UNIVERSITÉ DE LIMOGES
École Doctorale Sciences pour l'environnement-ED-523
FACULTÉ DE PHARMACIE
Laboratoire de Chimie des Substances Naturelles (LCSN)

Thesis

To obtain the degree

DOCTOR OF THE UNIVERSITY OF LIMOGES

Discipline / Specialization: applied Chemistry

Non-covalent interactions in natural products

Presented and defended by
Imène Bayach

JURY:

Reviewers

Pr. Juan Carlos SANCHO-GARCIA	University of Alicante, Spain
Dr. Frédéric CASTET	University of Bordeaux 1, France
Pr. Zoran MARKOVIC	University of Novi Pazar, Serbia

Examinators

Pr. Jean-Luc DUROUX	University of Limoges, France
Dr. Patrick TROUILLAS (supervisor)	University of Limoges, France

2014
10th of October

À la mémoire de mon père Said BAYACH,

À ma chère maman Souad Gouja,

À mes frères, sœurs et beaux-frères

“La réflexion est la bougie du cœur. *Si elle le quitte, le* cœur *n'aura plus de lumière."*

“Reflection is the lamp of the heart. If it departs, the heart will have no light.”

Abd Allah Ibn Alawi Attas

Acknowledgments

La présente thèse a été effectuée dans le laboratoire de Biophysique de la Faculté de Pharmacie de l'Université de Limoges appartenant au Laboratoire de Chimie des Substances Naturelles (LCSN) affilié à l'école Doctorale Gay Lussac ED-523 et financée par l'Association Djerbienne en France (ADF). Ce travail n'aurait pas été possible si je n'avais pas l'aide de plusieurs personnes envers lesquelles je suis reconnaissante.

Je remercie tout d'abord très sincèrement mon directeur de thèse **Dr Patrick Trouillas** pour ses qualités scientifiques et humaines. J'estime avoir de la chance de faire ma thèse sous ta direction. Je te remercie fortement de m'avoir former à la chimie théorique avec tant de gentillesse, de patience et de compréhension. Je m'excuse aussi de tous les moments difficiles par lesquels j'ai passé et qui ont influencé mon attitude et mes comportements. Je te remercie pour les différentes aides pendant ma thèse et pendant la correction de mon manuscrit ainsi que les efforts extraordinaires que t'as effectué.

Je tiens également à remercier **Prof. Jean-Frédéric F. Weber** (UiTM Puncak Alam, Malaisie) qui m'a proposé cette thèse et m'a donné l'opportunité de travailler sur son projet (Oligostilbenoids) dont il tient à coeur. Je vous remercie profondément de m'avoir choisi pour ce projet parmi vos étudiants, de m'avoir fais confiance et d'avoir cru en moi. Je vous remercie pour toutes les discussions scientifiques ou générales et de vos conseils pendant mon séjour en Malaisie. Je vous remercie également pour vos encouragements, votre soutien, vos critiques toujours constructifs. Malgré les difficultés, le manque d'échange, l'échec de la cotutelle, j'ai toujours un énorme respect pour vous. J'apprécie toutes les qualités humaines et scientifiques que vous possédez. Je vous remercie aussi de m'avoir présenter Dr Patrick Trouillas, c'est grâce à vous que j'ai pu connaitre une personnelle exceptionnelle comme lui. Merci aussi à Mme Aida pour ces divers aides et sa gentillesse.

Je remercie fortement **Prof Juan Carlos Sancho-García** (Université d'Alicante, Espagne) pour avoir accepté d'être rapporteur de cette thèse mais aussi pour m'avoir accepter dans son laboratoire pour des séjours scientifiques et m'avoir beaucoup aider. Je te remercie beaucoup de ta gentillesse, de tes conseils et ton aide inconditionné.

Je remercie sincèrement **Dr Frédéric Castet** (Université de Bordeaux 1) pour avoir accepté d'être rapporteur de ces travaux. Je vous remercie également de m'avoir accueilli dans votre laboratoire au cours de ma 2ème année de thèse.

I would like to thank sincerely **Dr. Zoran Marković** (University of Novi Pazar, Serbie) for having

agreed to judge this work. I will be pleased of knowing you.

Mes sincères remerciements vont également à **Prof Jean-Luc Duroux** (Université de Limoges) d'avoir accepté de juger ce travail.

Dans notre Labo, je remercie mon collègue **Dr Gabin Fabre**, pour ses différents aides notamment "informatiques", pour ses qualités humaines et pour sa bonne humeur. Je te souhaite encore plus de brillance et beaucoup de succès pour ta dernière année de thèse. Mes encouragements amicaux à **Tahani Ossman** pour la suite de sa thèse. Je te remercie sincèrement pour ton engagement dans le scan de ma thèse lors des dernières corrections et des différents services que tu m'as rendu. Je remercie également mon ami **Michal Biler** pour ses qualités humaines et sa bonne ambiance. Je suis très sincèrement ravie de t'avoir connu et je te souhaite beaucoup de brillance sur le sillon de la réussite. Je remercie également **Dr Claude Calliste**, pour ses discussions et sa bonne sympathie pendant les pauses café dont je suis rarement présente. Je remercie par ailleurs **Florent**, **Thomas**, **Nicolas** et **Assia** qui ont été présents au début de ma thèse. Je remercie également tous les membres de l'équipe LCSN, en particulier **Amandine Bonet** et **Olivier Rezazgui** pour leur amitié, **Pr Vincent sol**, **Dr Rachida Zarrouki** et **Mme Adeline Riguad** pour leur différents aides et surtout leur compréhension et gentillesse.

Je remercie également mon amie **Dr Laura Rustituoni** pour la bonne ambiance qu'elle a crée au labo pendant son séjour à Limoges, pour son amitié, son accueil chaleureux à Milano et tous les bons moments. Je t'ai connu pendant une courte période mais ton ouverture d'esprit, ta sympathie et tes qualités humaines font de toi une personne originale dont je suis ravie de connaître. Mes salutations vont à **Francisco** et **Delphy** ☺

From Malaysia, I want to thank all my friends from Atta-ur-Rahman Research Institute for Natural Product Discovery, especially **Zuhra** and **Fatimah** whom I consider my sisters. I am really very pleased to know you. I also thank my friends **Dr Rasha**, **Salwa**, **Najwa**, **Dr Mahdi** and **Dr Anouar**.

Par ailleurs, j'exprime ma gratitude envers l'association Djerbienne en France pour le financement d'une partie importante de ma thèse. Je remercie notamment le comité sociale et en particulier **Mr Faouzi Madani**, **Mr Hedi Raged** et **Mme Chedlia Ragued**, **Mr Jamel Ouersighni**, **Mr Taoufik Gouja**, **Mr Monir Gouja**, **Mr Mongi Ghandr**i, **Mr Ahmed chououi** et **Mr Soufien Mestaoui** de tous leurs efforts « bénévoles » et exceptionnels à mon égard. Mers remerciements vont également à tous les autres comités, les personnels ainsi que tous les membres y compris les étudiants pour l'accueil familial et la bonne ambiance au sein du siège de l'association.

Je remercie toute ma famille à Paris qui m'a toujours supporté et accueillie avec tant de chaleur

familiale. Je cite particulièrement **Mme Chedlia Ben Maamar**, **Mr Aroussi Bayach**, **Mr Chokri Bayach** et mes cousins et cousines notamment **Najet**, **Sarah et Maher** pour leur générosité, encouragements et soutiens financier et moral. Mes remerciements vont également à mes amies parisiennes **Hena** (et sa famille), **Raja** (son mari et son frère), **Jamila** (et sa famille), **Karamoko** (maintenant Canadien), mon cousin **Jamel BAYACH** et sa femme **Houda** et à tous mes amis, cousins et cousines partout.

Finalement, je dédie cette thèse à ma chère **maman Souad Gouja** qui compte tout pour moi, rien n'est plus cher que toi maman, je te remercie profondément de ta confiance, de ta patience, de toutes les valeurs que tu m'as transmis, de ton amour inconditionné, ton soutien, impossible d'exprimer ma reconnaissance et ma gratitude envers toi, que Dieu te préserve de tout mal, je m'excuse que je n'ai pas pu être souvent à tes cotés. À la mémoire de **mon père Saïd Bayach** (que Dieu lui accorde Sa Grâce et Sa Miséricorde et l'accueille en son vaste Paradis), papa qui nous a quitté vite sans voir un des rêves de sa fille se réaliser, papa qui m'a toujours fais confiance et qui a laissé de côté les vielles coutumes de la région pour que je puisse suivre mes études universitaires dans un pays étranger, cette thèse est à ton honneur même si tu n'es plus parmi nous. Un grand merci à mes sœurs **Olfa**, **Boutheina** et **Sondes** et mes frères **Radhouen** et **Hatem** qui m'ont toujours fais confiance et soutenus, à mes trois beaux-frères, mes chers neveux et nièces (**Malek**, **Aziz**, **Maram**, **Rayen** et **Rayssen**) et à toute la grande famille **BAYACH** de la ville de poterie à l'ile de Djerba.

Table of contents

Acknowledgments 4

Acronyms 10

Introduction 14

Chapter 1 – Natural products 17

1. Flavonoids 19
1.1. Structures and diversity 19
1.2. Distribution 21
1.3. Biosynthesis 21
1.4. Biological roles and activities 22
1.4.1. Antioxidant activity 23
1.4.2. Anti–inflammatory activity 24
1.4.3. Antimicrobial activity 24
1.4.4. Other biological activities 25

2. Stilbenoids 25
2.1. Structures and diversity 26
2.1.1. Stilbenes 26
2.1.2. Oligostilbenes 27
2.1.3. Bibenzyls 28
2.1.4. Bisbibenzyls 28
2.1.5. Phenanthrenoids 29
2.1.6. Other Stilbenoids 29
2.2. Distribution 30
2.3. Biosynthesis 30
2.4. Biological roles and activities 34
3.4.1. Antioxidant activity 34
3.4.2. Anti–Inflammation and Immunomodulating Activity 34
2.4.3. Anti–Microbial activity 35
3.4.4. Anticancer/antitumor activity 37
3.4.5. Other biological activities 38

Chapter 2 – Non-covalent interactions 41

1. A general definition of non-covalent interactions 41
1.1. vdW Interactions 42
1.2. Hydrogen bond 44
1.3. π-stacking 44

2. Non-covalent bonding in nature 46
2.1. Proteins 46
2.2. DNA 48
2.3. Copigmentation 50
2.4. Natural graphite 52
2.5. Non-covalent interactions in synthetic compounds 53

Chapter 3 – Theoretical methods 56

1. Basic concepts and general view on methods of calculation 56
1.1. The Born–Oppenheimer approximation 56
1.2. The Hartree-Fock approximation 57
1.2.1. The Slater determinant 57
1.2.2. The Hartree–Fock approximation 58

1.2.3. Restricted and unrestricted Hartree–Fock formalisms....59
1.3. Roothaan-Hall equations....60
1.4. Basis sets....61
1.4.1. Usual basis sets....62
1.4.2. Basis Set Superposition Error (BSSE)....63
1.5. Post Hartree-Fock methods....64
1.5.1. Coupled–cluster (CC) methods....64
1.5.2. Perturbation Theory (PT)....65
1.5.3. Møller-Plesset (MP) methods....66
1.5.4. SCS–MP2 methods....67
1.6. Semi-empirical methods....68
2. Density functional theory (DFT)....68
2.1. Thomas and Fermi....68
2.2. Hohenberg and Kohn theorems....69
2.3. Kohn–Sham....70
2.3. Exchange–correlation functionals....71
2.3.1. Local density approximation....71
2.3.2. Generalized gradient approximation....72
2.3.3. Hybrid functionals....73
3. Further developments of DFT....73
3.1. Self–interaction error....74
3.2. Dispersion–corrected functionals....74
3.2.1. DFT–D....74
3.2.2. DFT–D2....75
3.2.3. DFT–D3....76
3.2.4. DFT–NL....77
4. Time–Dependent DFT (TD–DFT)....77
Chapter 4 – Methodology....80
π–Stacked polyphenolic dimers: A case study using dispersion–corrected methods....80
1. Introduction....81
2. Theoretical methods....82
2.1. Modeling dispersion effects....82
2.2. Technical details....84
3. Results and discussion....86
3.1. Optimized geometry of the complex....86
3.2. Reference data....86
3.3. Assessment of DFT–based dispersion corrections....88
4. Conclusions....92
Chapter 5 – Methodological assessments of dispersion between prototypes of polyphenol non-covalent complexes....95
Oligostilbenoids from the heartwood of *N. heimii*: role of non–covalent association in their biogenesis....95
1. Introduction....96
2. Results and Discussion....96
3. Conclusion....116
4. Method Section....117

Chapter 6 – Antioxidants 122

Section I. Antioxidant properties of phenolic Schiff bases: Structure activity relationship and mechanism of action 123

1. Introduction 125

2. Methodology 128

3. Results and discussion 130

5. Conclusion 142

Section II. Atomistic description of collaborative antioxidant effects between vitamins E, C and natural polyphenols in lipid–bilayer membranes 143

1. Results/Discussion 144

1.1. Association energies 144

1.2. Critical analysis of the association Gibbs energy evaluation 145

2. Methods 146

❖ **Quantum mechanics calculations** 146

4. Conclusion 147

Chapter 7 – Tuning optical properties of chalcone derivatives 149

1. Introduction 149

2. Methodology 150

3. π–π non–covalent chalcone dimers 152

3.1. 3D arrangements issued from X-ray crystal structures 152

3.2. Non–restrained conformational analysis 154

4. Optical properties 159

4.1. Monomers 1 and 2 159

4.2. Non–covalent complexes 160

5. Conclusion 168

Conclusion 171

Annex 196

Acronyms

BDE Bond Dissociation Enthalpy

BSSE Basis Set Superposition Error

CC Coupled Cluster

CC2 Second−order approximate Coupled Cluster singles and doubles

CD Circular Dichroism

COSMO COnductor−like Screening Model

CT Charge Transfer

DFT Density Functional Theory

DFT-D Dispersion−corrected DFT

DNA DesoxyriboNucleic Acid

ES Excited State

ES-CT Excited State Charge Transfer

GEA Gradient Expansion Approximation

GGA Generalized Gradient Approximation

GS Ground State

GTO Gaussian−Type Orbital

HAT H−Atom Transfer

HF Hartree−Fock

HK Hohenberg−Kohn

HOMO Highest Occupied Molecular Orbital

HSV Herpes Simplex Virus

IP Ionization Potential

IR Infrared

KS Kohn−Sham

LCAO Linear Combination of Atomic Orbital

LDA Local Density Approximation

LDL Low–Density Lipoprotein

LPS Lipopolysaccharide

LSDA Local Spin Density Approximation

LUMO Lowest Unoccupied Molecular Orbital

MI Molecular Interaction

MO Molecular Orbital

MP Møller–Plesset

MP1 First–Order Møller–Plesset

MP2 Second–Order Møller–Plesset

MP3 Third–Order Møller–Plesset

MP4 Fourth–Order Møller–Plesset

MP5 Fifth–Order Møller–Plesset

NLNnon–Local

NMR Nuclear Magnetic Resonance

PAL Phenylalanine Ammonia Lyase

PCET Proton–Coupled Electron Transfer

PCM Polarizable Continuum Model

PT Perturbation Theory

QM Quantum Mechanics

RHF Restricted Hartree–Fock

ROHF Restricted Open–Shell Hartree–Fock

ROS Reactive–Oxygen–Species

SCF Self Consistent Field

SCS Spin–Component–Scaled

SHS Chalcone Synthase

SOMO Single Occupied Molecular Orbital

SOS Scaled–Opposite-Spin

SPLET Sequential Proton Loss Electron Transfer

STO Slater−Type Orbital

STS Stilbene Synthase

TD Time−Dependent

UHF Unrestricted Open−Shell Hartree-Fock

UV/Vis Ultraviolet/Visible

vdW van der Waals

XC Exchange−Correlation

Introduction

Introduction

Technological progress makes our lives much easier and more comfortable. Particularly, since the invention of the computer in the 20th century, the world has been revolutionized opening an unimaginable number of uses that have globally improved life. Moreover, the revolution of computers has allowed scientists to develop Quantum Mechanics (QM), a powerful tool that may support experimentalists either chemists or biologists. This has allowed rationalizing many scientific issues. For example, in the research on natural products, one of the most difficult and prevalent issues concerns the determination of stereochemistry in the design of new compounds. In fact, CD (Circular Dichroism) either ECD (Electronic Circular Dichroism) or VCD (Vibrational Circular Dichroism) is fast becoming a major method when NOE contacts are unobserved or ambiguous in NMR spectroscopy. However, to determine absolute configuration, CD requires similar compounds to be used for comparison purpose, while there are not always available. At this stage, QM may provide fruitful supports. Calculations of chemical shifts and coupling constants have reached high accuracy, which may also contribute to distinguish different isomers.

Another area in which QM becomes handy concerns synthetic/biosynthetic mechanisms. QM allows testing various hypothesized reaction mechanisms. Many other related properties can be accurately evaluated. Whereas the fields of application of QM are large, this PhD focuses on the role of this tool at describing non−covalent interactions, a crucial type of interactions that exist everywhere in Nature.

Non-covalent interactions make fascinating molecular architectures and designs with more or less complex inter− and/or intra−molecular arrangements. These interactions provide “artistic” touch and original conception for molecules, which may in turns provide different biological and pharmacological actions.

This thesis focuses on non-covalent interactions between natural polyphenols. These compounds constitute a well−known family of natural products found in fruit, vegetables, spices and beverages made from plants like (herbal) teas, wines and fruit juices. They are very trendy for their antioxidant properties that decrease oxidative stress and consequences such as skin aging.

Chapter 1 describes two main families of polyphenols, namely flavonoids and stilbenoids focusing on their biosynthetic pathways, their diverse and fascinating chemical structures as well as their pharmaceutical roles and biological activities. Interestingly, these polyphenols can form non−covalent complexes with various applications.

Chapter 2 rationalizes this type of interactions briefly reminding the different types of non−covalent interactions in terms of their physical−chemical particularities. The importance of these interactions is then exemplified by different examples showing their implications and contributions in Nature.

Chapter 3 details basic concepts of quantum chemistry in an attempt to introduce the different methods of calculations used in the present work.

The theoretical strategies to evaluate non-covalent interactions are still under development. In Chapter 4, which is a published article, we proposed a new parameterization for the B3P86−NL functional, in which dispersive interactions are accounted by a non-local approach.

In our work, we provide three new applications of non-covalent interactions in polyphenols. First, non−covalent complexation between oligostilbenoids, isolated from *Neobalanocarpus heimii*, a common tree found in abundance in the rainforests of Malaysia, has been studied. Malaysia offers probably the greatest plant biodiversity in the world, perhaps higher than the Amazonian rainforest. Chapter 5, a submitted article, shows how non−covalent association may drive regio− and stereo−selectivity of oligomerisation reactions. This QM study is aiming at a support to synthesis of new active agents for the pharmaceutical, cosmetic and food industries.

Second, Chapter 6 shows how non-covalent interactions may influence antioxidant properties *i)* in pre-reaction complexes before hydrogen and electron transfers from the polyphenol to the free radical; and *ii)* in stable non−covalent antioxidant complexes, which may favor antioxidant regeneration.

Third, Chapter 7 consists at elucidating the role of non−covalent interactions in the modulation of optoelectronic properties of molecules derived from natural polyphenols. These molecules that efficiently absorb light can be applied to the bioinspired design of new photovoltaic cells.

Chapter 1 – Natural products

Chapter 1 – Natural products

Natural products are all compounds derived from natural sources including all plant tissues, marine organisms and microorganisms. Many natural compounds exhibit pharmacological or biological activities and may also inspire the design of new drugs. Their diverse biological activities and medicinal potentials have increasingly attracted the attention of scientists over the past decades. Even if chemical and biological tools have shed light on many biological issues regarding natural compounds, many others are still open. In particular, biosynthesis of many natural polyphenols (e.g., flavonoids and stilbenoids) is still not fully elucidated. Flavonoids and stilbenoids are two important groups of natural polyphenols, widely distributed in the plant kingdom and present in human diet. This chapter presents these two families of polyphenols, which derive from the same precursors but differ in the further steps of the biosynthesis.

Both stilbene synthase (STS) and chalcone synthase (CHS) are related type III Polyketide synthase (PKS) enzymes that catalyze the formation of identical linear tetraketide intermediate from a CoA–tethered phenylpropanoid starter and three molecules of malonyl–CoA. Each enzyme catalyzes the cyclization of this intermediate but using different cyclization mechanisms to produce different chemical scaffolds for a variety of plant products (Fig. 1). This is a key step for which the synthetized tetraketide is further folded differently depending on the enzyme and subjected to aldol or Claisen condensation to yield either stilbene or chalcone. CHS, ubiquitous in the plant kingdom, catalyzes a C6→C1 Claisen condensation to form the core chalcone scaffold of all natural flavonoids. STS enables divergence from CHS, and instead catalyzes a C2→C7 aldol condensation that forms the stilbene backbone of resveratrol and related antifungal phytoalexins (Fig. 3).

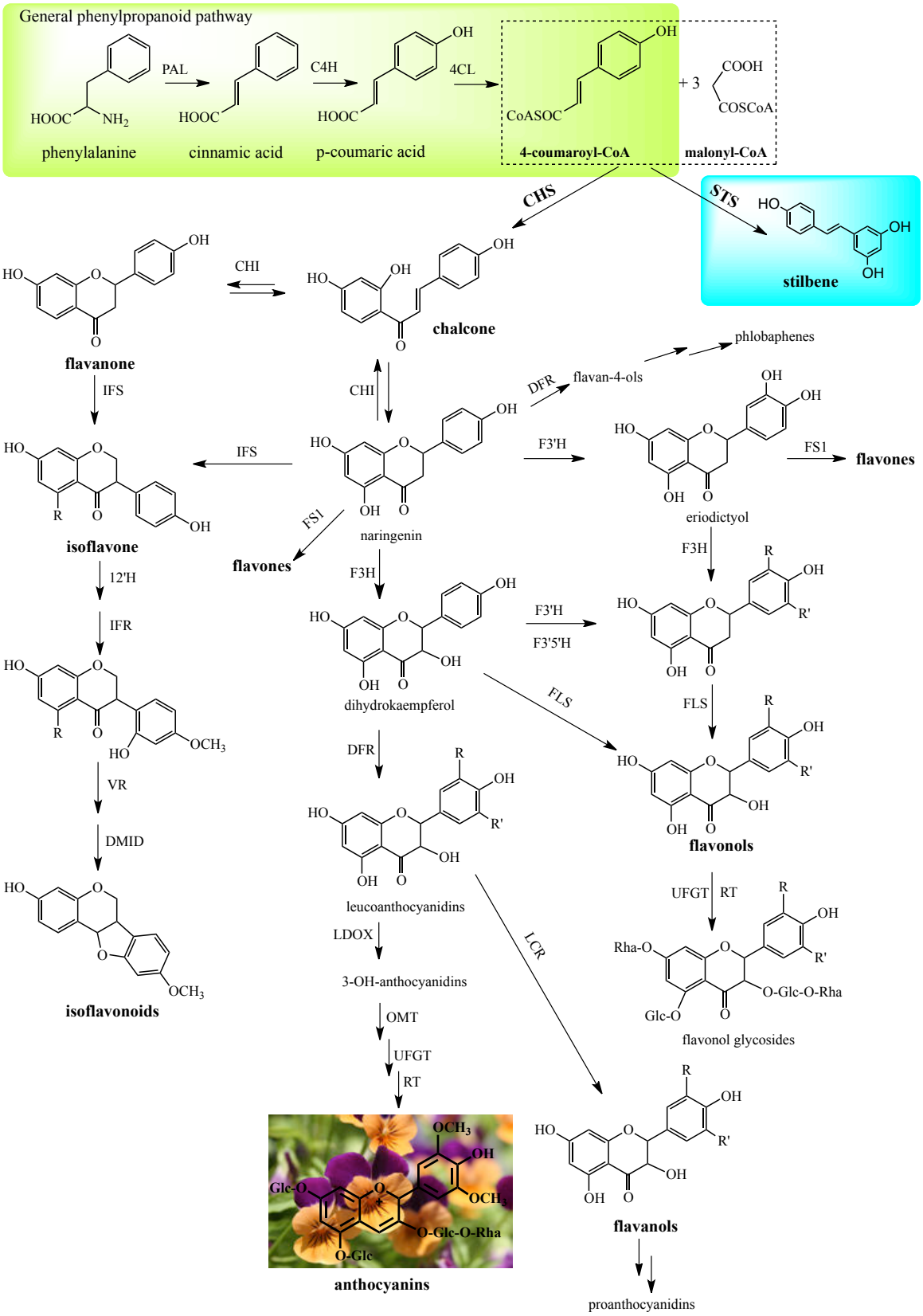

Figure 1. Major branch pathways of flavonoid biosynthesis.

The exact mechanisms of action of these enzymes are still unknown but many pathways have been hypothetized.[1]

1. Flavonoids

Flavonoids constitute the largest and the most studied family of polyphenols with more than 8000 different substances found in virtually all plants. They are responsible for many plant colors covering all visible spectrum. In oriental medicine, plants rich in flavonoids have been used for centuries e.g., scultellaria root, cornus fruit, licorice, and green tea are examples of flavonoid containing plant foods widely used in oriental medicine.

1.1. Structures and diversity

All flavonoids have a common chemical skeleton. They are generally made of two aromatic rings, each containing at least one hydroxyl, which are connected through a three-carbon "bridge" within a six-member heterocyclic ring (Fig.2).

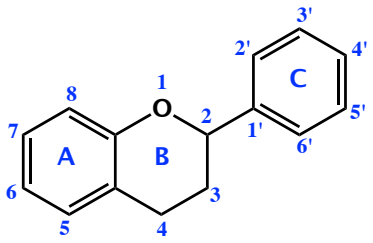

Figure 2. Flavonoids basic structure.

Flavonoids are divided into subclasses according to aromaticity of the heterocyclic ring, oxidation state and functional groups of the heterocyclic ring. The major subgroups are flavones, flavonols, flavanones, flavanonols, flavanols, chalcones and dihydrochalcones, isoflavones, anthocyanins and anthocyanidins (Table 1). The individual compounds of each subclass are characterized by specific hydroxylation and conjugation patterns.

Natural flavones are characterized by the presence of a keto group at C4 and a 2,3−double bond (Table 1). They include apigenin, luteolin, tangeritin, chrysin, 6−hydroxyflavone, baicalein, scutellarein and wogonin.* All compounds quoted in the manuscript are referenced in the Annex section.

Flavonols are flavones having a hydroxyl group at C3 (Table 1). They are widely distributed in fruits as well as vegetables. Their diversity derives from the different positions of the phenolic OH−groups. The most common are quercetin, kaempferol, rhamnazin, pachypodol and myricetin.

* All compounds quoted in the manuscript are referenced in the Annex section.

Flavanones are characterized by the presence of a keto group at C4 and an asymmetric carbon at C2 (Table 1). They are generally glycosylated by a disaccharide at C7 to give flavanone glycosides. The most common are naringenin, eriodictyol and hespertin.

Flavanonols, also called dihydroflavonols, exhibit two asymmetric carbons, C2 and C3, with a hydroxyl group at C3 (Table 1). The most common examples are aromanderin and taxifolin.

Flavanols (not to be confused with flavonols), also called flavan−3−ols, are derivatives of flavans and are characterized by a 2,3 single bond and the absence of the keto group at C4 (Table 1). Catechin and epicatechin are the most widely distributed flavanols and they are partly responsible for the beneficial effects of green tea. This class includes also epicatechin gallate, epigallocatechin, epigallocatechin gallate, proanthocyanidins, theaflavins and thearubigins.

Chalcones or chalconoids are open−chain flavonoids, in which the two aromatic rings are linked by an α,β-unsaturated carbonyl system (Table 1). Chalcones therefore exist as two stereoisomers (*E* and *Z*) according to the arrangement of substituents around the central double bond. Benzylideneacetophenone is the parent member of the chalcone series. The transformation of chalcone to flavanone is possible and catalysed by the chalcone isomerase.

Isoflavones are widely studied, mainly, for their pseudo-estrogenic properties. They are isomers of flavones, with an almost identical structure, the only difference being the position of the phenyl group, which is bonded at C3 instead of C2 for the flavones (Table 1). Almost exclusively, isoflavones are produced by the members of the *Fabaceae* family i.e., *Leguminosae* or bean.

Anthocyanidins and anthocyanins are characterized by the presence of a cationic charge (Table 1). Anthocyanidins are common plant pigments and typically not found as free aglycones. Most of them are partly responsible for color variation in fruit and flowers. The five main anthocyanidins are cyanidin, delphinidin, pelargonidin, malvidin, peonidin and petunidin. Anthocyanins are the glycosides of anthocyanidins, they are water−soluble vacuolar pigments that may appear red, purple, or blue depending on pH. They are found in many fruits and vegetables including purple cabbage, beets, blueberries, cherries, raspberries and purple grapes. They occur in all tissues of higher plants, including leaves, stems, roots, flowers and fruits.

Table 1. Chemical structures of the principal flavonoid subclasses.

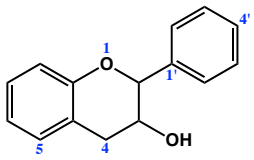 Flavanols	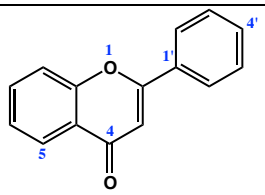 Flavones	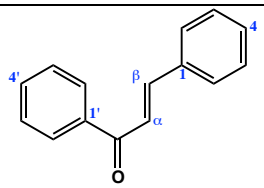 Chalcones
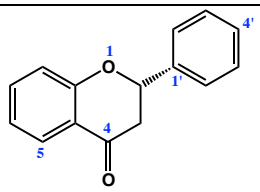 Flavanones	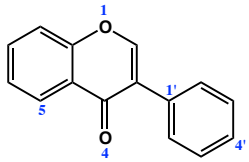 Isoflavones	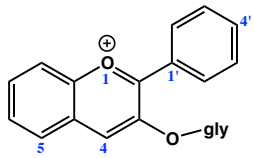 Anthocyanins
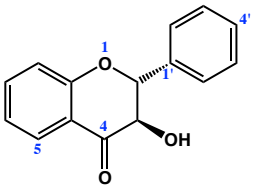 Flavanonols	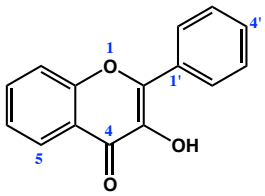 Flavonols	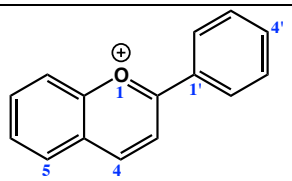 Anthocyanidins

1.2. Distribution

Virtually all fruits, vegetables, herbs and spices contain flavonoids. Beverages made from plants e.g., wines, tea and fruit juices also contain a wide variety of flavonoids.[2] Berries have high content of anthocyanins. Black raspberries, for example, may contain up to 100 milligrams of anthocyanins per ounce.† Green tea has high content of catechins, reaching 1 g per cup. Skin of fruits is known to contain high concentration of flavonoids. Flavonoids can be colored but also colorless, thus being less noticeable in food. Orange flavonoids can be found in the white pulpy portion inside the skin.

1.3. Biosynthesis

The discovery of the first enzyme involved in the phenylpropanoid pathway for flavonoid biosynthesis was achieved in 1961 by Koukol and Conn.[3] Later, it was demonstrated, using radioactively labeled compounds, that flavonoids were originated from acetate units and a phenylpropanoid intermediate derived from the shikimic acid pathway.[4] In short, ring A is formed by head–to–tail condensation of three acetate units and ring B as well as C2, C3 and C4 atoms from a phenylpropanoid precursors (Fig.1).[5] The primary enzyme specific for the flavonoid pathway is CHS that produces chalcone scaffolds from which all flavonoids derive (Fig. 3). Although the central pathway for flavonoid

† 1 ounce ≈ 28 g.

biosynthesis is conserved in plants, depending on the species, a group of enzymes, such as isomerases, reductases, hydroxylases, and several Fe^{2+}/2–oxoglutarate–dependent dioxygenases modify the basic flavonoid skeleton, leading to the different flavonoid subclasses.[6] Finally, tranferases modify the flavonoid backbone with sugars, methyl groups and/or acyl moieties, thus modulating the physiological activity of the resulting flavonoids by altering their solubility, reactivity and interaction with cellular targets.[7], [8]

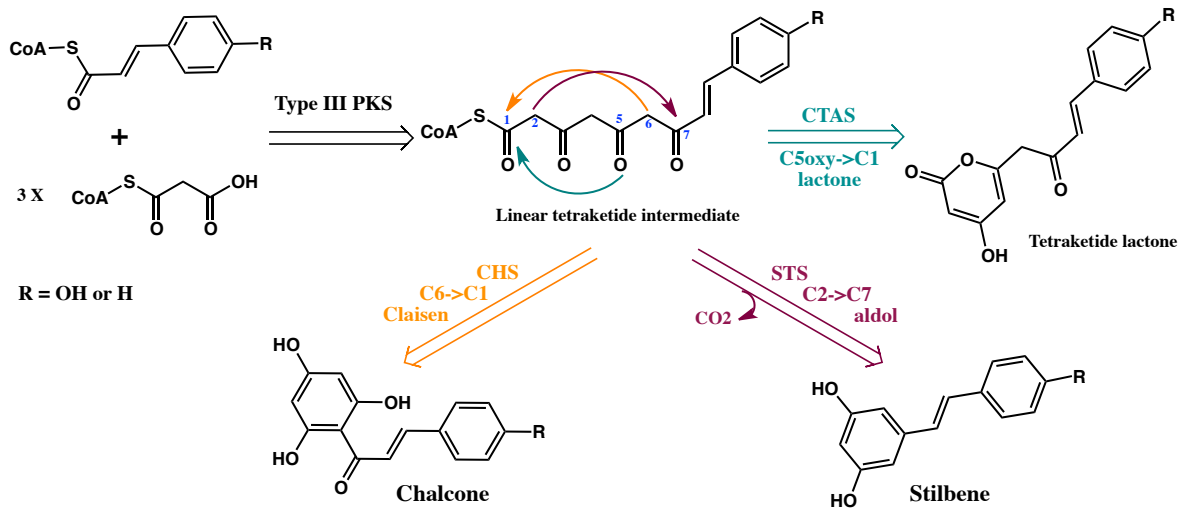

Figure 3. Type III Polyketide Synthase Enzymes and Tetraketide Cyclization

1.4. Biological roles and activities

Whereas nearly all organisms possess antioxidant defense and repair systems to protect them against oxidative damage leading to cancer, aging, atherosclerosis, ischemic injury, inflammation and neurodegenerative diseases, these systems may fail at preventing all oxidative damages.[9] Food antioxidant-containing diets may contribute to be used to help the human body to reduce oxidative stress.[10] Also the use of antioxidant food supplements have been envisaged, but such a use is controversy, beneficial effects being not systematically proved [11] and negative (pro–oxidant) effects being suggested in case of mega doses of antioxidants.[12]

Flavonoids have been extensively studied for their biological roles (in plants) and activities (in mammals). Many analyses have focused on the understanding of their roles in i) plant–microbe interactions, ii) protection against ultraviolet (UV) light, iii) (red, purple, orange, yellow, blue) plant pigmentation and iv) implication in male fertility process. These studies show importance of chemical flavonoid structures to rationalize a wide range of activities, but also highlight the flavonoid pathway as a paradigm for the study of the evolution of plant metabolism.[13] Consequently, these secondary plant metabolites have gained much attention, especially in their potential role to explain some of the human

health benefits associated diets rich in fruit and vegetables including apples, apricots, blueberries, pears, raspberries, strawberries, black beans, cabbage, onions, parsley, pinto beans and tomatoes.[14]

1.4.1. Antioxidant activity

Most of flavonoids exhibit antioxidant activities.[15] As antioxidants, they can participate in neutralization of reactive−oxygen−species (ROS) overproduction, subsequently preventing related cell damages. Flavonoids are powerful in vitro antioxidants, being able to scavenge many free radical species. While flavonoids may exert their cell structure protection through a variety of mechanisms, one of their potent effects may be through their ability to increase levels of glutathione, a powerful antioxidant, as suggested by various research studies. The capacity of flavonoids to act as antioxidants, depends mainly upon their molecular structures. The position of hydroxyl groups and other features in the chemical structure of flavonoids plays a key role on their free radical scavenging activities. Quercetin, the most abundant dietary flavonol found in its glycoside form, is a potent antioxidant because exhibiting most of structural requirements for an effective free radical scavenging capacity.[15]

The capacity of prenylated flavonoids to inhibit LDL (low-density lipoprotein) oxidation induced by copper was evaluated as an indicator of antioxidant activity. It was a comparative study of quercetin (a flavonol), genistein (the major isoflavone in soy), chalconaringenin (a non−prenylated chalcone), naringenin (a non-prenylated flavanone) and vitamin E (Fig. 4). The prenylchalcones and prenylflavones are effective in preventing LDL oxidation, the prenylchalcones having generally greater antioxidant activity than the prenylflavanones. Xanthohumol, the major prenylchalcone in hops and beer, is more powerful than vitamin E or genistein, whereas xanthohumol was less potent than quercetin. The potency of xanthohumol as an antioxidant is clearly increased when combined with an equivalent amount of vitamin E.

The prenyl group plays an important role in the antioxidant activity of certain flavonoids. Indeed, a flavonoid chalcone (chalconaringenin) and a flavanone (naringenin) without prenyl groups act as pro−oxidants, i.e. they promote rather than limit LDL oxidation. However, adding a prenyl group to these flavonoids counteracted their pro−oxidant activities. This observation that prenyl groups are important in conferring antioxidant activity to certain flavonoids may lead to the discovery or synthesis of novel prenylated flavonoids as preventive or therapeutic agents against human diseases associated with free radicals.

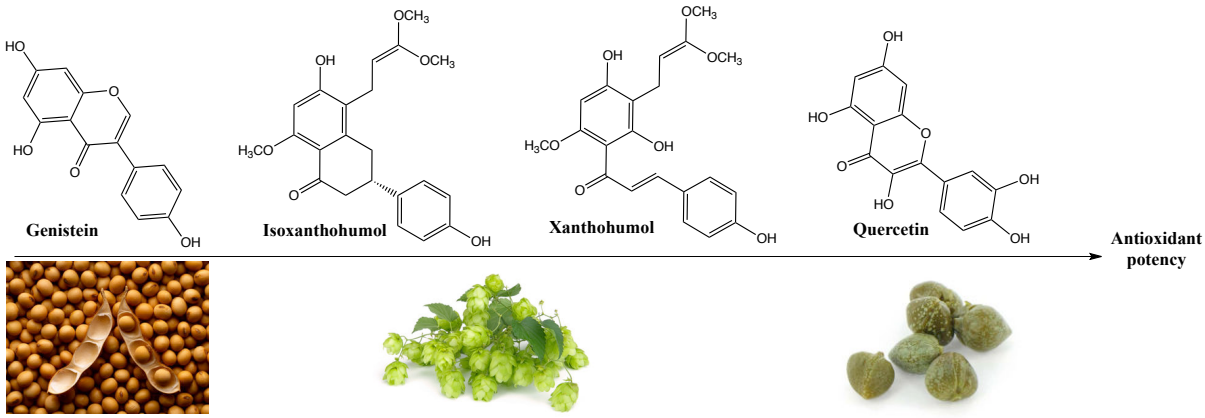

Figure 4. Examples of antioxidant flavonoids.

1.4.2. Anti–inflammatory activity

The natural response of the human organism to external aggression is continuously regulated to prevent over–activation of the immune system and unwanted immune responses. Many types of cells involved with the immune system including T cells, B cells, NK cells, mast cells, and neutrophils have been shown to alter their behavior in the presence of flavonoids. Many investigations have proved anti–inflammatory activities of many flavonoids.[16] Flavonols (quercetin, rutin and morin) and flavanones (hesperetin and hesperidin) were investigated in acute and chronic inflammation animal models.[17] Only flavanones were effective on neurogenic inflammation induced by xylene. Quercetin represents the most important compound in reducing paw edema induced by carrageenan.[17] Paradkar et al. demonstrated that diet rich in the isoflavones daidzin, glycitin, genistein and their glucosides, modulate the inflammatory reaction in the mouse intestine and liver after LPS (lipopolysaccharide) injection.[18] Genistein (isoflavone) constitutes one of the most studied among a great variety of natural flavonoids in different models of inflammation. Its anti-inflammatory effect can be mediated by inhibition of the tyrosine kinase signaling cascade.[19] Besides, other flavonoids were effective in preventing adjuvant arthritis in the rat. Daily intraperitoneal administration of rutin, quercetin and hesperidin, inhibited both acute and chronic phases in this experimental model of inflammation, with rutin being the most active compound in the chronic phase.[20]

1.4.3. Antimicrobial activity

- Antifungal activity

Flavonoids have been proposed for use against fungal pathogens because of their widespread ability to inhibit spore germination of plant pathogens. For example, galangin, a flavonol commonly found in

propolis samples has been shown to inhibit *Aspergillus tamarii*, *A. flavus*, *Cladosporium sphaerospermum*, *Penicillium digitatum* and *Penicillium italicum* effects.[21]

- Antiviral activity

Several research groups have investigated the relationship between flavonoid structure and inhibitory activity against HIV−1 and related enzymes.[22]–[25] Flavonoids also exhibit activity against other viruses. For example, quercetin, morin, rutin, dihydroquercetin, dihydrofisetin, leucocyanidin, pelargonidin chloride and catechin possess activity against up to seven types of viruses, including herpes simplex virus (HSV), respiratory syncytial virus, poliovirus and Sindbis virus.[23], [24]

- Antibacterial activity

The antibacterial activity of flavonoids is being increasingly documented. For example, flavonoid−rich plant extracts from *Hypericum*, *Capsella* and *Chromolaena* have been reported to possess antibacterial activities.[25], [26] Many other phytochemical preparations with high flavonoid content have also been reported to exhibit antibacterial activity.[27]–[29]

1.4.4. Other biological activities

Flavonoids have been reported to possess many other useful properties, including oestrogenic activity, enzyme inhibition, antiallergic activity, vascular activity and cytotoxic antitumor activity.[31]

2. Stilbenoids

This section is more detailed than that on flavonoids because of i) the huge number of articles in literature dedicated to flavonoids compared to stilbenoids as well as previous theses from our laboratory and ii) the particular interest of oligostilbenoid molecules in this present thesis.

Stilbenoids constitute a family of polyphenols known for their structural complexity and for their diverse biological activities. They occur with a limited and heterogeneous distribution in the plant kingdom. The plant family Vitaceae is one of the richest sources of stilbenes, together with other families, such as Dipterocarpaceae, Gnetaceae and Fabaceae. Stilbenoids were isolated from the plants for the first time in 1899 [31] but only named as it in 1980 by Gorham.[32]

Their chemical diversity and their bioactivities are attracting increasing interest in particular due to resveratrol (i.e., 3,5,4'−trihydroxystilbene), known for promising biological activities. Currently, the number of stilbenoids isolated from plants exceeds 1000 molecules against ca. 300 in 1995 and only 100 in 1980. A large number of these compounds have been investigated mainly for their roles in plant resistance to fungal pathogens but also for their diverse biological activities.

2.1. Structures and diversity

Over the last few years, more than 800 novel stilbenoids have been identified.[33] While the constituent unit is simple, their structures emphasize chemical diversity through different alternatives and various oligomeric features. Their structures are made of 1,2−diphenylethylene or 1,2−diphenylethane moieties. According to their structural characteristics, stilbenoids can be classified into five groups including stilbenes, oligostilbenes, bibenzyls, bisbibenzyls and phenanthrenes.

2.1.1. Stilbenes

The essential structural stilbene skeleton includes two aromatic rings linked by a methylene bridge. Due to the double bond (i.e., no free rotation allowed), stilbene may have either *trans* or *cis* configuration. The *trans−(E)* configuration is often common among naturally occurring stilbenes, but the *cis−(Z)* configuration has also been encountered. From this relatively simple structure, hydroxyl groups may be substituted together with sugar, methyl, methoxy and other moieties. More than 120 stilbenes and their glycosides have been isolated and classed as spermatophytes‡.[34] Stilbenes represent the most widely investigated small stilbenoids, due to their bioactivities, especially resveratrol and its analogues.[35]

Table 2. Chemical structures of a few examples for all five subclasses of stilbenoids

A	B	C	D	E
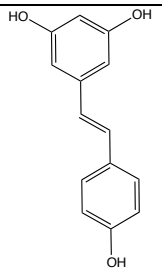 Resveratrol	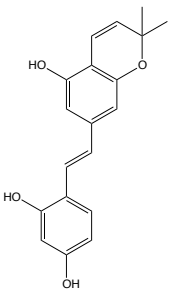 Artocarbene	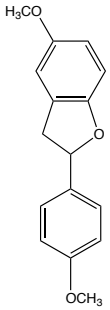 Corsifuran C	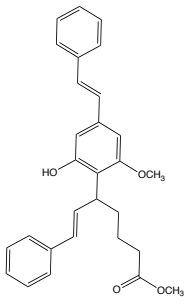 Idenburgene	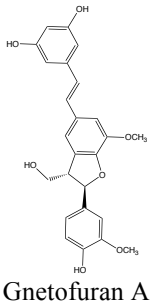 Gnetofuran A

‡ Spermatophytes are plants that produce seeds.

One can classify stilbenes according to their chemical structures into subclasses A–E (Table 2), namely A) simple stilbenes (e.g., resveratrol) that contain molecules having oxygen functions on the aromatic rings and including the methylenedioxy derivatives and glycosides; B) prenylated and geranylated stilbenes (e.g., artocarbene) independently of the substitution position and including cyclized derivatives; C) aryl benzofuran derivatives (e.g., corsifuran C); D) carbon substituted stilbenes other than C–glycosides and those of groups B and C (e.g., idenburgene); as well as E) other hybrid stilbenes (e.g., gnetofuran A).

2.1.2. Oligostilbenes

Stilbene oligomers or oligostilbenes display high chemical diversities as a result of homogeneous or heterogeneous coupling between monomeric stilbenes. Coggon et al. reported in 1965 the first naturally occurring resveratrol tetramer, namely (-)–hopeaphenol.[36] Currently, the octamer vateriaphenol A isolated from the stem bark of *Vateria indica,* which belong to the Dipterocarpaceae family, is the most condensed naturally occurring oligomer. In 1993, Sotheeswaran and Pasupathy proposed to classify oligostilbenes into two groups, namely Group A that includes at least on five–membered oxygen heterocycle (usually the trans–2–aryl–2,3–dihydrobenzofuran moiety), and Group B that contains no oxygen heterocycle.[37] Sotheeswaran et al. suggested that all naturally occurring resveratrol oligomers from group A were formed from resveratrol through the dimer ε–viniferin (see annex). It is worth noting that (+)–ε–viniferin occurs only in *Vitaceae*, whereas (-)–ε–viniferin is found in *Dipterocarpaceae*, *Cyperaceae*, *Gnetaceae* and *Leguminosae*.

The Sotheeswaran's classification is restricted to resveratrol oligomers. Thus, Lin et al. has extended the definition and has proposed that oligomeric stilbenes may be divided into five major groups according to constituent units, each group being split into two subgroups according to Sotheeswaran's scheme. Recently, many novel oligomers have been discovered, and the newly discovered stilbene oligomers have been classified according to their degree of polymerization, namely as dimers (e.g., viniferin), trimers (e.g., caraphenol A), tetramers (e.g., gnemonol B) and higher oligomers (Fig. 5).

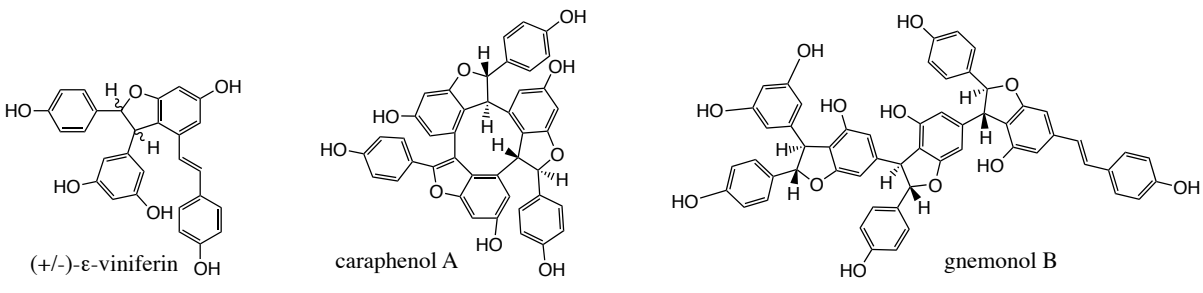

Figure 5. Oligostilbene examples.

Structural identifications and characterizations of oligostilbenes by NMR is sometimes a challenging task due to complex structures, with confusing stereochemistry due to huge possibilities of diastereoisomers, epimers, enantiomers and conformers (e.g., gneafricanin F, upunaphenols I and J, see annex).[38], [39] The basic units of stilbene oligomers are resveratrol, isorhapontigenin, piceatannol, oxyresveratrol, rhapontigenin, gnetol and pterostilbene. The various stilbene oligomers may combine in either homo– or hetero–polymerization processes, giving rise to huge chemical diversity from only a few monomer units.

2.1.3. Bibenzyls

One of the richest sources of bibenzyls is liverwort (a group of plants belonging to the bryophytes). According to their structures, bibenzyls are classified into four groups (Table 3) as follow, A) simple bibenzyls having oxygenated functions on the aromatic rings, including methylenedioxy derivatives and glycosides (e.g., bulbophyllin); B) prenylated, geranylated and farnesylated bibenzyls (e.g., glepidotin D); C) 4–hydroxybenzyl substituted bibenzyls (e.g., shanciguol); and D) other bibenzyls (e.g., lespedezol H).[31]

Table 3. Examples of bibenzyls structures: groups A-D.

A	B	C	D
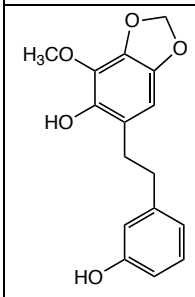	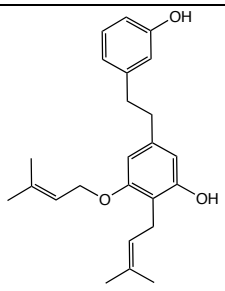	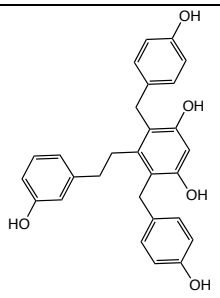	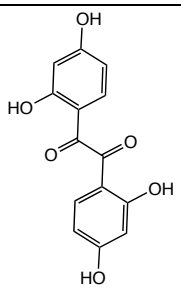
Bulbophyllin	Glepidotin D	Shanciguol	Lespedezol H

2.1.4. Bisbibenzyls

Bisbibenzyls are usually distributed in liverworts and were rarely discovered in other species. Indeed, the first occurrence of bisbibenzyls other than from liverworts was perrottetin H that was isolated from a pteridophyte, *Hymenophyllum barbatum*. It is a derivative of cyclic bisbibenzyl, which was isolated from the liverwort *Jubula japonica*. The occurrence of bisbibenzyls in both pteridophytes and liverworts is very important to understand evolutionary of terrestrial green plant spores.

Due to their structural diversity and biological activities, bisbibenzyls have attracted much interest from chemists for synthesis. Gorham has identified nine types of bisbibenzyls based on different modes of cyclization.[31] Other highlights in bisbibenzyl research must be mentioned including elucidation of

absolute configuration of isoplagiochins C and D and structurally related bazzanins, the first linkage found between a bibenzyl and a phenanthrene.[31]

2.1.5. Phenanthrenoids

Phenanthrenoids are usually abundant in Orchidaceae, Juncaceae, Stemonaceae and liverworts. They may occur also in Euphorbiaceae, Dioscoreaceae and Ulmaceae. Phenanthrenoids are classified according to their structure into five subclasses, namely phenanthrenes, 9,10−dihydrophenanthrenes, dimeric phenanthrenoids, phenanthrene alkaloids and other phenanthrenoids.[31]

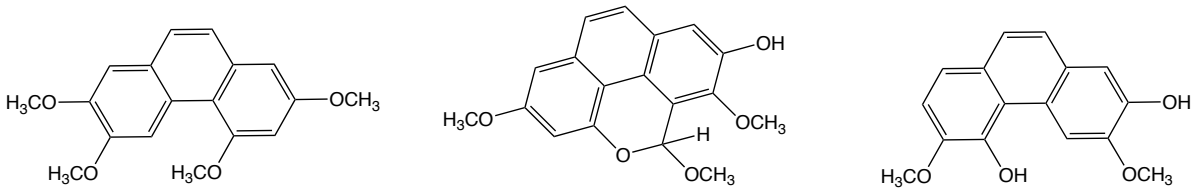

Figure 6. Examples of phenanthrene structures.

2.1.6. Other Stilbenoids

In addition to the structures mentioned above, there are other stilbenoids with specific structural features so do not allow classification into the above five types. They are oligostilbenes related derivatives or hybrids conjugated with flavonoids and lignans.

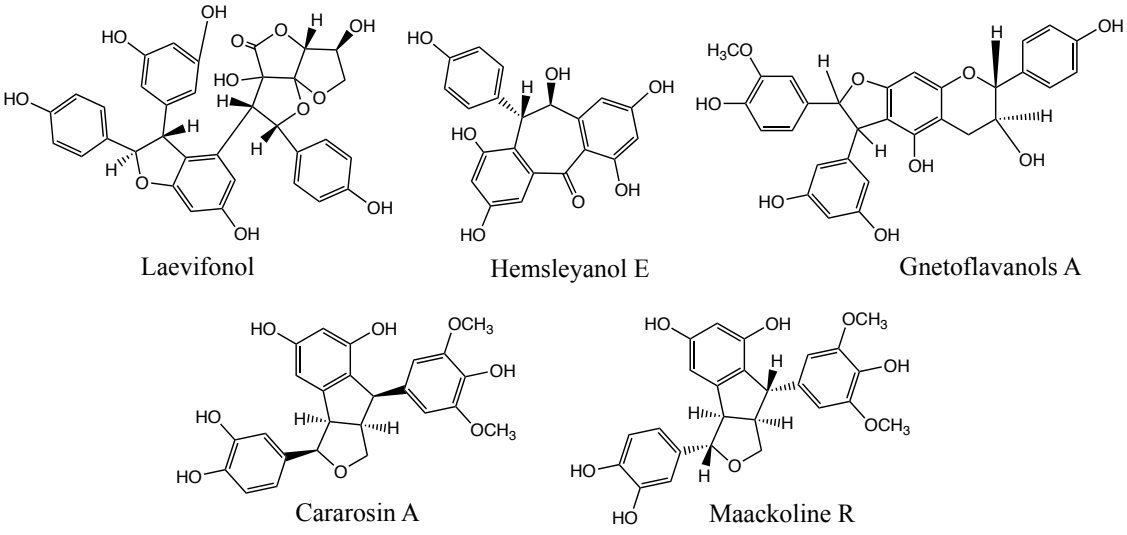

Figure 7. Examples of other stilbenoid structures.

One example is laevifonol, an ε−viniferin ascorbic acid hybrid isolated from the heartwood of *Shorea laeviforia*, which possesses a five membered lactone ring (Fig. 7). Another example is hemsleyanol E

isolated from the stem bark of *Shorea hemsleyana* (Dipterocarpaceae). It is the stereoisomer (+)−parviflorol, which was initially isolated from the bark of *Hopea parviflora* (Fig. 7). This subclass contains also flavonostilbenes (e.g., gnetoflavanols, Fig. 7), resulting from coupling between flavanone and stilbene. Stilbenolignans (e.g., maackoline R (optically inactive) or cararosin A (optically active, Fig. 7) are phenolic compounds formed from stilbenoids (e.g. stilbene) and lignans (e.g. phenylpropanoid).

2.2. Distribution

The interest of stilbenoids is related to the increasing number of new molecules; for instance, between 1995 and 2008, 125 new monomeric stilbenes and 275 new oligomeric stilbenes were reported. Monomeric and oligomeric stilbenes have mainly been found in the species of twenty−three families e.g., Cyperaceae, Dipterocarpaceae, Gnetaceae, Iridaceae, Leguminosae (Fabaceae), Moraceae, Orchidaceae and Polygonaceae. Stilbene oligomers have been found mainly in Dipterocarpaceae, Gnetaceae, Vitaceae, Cyperaceae, Leguminosae, Moraceae, Welwitschiaceae, Umbelliferae, Iridaceae, Celastraceae, Paeoniaceae and Haemodoraceae families. Especially, Dipterocarpaceae, Vitaceae and Gnetaceae constitute a large number of oligostilbenes. The Dipterocarpaceae was the richest source of new oligomeric stilbenes.

2.3. Biosynthesis

- **Biosynthesis of stilbenes**

Over the past years, great efforts have been dedicated at rationalization of stilbenoid biosynthesis. Sotheeswaran studied the biosynthetic pathway of stilbenes in 1993, where ε−viniferin was recognized as an important intermediate involved in the biosynthesis of stilbenes containing benzofuran moieties.[37] Indeed, the biosynthesis of simple stilbenes has been well characterized, in which the last step is catalyzed by STS, a key enzyme in the biosynthetic pathway. STS catalyzes the sequential decarboxylative addition of three acetate units from malonyl-CoA to a *p*−coumaroyl−CoA precursor molecule derived from phenylalanine through the general phenylpropanoid pathway (Fig.8).[40] For instance, STS condenses three molecules of malonyl−CoA and one molecule of *p*−coumaryl−CoA to form resveratrol. It must be reminded that CHS can catalyze the formation of chalcone by *p*−coumaroyl−CoA and malonyl−CoA via the intramolecular cyclization and aromatization of the resulting linear phenylpropanoid tetraketide.[41] Different types of enzymes are involved in the biosynthetic pathway of stilbenes e.g., phenylalanine ammonia lyase (PAL), 4−coumarate−CoA ligase (4CL), cinnamate 4−hydroxylase (C4H), pinosylvin methoxy-transferase (PMT) in combination to STS.

All these enzymes can be classified according to their substrate specificity i.e., specific stereochemical enzymes that catalyze the formation of the stilbene backbone and enzymes catalyzing the modification reaction of products. PAL, CHS, and STS are the first type enzymes. The stilbene backbone is synthesized from cinnamoyl–CoA and malonyl–CoA by STS. The use of unusual substrates with STS showed that only minor changes can form a variety of different and new products.[42] The second type of enzymes includes hydroxylation enzyme, dehydrogenase, oxidase and the glycosyl-transferase.

The regulation mechanism of metabolic channeling also plays an important role in the induction and accumulation of end stilbenoid products. The activation of metabolic channeling and biosynthesis pathways of homologous synthesis is determined by the expression of key enzymes, but accumulation is determined by expression of rate-limiting enzymes in plants. These rate-limiting enzymes that can usually be found at the branch point or downstream biosynthetic pathways of secondary metabolites in plants are responsible for the synthesis of precursors of many secondary metabolites.[43]. Relevant enzymes can form multi-enzyme complexes and coordinated expression in different parts of the cell. Enhanced expression in enzyme complexes can lead to a dramatic accumulation of end products. For example, induced coordinate expression of PAL and STS in the biosynthetic pathways of stilbene can affect the synthesis of stilbene.[44]

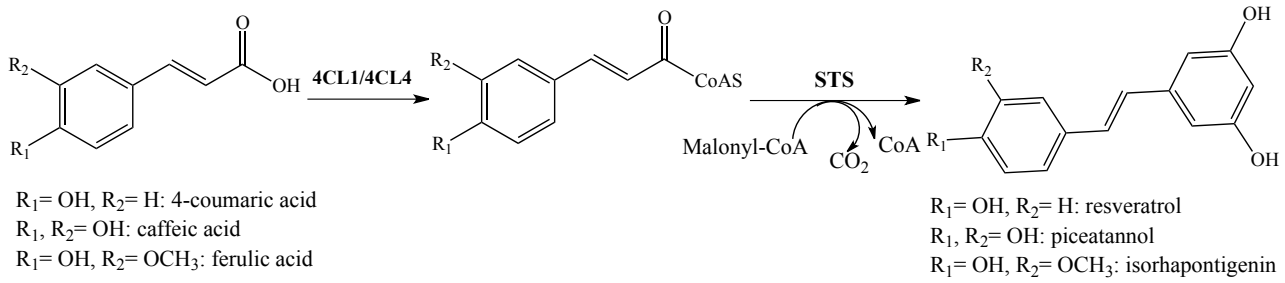

Figure 8. Biosynthesis pathway of stilbenes.[45]

❖ **Biosynthesis of oligostilbenes**

Oligostilbenoid biosynthesis plays a role in wood durability, paper and other wood side–products. It is recognized that most of these compounds are derived from resveratrol and two derivatives isorhapontigenin and pterostilbene.[46]

A plausible biosynthesis of stilbene oligomers in the Vitaceae family was proposed as seen in Figure 9.[47] The biosynthesis of oligostilbenes from dipterocarpaceaeous, cyperaceaeous, gnetaceaeous and leguminosaeous plants has been assumed to follow a similar pathway.[46], [48], [49]

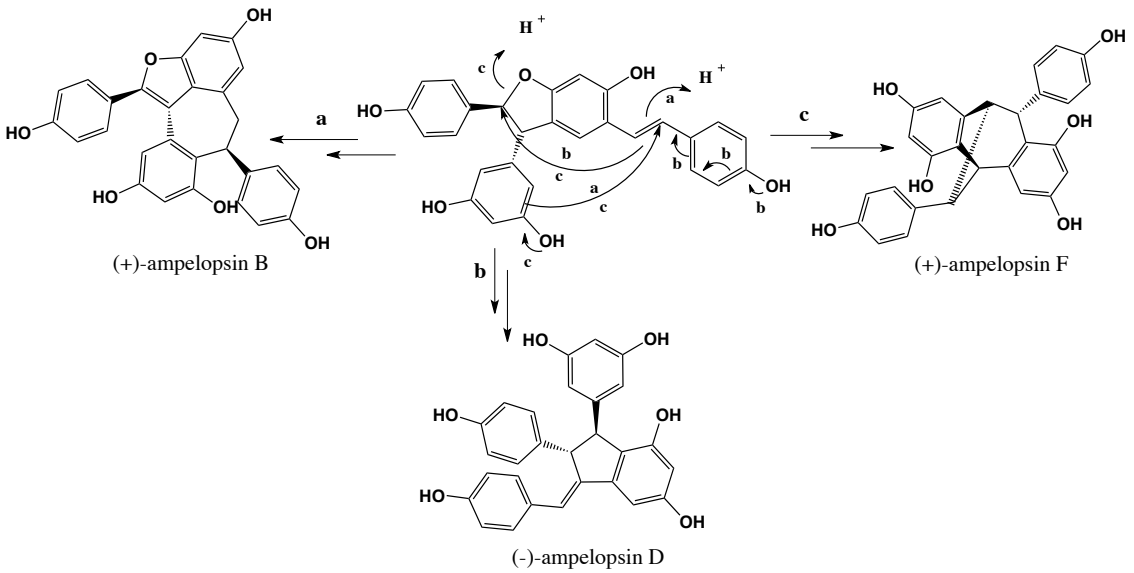

Figure 9. Plausible biosynthesis of stilbene dimers.

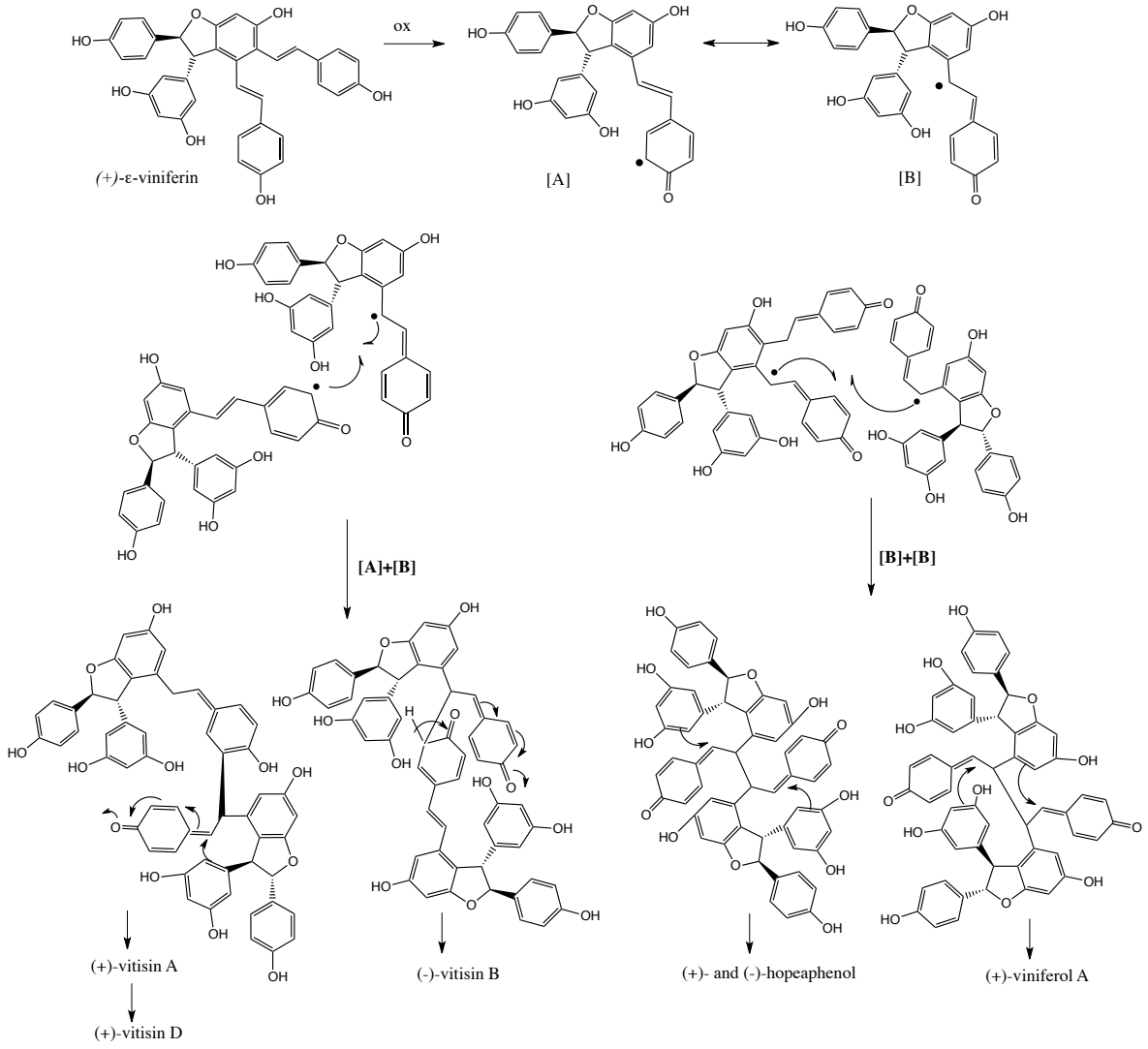

Figure 10. Plausible biosynthesis of examples of stilbene tetramers.

The attempts to rationalize oligostilbene biomimetic synthesis have not provided convincing mechanisms to explain reaction selectivity and the apparent discrepancies between all results.[50]–[54] Snyder et al. elegantly described stereo-control of resveratrol oligomer synthesis by the introduction of a novel reagent of bromination.[55] Moreover, Velu et al. explained the formation of different oligostilbenoids and argued on their regio– and stereo–selective biosynthesis.[56], [57] It appears that the biosynthesis of most components of dipterocarpaceae is driven by non–covalent interactions (see chapter 5).[58]

- **Biosynthesis of bisbibenzyls**

The biosynthesis of marchantin A was investigated using thallus tissue of *Marchantia polymorpha.* Experiments demonstrated that rings A and C of marchantin were derived from the benzene ring of L–phenylalanine through cinnamic acid (clinnamate) and p–coumaric acid. Dihydro–p–coumaric acid is an intermediate of the marchantin biosynthesis. The phenylpropane or polymalonate pathway using dihydro-p-coumaric acid and acetate or malonate was proposed to understand biosynthesis of bibenzyl monomers, which have been confirmed as the constituent elements leading to marchantin. Therefore, the bibenzyls are coupled in a unique manner.[59] The cell suspension cultures of *Marchantia polymorpha* analysis revealed the presence of two specific cytochromes P450 enzymes having different roles. The first catalyzes coupling of two lunularic acid molecules to form marchantin C together with CO_2 release. The second hydroxylates marchantin C to marchantin A (Fig. 11). The polyketide synthase (PKS) is a key enzyme that uses dihydro-4-coumaroyl-CoA as starter and performs three condensation reactions marked by colors. This is followed by a STS–type ring-folding with retention of the terminal carboxyl group that is removed in the standard STS-type reaction. The first identified product *in vivo* is prelunularic acid,[60] for which the biosynthesis requires an additional reduction step through a polyketide reductase (PKR) i.e., it reduces carbonyl group to hydroxyl group.[61]

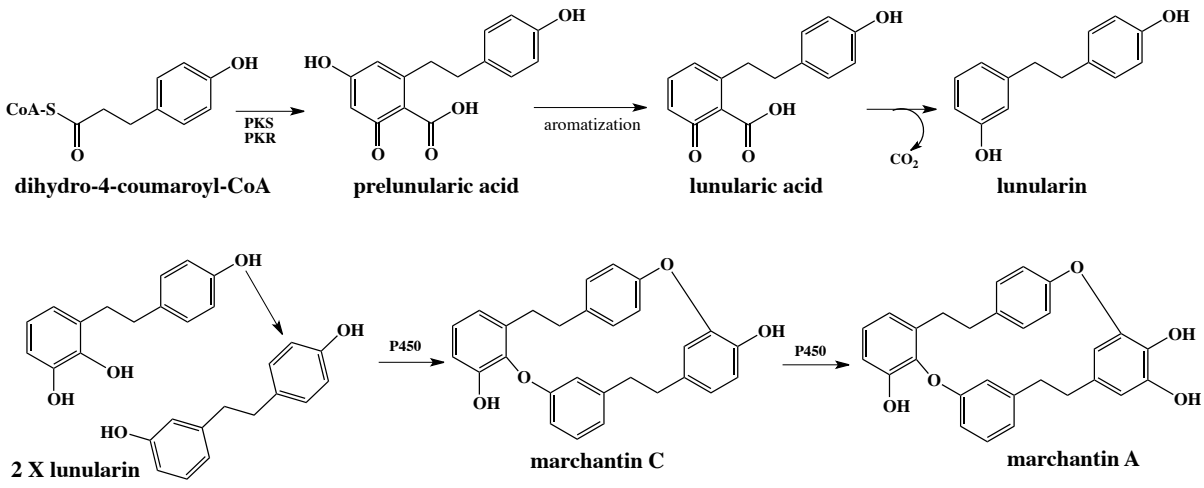

Figure 11. Biosynthesis pathway of two simple bisbibenzyls.

2.4. Biological roles and activities

Due to their structural diversity, stilbenoids exhibit a multiple of biological roles and activities that are listed in this section, as exhaustively as possible.

3.4.1. Antioxidant activity

Most of stilbenoids possess antioxidant activities thanks to the phenolic groups. Resveratrol is a major stilbenoid antioxidant, with adequate structural feature for efficiency. Resveratrol analogs have widely been studied for their antioxidant properties, and some were found more active than resveratrol. Several resveratrol derivatives from *Yucca periculosa* have showed inhibitory activity on crocin bleaching induced by alkoxyl radicals and DPPH scavenging activities. Many natural stilbene glycosides have also significant antioxidant activities e.g., (Z)-astringin and (E)- and (Z)- resveratrol-4'-O-β-D-glucopyranoside, 2,3,4',5-tetrahydroxystilbene-2-O-β-D-glucopyranoside. [62]

Different oligostilbenes have exhibited antioxidant activities, namely gneafricanins A, longusol A and bisisorhapontigenin B. Bisisorhapontigenins E–G and 13-b-methoxy bisisorhapontigenin G have also highlighted potent antioxidant activity comparable to vitamin E.[31]

Other stilbenoids for which activities were much stronger than vitamin E, such as the flavonostilbenes gnetoflavanols A, E and F, have showed inhibition of lipid peroxidation and superoxide produced within a xanthine–xanthine oxidase system.

Tyrosinase (a copper–containing enzyme) inhibitors are antioxidants; they are widely used in dermatological treatments and also applied in cosmetics (e.g., as skin whitening agent). Some stilbenoids have been reported to possess tyrosinase inhibition activity e.g., the oxyresveratrol, exerting inhibition on murine tyrosinase. Resveratrol oligomers from dipterocarpaceae plants have also been reported to have inhibitory effects on murine tyrosinase activity. The double bond in the stilbene skeleton was critical for inhibition.[63]

3.4.2. Anti–Inflammation and Immunomodulating Activity

Different stilbenes e.g., resveratrol and piceatannol as well as their derivatives have been regarded as potent anti–inflammatory agents and still attract attention.[64]–[68] Stilbene derivatives e.g., from *Artoccarpus dadah* showed inhibitory effects against COX-1 and COX-2.[69]

(+)-α-Viniferin from the root of *Carex humilis* is an inhibitor of prostaglandin H2 synthase 3-4-fold,

stronger than resveratrol. Moreover, it has displayed a significant anti−inflammatory activity on carrageenin−induced paw edema in mice due to inhibitory effect on the release of prostanoids and NO. [70], [71] Viniferin and miyabenol C exhibited protein kinase C (PKC) inhibitory activity at low micromolar concentrations.

There are many bibenzyls and bisbibenzyls that have exhibited anti−inflammatory activities. Bibenzyls from the tubers of *Gymnadenia conopsea,* (including the structure gymconopin D) were found to inhibit the antigen-induced degranulation in RBL-2H3 cells.[72] Some bisbibenzyls have exhibited anti−inflammatory activities through inhibition of LPS-induced nitric oxide synthase (NOS) e.g., marchantin A involved in the inhibition of LPS-induced Inducible nitric oxide synthase (iNOS) Messenger Ribonucleic acid (mRNA) expression, is considered as the most potent. The presence of phenolic hydroxyls and saturation at C−7, C−8 and/or C−7'/C−8' are required for an efficient inhibition of NO production.[73]

The phenanthrenoidsgymconopin B and blestriarene A isolated from *Gymnadenia conopsea* were found to inhibit the antigen−induced degranulation in RBL-2H3 cells. Otherwise, stemanthrene A and D showed strong inhibition of leukotriene biosynthesis (IC_{50}=8.5 and 4.8$\mu M,$ respectively). Another example is dendrochrysanene from the stems of *Dendrobium chrysanthum,* which was proved to suppress mRNA level of *TNF−*$\alpha,$ IL8, ILI0, and iNOS in murine peritoneal macrophages stimulated by LPS.[74]

Other stilbenoids, e.g., artocapol C, have inhibited the release of histamine and β−glucuronidase from mast cell degranulation in concentration-dependent way. It has also displayed inhibitory effect on the formyl−peptide−simulated superoxide anion formation in neutrophils.[75] Racemosol and 10−*O*−demethylracemosol as well as their synthetic derivatives have exhibited potent *in vitro* inhibitor activities against COX-l and COX-2.

2.4.3. Anti−Microbial activity

As other stilbenoids, resveratrol has antifungal and antibacterial effects, as well as antiviral effects against HIV−1 (human immunodeficiency virus), HSV−1 (herpes simplex virus) and human cytomegalovirus.[66], [76], [77]

- Phytoalexin function

Many stilbenoids behave as phytoalexins that are antimicrobial substances synthesized by plants, which accumulate rapidly in microorganisms.[40] Their actions derive from multiple defense reactions. For

example, it was shown that transfer of two genes from grapevine (VST1 and VST2) to tobacco increase resistance of the latter to various diseases including infection by *Botrytis cinerea*.[78] Thereafter, a series of gene transfers were conducted in many plants such as rice, tomato, wheat, papaya.[79], [80]

- Antifungal

Many stilbenoids act as antifungal i.e., they selectively eliminate fungal pathogens from a host with minimal toxicity. Stemofurans displayed antifungal activity against four microfungi, namely *Alternaria citri*, *Fusarium avenaceum*, *Pyricularia grisea* and *Botrytis cinerea*. Stemofuran B showed the highest activity against the four pathogenic fungi (EC_{50}=1.4 μg/ml against *Pyricularia grisea*), but only weak effects against *C. herbarum*. Stemofuran E and stilbostemin B showed high activities, while stemanthrenes showed negligible inhibition.[81]

The 3−hydroxy−4'-methoxybibenzyl isolated from the liverwort *Frullania muscicola* Steph showed potent inhibitory effects against certain fungi, especially *Trichophyton rubrum* and *Trichophyton gypseum*. The 3,4−dimethoxy−4−hydroxybibenzyl from the same plant exhibited moderate inhibition.[82]

Bazzanin B, isoplagiochin D and bazzanin S are three bisbibenzyls from the liverwort *Bazzania trilobata* showing antifungal activity against a variety of phytopathogenic fungi, in particular *Pyricularia oryzae*. The antifungal activity against *Trichophyton mentagrophytes* was also reported for marchantin C, neomarchantins A. Plagiochin E, neomarchantin A and 13,13'−*O*−isoproylidenericcardin D against *Candida albicans*. [82], [83]

Stilbene tetramers may prove to be valuable agents against, rice-blast disease. For example carasiphenol D inhibited the mycelial growth of *Pyricularia oryzae* by curling and swelling effect.[84] On the other hand, dimeric stilbenes (*trans* and *cis* ε−viniferins) have showed higher antifungal activity than resveratrol. There are many other examples reported antifungal activities of resveratrol dimers, such as cyphostemmins A and B.[85]

- Antibacterial

Many stilbenoids are reported as antibacterials. For example, combretastatin B5 from *Combretum woodii* leaf powder displayed significant activity on *S. aureus* but with lower activity toward *P. aeruginosa* and *E. faecalis* and slight activity towards *E. coli*. Stilbenes isolated from *Rumex hymenosepalus*, Mexican medicinal plants, showed moderate antimycobacterial activities.[86] The prenylated stilbene isolated from the aerial parts of *Artocarpus integer* showed antibacterial activity against *Bacillus subtilis*. Lakoochins A and B demonstrated antimycobacterial activity. The bisbibenzyls marchantin C, neomarchantin A and B

showed moderate activity against *Bacillus subtilis*. Gnetin E, parthenocissin A, ε−viniferin, α−viniferin, hemsleyanols B and D, vaticanol B and davidiol A inhibited the growth of MRSA (methicillin-resistant Staphylococcus aureus, a type of staph bacteria). Hemsleyanol D was found to be the most effective compound i.e., Minimal Inhibitory Concentration (MIC) of 2μg/ml vs. 1 μg/ml of vancomicin.[87] Hopeaphenol A and vaticaphenol A displayed moderate inhibitory activity against MRSA and methicillin-resistant *Mycobacterium smegmatis*.[88]

The antibacterial activity pattern of the two photosensitizers, dehydroeffusol and juncusol against methicillin-resistant and sensitive *S. aureus* and *B. subtilis* was similar to that of their antifungal activity.[89]

- Antivirus

The main anti−virus activity researches concerning stilbenoids focuse on HIV. For instance, glepidotin D, which is isolated from the leaves of *Glycyrrhiza lepidota*, is considered as the compound responsible for the antiviral activity.[90] Dimers scirpusin A and B (oligostilbenes) were isolated from *Caragana rosea* with EC_{50} values of 10 and 7 μg/ml against HIV-1 III-B, respectively.[91] The dimer balanocarpol and the tetramer dibalanocarpol from the leaves of *Hopea malibato* exhibited very modest HIV-inhibitory activity (EC_{50} of 46 and 20 μg/ml, respectively). However, malibatols A and B from the same plant were cytotoxic to the host cells. Riccardin C and F were weakly active against HIV-1 reverse transcriptase.[92]

3.4.4. Anticancer[§]/antitumor[**] activity

To find new chemopreventive agents from stilbenoids has attracted much attention. The different groups of stilbenes are reported to be potentially important cancer chemoprotective agents, being able to inhibit cellular events associated with carcinogenesis, including tumor initiation, promotion, and progression. Stilbenes, especially resveratrol and its analogs play a role in the prevention of carcinogenesis. Their effects on human cancer cell lines (and on animal models) have been carried out extensively.[93]–[95] Combretastatin A−4 is seen as a promising tubulin inhibitor targeting tumor vasculature to induce rapid and selective vascular dysfunction in tumors. The combretastatin A−4 phosphate (fosbretabulin), a prodrug of combretastatin A-4, is now in phase II of clinical trials.[96], [97] Since Jang et al. published the anticancer effects of resveratrol, there have been a few studies on their potential therapeutic roles in the prevention cancer, as well as of the corresponding oligomers.[98], [99] Anticancer effects of stilbenoids are cytotoxicity, proliferation inhibition and apoptosis of tumor cells.

---

§ anticancer is an activity restricted to clinical effect on humans

** antitumor would also refer to biological effect on animal models, such as xenografts

Many oligostilbenes have been tested for their antitumor effects. For example, vaticanol C (resveratrol tetramer) have induced cytotoxicity in different cell lines and have exhibited growth suppression in colon cancer cell lines at low concentration via apoptosis induction.[100], [101] A noticeable progress of oligostilbene anticancer activities comes from the discovery of their inhibitory activity of DNA Topoisomerase II (topoisomerase II inhibitors are used as anticancer drugs). For instance, nepalensinols isolated from the stem of *Kobresia nepalensis* (Cyperaceae) have presented potent inhibitory effect on topoisomerase II; some even stronger than etoposide or daunorubicin. Particularly, nepalensinol B has exhibited the most potent activity (~1000 times stronger than etoposide).[102], [103] Different bibenzyls (e.g., 3,3'-dihydroxy-2',6'-bis(4−hydroxybenzyl)-5−methoxybibenzyl and 3',5−dihydroxy−2-(4−hydroxybenzyl)−3−methoxybibenzyl from *Bletilla striata*) and bisbibenzyls (e.g., neomarchantins A and B and marchantin C) have also showed anticancer activity as well as some phenanthrenoids (e.g., 4,7-dihydroxy-2-methoxy-9,10-dihydrophenanthrene and 2-methoxy-3,4,7-trihydroxy−phenanthrene).[104], [105] Many other stilbenoids have exhibited antitumor activity, for example, racemosol and demethylracemosol exerted cytotoxicity against KB and breast cancer cell lines.[106]

3.4.5. Other biological activities

Stilbenoids have different other activities including phytotoxicity;[107], [108] ecdysteroid antagonistic activity;[109]–[111] 5−α−Reductase inhibitory activity; [112], [113] estrogenic/antiestrogenic activities; [65], [114], [115] neuroprotective activity; [116], [117] antiplatelet activity;[118], [119] antidiabetic activity;[120]–[122] hepatoprotective and hepatotoxic activities; [123] spasmolytic activity;[124]–[126] aromatase inhibitory activity (e.g., ε−viniferin); human cytochrome P450 enzyme inhibitory activity (e.g., bibenzyls moscatilin and gigantol from *Dendrobium nobile*, *trans*− and *cis*−ε−viniferin, gnetin H, suffruticosols A and B); antimutagenic activity; and stimulation of osteopath growth activity (e.g., karakinos A−C, leachianol C and cararosinol A from the roots of *Caragana sinica*).[127]–[129]

In conclusion, flavonoids and stilbenoids have attracted increasing interest due to their shown or assumed beneficial health effects. There is no doubt concerning their importance, however there are a lot of confusions and misunderstanding in the related literature and in their use for cosmetic, food and pharmaceutical applications. *In vivo*, food intake is not systematically well documented e.g., quid inapetant effects. Also, many in vitro studies lead authors to overestimate the real effects on human, as for anticancer or antitumor activities. Because the related epidemiological studies are delicate to conduct (too many crossed parameters and too low population), there is no clear evidence of beneficial effects of polyphenol−rich foods. In particular *in vivo* antioxidant activities from polyphenol−rich diets is still under

debate.[130] Thereby, care must be systematically given before claiming polyphenols actions. Nowadays, virtually no polyphenol–derived drugs are clinically available.

Chapter 2 – Non–covalent interactions

Chapter 2 – Non-covalent interactions

Nature designs fantastic supramolecular architectures and provides fascinating molecules that are stabilized by mixture of covalent and non−covalent interactions. It is necessary to well understand and rationalize the role of these interactions; here we are mainly interested in non-covalent interactions.

To better define what are non−covalent molecular assemblies and their importance in modern molecular sciences, this chapter provides *i)* physical-chemical definition of the different chemical bonding and *ii)* a series of examples existing in Nature.

1. A general definition of non-covalent interactions

In covalent bonds, atoms share their electrons that belong to common molecular orbitals. The optimum intermolecular distance is usually shorter than 2 Å. Also the angles formed between covalently bonded atoms are specific and characteristic, providing molecules definite and predicable shapes. Non−covalent bonds do not strictly share electrons from the two atoms involved in the bond. This implies more conformational variability inherent to dispersive and electromagnetic interactions between atoms or molecules non-covalently linked. Understanding the nature of non−covalent interactions is more delicate and theoretical calculations have been repeatedly in conflict with experimental data. The basic principles of non-covalent interactions were formulated by Pauling in the 1930's.[131], [132] However, many developments have been required and still nowadays the theoretical evaluation must be carefully conducted to agree with experiments.

An important feature of non−covalent association is the contribution not only of classical Coulomb electrostatic interaction but also of multipole−electric interactions. Non−covalent bonds are often called 'weak bonds', which can be inadequate as these bonds can maintain supramolecular assemblies. Anyway, non−covalent interactions are weak compare to covalent bonding with stabilizing energies often lower than -30 $kJ.mol^{-1}$ per fragment. Consequently, according to the environment, these bonds may be continuously formed and broken. Adding many non−covalent contributions in extended complexes (up to 100 atoms) may stabilize conformations. Non−covalent interactions are driven by electrostatic and vdW (van der Waals) forces. Whereas electrostatic interactions are extensively taught in basic physic and chemistry lessons, vdW do not systematically deserve deep attention. Therefore, we propose to detail the latter interaction.

1.1. vdW Interactions

vdW Interactions are attractive and repulsive forces between molecular entities other than electrostatic interactions. They are short–range and weak interactions. They were first introduced by Johannes D. van der Waals for real gas properties i.e. correcting ideal gas by accounting for intermolecular interactions. The theory appeared also applicable to liquids and solids, in which vdW forces may also participate in molecule linkage. There exist vdW solids in which the packing between molecules is insured by vdW forces. They have lower melting points and are softer compare to classical solid formed only by ionic, covalent and metallic bonds.

vdW Forces are issued from dipole – dipole interactions either permanent dipole – permanent dipole, permanent dipole – induced dipole and instantaneous dipole – instantaneous dipole (dispersion). The three-vdW contributions are also classified as orientation (Keesom), induction (Debye) and dispersion (London) interactions, respectively. The first contribution is calculated as the interaction between two permanent dipoles m_1 and m_2:

$$w(r) = -\frac{\mu_1^2 \mu_2^2}{3(4\pi\varepsilon\varepsilon_0)^2 k_B T r^6} \quad (eq.1)$$

The Debye interaction is developed between a permanent dipole and an induced dipole. The corresponding interacting energy, which include polarizabilities, is given by:

$$w(r) = -\frac{(\mu_1^2 \alpha_{02} + \mu_2^2 \alpha_{01})}{(4\pi\varepsilon\varepsilon_0)^2 r^6} \quad (eq.2)$$

The dispersion term was first rationalized by Fritz London[133] in 1937. vdW Forces possible between all types of atoms and molecules regardless existence of permanent dipoles. In fact, even non–polar and uncharged atoms and molecules, exert attractive forces on each other due to their atomic polarizability (α_0). There are repulsive or attractive contributions. Indeed, there exists a temporary attractive force between atoms and molecules, resulting from quantum electron fluctuations. The dispersion contribution is fully rationalized from a quantum point of view but a classical interpretation is easily provided as well, as the electron motion induce instantaneous dipoles, so that the interaction is often described in terms of instantaneous dipole – instantaneous dipole or instantaneous dipole – induced dipole. In a first approximation, the attractive dispersion energy was shown to vary as $-\frac{C_6}{r^6}$, where C_6 was given for two dissimilar and non–polar molecules by:

$$C_6 = \frac{3{\alpha_{01}}^2{\alpha_{02}}^2 I_1 I_2}{2(4\pi\varepsilon_0)^2(I_1 + I_2)} \quad (eq.3)$$

where I_i is the first ionization potential of each molecule *i,* α_{0i} is the polarizability, and r is the distance between both molecules. Note that this expression was obtained in a classical way and does not account explicitly for the quantum fluctuation and quantum mechanic theory. In the perturbative quantum scheme, electron fluctuation can be described as a sum over single excitations. Consequently the dispersion energy is given by:

$$E_{disp} = -\sum_{ia}\sum_{ib} \frac{(ia|jb)[(ia|jb) - (ib|ja)]}{\varepsilon_a + \varepsilon_b - \varepsilon_i - \varepsilon_j} \quad (eq.4)$$

where the sum is over all possible single excitation $i \rightarrow a$ (on fragment A) and excitation $j \rightarrow b$ (on fragment B), $(ia|jb)$ is a two−electron integral and ε the corresponding orbital energy.

The dispersion energy can also be given as:

$$\omega(r) = -\left[\frac{C_6}{r^6} + \frac{C_8}{r^8} + \frac{C_{10}}{r^{10}} + \cdots\right] \quad (eq.5)$$

There exists also a repulsive term, when molecules are too close to each other, for which no exact form is known. Variation in $\frac{1}{r^n}$ is used with n=12 to form, as a first-order approximation, the Lennard−Jones potential:

$$\omega(r) = \frac{C_{12}}{r^{12}} - \frac{C_6}{r^6} \quad (eq.6)$$

The total attractive vdW energy that includes the three possible contributions (Keesom, Debye and London) is expressed as:

$$w_{vdW}(r) = -\frac{C_{vdW}}{r^6} = -\frac{[(1) + (2) + (3)]}{r^6} \quad (eq.8)$$

$$= -\frac{\left[(\mu_1^2\alpha_{02} + \mu_2^2\alpha_{01}) + {\mu_1^2\mu_2^2}/{3kT} + {3\alpha_{01}\alpha_{02}hV_1V_2}/{2(V_1 + V_2)}\right]}{(4\pi\varepsilon_0)^2 r^6}$$

The equation $(eq.8)$ has two main limits since it *i)* assumes that all atoms and molecules have only one ionization potential and so one absorption frequency and *ii)* fails at prediction of interactions between molecules in solvent.

1.2. Hydrogen bond

H-bonds play a key role in chemistry, physics and biology. For instance, they are responsible for the structure and properties of an essential compound for life, namely water. Furthermore, H–bonds also play a key role in determining the shapes, properties and functions of biomolecules like proteins and DNA. Molecules may establish intra–or inter–molecular H–bond. H–bonding has been discussed in literature for almost a century due to its high importance.[134]–[136] H–bond may represent the strongest and the most common type of non–covalent interactions.

H–bond is an attractive interaction between two fragments (atoms, groups, molecules) in a structural arrangement where one hydrogen of one fragment, covalently linked to a sufficiently electronegative atom (e.g., N, O or F), is non–covalently linked to an electron–rich atom of the other fragment.[137]

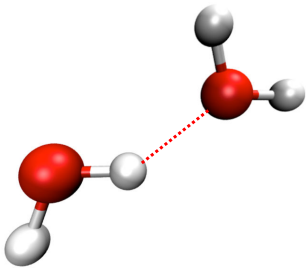

Figure 3. Example of H-bond (represented by a dotted line) between two molecules of water.

H–bonds can be strong if the two atom of both fragments (donor and acceptor, respectively) are collinear. The length of hydrogen bonds is typically less than 3.0 Å but strongly depends on the chemical neighboring.[138]

1.3. π-stacking

π–Stacking (also called π–π interaction) constitute one of the most fascinating non–covalent interactions and corresponds to the non–covalent attraction between aromatic rings when they are oriented favorably. As it is known, to be aromatic, molecule must have *i)* a cyclic and planar arrangement of p orbitals and *ii)* (4n+2) electrons in the p system.

π-Stacking interactions are caused by intermolecular overlapping of p–orbitals in π–conjugated systems, thus they become stronger as the number of π–electrons increases. There is three general types of π–stacking arrangements namely displaced (or slip stacked), edge–to–face (or T–shape) and sandwich (Fig. 4), the latter being less favorable due to electrostatic repulsion.

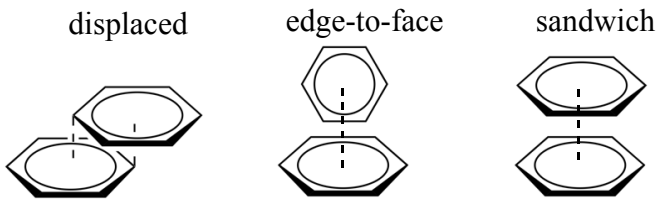

Figure 4. π–π interactions of benzene.

The attractive interaction between the π–systems of both partners is partly driven by electrostatics and dispersion, when both π systems have very similar electron densities. In case of different electron density (i.e., one is electron–rich and the other electron–deficient systems), induction interactions becomes important.[139], [140]

The study of the interaction between two benzene rings has been intense over the past decades both experimentally and theoretically. Experiments consider that attraction greatly affects the interaction of phenyl rings in solution or other environments. [141] For the benzene dimer, the T–shape conformer is the most stable but is nearly isoenergetic to the parallel–displaced conformation. Consequently, the isolated benzene dimer is highly flexible and both forms may coexist. Substitution effect influences edge-to-face aromatic interaction, the electron density at the para position is an important stabilizing factor for the axially substituted aromatic systems. The stabilization by substitution of an aromatic ring is significantly affected by the electrostatic energy, while the dispersion energy is mostly canceled out by the exchange repulsion.[142] As a consequence, the stabilization (or destabilization) by substitution is governed mainly by electrostatics. Furthermore, the aromatic system facially substituted depends on the electron donating ability, which is responsible for the electrostatic energy as well as the dispersion interaction and exchange repulsion. The dispersion energy is the most dominating interaction in both axial and facial substitutions, however it is almost canceled by the exchange repulsion in the axial substitution. Whereas in the facially substituted aromatic systems, together with the exchange repulsion it augments the electrostatic energy.[143] As an amazing electrochemically controllable nanomechanical application, using the flipping/flapping motion from edge–to–face to face–to–face, a molecular flipper has been designed.[144] Electrochemically and photochemically active π systems may be utilized to maximize control of this interconversion. While both T–shaped and displaced-stacked structures of the benzene dimer are almost isoenergetic, the latter π–stacked structure tends to be more favored with aromatic N–heterocyclic rings except for the tetraazine dimer.[145]

2. Non-covalent bonding in nature

Non−covalent interactions are key factors of numerous natural three−dimensional architectures. Among many other examples, non−covalent interactions participate in supramolecular arrangements of proteins, DNA, natural graphite. A less long−term studied process, in which these interactions are major actors, is the copigmentation association between natural polyphenols that modulate optical properties on e.g. berries, wine and flowers.

2.1. Proteins

The primary structure of proteins is driven by covalent bonds (peptide backbone), whereas disulfide bonds and non-covalent interactions (H−bond, hydrophobic effect, electrostatics and vdW) drive the secondary structure. This allows appreciating how proteins work, in their wide variety according to specific domains. Further non−covalently−driven folding and reorganization lead to tertiary structure. Secondary and tertiary structures reflect the most (thermodynamic) stable conformation of the protein, resulting from non-covalent interactions between the various amino acid side−chains (intramolecular) and with the surrounding water molecules (intermolecular). The solvent accessible surface of protein may also be involved in non−covalent interactions with other molecules, including other proteins. Protein−protein interactions result in the quaternary structure (Fig. 5).

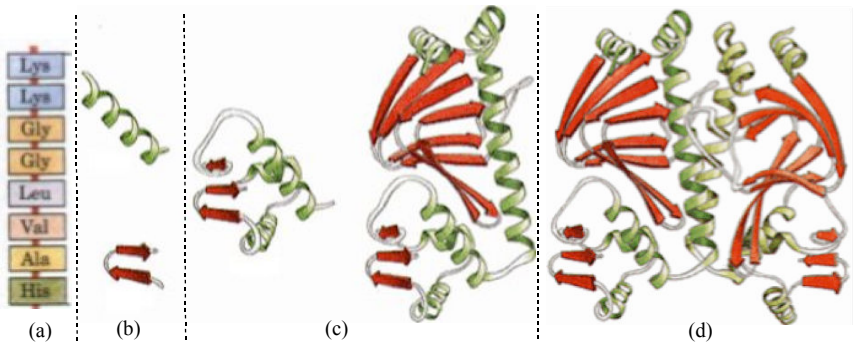

Figure 5. (a) Primary, (b) secondary, (c) tertiary and (d) quaternary structures of protein.

❖ ***H-bonds***

H−bonds influence the three-dimensional structure of proteins. It results from the contribution of both polar amino acid side−chains and peptide bonds (carbonyl oxygen and amide proton). Forming H−bond is usually energetically favorable in these cases. Even if H−bonds are thermodynamically weaker

(ΔH~ 10–20 kJ/mol) than covalent bonds (ΔH ~ 400 kJ/mol), they become important since proteins contain a large number of donors and acceptors.

Intermolecular H–bonding with solvent usually weakens intramolecular H–bonds, therefore inside protein hydrophobic cavities, where solvent is excluded, H–bonds tend to be rather important. Similar considerations are important for the transmembrane portion of membrane proteins.

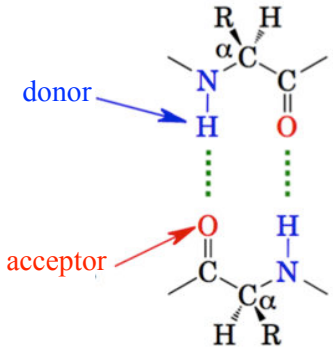

Figure 6. Example of H–bonds (green dotted line) in proteins.

❖ ***Electrostatics***

The particularity of electrostatic interactions compared to the other types present in proteins is that these interactions are effective at relatively long ranges, especially in environments of low dielectric constant (ε). Electrostatic interactions result either from ionizable residue side–chains or from free ionized groups of the amino– and carboxy–termini. Polar groups and secondary structural elements can also contribute to the electrostatic ion–dipole or dipole-dipole interactions. Ionic interactions are weakened by high salt concentrations inducing competition between interactions. Electrostatic interactions are much stronger in nonpolar environments (ε 2–5) than in aqueous solvent (ε=78), the strength of the interaction being inversely proportional to ε. The interactions between oppositely charged groups usually contribute to about 20 kJ/mol per interaction to protein folding under cellular conditions.

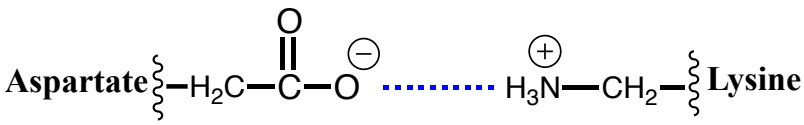

Figure 7. An example of electrostatic interactions.

❖ ***Van der Waals***

The other important bonding type that helps stabilizing protein structure is vdW. vdW Interactions contribute to the strength of hydrophobic effects because non–polar atoms are prone to vdW interactions. For instance, in the coiled–coil protein (Fig. 8), involved in the regulation of gene expression, there are

Heptad repeats (i.e. repeated every seven residues) forming alpha helices. vdW Interactions occurrence depends on hydrophobicity of residues, for instance if these repeating residues are hydrophobic, such as leucine, vdW interaction will be formed to stabilize this protein structure.

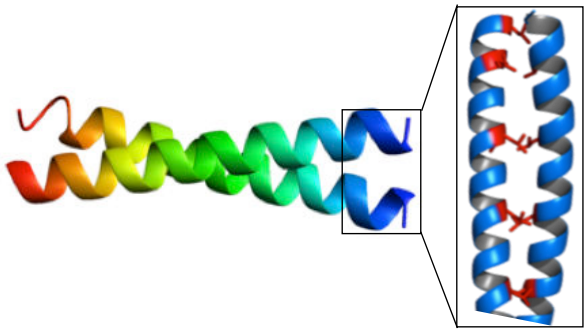

Figure 8. The GCN4 leucine zipper structure: a classical (parallel and left–handed homodimer) example of a coiled coil protein (leucine residues in red).

❖ ***Hydrophobic effect***

Hydrophobic effects are often considered as a specific interaction, it is however definitely not an interaction by itself. It results from the combination of other interactions, where non–polar side chains interact with each other to avoid direct interaction with water. It is a major driving force for protein folding.

2.2. DNA

As for proteins, non-covalent interactions play a central role in stabilizing DNA structure. Again all types of interactions (ionic, H–bonds, base-stacking, hydrophobic interactions and vdW) have a role in DNA structure, however *i)* H–bonds between two adjacent bases from opposite strands (forming a Watson–Crick pair), and *ii)* base–stacking interactions between two bases within the same strand are major components. Non–covalent interactions involved in DNA structure, such as H–bonding are well understood by high–level DFT calculations.[146]

❖ ***Hydrogen Bonding***

The DNA double helix is stabilized by H–bonds between the opposite strands. Each type of the four nucleic bases (adenine (A), cytosine (C), guanine (G) and thymine (T)) has the capacity to make H–bond with its complementary base i.e. purines form H-bonds with pyrimidines A–T and C–G. This arrangement of two nucleotides binding together across the double helix is called a base pair.

Interestingly, using modified DNA bases increases the DNA duplex stability. For instance, the 2–aminoamine–T which include three H–bonds (i.e., one more than A–T base pairs) stabilizes the DNA duplex by increasing the melting temperature (T_m) by about 3°C per substitution compared to A–T base pair (Fig. 9). The other example is the G–G–clamp (four H–bonds), in which T_m is increased by 18°C compared to G–C (three H-bonds, Fig. 9).

Moreover, slight variations in the DNA sequence can induce dramatic effects on the stability of the DNA duplex. For instance, errors at the DNA replication stage induce mutations in the base sequence that lead to relatively unstable duplexes. This instability is rectified through proofreading enzymes that recognize the mutation and replace it by the correct nucleotide.

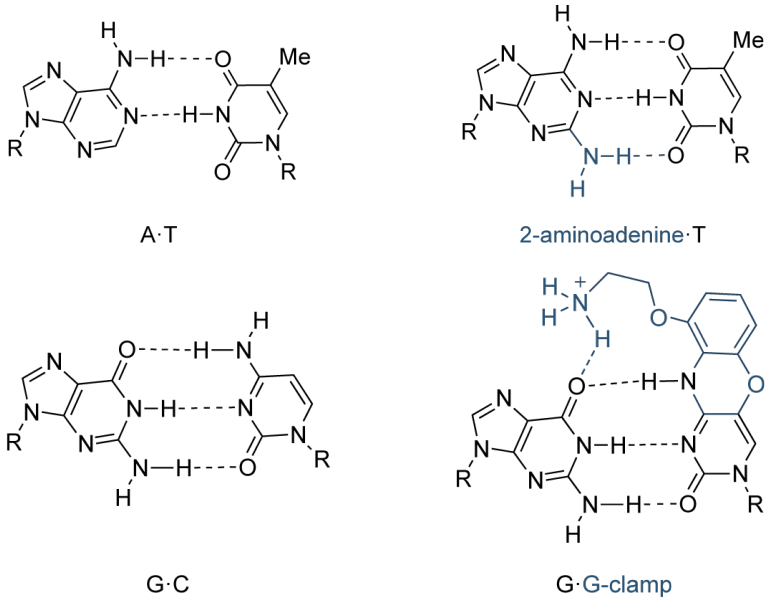

Figure 9. Role of H–bonds between bases in stabilizing DNA.

❖ ***Base-stacking interactions***

As for H–bonds, the individual base stacking forces are weak but become a major stabilizing factor when they are cumulated over several thousand base pairs. In nature, base–stacking interactions within nucleic acid duplexes are partially intra– and partially inter–strands.

The degree of stabilization provided by base–stacking depends on the DNA sequence. Base-stacking interactions and therefore DNA duplex stability increase with salt concentration, because the high concentration of salt hides the destabilizing charge repulsion between the two negatively charged phosphodiester backbones. Divalent cations (e.g., Mg^{2+}) are more stabilizing than monovalent ions (e.g., Na^{+}). In addition, some metal ions bind specific loci on the DNA duplex.

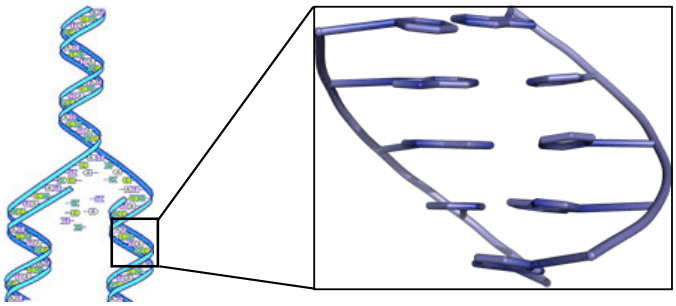

Figure 10. Base stacking in a DNA double helix.

❖ ***Others***

Different other types of interactions contribute to the DNA stability such as ionic bonds as DNA contains a phosphate backbone consisting of phosphorus and oxygen atoms. DNA can complex with histone proteins; these non−specific interactions are formed through basic residues in the histones making ionic bonds to the acidic sugar−phosphate backbone of DNA.

Moreover, hydrophobic interactions participate in DNA stability. In fact, base faces (as opposed to edges) are hydrophobic so that bases are protected from interaction with water within the double helix structure.

2.3. Copigmentation

Copigmentation is a stabilizing process of a pigment by another molecule, a copigment. This occurs in plants especially with anthocyanin pigments that can form non-covalent complexes with other natural polyphenols. As described in Chapter 1, flavonoids are responsible for colors of flowers, fruits and vegetables. Due to more or less extended π-conjugated systems, these compounds are prone to associate to each other with π−stacking interactions. This non-covalent association stabilizes the flavylium cation form of anthocyanins, which stabilizes and modulate color. The copigmentation phenomenon has long been mentioned in flowers and fruits; The concept was later used for grape wine in 1931.[147] Grape and wine anthocyanins may exist in their flavylium cation form (AH+), responsible for the wine red color. However this form only exists at pH < 2. In fact, various natural processes stabilize AH+ to preserve the red color, in particular by non-covalent complexation with copigments, e.g., with flavonols (Fig. 11).[148] In red wine, copigmentation leads to *i)* bathochromic shifts transforming color towards purple and *ii)* hyperchromic effects that can be followed by UV/Vis absorption spectroscopy. Also nuclear magnetic resonance (NMR) and circular dichroism (CD) may provide a partial structural picture of copigmentation complexes. Theoretical chemistry e.g., DFT including dispersive effects allow evaluating conformational arrangements involving π−stacking and intermolecular H−bonding. Moreover,

copigmentation has been rationalized by using TD–DFT, showing that the observed bathochromic shift was attributed to the formation of a charge transfer excited state (ET–CT) (see Chapter 3). The copigmentation of C:Q [3–*O*–Methylcyanidin (anthocyanin pigment) and quercetin (copigment)] complex was totally elucidated and there optical properties understood from a molecular orbital analysis (Fig. 12).[149]

Wine color has been of great importance to food industry since color influences consumer satisfaction. The experimental quantification of phenolic composition in wine, as well as evaluation of their physicochemical properties, is still challenging.[150], [151] Theoretical chemistry may appear as a new analytical tool to support rationalization of chemical and optical features of wine polyphenols. This molecular understanding may help food industry to achieve optimum balance of wine pigmentation. One can also envisage new opportunities for designing new dyes for food and cosmetics.

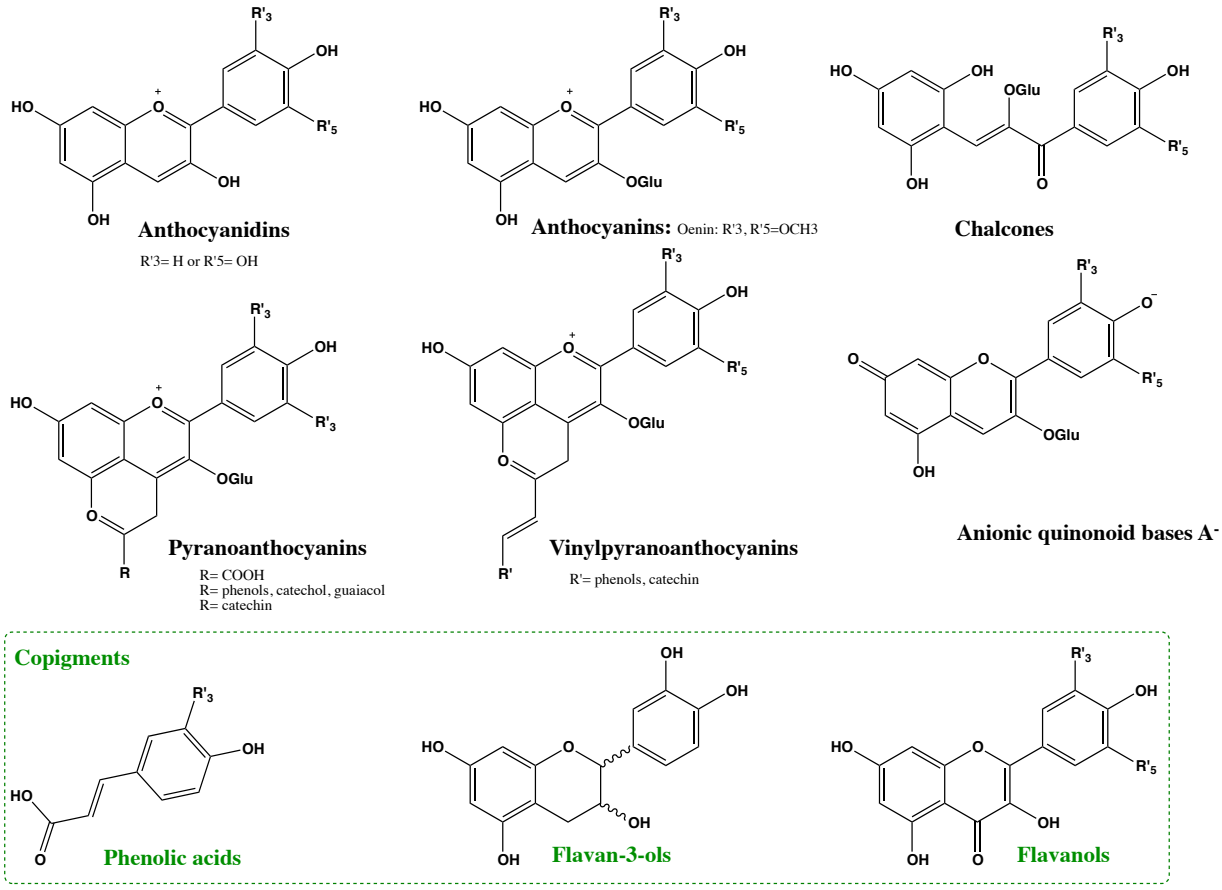

Figure 11. Chemical structures of some important examples of wine pigments and copigments.

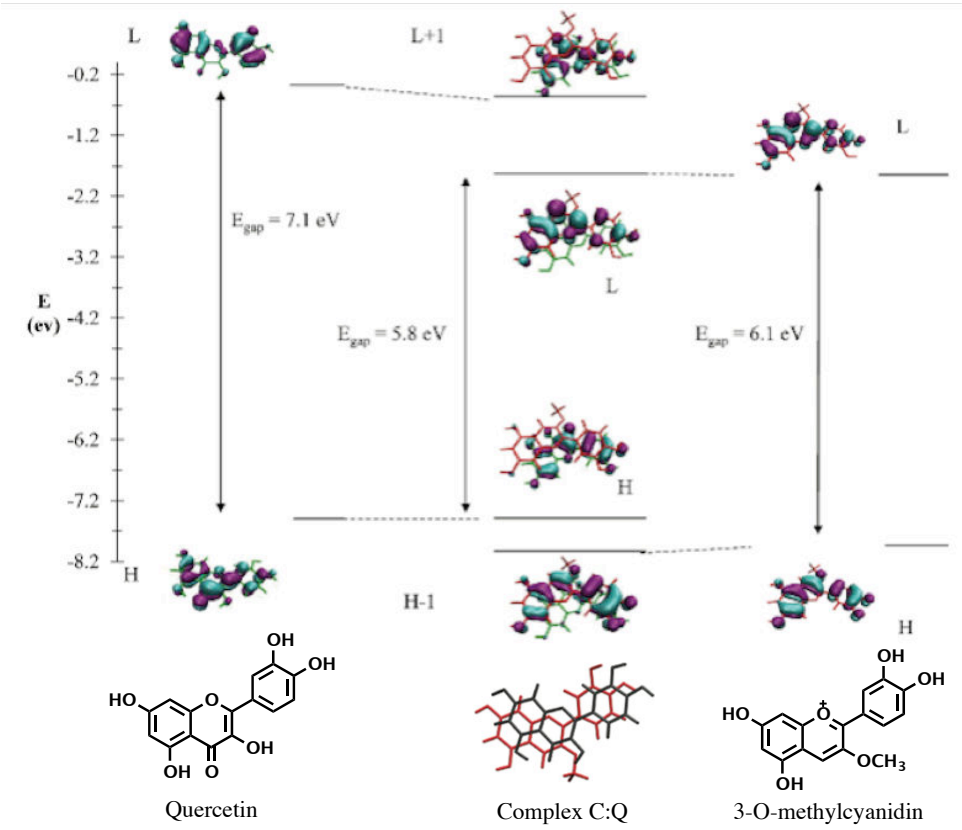

Figure 12. MO correlation diagram of quercetin, complex C: Q and 3−O−methylcyanidin.[149]

2.4. Natural graphite

Natural graphite is a multilayer, each single planar layer (graphene) being constituted by carbon atoms arranged in a hexagonal lattice. The interlayer distance is 0.335 nm (Fig. 13), stabilized by face−to−face π−stacking interactions. It has two known forms, alpha (hexagonal) and beta (rhombohedral), that have very similar physical properties, except that the graphene layers stack slightly differently. In each unit, carbon atoms are covalently bonded and π electrons are highly mobile which explains the high electrical and thermal conductivity as well as the black color of graphite. Layers are non−covalent bonded, which explain cleavage and low hardness. It is used for refractories, batteries, steelmaking, expanded graphite, brake linings, foundry facings and lubricants.[152], [153] Furthermore, natural graphite is an essential source of graphene.[154]

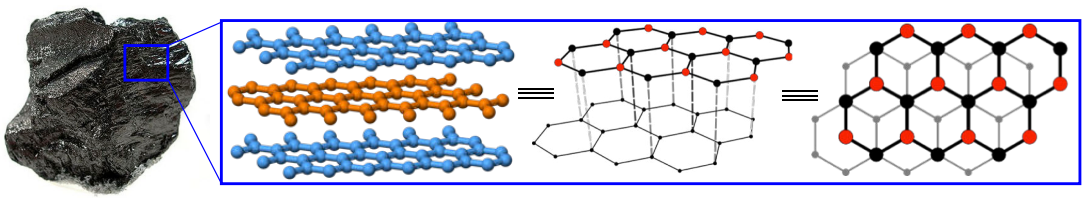

Figure 13. Different views of layer stacking forming the graphite structure.

2.5. Non-covalent interactions in synthetic compounds

The understanding of different natural (biological) processes is fundamental and increasingly developed through the understanding of non–covalent interactions. This guides the development and design of synthetic structures based on non-covalent interactions such as micelles, micro-emulsions, foldamer (Fig. 14) that allows protein folding, nucleic acids, polysaccharides and other molecules into predictable and well–defined conformations.

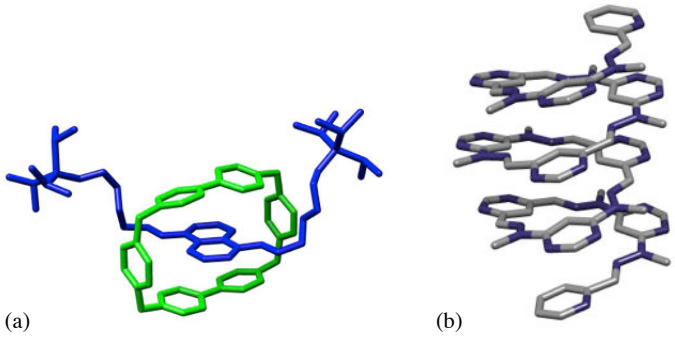

Figure 14. Non–covalent interactions stabilizing two synthetic structures: (a)[††] rotaxane (blue) with cyclobis(paraquat–p–phenylene) macrocyle (green) and (b)[‡‡] foldamer.

The non–covalent interactions constitute a major driving force for supramolecular self–assemblies, therefore its control is crucial for designing and synthesizing novel organic nanostructures.[155]

- ***Materials science***

Many non-covalent synthetic polymers have been developed. For instance, conjugated polymers have attracted much interest over the last three decades due to their large application in flexible, lightweight and low-cost electronic devices. They are used in organic light-emitting diodes (OLEDs), field–effect transistors (FETs), plastic lasers and photovoltaic cells.

Furthermore, these materials, when key structural requirements are met, may combine the mechanical properties of polymers with the electrical and optical properties of functional organic molecules. They exhibit specific properties such as solution processability, large charge transporting capabilities as well as broad optical absorption properties.[156]

[††] Eur. J. Org. Chem. 1998 (11): 2565–2571.

[‡‡] Helvetica Chimica Acta 2003, 86 (5): 1598.

At the end of the 20th century, the new concept emerged of supramolecular polymers, which are self–assembled small molecules held together by reversible non–covalent interactions, such as hydrogen bonds, metal–ligand complexation and π–stacking.

- ***Catalysis***

Non-covalent interactions are important in catalysis, binding reactants into conformations suitable for reaction and decreasing transition state energies. Template-directed synthesis is a special case of supramolecular catalysis. Encapsulation systems such as micelles and dendrimers are also used in catalysis to create microenvironments suitable for reactions.[157]

- ***Medicine***

The importance of non-covalent complexation is also appreciated by the development of new pharmaceutical candidates through the understanding of the interactions at a drug-binding site mostly controlled by this type of interactions. The field of drug delivery has also made important advances as a result of supramolecular chemistry providing encapsulation and targeted release mechanisms.[158] Furthermore, non-covalent systems have been designed to disrupt protein-protein interactions that are crucial to cellular function.[157], [159]

- ***Green and organic chemistry***

Understanding of non-covalent interactions has also application in green chemistry by proceeding within solid state directed by non-covalent bonding, thus decreasing the use of solvents during synthesis.[157]

- ***Others***

Non-covalent complexation often allows developing of new functions that cannot exist in single molecule (fragment). These functions also include magnetic properties, light response, self–healing polymers, synthetic ion channels and molecular sensors. Moreover, these interactions have been applied to e.g., develop high-tech sensors, processes to treat radioactive waste and contrast agents for Computed Axial Tomography (CAT) scans.[157]

To conclude, it is evident that the role of non-covalent interactions in Nature is crucial. They are responsible for stabilizing and maintaining many natural and synthetic molecules. In other words, some original (supra)molecular assemblies “made in Nature” would not be the same without non–covalent interactions.

Chapter 3 – Theoretical methods

Chapter 3 – Theoretical methods

1. Basic concepts and general view on methods of calculation

1.1. The Born–Oppenheimer approximation

The resolution of the Schrödinger equation[160] is only possible for mono–electron systems, namely hydrogen atom or the helium monocation. The exact solution of many-particle equation is not possible, in this case, using approximations is mandatory. Born and Oppenheimer proposed a first approximation[161], [162], based on which the motion of electrons and nuclei can be considered separately. This is allowed because electrons, being lighter than nuclei, are much faster. Therefore, when considering the motion of electrons, we can consider nuclei as immobile, and the electronic wave function depends only on electron coordinates. That does mean also that the kinetic energy of nuclei is zero when electrons are moving in a field of nuclei. The total wave function of the system is divided into its electronic and nuclear components:

$$\Psi_{total} = \Psi_{electronic}\,\Psi_{nuclear} \quad (eq.1)$$

The electronic Schrödinger equation for a molecular system is:

$$\widehat{H}_e\Psi_e = E_e\Psi_e \quad (eq.2)$$

where Ψ_e is the electronic wave function, E_e is the electronic energy and H_e is the electronic Hamiltonian operator given by:

$$\widehat{H}_e = -\sum_{i=1}^{N}\frac{1}{2}{\nabla_i}^2 - \sum_{i=1}^{N}\sum_{A=1}^{M}\frac{Z_A}{r_{iA}} + \sum_{i=A}^{N}\sum_{j>i}^{N}\frac{1}{r_{ij}} \quad (eq.3)$$

The total energy (E) is the sum of the electronic energy (E_e) and the constant nuclear repulsion energy between nuclei:

$$E = E_e + \sum_{A=1}^{M}\sum_{B>A}^{M}\frac{Z_A Z_B}{r_{AB}} \quad (eq.4)$$

This first approximation gave rise to the quantum chemistry or quantum mechanics (QM) methods. The

second side within the Born–Oppenheimer approximation[163] describing explicitly the motion of nuclei and in which atoms are balls and bonds are springs, gave rise to molecular mechanics (MM) methods.

1.2. The Hartree-Fock approximation

1.2.1. The Slater determinant

According to the molecular orbital (MO) theory, each electron is described as belonging to a spin–orbital wave function $\chi\ (x_i)$:

$$or \begin{cases} \chi(x_i) = \varphi(r_i)\alpha(\omega_i) \\ \chi(x_i) = \varphi(r_i)\beta(\omega_i) \end{cases} \quad (eq.5)$$

where $\varphi\ (r_i)$ is the spatial orbital, $\alpha(\omega_i)$ and $\beta(\omega_i)$ are the spin Eigen–function corresponding to spin up and spin down, respectively, x_i and ω_i correspond to spatial and spin coordinates, respectively.

The total wave function Ψ of a poly–electronic system (N electrons), can elegantly be given by a Slater determinant, which satisfies the anti-symmetry principle[164] and is solution of the Schrödinger equation:

$$\Psi\ (x_1, x_2, \dots, x_N) = \frac{1}{\sqrt{N!}} \begin{vmatrix} \chi_i(x_1) & \cdots & \chi_k(x_1) \\ \cdots & \ddots & \dots \\ \chi_i(x_N) & \dots & \chi_k(x_N) \end{vmatrix} \quad (eq.6)$$

where $\frac{1}{\sqrt{N!}}$ is the normalization factor, χ_i is the individual spin orbital as a function of spatial and spin coordinates of electron *i*. If there are two identical lines i.e., identical electrons, the determinant equals zero. This satisfies the Pauli principle, which states that two electrons cannot have both the same spin at the same spatial location. Also, the sign of the Slater determinant changes when two lines are exchanged; this satisfies the non–distinguishability of electrons.

When introducing the Salter determinant into the total energy expression, it is written as the sum of three variable terms plus one constant:

$$E = \sum_{i=1}^{N} H_i + \sum_{i}^{N} \sum_{j>i}^{N} \left(J_{ij} - K_{ij}\right) + H_0 \quad (eq.7)$$

where:

- H_i is the kinetic energy and the potential energy of each electron moving in the field of nuclei:

$$H_i = E_{total}^{core} = \sum_{i=1}^{N} \int d\tau_1 \chi_i(1) \left(-\frac{1}{2} {\nabla_i}^2 - \sum_{A=1}^{M} \frac{Z_A}{r_{iA}} \right) \chi_i(1) \quad (eq.8)$$

- J_{ij} is the classical Coulomb repulsion between electrons in the *i* and *j* spin−orbitals:

$$\sum_{ij} J_{ij} = E_{total}^{Coulomb} = \sum_{ij} \int d\tau_1 d\tau_2 \chi_i(1) \chi_i(2) \frac{1}{r_{12}} \chi_j(1) \chi_j(2) \quad (eq.9)$$

- K_{ij} is the non−classical (purely quantum) exchange interaction, which describes correlation between electrons with parallel spin:

$$\sum_{ij} K_{ij} = \sum_{ij} \int d\tau_1 d\tau_2 \chi_i(1) \chi_j(2) \frac{1}{r_{12}} \chi_i(2) \chi_j(1) \quad (eq.10)$$

- H_0 is a constant that represents the repulsion potential between nuclei.

1.2.2. The Hartree−Fock approximation

The Hartree−Fock (HF) approximation consists in replacing the complicated many electron problem by a one-electron problem. In fact, in N−electron systems, the motions of all electrons are correlated. Hartree suggested to exchange the influence of all N−1 electrons on a single electron by a mean potential field. In other words, every electron behaves as being in this potential field, which is due to the other electrons. Each electron is described by its own wave function Ψ_i:

$$\widehat{H}_i \Psi_i = \mathcal{E}_i \Psi_i \quad (eq.11)$$

Within the Hartree approximation, the N−electron Hamiltonian is defined as the sum of all one−electron Hamiltonians, H_i:

$$\widehat{H} = \sum_{i=1}^{N} H_i = \sum_{i=1}^{N} \left(-\frac{1}{2} \nabla_i^2 - \sum_{\alpha=1}^{A} \frac{Z_\alpha}{|R_{\alpha i}|} + V_i \right) \quad (eq.12)$$

The N−electron wave function as defined by Hartree is not anti−symmetrical, it is the product of the one−electron wave functions:

$$\Psi_{HF} = \Psi_1 \Psi_2 \dots \Psi_N \quad (eq.13)$$

Fock considered the wave function as a Slater determinant. Thus, within the Hartree-Fock approximation the exchange contribution was included:

$$\left(H^{core} + \sum_{i \neq j}^{N} J_j(x_1) - \sum_{i \neq j}^{N} K_j(x_1)\right)\chi_i(x_1) = \sum_j \varepsilon_{ij}\chi_j(x_1) \quad (eq.14)$$

where H^{core} is the core potential for electron i, J_j is the Coulomb repulsion operator and K_j is the exchange operator. The term in brackets is the so-called Fock operator ($\hat{f}_i$):

$$\hat{f}_i = -\frac{1}{2}\nabla_i{}^2 - \sum_{A=1}^{M}\frac{Z_A}{r_{iA}} + v_i^{HF} \quad (eq.15)$$

where the one-electron equation can be written as:

$$\hat{f}_i\chi_i = \varepsilon_i\chi_i \quad (eq.16)$$

ε_i is the energy of a given spin-orbital χ_i.

The HF Hamiltonian is defined for N–electron systems by:

$$\hat{H}^{HF} = \sum_i^N f_i = \sum_i^N H_{ii}^{core} + \sum_i^N \sum_{j>i}^N \left(J_j(i) - K_j(i)\right) \quad (eq.17)$$

where H_{ii}^{core} is the monoelectronic core operator that includes kinetics and electron–nuclei interactions.

1.2.3. Restricted and unrestricted Hartree–Fock formalisms

The HF equations must be solved within a SCF (self–consistent field) procedure. The guessed wave function is a Slater determinant chosen as a trial wave function and it is introduced in the equations to calculate a first approximation of the energy and a new wave function. This is used for a new loop until self-convergence is reached, namely no significant difference in energy and gradient.

According to the variational principle, the total energy obtained from the HF approximation is overestimated compared to the energy of the exact solution of the Schrödinger equation. The missing part is mainly the electron correlation energy, which is not taken into account with the HF approach.

Depending on the number of electrons, the approaches used for the resolution of the HF equation are different. For systems with pair number of electrons, restricted Hartree–Fock (RHF) is used, in which, electrons with α– and β–spins must occupy the same spatial orbitals $\phi_i(r_i)$. The advantage of this

approach is that the wave function is an eigenfunction of $\langle S^2 \rangle$ operator.

The corresponding energy is given by:

$$E = 2\sum_{i=1}^{N/2} H_{\mathrm{ii}}{}^{core} + \sum_{i}^{N/2}\sum_{j>i}^{N/2}(2J_{ij} - K_{ij}) \quad (eq.18)$$

However, the constraint of two electrons with α and β spins occupying the same spatial orbital ignores the correlation between two electrons with opposed spins (spin correlation). This is of particular importance for systems having odd number of electrons in their outer shells, e.g., radicals. In this case either restricted open−shell Hartree−Fock (ROHF) or unrestricted open−shell Hartree−Fock (UHF) can be used. The advantage of the UHF is that there is no imposed restrains on the spatial nature of orbitals (ϕ_i) because it takes the correlation between electrons with opposed spins into account. Nevertheless, the corresponding wavefunction is not an eigenfunction of $\langle S^2 \rangle$. This unrestricted set is written as:

$$\begin{cases} \chi_i = \phi_i^{\alpha}\alpha(\omega) \\ \chi_{i+1} = \phi_i^{\beta}\beta(\omega) \end{cases} \quad (eq.19)$$

1.3. Roothaan-Hall equations

The most popular strategy to make the direct solution of the HF equations more practical was developed by Roothaan and Hall.[165], [166] They proposed to describe each MO as a linear combination of atomic orbitals (LCAO-MO) approximation:

$$\chi_i = \sum_{v=1}^{k} c_{vi}\phi_v \quad (eq.20)$$

where ϕ_v are the atomic orbitals and C_{vi} are the linear coefficients that must satisfy the variational theorem:

$$\frac{\partial E}{\partial c_{vi}} = 0 \quad (eq.21)$$

The insertion of these atomic orbitals into the HF equation leads to the following form:

$$\sum_{v} F_{\mu v}C_{vi} = \sum_{v} \varepsilon_i S_{\mu v}C_{vi} \quad (eq.22)$$

where $F_{\mu\upsilon}$ are the terms of the Fock matrix:

$$F_{\mu v} = \int dr_1 \phi_\mu(1) f_i(1) \phi_v(1) \quad (eq.23)$$

$$\hat{f}_i = h_i + \sum_{j=1}^{N/2} 2J_j(r_i) - K_j(r_i) \quad (eq.24)$$

$S_{\mu\upsilon}$ is the overlap between two atomic orbitals φ_μ and φ_υ. When the orbitals are located on different atoms, this overlap is different from zero:

$$S_{\mu v} = \int dr_1 \phi_\mu(1) \phi_v(1) \quad (eq.25)$$

The current form of the Roothaan–Hall equations is written as follows:

$$\sum_v F_{\mu v} c_{vi} = \sum_v \mathcal{E}_i S_{\mu v} c_{vi} \quad (eq.26)$$

or in its matrix form:

$$FC = SCE \quad (eq.27)$$

where C is a matrix containing the coefficients $c_{\upsilon i}$ and E is a diagonal matrix describing orbital energies:

$$C = \begin{vmatrix} c_{11} & c_{12} \cdots & c_{1k} \\ c_{21} & c_{22} \ldots & c_{2k} \\ \vdots & \vdots & \vdots \\ c_{k1} & c_{k2} \cdots & c_{kk} \end{vmatrix} \qquad E = \begin{vmatrix} \mathcal{E}_1 & 0 \cdots & 0 \\ 0 & \mathcal{E}_2 \cdots & 0 \\ \vdots & \vdots & \vdots \\ 0 & 0 \cdots & \mathcal{E}_k \end{vmatrix}$$

The solvation is then a matter of solving an eigenvalue equation. However, again, since F depends on its own solution (through the orbitals), the process must be done self–consistently (iteratively). So, for a given nuclei geometry, one provides a guess C matrix, then to enter in a SCF procedure.

1.4. Basis sets

The description of the atomic orbitals is achieved by the basis set, which has a huge impact on the quality of the results; so that it should be carefully chosen.

1.4.1. Usual basis sets

In the LCAO theory, the MOs (χ_i) are written as:

$$\chi_i = \sum_{\mu=1}^{m} C_{\mu i}\phi_\mu \quad (eq.28)$$

and atomic orbitals (ϕ_μ) are described by Slater–type orbital (STO) functions:

$$f_{STO} = P(x,y,z)e^{-\alpha r} \quad (eq.29)$$

The resolution of HF equations with f_{STO} is a complex mathematical issue, that can be simplified by replacing the STO by Gaussian-type orbital (GTO) functions:

$$f_{GTO} = P(x,y,z)e^{-\alpha r^2} \quad (eq.30)$$

A proper description of the Slater orbitals requires at least three Gaussian functions and the precision increases with the number of Gaussian functions. Each orbital χ_μ is thus replaced by a linear combination of (primitive) Gaussian functions. The basis sets, in which each contraction is developed by n primitives ($1 \leq n \leq 6$) are called the STO–nG basis sets. The most famous is the STO–3G.[167]

The minimal basis set does not provide accurate results because it describes only occupied atomic orbitals. Therefore, to improve accuracy, virtual orbitals are added to the description. Also core and valence electrons can be described by two different sets of Gaussian function. If the number of contractions is doubled for valence electrons, the basis set is called a double–dzeta. The mathematical expression is given by two contractions and allows more flexibility in the description of atomic orbitals. By the same way, there exist the triple- and quadruple–dzeta.

To improve further the accuracy, polarized functions can be added to the basis set. It consists to add p– and d–type contraction on hydrogen and heavy atoms, respectively.

Adding diffuse primitives improves the description far from the nucleus. These basis sets are indicated with "+ " and "+ +" for heavy and hydrogen atoms, respectively.

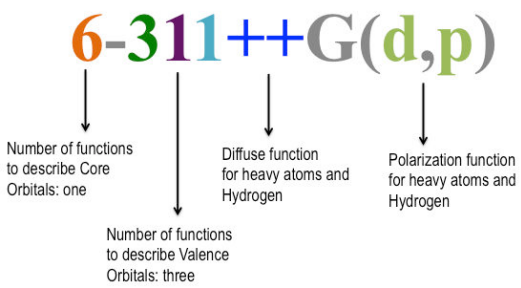

Figure 1. Example of a Pople's basis set with attribution

Other basis sets than Pople-type basis sets exist, namely natural orbital basis sets also called correlation consistent basis sets (Dunning–type),[168] e.g., cc–pVDZ, cc–pVTZ and cc–pVQZ, where "cc" mean that we introduce correlation consistent basis sets, p designates polarization function and the last three letters describe valence electrons i.e., valence double or triple or quadruple-dzeta. The prefix "aug" is added when introducing diffuse functions.

1.4.2. Basis Set Superposition Error (BSSE)

The basis functions of atoms from two molecules may overlap when the two atoms are close to each other (e.g., in non–covalent dimers). Each fragment somehow borrows the functions from the other fragment, thus artificially increasing basis set description, and consequently inadequately improving the calculated properties, such as energy. This issue can be solved by using the counterpoise approach (CP). In CP, one calculates the BSSE by re-performing all calculations using the mixed basis sets, through introducing "ghost orbitals", and then subtracts this error *a posteriori* from the uncorrected energy:

$$\Delta E_{bind}^{CP}(AB) = [E_{AB}^{AB}(AB) - E_{AB}^{AB}(A) - E_{AB}^{AB}(B)] + [E_{AB}^{A}(A) - E_{A}^{A}(A)] + [E_{AB}^{B}(B) - E_{B}^{B}(B)] \quad (eq.31)$$

where $E_{AB}^{AB}(A)$ and $E_{AB}^{AB}(B)$ are the energies of two given parteners A and B, respectively as obtained in the AB complex geometry with the AB basis set, $E_{AB}^{A}(A)$ and $E_{AB}^{B}(B)$ are the energies of A and B, respectively as obtained in the AB complex geometry with the A and B basis sets, respectively.

BSSE is reduced when using large basis sets. In conclusion, there are some criteria to make the best choice of basis set, e.g.,

- ✓ Double–dzeta at least
- ✓ Including polarization of heavy atoms
- ✓ Including diffuse functions for anions and systems stabilized by H-bonding
- ✓ Accounting for BSSE correction when necessary

1.5. Post Hartree-Fock methods

The HF method fails at describing the dissociation of molecules into open-shell fragments. For example, the phenol BDE (bond dissociation enthalpy) obtained by HF methods is 49.5 kcal.mol^{-1} while the experimental value is about 87 kcal.mol^{-1}. To reach the exact energy (E), the missing part of the correlation energy (E_{corr}) must be added to the HF energy (E_{HF}). This correlation contribution mainly describes the correlation motion of electrons having antiparallel spins. The HF−derived methods that account for E_{corr} are called post−HF methods namely configuration interaction, coupled cluster, and perturbation theory.

1.5.1. Coupled−cluster (CC) methods

The coupled−cluster approach uses an exponential operator for the wave function:

$$\Psi = e^{\hat{\mathrm{T}}}\Phi_0 \quad (eq.32)$$

in which the exponential operator can be transformed into a Taylor expansion:

$$e^{\hat{\mathrm{T}}} = 1 + \hat{\mathrm{T}} + \frac{1}{2!}\hat{\mathrm{T}}^2 + \cdots + \frac{1}{n!}\hat{\mathrm{T}}^n = \sum_{i=0}^{n}\frac{\hat{\mathrm{T}}^i}{i!} \quad (eq.33)$$

where $\hat{\mathrm{T}}$ is the cluster operator obtained as the sum of operators that generate N-excited determinants, i.e., $\hat{\mathrm{T}}_1$ and $\hat{\mathrm{T}}_2$ mono− and bi−excited, respectively:

$$\hat{\mathrm{T}} = \sum_{i=1}^{N}\hat{\mathrm{T}}_i \quad (eq.34)$$

$$\hat{\mathrm{T}}_1\phi_0 = \sum_{i}^{O}\sum_{a}^{V} t_i^a\,\phi_i^a \quad (eq.35)$$

$$\hat{\mathrm{T}}_2\phi_0 = \sum_{i<j}^{O}\sum_{a<b}^{V} t_{ij}^{ab}\,\phi_{ij}^{ab} \quad (eq.36)$$

where t_i^a and t_{ij}^{ab} are the amplitudes, O and V are the number of occupied and virtual orbitals, respectively.

The operator $\hat{\mathrm{T}}$ is divided into $\hat{\mathrm{T}}_1$ and $\hat{\mathrm{T}}_2$ within the (CCSD) model and the energy is given by:

$$E_{CCSD} = \langle \Psi_0 | \hat{H} | \Psi_0 \rangle + \langle \Psi_0 | \hat{H} | \hat{\mathrm{T}}_1 \Psi_0 \rangle + \left\langle \Psi_0 \middle| \hat{H} \middle| \left(\hat{\mathrm{T}}_2 + \frac{\hat{\mathrm{T}}_1^2}{2} \right) \Psi_0 \right\rangle \quad (eq.37)$$

The first term corresponds to the HF energy (E_{HF}), the second term equals zero according to the Brillouin's theorem and the third term is the CC correlation energy (E_{CCSD}^{cor}):

$$E_{CCSD}^{cor} = \sum_{a,b,i,j} \left(t_{ij}^{ab} + t_i^a t_j^b - t_i^b t_j^a \right) \langle \Psi_0 | \hat{H} | \Psi_0 \rangle \quad (eq.38)$$

Currently, the CCSD(T) method allows reaching high accuracy and providing the best results concerning ground-state calculations. However, the corresponding computational time is dramatically increased with respect to other methods (following a N^7 law, N being the number of basis functions). It is thus limited to rather small molecular systems containing ca. twenty heavy atoms. Nevertheless, this method is often used as a reference to validate *e.g.*, "single point" energy calculation.

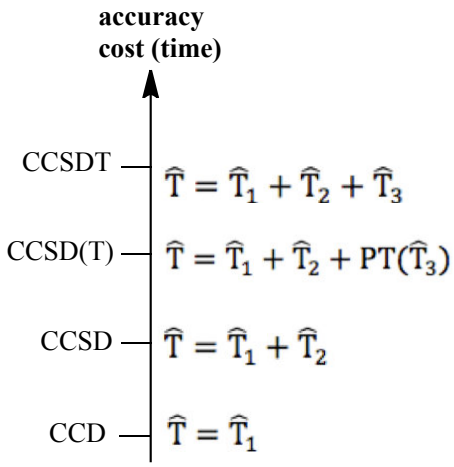

Figure 2. CC methods ranking and corresponding operators.

1.5.2. Perturbation Theory (PT)

The perturbation theory consists in adding a correcting contribution to the Hamiltonian operator. In a general way, the expression of a physical property is given as a perturbation series:

$$\mathrm{A} = \mathrm{A}_0 + \mathcal{E}^1 \mathrm{A}_1 + \mathcal{E}^2 A_2 + \cdots + \mathcal{E}^n A_n \quad (eq.39)$$

where A_0 is the first approximation (e.g. HF solution) and A_n is the higher-order terms. The first order perturbation is given by:

$$\mathrm{A} \approx \mathrm{A}_0 + \mathcal{E}^1 \mathrm{A}_1 \quad (eq.40)$$

1.5.3. Møller-Plesset (MP) methods

The perturbation theory is developed for treating an n electrons system in which the HF solution appears as the zero–order approximation. The Møller–Plesset (MP) correlation energy is the perturbation to the total energy given as:

$$\lambda\hat{V} = \hat{H} - \hat{H}_0 = \frac{1}{2}\sum_i \sum_j \frac{1}{r_{ij}} - \sum_i \hat{v}_i^{HF} \quad (eq.41)$$

From $eq.41$ that includes the HF Hamiltonian, the energy can be written as the sum of the HF energy (E_{HF}) and the electron–electron term (E_{ee}). The first–order Møller–Plesset (MP1) method provides the HF energy:

$$E_{MP1} = E_0^{(0)} + E_0^{(1)} = E_{HF} \quad (eq.42)$$

where $E_0^{(0)} = -E_{ee}$

The development of the higher approximation involves only calculations based on a definite one-body problem.[169] The second–order Møller–Plesset (MP2) energy [170], [171] is written as:

$$E_0^{(2)} = \sum_{\substack{possibles \\ diexcitations}} \frac{\left|\left\langle \psi_{HF} \middle| \sum_{i>j} \frac{1}{r_{ij}} \middle| \psi^D \right\rangle\right|^2}{E_0^0 - E_0^D} = \sum_{s>r}\sum_{b>a} \frac{|\langle ab|rs\rangle|^2}{(\mathcal{E}_r - \mathcal{E}_a) + (\mathcal{E}_s - \mathcal{E}_b)} \quad (eq.43)$$

where a and b are the spin-orbitals occupied by electrons 1 and 2 for the reference (ground state) configuration, while r and s are the spin-orbitals occupied by electrons 1 and 2 in the excited configuration, ψ^D is the double-electron wave function.

It must be reminded that the MP method does not use the variational principle and so it is possible to have: $E_{MP} < E_{exact}$. While MP2 provides highly accurate results with respect to experimental data, these methods are expensive in terms of computational time particularly when using large basis sets. The molecule size is limited to ca. fifty atoms. In the case of using small basis sets, the accuracy is prone to be limited. The other limitations of these methods consist in the bad description of dispersion interactions. Even with the third–order Møller–Plesset (MP3) method, the results do not improved while the computational time dramatically increased.[172] MP4 significantly improved the accuracy, but again the computational time dramatically increases as a function of N^7.[173] The fifth order Møller–Plesset (MP5) method is rarely used because of its cost.[174]

1.5.4. SCS–MP2 methods

Recently, MP2 has been improved by developing new methods; the most common are the spin–component-scaled (SCS) methods. The MP2 correlation energy is expressed as:

$$E_{c,MP2} = E_0^{(2)} = \frac{1}{2}(E^{\uparrow\uparrow} + E^{\downarrow\downarrow}) + E^{\uparrow\downarrow} \quad (eq.44)$$

where $E^{\uparrow\downarrow}$ corresponds to the energy of spin-paired and $(E^{\uparrow\uparrow} + E^{\downarrow\downarrow})$ to the spin-unpaired double-excited electron systems.

The SCS–MP2 method was parameterized by Grimme in 2003 to correct the underestimation of the spin-paired energy and the overestimation of the spin-unpaired energy. The SCS–MP2 correlation energy is given by:

$$E_c^{SCS-MP2} = E_0^{(2)} = c^{\uparrow\uparrow}\left(\frac{1}{2}E^{\uparrow\uparrow} + \frac{1}{2}E^{\downarrow\downarrow}\right) + c^{\uparrow\downarrow}E^{\uparrow\downarrow} \quad (eq.45)$$

where $c^{\uparrow\uparrow}$ and $c^{\uparrow\downarrow}$ are the scaling factors for spin–unpaired and spin–paired electron contributions, respectively.

In 2004, Jung et al. proposed to improve SCS–MP2 by neglecting the $(c^{\uparrow\uparrow})$ and changing the $(c^{\uparrow\downarrow})$ parameter to 1.3. This improvement led to the scaled–opposite–spin–MP2 (SOS–MP2) method.[175]

SCS–MP2 methods can also be parameterized for specific chemical purposes e.g., to describe long-range interactions by using SCS–MI–MP2 and SCS–S66–MP2 methods as proposed by Hobza's group. There have already been a number of studies of the SCS approach for the calculation of non-covalent interactions.[176]–[178] The different $c^{\uparrow\uparrow}$ and $c^{\uparrow\downarrow}$ values are given in Table 1.

Table 1. $c^{\uparrow\uparrow}$ and $c^{\uparrow\downarrow}$ component factors for SCS–MP2–type methods.

Method	MP2	SCS-MP2	SOS-MP2	SCS-MI-MP2*	SCS-S66-MP2*
$c^{\uparrow\uparrow}$	1.00	1.20	1.30	0.17	0.14
$c^{\uparrow\downarrow}$	1.00	0.33	0.00	1.75	1.88

* cc-pVTZ basis set

1.6. Semi-empirical methods

To simplify the HF and related methods and to decrease computational time, semi−empirical methods have been developed. These methods offered the possibility to treat large molecules in reduced time by adding several approximations (e.g., neglecting some integrals for certain long−range−interactions, choosing the minimal basis set and using fitted parameters for bi−electronic integrals). Due to these approximations, some properties are not well described (e.g., non−covalent interactions) and will not be considered in this work. There are a variety of semi-empirical methods. The most common is AM1 (Austin Model 1), which has been developed in 1985 and still give reliable results for a very efficient computational time, as compared to HF and DFT. There are also CNDO (Complete Neglect of Differential Overlap), INDO (Incomplete neglect of Differential Overlap), MNDO (Medium Neglect of Differential Overlap) and PM3 (third parameterization of MNDO).

The difference between semi−empirical and Hartree−Fock methods is that i) the parameterization of the former includes all thermochemical corrections to yield heat of formation at T=300K, while the latter do not, and ii) the semi−empirical parameterization which refers to experimental data methods could recover some part of electron correlation effects only for the ground states and not for the transition or excited states.

2. Density functional theory (DFT)

While it was originally used only in solid−state physics, density functional theory (DFT) has more recently become popular in various fields of chemistry and biology.

2.1. Thomas and Fermi

While post−HF methods allow accuracy, only rather small molecules can be studied. DFT has been developed to treat bigger systems at a lower computational cost. The wave function does not have any physical meaning in its native form but its square module corresponds to the electron density. The DFT formalism has proposed to replace the wave function by the electron density as a variable, which can be experimentally measured (e.g., by X-ray diffraction).

The electron density $\rho(r_1)$ defines the probability of finding one electron at a given location r_1. It is described by three coordinates, and the expression for one electron is:

$$\rho(r_1) = N \int \dots \int \psi^*(x_1, \mathrm{x}_2 \dots x_N)\psi(x_1, x_2, \dots x_N) ds_1 dx_2 \dots dx_N \quad (eq.46)$$

Thomas and Fermi proposed to write the total energy as a function of ρ. The energy of the system is so a functional i.e., a function of a function:

$$E[\rho] = T_{TF}[\rho] + V_{ne}[\rho] + V_{ee}[\rho] \quad (eq.47)$$

The model proposed by Thomas and Fermi was accurate for solid−state physics but it totally failed at describing chemical properties due to the local approximation inherent to this formalism. Hohenberg and Kohn proposed two theorems to improve DFT.

2.2. Hohenberg and Kohn theorems

❖ **The first theorem**

This theorem states that the external potential (V_{ext}) is determined, within a trivial additive constant, by the electron density.[179] In other words, all physical properties can be obtained from ρ e.g., the external potential, the Hamiltonian H and the wave function. The electronic energy is given by:

$$E[\rho] = V_{ext}[\rho] + T[\rho] + V_{ee}[\rho] = T[\rho] + \int V_{ext}(r)\rho dr + V_{ee}[\rho] \quad (eq.48)$$

where V_{ext} corresponds to the interaction between nuclei and electrons in absence of any other external field, this is system-dependent:

$$v_{ext}[\rho] = V_{ne}[\rho] = -\sum_{A=1}^{K}\sum_{i=1}^{N}\frac{Z_A}{r_{Ai}} \quad (eq.49)$$

$T[\rho]$ and $V_{ee}[\rho]$ correspond to the kinetic energy and the potential energy of the electron-electron interaction, respectively; they are not system−dependent.

❖ **The second theorem**

The second theorem is the variational principle for the energy functional. From the first theorem, the exact electron density ρ_0 of the ground state corresponds to the exact energy E_0. Thus, for a trial ρ the corresponding energy E is such as:

$$E_0 \leq E$$

the energy is given by:

$$\mathrm{E}[\rho(r)] = F^{HK}[\rho(r)] + \int v_{ext}(r)\rho(r)dr \quad (eq.50)$$

$F^{HK}[\rho(r)]$ is the universal system-independent HK functional given by:

$$F^{HK}[\rho(r)] = T[\rho(r)] + V_{ee}[\rho(r)] \quad (eq.51)$$

The electron–electron interaction can be split into the Coulomb (J) and the non–classical and correlation (E_{ncl}) contributions, the F^{HK} expression becomes:

$$F^{HK}[\rho(r)] = T[\rho(r)] + J[\rho(r)] + E_{ncl}[\rho(r)] \quad (eq.52)$$

where the Coulomb term is given by:

$$J[\rho(r)] = \frac{1}{2}\int\int \frac{\rho(r_1)\rho(r_2)}{r_{12}} dr_1 dr_2 \quad (eq.53)$$

2.3. Kohn–Sham

The electron–electron interaction is not known at this stage and Kohn and Sham proposed to calculate the kinetic energy introducing a non-interacting electron system:

$$T_{KS} = \sum_i^N \left\langle \psi_i \left| -\frac{1}{2}\nabla^2 \right| \psi_i \right\rangle \quad (eq.54)$$

and the total energy is given by:

$$E[\rho] = T_{KS}[\rho] + V_{ne}[\rho] + V_{ee}[\rho] + T_c[\rho] + E_{ncl}[\rho] \quad (eq.55)$$

where $T_c[\rho]$ is a correction added to the kinetic energy, which is combined to the non–classical interaction $E_{ncl}[\rho]$ to form the exchange–correlation energy E_{xc}:

$$E_{xc}[\rho] = T_c[\rho] + E_{ncl}[\rho] = (T[\rho] - T_{KS}[\rho]) + (E_{ee}[\rho] - V_{ee}[\rho]) \quad (eq.56)$$

The equations can be written with the one-electron operator f_S^{KS} within the non–interacting system given by:

$$\hat{f}_S^{KS}\psi_i = \varepsilon_i \Psi_i \quad (eq.57)$$

$$\hat{f}_S^{KS} = -\frac{1}{2}\nabla^2 + \upsilon_{eff}(r) \quad (eq.58)$$

where $\upsilon_{eff}(r)$ is the effective potential:

$$\upsilon_{eff}(r) = \upsilon_{ne}(r) + \int \frac{\rho(r_2)}{|r_{12}|} dr_2 + \upsilon_{xc}(r) \quad (eq.59)$$

2.3. Exchange–correlation functionals

The only unknown term in the total energy expression is the exchange-correlation functional (E_{xc}), which contains the non–classical contribution of the electron–electron interaction and the correction to the kinetic energy. Different approaches were proposed to describe this functional.

2.3.1. Local density approximation

The local density approximation (LDA) is based on the concept of the uniform gas of electrons, i.e., the jellium model, in which the electron density is defined locally, that is at a certain r. The corresponding exchange-correlation energy is:

$$E_{xc}[\rho] = \int \rho(r)\varepsilon_{xc}\big(\rho(r)\big)dr \quad (eq.60)$$

where $\varepsilon_{xc}\big(\rho(r)\big)$ is the exchange–correlation energy per electron, which is usually divided into the exchange and correlation contributions:

$$\varepsilon_{xc}\big(\rho(r)\big) = \varepsilon_x\big(\rho(r)\big) + \varepsilon_c\big(\rho(r)\big) \quad (eq.61)$$

The most known LDA functional is SVWN, in which the exchange part was described by the Slater exchange obtained from the HF approximation, and the correlation part was suggested by Vosko, Wilk and Nusair. The LDA formalism overestimates the correlation energy and underestimates the exchange energy. It is accurate only for homogenous systems. A better description is obtained when separated both α and β contributions (ρ_α, ρ_β), corresponding to the local spin-density approximation (LSDA), for which the energy is:

$$E_{xc}[\rho_\alpha, \rho_\beta] = \int \rho(r)\varepsilon_{xc}\left(\rho^\alpha(r), \rho^\beta(r)\right) dr \quad (eq.62)$$

When the number of α–electrons is equal to the β–electrons, the energies obtained from LSDA and LDA must equals, considering the spin polarization function:

$$f(\xi) = \frac{(1+\xi)^{4/3} + (1-\xi)^{4/3} - 2}{2^{4/3} - 2} \quad (eq.63)$$

where $\xi(r) = \frac{\rho^{\alpha} - \rho^{\beta}}{\rho^{\alpha} + \rho^{\beta}}$

LSDA is not accurate for heterogeneous systems, but it is accurate for e.g., conductor and semi−conductor systems.

2.3.2. Generalized gradient approximation

To improve the LDA description and decrease the local character, the density gradient is included to treat also non-homogenous systems. GEA (gradient expansion approximation) was the first attempt, where the exchange-correlation energy is:

$$E_{xc}[\rho(r)] = \int \rho(r)\varepsilon_{xc}^{LDA}[\rho(r)]dr + \sum_{\alpha}\sum_{\beta}\int C_{xc}^{\alpha,\beta}\left(\rho(r)^{\alpha}, \rho(r)^{\beta}\right)\frac{\nabla\rho(r)^{\alpha}}{(\rho(r)^{\alpha})^{2/3}}\frac{\nabla\rho(r)^{\beta}}{(\rho(r)^{\beta})^{2/3}}dr + \cdots$$

$$(eq.64)$$

The improvement given by GEA had not appeared sufficient to describe non-homogenous systems. An improved version was then proposed, namely GGA (generalized gradient approximation), for which the exchange-correlation functional is given by:

$$E_{xc}^{GGA}\left[\rho, \nabla_{\rho}, \nabla^2\rho\right] = \int \varepsilon_{xc}^{GGA}\left[\rho^{\alpha}, \rho^{\beta}, \nabla\rho^{\alpha}, \nabla\rho^{\beta}\right]dr \quad (eq.65)$$

The GGA functionals were empirically tested by comparison to experimental data, e.g., G2 test (atomization energies of 50 small molecules), and provided much accurate results. Two types of GGA exchange functionals were developed. First, those fitted on the exchange energy of rare gas, as the first popular GGA exchange functional, developed by Becke (B) or e.g., FT97, O, PW, *m*PW. Second, those mathematically developed and based on rational function expansions, as the one developed by Perdew (P) or e.g., P86, LG, P, PBE (PBE is an improvement of PW86), *m*PBE. These functionals do not include any empirically optimized parameters. Besides, the correlation functionals are empirically built. The corresponding mathematical expressions are rather complicated and cannot be understood with simple physical rules e.g., LYP (Lee Yang Parr), P86 and PW91. The exchange−correlation GGA functionals are the combinations of both exchange and correlation e.g., BLYP. The further improvements (meta−GGA functionals) were to include the second derivative of the density or the Laplacian $(eq.66)$ e.g., B95, B98, ISM, KCIS, PKZB, tHCTH, TPSS and VSXC.

$$E_{xc}^{m-GGA}[\rho, \nabla_\rho, \nabla^2\rho] = \int \varepsilon_{xc}^{m-GGA}[\rho, \nabla\rho, \nabla^2\rho]dr \quad (eq.66)$$

2.3.3. Hybrid functionals

The main limitation of GGA and meta−GGA is that the exchange contribution is overestimated, while the HF−theory provides the exact exchange E_x. The original idea of the hybrid functionals was to use the exact HF−exchange and DFT−correlation, and so to write the exchange−correlation functional as:

$$E_{xc} = E_x^{HF} + E_c^{KS} \quad (eq.67)$$

This approximation is accurate only for atoms and totally failed to describe molecules. As an improvement, the hybrid functionals include one part of the exact HF exchange, the rest being of DFT−type; the correlation contribution is purely DFT:

$$E_{xc} = aE_x^{HF} + (1-a)E_{xc}^{DFT} \quad (eq.68)$$

For example, this functional is called half−and−half (HandH) when a = 0.5, meaning that the combination is 50% of HF−exchange and 50% of DFT-exchange. There are virtually an infinity of functionals that can be built based on this principle. One of the most used is B3-type[180] in which the exchange correlation functional is described by three parameters:

$$E_{xc}^{B3} = E_{xc}^{LSD} + a(E_{xc}^{HF} - E_x^{LSD}) + bE_x^B + cE_c^{PW91} \quad (eq.69)$$

where a, b and c are known as: a = 0.20, b = 0.72 and c = 0.81.

The hybrid−meta GGA functionals were accurate to describe specific properties, e.g., delocalized systems and kinetics of reactions. As an example, the results obtained with the MPWB1K functional, which was parameterized to describe kinetics, is in agreement with many experimental data, e.g., H atom transfer reactions.

3. Further developments of DFT

For many chemical systems, DFT methods provide an adequate compromise between accuracy and computational time. Among the most important drawbacks of DFT is that this method introduce self−interaction error and fails at describing non−covalent interactions.

3.1. Self–interaction error

Within the HF theory, for a single-electron system, the Coulomb term (J_{ij}) is exactly cancelled by the exchange term (K_{ij}), which is not the case with DFT functionals that introduce an artificial interaction of one electron with itself. This is the SIE (self–interaction error), which may influence also many–electron systems. Perdew and Zunger[181] proposed to correct this error by using the SIC (Self–Interaction Correction) procedure, which basically ensure equality between J_{ij} and K_{ij}, according to:

$$E_{xc}^{SIC}[\rho^{\alpha},\rho^{\beta}] = E_{xc}[\rho^{\alpha},\rho^{\beta}] - \sum_{i}\sum_{s}(J[\rho_i^s] + E_{xc}[\rho_i^s,0]) \quad (eq.70)$$

where the second sum runs over α– and β–spins

3.2. Dispersion–corrected functionals

The classical vdW interaction is described by the Lennard–Jones–type potential, which is expressed for a M–atom system as:

$$E_{VdW} = \sum_{A}^{M-1}\sum_{B>A}^{M} \varepsilon_{AB}\left(\frac{r_{0,AB}}{{R_{AB}}^{12}} - \frac{r_{0,AB}}{{R_{AB}}^{6}}\right) \quad (eq.71)$$

where ε_{AB} and $r_{0,AB}$ are atom–couple dependent parameters, R_{AB} is the inter–atomic distance, $\left(\frac{1}{{R_{AB}}^{12}}\right)$ and $\left(\frac{1}{{R_{AB}}^{6}}\right)$ are the repulsive and attractive terms, respectively.

Regular DFT functionals do not properly account for dispersion, which is crucial to describe non–covalent interactions e.g., H–bonding and π–stacking. Over the past decade, various solutions have been proposed to account for the dispersive contribution. The main improvements were based on the explicit introduction of R^{-6} (i.e., DFT–D and DFT–D2), $R^{-8}$and R^{-10} (i.e., DFT–D3) decay functions.

3.2.1. DFT–D

To improve the DFT energy, Grimme proposed to simply add a carefully parameterized dispersion correction to the KS–DFT energies.[182] Therefore, the total energy is written as:

$$E_{DFT-D} = E_{DFT} + E_{disp} \quad (eq.72)$$

The dispersion correction is given by:

$$E_{disp} = -s_6 \sum_{i}^{M-1} \sum_{j>i}^{M} \frac{C_6^{ij}}{R_{ij}^6} f_{dmp}(R_{ij}) \quad (eq.73)$$

where s_6 is a scaling factor that is a functional−dependent parameter that must be adjusted to reach accuracy; C_6^{ij} is the dispersion coefficient of a given ij atom pair; f_{dmp} is the damping function that avoid near−singularities for small interatomic distances and double−counting effects of correlation at intermediate distances:

$$f_{dmp}(R) = \frac{1}{1 + e^{-d\left(\frac{R}{R_0}-1\right)}} \quad (eq.74)$$

where d indicates the slope of the damping function and R_0 is the sum of the respective vdW radii of both atoms involved.

The DFT−D methods is not only used for molecular complexes; other workers extended this correction to periodic systems.[183], [184]

3.2.2. DFT−D2

The DFT−D2 dispersion correction is given by the same equation as for DFT−D, but it differs by the slope of the damping function (d) and the atomic and atom-paired dispersion coefficients (Table 2).

Table 2. Comparison between DFT−D and DFT−D2 methods.

Parameter	DFT-D	DFT-D2
C_6^A	Ref.[185]	$0.05NI_p^A\alpha_p^{A*}$
C_6^{AB}	$2\frac{C_6^A C_6^B}{C_6^A + C_6^B}$	$\sqrt{C_6^A C_6^B}$
d	23	20

**N equals 2, 10, 18, 36 and 54 for atoms from rows 1-5 of the periodic table, I_p^A and α_p^A are the ionization potential and static dipole polarizabilities of atom A.*

The scaling factor s_6 is a key parameter in this formalism. It must be carefully parameterized in agreement with high−level post−HF methods and/or experimental data when available.

3.2.3. DFT−D3

Grimme [186] has improved his previous model by including a three-body term and higher order dispersion terms. A significant change in this so-called DFT−D3 method is that the C_6 dispersion coefficients are dependent on the molecular structure, which accounts for subtle effects. The new formalism of the dispersion energy is written as the sum of the two− (E_2) and three−body (E_3) terms:

$$E_{disp} = E_2 + E_3 \ (eq.75)$$

The two−body term includes the higher n^{th} −order classical dispersion terms:

$$E_2 = \sum_{A}^{M-1} \sum_{B>A}^{M} \sum_{n=6,8,\dots} s_n \frac{C_n^{AB}}{R_{AB}^n} f_{dmp,n} \quad (eq.76)$$

Differently from the empirically derived interpolation formula of DFT−D2, the atom-pair dispersion coefficients C_8^{AB} are calculated from the geometrical average of atomic quantities C_8^A and C_8^B. These coefficients are obtained by using multiple expansion of the atomic density.

Chai and Head−Gordon have developed the damping function used in DFT−D3, which is numerically stable for all n$^{\text{th}}$−orders. Nevertheless, other functions may be used as the (BJ) function:[187]

$$f_{dmp,n}(R) = \frac{1}{1 + 6\left(R/_{s_{r,n}R_{cut}}\right)^{-\alpha_n}} \quad (eq.77)$$

where $s_{r,n}$ is the n$^{\text{th}}$−order−dependent scaling factor of the cutoff radii and α_n is the steepness factor.

The three−body terms is expressed as:

$$E_3 = \sum_{A}^{M-1} \sum_{B>A}^{M-1} \sum_{\substack{C>A \\ C>B}}^{M} \frac{C_9^{ABC}(3cos\theta_a cos\theta_b cos\theta_c + 1)}{(R_{AB}R_{BC}R_{AC})^3} f_{dmp,(3)(\bar{r}_{ABC})} \quad (eq.78)$$

where θ_a, θ_b and θ_c are the internal angles of the triangle formed by the AB, BC and AC segments. C_9^{ABC} is the geometrical average of the previously defined atom-pair dispersion coefficients:

$$C_9^{ABC} \cong -\sqrt{C_6^{AB}C_6^{AC}C_6^{BC}} \quad (eq.79)$$

DFT−D3 is accurate for complex systems for the high-order dispersive term n=8, however it provides

unstable results with higher-order term as n=10.

3.2.4. DFT−NL

The dispersion energy can be directly obtained from a NL (non−local) correlation functional, which inherently accounts for this contribution.[188]–[190] The total energy is then $E_{DFT-D} = E_{DFT} + E_{NL}$, E_{NL} being a correction covering long−ranged interactions as those between fluctuating induced local dipoles; it is given by:

$$E_{NL} = \int dr\rho(r)\left[\beta(\boldsymbol{b}) + \frac{1}{2}\int dr'\rho(r')\Phi(r,r')\right] \quad (eq.80)$$

where $\Phi(r,r')$ depends on two electron coordinates simultaneously, including non-locality.

Using the specific construction called VV10[190] for the non-local $\phi(r_1,r_2)$ kernel. Note that in the NL−approach, a short−range attenuation functional-dependent parameter dubbed b; $\beta(b)$ is required to efficiently couple the total correlation energy to any particular exchange form used. Note also that a (more costly) double integration is required for E_{NL}, which implies the use of an additional numerical grid on top of the grid used for the local exchange–correlation functional; however, thanks to recent techniques this step is not a bottleneck for real calculations.[191]

The DFT−NL allows high accuracy in studying not only non−covalent interactions, but it is readily applicable to a large range of chemical elements and therefore particularly recommended for more general applications.[192] However, it requires more computational times compared to regular DFT functionals.

4. Time−Dependent DFT (TD−DFT)

While the description of the potential energy surface of ground states (GS) can be achieved by classical quantum methods (HF, DFT, semi−empirical), the potential energy surface of ES (excited state) is usually badly reproduced. The challenge of modern quantum chemistry is to provide an accurate description of ES as well as for GS. Different methods were developed (e.g., time−dependent HF and time−dependent configuration interaction). Most of the methods have proposed to solve the problem within the perturbation theory, in which the perturbation is a time-dependent excitation. The time−dependent DFT (TD−DFT) has been relatively recently developed. Most of their uses are achieved within a linear response theory, which is enough to reproduce the behavior of most of the physical systems (e.g.,

UV/visible absorption).

Runge and Gross have established a generalized Hohenberg–Kohn–Sham formalism within a time–dependent formalism.[193] Their idea consists on proving that for two different external potentials differing by a time-dependent constant $v_2(t) \neq v_1(t) + c(t)$, the corresponding time–dependent densities $\rho_1(r,t)$ and $\rho_2(r,t)$ are different. The Runge–Gross theorem, which is the time-dependent equivalence of the HK theorem, states that as soon as $\rho(r,t)$ is defined, all observables can be obtained.

The time–dependent KS equations are:

$$\left[-\frac{\nabla^2}{2} + v_{KS}(r,t)\right]\Phi_i^{KS}(r,t) = i\frac{\partial}{\partial t}\Phi_i^{KS}(r,t) \quad (eq.81)$$

in which:

$$v_{KS}(r,t) = v_{ext}(r,t) + v_{hartree}(r,t) + v_{xc}(r,t) \quad (\mathrm{eq.82})$$

where $v_{ext}(r,t)$ is the external potential, $v_{hartree}(r,t)$ is the classical electrostatic interaction between electrons and $v_{xc}(r,t)$ is the exchange-correlation potential.

The time-dependent KS equation can thus be written as:

$$\left[-\frac{1}{2}\nabla^2 + v_{ext}(r) + \int \frac{\rho'}{|r-r'|}dr' + v_{xc}(r)\right]\psi_i(r,t) = i\hbar\frac{\partial}{\partial t}\psi_i(r,t) \quad (eq.83)$$

TD–DFT allows characterizing ESs and subsequently UV/Vis absorption wavelengths and oscillator strengths.

Chapter 4 – Methodology

Chapter 4 – Methodology

Note for readers: *This article has been published in Chemical Physics Letters (I. Bayach et al., Chem. Phys. Lett., vol. 578, pp. 120–125, Jul. 2013). My contribution concerns the calculations of the association energies of the oligostilbenoid complex.*

The figure and reference formats and positions are sometimes modified compared to the original article to keep homogeneity of the thesis.

π–Stacked polyphenolic dimers: A case study using dispersion–corrected methods

I. Bayach [a,d], J.C. Sancho-García [b,c,*], F. Di Meo [a], J.-F.F. Weber [d], P. Trouillas [a,c,e]

Abstract: The accuracy of dispersion-corrected calculations (DFT–D2, DFT–D3 and DFT–NL) is assessed here, with large basis sets (def2–QZVP) to avoid incompleteness effects, for the most stable structure of a real-world polyphenol dimer chosen as an appropriate model. Natural polyphenols form such complexes with π–stacking playing a key-stabilizing role. Our benchmark calculations predict its existence favored by 22–24 kcal/mol with respect to the isolated monomers, mainly driven by both π–π and H–bonding interactions. The adequate comparison of lower-cost DFT–based methods allowed bracketing their expected accuracy. These results thus pave the way towards reliable studies of challenging aggregation processes of natural products.

[a] LCSN, Faculté de Pharmacie, Université de Limoges, 87025 Limoges, France

[b] Departamento de Química Física, Facultad de Ciencias, Universidad de Alicante, 03080 Alicante, Spain

[c] Laboratory for Chemistry of Novel Materials, University of Mons, 7000 Mons, Belgium

[d] Atta-ur-Rahman Research Institute for Natural Product Discovery, Faculty of Pharmacy, Universiti Teknologi MARA, 42300 Puncak Alam, Malaysia

[e] Department of Physical Chemistry, Faculty of Science, Palacky University, 771 46 Olomouc, Czech Republic

* Corresponding author at: Departamento de Química Física, Facultad de Ciencias, Universidad de Alicante, 03080 Alicante, Spain.

1. Introduction

Polyphenols *sensu lato* [194] (e.g., lignans and lignins, chalconoids and flavonoids, condensed and hydrolysable tannins, phlorotannins, depsides, stilbenoids, curcuminoids, anthraquinoids, etc.) constitute one of the most important groups of natural products, with some 10^5 defined structures.[195] They have been isolated from all plant organs (e.g., bark, wood, roots, leaves, flowers, fruit, and seeds) in which they may accumulate in substantial amounts. Therefore, they are quite abundant in human diets (e.g., fruit, vegetables, spices and beverages) exhibiting various potential health benefits (see for example [196], [197]). In order to fully rationalize and increase these beneficial effects, particular attention is paid to the chemical properties involved in e.g., (i) their biological properties and (ii) their biomimetic syntheses. Non−covalent complexes have been suggested in last decades to play an important role in these chemical properties. The high π−delocalization observed in the polyphenol backbone would allow monomer self−association, while the presence of OH substituents allows additional formation of strong intermolecular H-bonds. For example, non−covalent interactions in polyphenols lead to complexes involved in many key natural processes including: (i) plant color persistence;[198], [199] and (ii) regio− and stereo−selective biogenetic reactions (see for example [200]). However, the definite role of these weak interactions in polyphenol compounds is still under scrutiny; theoretical predictions are thus of (expectedly) high value for the rationalization of these processes and they appear as the only current way to provide a direct molecular visualization of these non−covalent dimers in solution. The theoretical results thus appear issued from a 'computational microscope' supporting the indirect experimental visualization (e.g., bathochromic shift observed in UV/Vis absorption measurements).

A small yet emblematic group of polyphenols is that of oligostilbenoids, biogenetically deriving from the oligomerisation of polyhydroxylated stilbene precursors. The large variety of their chemical structures allows for a broad range of biological activities including antibacterial, antioxidant, anti−fungal and anti−inflammatory properties.[201] Oligostilbenoid polymerization is a typical case where the importance of non−covalent interactions has been recently highlighted: regio− and stereo−selective synthesis is largely driven by the ability of these compounds to self−assembly in solution prior to the oxidative initiation stage.[48], [202] The extended π−delocalization of ε−viniferin derivative (Figure 1) is known to allow long−range interactions in solution,[202], [203] as it is indeed confirmed by NMR−based dynamical and structural studies.[204] Therefore, if theory aims at describing a complete picture of these interactions and corresponding supramolecular association at the molecular scale, the treatment of weak interactions is mandatory. Note also that regarding the large size of the (if any) dimer involved precludes

the use of methods that unfavorably scale with system size. Thus, Density Functional Theory (DFT) becomes the favored and more judicious choice here, also keeping in mind that such methodology should be used for large series of compounds similar in size, as a predictive tool in the near future. Taken into account these issues, the present study deals with structure and energetics of the non–covalent dimer of ε–viniferin, which is used as a prototype to tackle as accurately as possible these effects leading to dimerization. Various DFT functionals including dispersive effects are used and the associated association energies are compared to reference results. To present the achievements towards the above goals, the manuscript is structured as follows: Section 2 presents the different DFT–based theoretical methods able to largely deal with non–covalent interactions at both intra– and intermolecular levels. Section 3 reports the careful application of these methods concomitantly with their benchmarking. This would then allow reaching predictive yet robust conclusions about the stability of this kind of complexes, and complementarily shedding light about the possible routes followed in their reactivity.

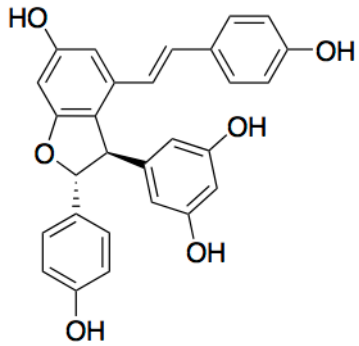

Figure 1. Chemical structure of the studied compound. The hydrogen atoms and corresponding C–H bonds have been omitted for clarity. Figure created with ChemDraw.

2. Theoretical methods

2.1. Modeling dispersion effects

Dispersion physics arises from locally induced interactions, be them intra– or intermolecular, after the response of the electronic cloud in one region to the presence of instantaneous and fluctuating charge densities in another.[205] In other words, whenever polarizable electronic clouds are present in two spatially separated but interacting fragments or subsystems, even if weakly overlapping, these correlated dipole–dipole interactions might clearly drive self–assembly or supramolecular organization. To account for these interactions is a real challenge for any theoretical method currently in use. A purely ab initio treatment would therefore imply the use of energy magnitudes depending simultaneously of properties at

two separate points in space **r** and **r'**. This is one of the reasons why classical Møller–Plesset perturbation theory truncated at second order (MP2) is able to partly capture the physics behind these interactions. It has been considered as the pioneering yet simplest theoretical method to be applied within this context. Contrarily to this, unmodified or poorly fitted DFT–based functionals completely fails due to the short–sight treatment of matter imposed by the dependence of common (semi–local) functionals on the density (ρ) and its gradient ($\nabla\rho$) on r exclusively. Here we briefly review the most common DFT–based dispersion methods currently applied [206] to overcome this undesired but generalized drawback.

Due to the difficulty to self–consistently introduce the dispersion energy (E_D) into the computational treatment, one normally adds this contribution to the electronic energy in a post self–consistent way:$E_{DFT+D} = E_{DFT} + E_D$, the density thus remains unaffected upon the dispersion treatment. The modeling of E_D term is based on the well–known pairwise additivity of effects between atoms A and B belonging to weakly overlapping fragments:

$$E_D = \sum_{B>A}^{N} -[\frac{C_6^{AB}}{R_{AB}^6} - \frac{C_8^{AB}}{R_{AB}^8} - \frac{C_{10}^{AB}}{R_{AB}^{10}} \dots] \quad (1)$$

where C_j^{AB} are interatomic dispersion coefficients and R_{AB} is the distance between the two atoms involved. The simplest approach, coined as D2 [207] truncates the expansion at first order providing the $1/R^6$ attractive term as found in the classical Lennard–Jones potential. This term is however weighted introducing a functional–dependent parameter (S_6) to efficiently couple both terms, E_{DFT} and E_D:

$$E_{D2} = -S_6 \sum_{B>A}^{N} \frac{C_6^{AB}}{R_{AB}^6} f(R_{AB}), \quad (2)$$

also relying on a damping function, $f(R_{AB})$, to efficiently and more physically switch from the infinite separate limit to distances belonging to the binding region.[208] This correction has been successfully applied for complexes of the most interest,[177], [209], [210] although a more sophisticated correction (D3) has been recently introduced to overcome some known limitations of the latter.[211] In this case the correcting term is given by:

$$E_{D3} = -\sum_{B>A}^{N} \sum_{n=6,8} S_n \frac{C_n^{AB}}{C_{AB}^n} f_n(R_{AB}), \quad (3)$$

expanding the former series and introducing now n^{th}–order dispersion coefficients allowing a better respond to changes in chemical environment. The mathematical form imposed to the damping function

introduces two new parameters, $S_{r,n}$, to be defined for each value of n,

$$f_n(R_{AB}) = \frac{1}{1 + 6(\frac{R_{AB}}{S_{r,n}R_0^{AB}})^{-\alpha}}, \quad (4)$$

with the ratio $R_0^{AB} = \sqrt{\frac{C_8^{AB}}{C_6^{AB}}}$. Note that the dumping function reduces to a simpler form for DFT–D2 and that more details about the form and (expectedly) negligible influence of other devised damping functions can be found in Ref.[212].

Interestingly, there is a recent renewed interest [213]–[215] to obtain the dispersion energy directly from the electron density through a non–local (NL) correlation functional, which inherently account for this contribution. The total energy is now $E_{DFT+D} = E_{DFT} + E_{NL}$, with E_{NL} being a correction covering mostly long–ranged interactions between these instantaneous and fluctuating induced local dipoles:

$$E_{NL} = \int dr\rho(r)\left[\beta + \frac{1}{2}\int dr'\rho(r')\phi(r,r')\right] \quad (5)$$

using the specific construction called VV10 [216] for the $\phi(r,r')$ kernel. Note that in the NL–approach a short–range attenuation functional–dependent parameter dubbed b, $\beta = \beta(b)$ is required to efficiently couple the total correlation energy to any particular exchange form used. Note also that a (more costly) double integration is required for E_{NL}, which implies the use of an additional numerical grid on top of the grid used for the local exchange–correlation functional; however, thanks to recent techniques [217] this step is not a bottleneck for real calculations.

2.2. Technical details

The choice of the exchange–correlation functionals BP86 and B3P86 is motivated by two features: (i) the excellent performance shown by the latter model for bond dissociation energies [218]–[220] and optoelectronic properties [221] of many different polyphenols; and (ii) the lower computational cost of the parent non–hybrid model (BP86), which would allow applications to larger real–world systems and large series, due to the pervasive trade–off between accuracy and computational resources. The related parameters of Eqs. (2)–(4) are reported in Table 1. Whereas these are taken from Grimme's work for BP86 (–D2 or –D3), we have recently extended the B3P86 model (–D2) in this way.[198] The attenuation parameter b required for the use of both models together with Eq. (5), BP86–NL and B3P86–NL, is also assessed here for the first time (to the best of our knowledge) in order to obtain (vide

infra) its optimum value (Table 1).

All calculations were performed with the ORCA program [222] with the built in def2−xVP family of basis sets, unless otherwise noticed, i.e., the hierarchy def2−SVP, def2−TZVP, and def2−QZVP. The cost of the calculations was reduced in all cases by the use of the 'resolution of the identity' (RI) [223] and/or the 'chain−of−spheres' (COSX) [224] algorithms, for Coulomb or exchange integrals, respectively; note that the largest calculations performed here involve 7500 primitive basis functions. Concerning numerical grids for integration, to be on the safer side, their size was always made larger than hardwired defaults: grid4 and grid6 for computing E_{DFT} and E_{NL}, respectively. Due to the (expected) flatness of potential energy curves around the equilibrium geometry, we also imposed larger than default thresholds for the optimization algorithm.

The intermolecular interaction or association energy (ΔE) was calculated as the difference between the energy of the complex (E_{CX}) and those of the free monomers I and II (E_{MON-I} and E_{MON-II}). A negative value for ΔE thus implies the existence of the complex with respect to the pair of isolated monomers.

The basis set superposition error (BSSE), which introduces a spurious (over stabilizing the dimer formation) energetic $\Delta E\ (BSSE)$ contribution to ΔE was calculated by the standard counterpoise method, giving thus rise to:

$$\Delta E = [E_{CX}^{CX}(CX) - E_{MON-I}^{MON-I}(MON-I) - E_{MON-II}^{MON-II}(MON-II)] - \Delta E(BSSE), \quad (6)$$

in which:

$$\Delta E\ (BSSE) = [E_{MON-I}^{CX}(CX) - E_{MON-I}^{CX}(MON-I) + E_{MON-II}^{CX}(CX) - E_{MON-II}^{CX}(MON-II)] \quad (7)$$

where $E_P^Q(R)$ is the energy of fragment P calculated at the optimized geometry of Q and with the basis set of R. Note how this procedure always implies an extra significant computational effort, which must be considered as a limit for further extensions of this methodology to large series of compounds. On the other hand, the BSSE can be nearly minimized, and thus the contribution $\Delta E\ (BSSE) \cong 0$, by applying a very large basis set, the def2−QZVP here; we will thus compare the results of both approaches to estimate the results at the Complete Basis Set (CBS) limit.

Table 1. List of parameters entering into the dispersion-corrected methods employed.

Method	S_6	$S_{r,6}$	S_8	$S_{r,8}$	b
BP86–D2	1.050	1.100	-	-	-
B3P86–D2	0.780	1.100	-	-	-
BP86–D3	1.000	1.139	1.683	1.000	-
BP86–NL	-	-	-	-	4.4
B3P86–NL	-	-	-	-	5.1

3. Results and discussion

3.1. Optimized geometry of the complex

The geometry of the complex has been calculated at the BP86–D2, BP86–D3, and B3P86–D2 levels with the def2–SVP basis set; the geometry is not expected to significantly change upon use of larger basis sets. Figure 2 shows two views of the head–to–tail complex formed, no matter the theoretical level employed: (i) a large π–stacking of the backbone upon resulting monomer interaction; (ii) a release of steric hindrance caused by the phenolic moieties acting as substituents after adopting (almost) perpendicular positions with respect to the central backbone; and (iii) the strong directionality and force of some intermolecular hydrogen bonds $O-H\cdots O$, occurring within the two heads or at the tails; to name just a few interesting facts. The dimer intermolecular distance, defined as the closest distance between carbon atoms of the central backbone belonging to both monomers, is around 2.99, 3.02, and 2.98 Å, at the BP86–D2, BP86–D3, and B3P86–D2 levels, respectively. These features clearly show how the choice of the exchange–correlation functional is of relatively little importance to describe the geometrical features, once a proper correction for dispersion is considered. Whereas the backbone of isolated monomers is almost completely planar, the strong intermolecular interactions (mainly H–bonds) slightly bent the monomers in the complex geometry. These hydrogen bonds located at the edges of the backbone reduce the intermolecular distance to values that are normally repulsive (the sum of C–C van der Waals radii is 3.5 Å); this effect has also recently been detected with halogenated polycyclic aromatic complexes.[225]

3.2. Reference data

The size (N) of the system tackled here precludes the use of highly sophisticated yet very costly ab initio

methods like CCSD(T) or some of its variants,[226] despite recent progress [227] to reduce its formal dependence with size: $O(N^7)$. The so-called Spin−Component−Scaled (SCS)[§§] MP2 method [228] was used as the current base−line to deal with dispersion effects. Note that despite being a method scaling as $O(N^5)$, which dramatically alleviates the computational cost with respect to CCSD(T) this (general purpose) method is known to provide remarkable accuracy for a wide variety of covalent and non−covalent interacting molecular systems,[229] including para−diiodobenzene [230] or anthracene [231] dimers extracted from crystalline structures and paracyclophane derivatives,[232] and will be thus used as reference in the following. Note that all these single−point calculations were performed here at the BP86−D3 optimized geometry for both the complex and the isolated monomers. As expected, the calculated SCS−MP2 interaction energy decreases, upon augmenting the size of basis sets: -21.8, -18.4, and -16.2 kcal/mol with the def2−SVP, def2−TZVP, and def2−QZVP basis sets, respectively. SCS-MP2 has been shown to slightly underestimate non-covalent association energies;[233] thus, within the SCS−MP2−D2 corrected method ($S_6 = 0.6$, obtained with a large TZVPP basis set [233]), the combination is somewhat considered as an artifact dropping the values to -24.3 and -22.1 kcal/mol with the def2−TZVP and def2−QZVP basis sets, respectively. However, the high stability of these complexes is confirmed with a new SCS−MP2 version, namely SCS−S66−MP2 [234] specifically suited for non−covalent interactions, which is additionally known to become very accurate in the description of strong hydrogen bonds. A -26.5 kcal/mol energy of complexation was obtained with the def2−TZVP basis set, which serves to firmly bracket the reference value and to validate afterwards the DFT−based approximations employed.

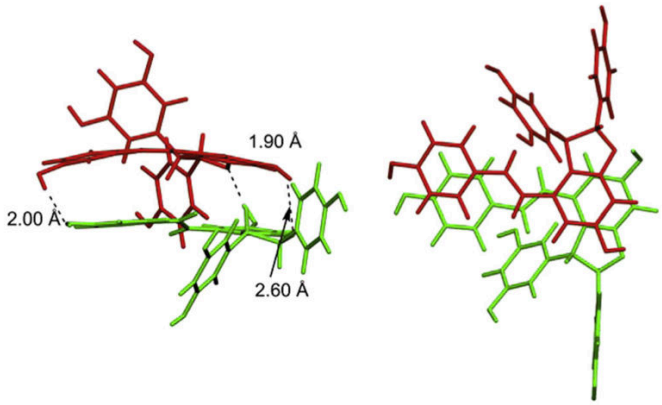

Figure 2. Optimized structure of the studied dimer from perpendicular (right) and side (left) views. Figure created with VMD.

[§§] This method scales differently the contribution to correlation energy arising from opposite- or same-spin contribution.

3.3. Assessment of DFT−based dispersion corrections

Further reduction of computational time and associated resources will necessarily proceed through the use of DFT−based approaches scaling as much as $O(N^4)$, e.g. B3P86, or even as $O(N^3)$, e.g. BP86. The association energies obtained with BP86−D2, BP86−D3, and B3P86−D2 are compared to the reference data in Figure 3. Note first that the complex is predicted to be unbound without these −D2 or −D3 corrections, independently of the functional employed. Note also that the calculations with the large def2−TZVP and def2−QZVP basis sets were done at the def2−SVP respective optimized geometries. The association energies are always largely affected by the BSSE: the energy decreases by 7–8 kcal/mol when going from the def2−SVP to the def2−TZVP, and only by 1.5–2.0 kcal/mol upon extension to the nearly saturated def2−QZVP basis set. The use of the counterpoise correction, see Eq. (7), brings the results close to those achieved by using the large def2−QZVP basis set, which can be thus considered near to the (unknown) CBS limit. As a matter of example, the counterpoise−corrected BP86−D3 association energies are -15.8, -18.5, and -18.6 kcal/ mol, with the def2−SVP, def2−TZVP, and def2−QZVP, respectively, as compared to the values obtained without BSSE correction, i.e., -28.0, -20.9, and -19.1 kcal/mol for the three basis set, respectively. The underlying BSSE can be thus estimated to be -12.2 (unacceptable), -2.4 (mildly acceptable), and -0.5 (within the 'chemical accuracy' range) kcal/mol, for the def2−SVP, def2−TZVP or def2−QZVP basis sets, respectively. This trend is similar to all the functionals tested here. Note also that this way to calculate the BSSE is believed to slightly overestimate its effect, and some authors even propose to scale it down by a factor between 0.5 and 1.0.[235], [236] This is the reason why in the following we will estimate (if any) the CBS limit as the average between the def2−QZVP values with and without the counterpoise−correction. As a matter of example, the BP86−D3/CBS result will be thus -18.8 ± 0.2 kcal/mol, being the error bar the difference of each method with respect to its averaged value.

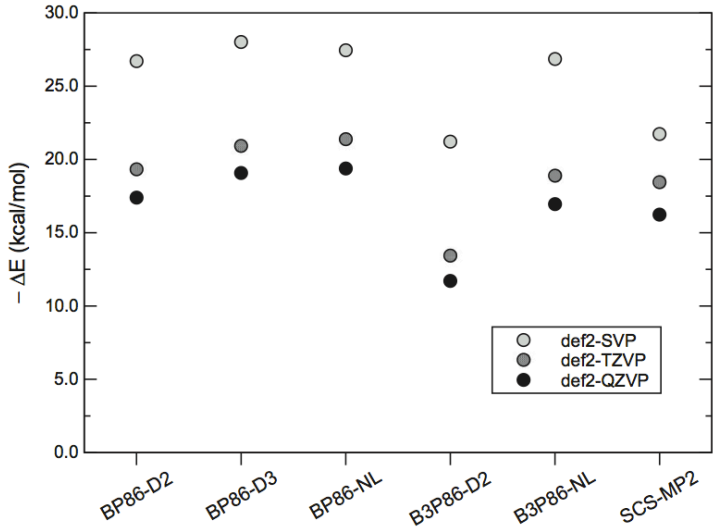

Figure 3. BSSE–uncorrected association energies (in kcal/mol) at several dispersion–corrected DFT levels, and with the sequence of def2–xVP (x = T,Q) basis sets. Figure created with Xmgrace.

The S_6 parameter entering into the B3P86–D2 form was originally assessed with the cc–pVTZ basis set for a non–covalent polyphenol dimer,[198] i.e., with very similar interaction than the present dimer. The effect of using a particular family (cc–pVxZ or def2–xVP) of basis sets has been also investigated here as a by-product. The cc–pVTZ value is -14.5 kcal/mol, which reduces to -11.2 kcal/mol after the corresponding counterpoise correction, which is compared to -13.4 (or -11.4 when BSSE–corrected) and –11.7 kcal/mol with the def2–TZVP or def2–QZVP, respectively. The S_6 parameterization is thus not expected to be significantly influenced by this basis set issue and would not significantly affect the association energies.

We also recognize at this stage that the corrections discussed so far are pairwise additive, which might be related to a slight tendency of BP86–D3 towards overbinding. A way to evaluate the (repulsive) amplitude of the three–body contribution is through the function [237]:

$$E_{3-body} = C_9^{ABC} \frac{(3cos\theta_a cos\theta_b cos\theta_c + 1)}{R_{AB} R_{BC} R_{AC}}, \quad (8)$$

where ABC are all the atom triples, θ_i are the internal angles of the triangle formed by $R_{AB}–R_{BC}–R_{AC}$, and the coefficient is approximated by $C_9^{ABC} = -\sqrt{C_6^{AB} C_6^{BC} C_6^{AC}}$. While this contribution is believed to be negligible for small complexes, around 2% of the association energy of the benzene dimer,[238] it might become crucial for larger systems, around 25% for two graphene layers.[237] In the present case, this contribution amounts for 1.2 kcal/mol (which is 6–7% of the association energy if we take for instance the BP86–D3/CBS result of -18.8 kcal/mol as reference for estimating the weight of this 3–body

correction). This correction thus reduces the difference between the BP86–D2 and BP86–D3 results and appears not negligible. However, it is not expected to significantly influence the conclusions about the relative performance of methods and the derived association energies.

The relevance of the BP86–NL and B3P86–NL models was also assessed for the present non–covalent polyphenol dimer. In this case, the exchange–correlation functional is defined by:

$$E_{XC}[\rho] = E_X[\rho(r)] + E_c^{local}[\rho(r)] + E_c^{non-local}[\rho(r), \rho(r')] \quad (9)$$

where E_X is the B and B3 exchange parts, respectively, and E_c^{local} ($E_c^{non-local}$) is P86 (VV10) in both functionals. Again the sequence of def2–xVP basis sets was used. The initial value imposed to the b parameter for an efficient coupling of non–local correction with the exchange–correlation part was the available values for related models,[239] i.e., b=3.5 (b=4.0) for BP86 (B3P86). Note that for the cases known up to now (BLYP vs. B3LYP and revPBE vs. revPBE0) the value of b turns to be always lower for pure than for hybrid methods, as it should be upon a careful inspection of the whole function $\beta = \beta(b)$ entering into Eq. (5). We then accordingly modified it in a systematic way to check the influence on the association energies. Table 2 presents the corresponding association energies, leading to the following conclusions: (i) going across the sequence def2–SVP/def2–TZVP/def2–QZVP largely reduces the BSSE in line with the observations made before; and (ii) the association energies depend on b values, B3P86 always providing larger stabilization energies than BP86 at same b–value. Figure 4 exemplifies the amplitude of this variation for both BP86–NL and B3P86–NL models when the large def2–QZVP basis set is employed.

Table 2. Association energies (in kcal/mol) at several non−local dispersion−corrected DFT levels, with the sequence of def2−xVP basis sets, as a function of the attenuation parameter.

Method	Basis set	ΔE (kcal/mol)				
		b = 3.5	b = 4.0	b = 4.5	b = 5.0	b = 5.5
BP86−NL	def2−SVP	-38.5	-32.3	-27.4	-23.5	
	def2−TZVP	-32.0	-25.5	-20.5	-16.4	
	def2−QZVP	-29.9	-23.5	-18.5	-14.4	
B3P86−NL	def2−SVP		-35.6	-30.8	-26.9	-23.6
	def2−TZVP		-28.6	-23.6	-19.6	-16.3
	def2−QZVP		-26.7	-21.7	-17.7	-14.4

In the hope to obtain a refined value of b for the use of this correction for polyphenol compounds, three systems (benzene–benzene, benzene–methanol, phenol–phenol, see Figure 5) were correspondingly selected. They are representative of the leading p–p, p–OH, and OH–OH interactions, respectively, as found in non−covalent polyphenol dimers. Note that very accurate CCSD(T)/CBS results are available in the literature for the association energy of these complexes of moderate size,[240], [241] which will thus serve to guarantee the lowest possible deviation with respect to any benchmark thought. To do that, the Mean Absolute Deviation (MAD) is reduced as much as possible for association energies calculated at the BP86−NL and B3P86−NL levels, according to the b values and with respect to the CCSD(T)/CBS association energies taken as reference. Note also that the large def2−QZVP basis set is used here to avoid any spurious BSSE. The following optimum b=4.4 and b=5.1 values were found, providing a MAD lower than 0.2 kcal/mol in both cases with respect to the CCSD (T)/CBS results. We thus now predict with these optimized b values, and again with the def2−QZVP basis set, association energies of -19.4 and -17.0 kcal/mol, with the BP86−NL and B3P86−NL models respectively, which are very close to the benchmark SCS−MP2−based results (Figure 3).

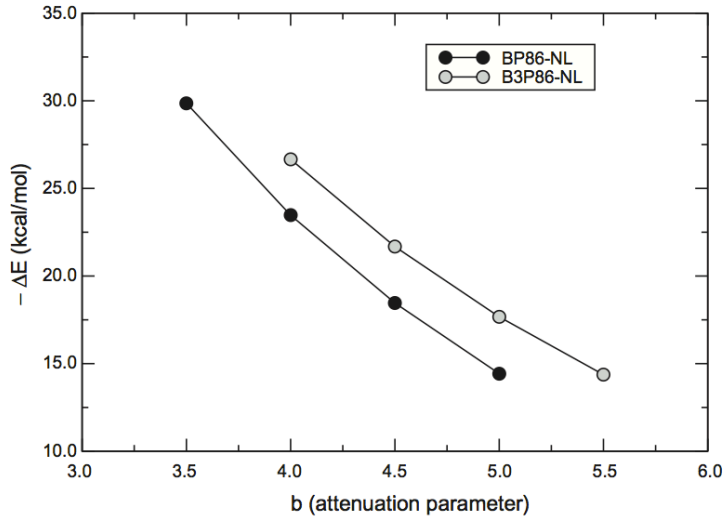

Figure 4. BSSE–uncorrected association energies (in kcal/mol) at several non–local dispersion–corrected DFT levels, with the def2–QZVP basis set, as a function of the attenuation parameter. Figure created with Xmgrace.

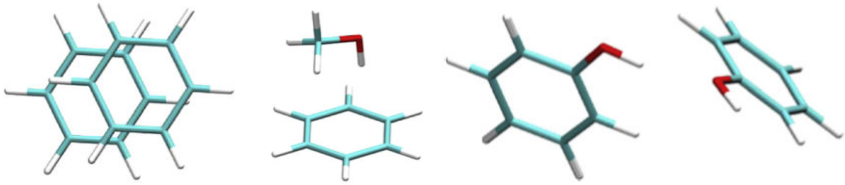

Figure 5. Selected interacting dimers for benchmarking. From top to bottom: Benzene–Benzene, Benzene–Methanol, and Phenol–Phenol. Figure created with VMD.

4. Conclusions

The association or interaction energy of a large real–world non–covalent polyphenol dimer has been elucidated by dispersion–corrected DFT methods using several flavors. First, benchmark calculations at improved second–order perturbation theory were performed to adequately bracket the stabilizing energy gained when the two monomers self–associate to form the complex. The use of large basis sets, up to the def2–QZVP, leads to sufficiently converged results. Interestingly, we estimate at the complete basis set limit (within an expected error bar or about 0.2 kcal/mol) complexation energies of -17.6 kcal/mol at both the BP86–D2 and BP86–B3 levels, the latter after taking into account the 3–body interactions, and of –11.5 kcal/mol at the B3P86–D2 level. When these functionals combine in a purely ab initio fashion with a correlation correction (the VV10 functional) and with an optimum value for the attenuation b–parameter entering into this non–local functional, the values are -19.4 and -17.0 kcal/mol (BP86–NL and B3P86–NL, respectively). All these schemes seem to slightly underestimate the

SCS−S66−MP2−based results although, however, it is satisfying to see that, even being fairly different in both the underlying density functional and the way in which they incorporate the missing dispersion forces, they predict enough stabilization energy to anticipate the existence of this kind of complexes almost independently of expected thermal or environmental conditions. Thus, a practical yet accurate combination of DFT−D2/ DFT−D3 searches along potential energy hypersurfaces, thanks to rapid evaluation of gradients with these levels and their moderate scaling with size, together with refinements employing DFT−NL might constitute a valid strategy for further future studies.

Chapter 5 – Methodological assessments of dispersion between prototypes of polyphenol non-covalent complexes

Chapter 5 – Methodological assessments of dispersion between prototypes of polyphenol non-covalent complexes

Note for readers: *This article is under minor revisions in Chemistry–An Asian Journal. It consists on an experimental and theoretical study of the biosynthesis of oligostilbenoids. I only participate to the theoretical elucidation. The entire manuscript is incorporated in this PhD to keep consistency.*

The figure and reference formats and positions are sometimes modified compared to the original article to keep homogeneity in the thesis.

Oligostilbenoids from the heartwood of *N. heimii*: role of non–covalent association in their biogenesis

Bayach, I.,[a,#] Manshoor, N.,[b, #] Sancho García,[c] J.C., Choudhary, M. I.,[d] Trouillas, P.,[e,f,g,*] and Weber, J. F. F.[b,*]

Abstract: Four new oligostilbenes, including one dimer and three tetramers of resveratrol, *i.e.* heimiols B-E (**1-4**) were isolated from the heartwood of *Neobalanocarpus heimii* (Dipterocarpaceae), together with thirteen known resveratrol oligomers (**5-17**). Examination of structural diversity of the isolated oligostilbenes led to hypothesise their biogenetic origin through a small number of versatile chemical pathways. These hypotheses are strongly supported by computational calculations (based on the density functional theory, DFT) that were performed to rationalize conformational rearrangements and thus provide insights into the mechanism of oligostilbenoid biosynthesis. Non–covalent complexes are believed to drive the regio– and stereo–selectivity of the oligomerisation reactions.

Keywords: Neobalanocarpus heimii • Oligostilbenes • Biosynthesis • DFT(–Dispersive) • Non–covalent interactions

[a] Imene Bayach: LCSN - Faculté de Pharmacie, Université de Limoges, 2 rue du Dr Marcland, 87000 Limoges, France

[b] Dr. Nurhuda Manshoor and Prof. Dr. Jean-Frédéric F.Weber: Atta-ur-Rhaman Institute for Natural Product Discovery (AuRIns), Faculty of Pharmacy, Universiti Teknologi MARA, 42300, Bandar Puncak Alam, Selangor, Malaysia. E-mail: jffweber@puncakalam.uitm.edu.my

[c] Prof. Dr Muhamad Iqbal Choudhary: H. E. J. Research Institute of Chemistry, International Center for Chemical and Biological Sciences, University of Karachi, Karachi, Pakistan.

[d] Dr. J.C. Sancho-García: Departamento de Química Física, Facultad de Ciencias, Universidad de Alicante, 03080 Alicante, Spain

[e] Dr. Patrick Trouillas: INSERM, UMR-S850, Faculty of Pharmacy, 2, Rue du Dr Marcland, 87025 Limoges Cedex, France. E-mail: patrick.trouillas@unilim.fr

[f] Regional Centre of Advanced Technologies and Materials, Department of Physical Chemistry, Faculty of Science, Palacký University, tř. 17 listopadu 12, 771 46 Olomouc, Czech Republic

[g] Laboratoire de Chimie des Matériaux Nouveaux, Université de Mons, Place du Parc 20, B-7000 Mons, Belgium

* Corresponding author # These authors contributed equally

1. Introduction

Oligostilbenes are major secondary metabolites of plants belonging to the Dipterocarpaceae family. About one third of oligostilbenes ever isolated were from dipterocarps,[242] which makes them relevant chemical markers for the family. They are found in various plant parts (the leaves, barks, woods and seeds), but were obtained most often from the heartwood. Most oligostilbenes found in this family include at least one oxygenated heterocyclic ring, usually in the form of a *trans*-2-aryl-2,3-dihydrobenzofuran ring.[243] In a preceding paper, we reported the characterization of a novel dimeric stilbene and four known oligostilbenoids from the heartwood of *Neobalanocarpus heimi*.[244] Further investigation of the methanol extract led to the isolation of four new resveratrol oligomers along with thirteen known oligostilbenes. We thus report herein the structural elucidation of a new stilbene dimer, namely heimiol B (**1**), and three tetramers, heimiols C (**2**), D (**3**) and E (**4**). After a complete description of the elucidated chemical structures, the biogenesis of these compounds is proposed as a result of close examination of the heartwood extract composition and recent insights in oligostilbene biosynthetic mechanisms.[203] The hypotheses based on supramolecular arrangements are elegantly supported by DFT (density functional theory) calculations, augmented by dispersive corrections (DFT-D) to properly account for non-covalent interactions.

2. Results and Discussion

Compounds **1-4** (Figure 1) are four new oligostilbenes that were isolated from the methanol extracts of the heartwood of *Neobalanocarpus heimii* by repeated chromatography on C18 silica-bonded columns.

❖ ***Heimiol B***

Heimiol B (**1**) was obtained as a light brown residue. It exhibited a $[M-H]^-$ ion at *m/z* 469.1288 in HR-ESI-TOF-MS compatible with the molecular formula $C_{28}H_{22}O_7$, suggesting **1** to be an oxidative dimer of resveratrol. This was supported by the ^{13}C-NMR spectrum (Table 1), which showed twenty-eight signals, assignable to four sp^3 and twenty-four sp^2-hybridized carbons. The ^{1}H-NMR spectrum of **1** (Table 1) displayed two sets of *ortho*-coupled aromatic hydrogen signals in AA'BB' spin systems at d 7.34, 7.03, 6.75 and 6.71 (2 H, each d, J = 8.7 Hz), assignable to two independent 4-hydroxyphenyl groups, two sets of meta-coupled aromatic hydrogen signals at d 6.36, 6.52, 6.24 and 6.08 (l H each, d, J = 2.1 Hz), assignable to two di-substituted resorcinol moieties, and four olefinic hydrogen signals at d 5.13, 4.90, 4.61 and 4.22 (l H each, d, J = 2.0 Hz). The HMBC cross peaks between methine protons and aromatic carbons (H-7a/C-1a, H-7a/C-9a, H-8a/C-9a, H-8a/C-10a, H-8a/C-14a, H-7b/C-1b, H-7b/C-2(6)b, H-7b/C-9b, H-8b/C-1b, H-8b/C-9b, H-8b/C-10b and H-8b/C-14b) allowed establishment of connections between aromatic rings and their corresponding benzylic methine groups as described in Figure 2.

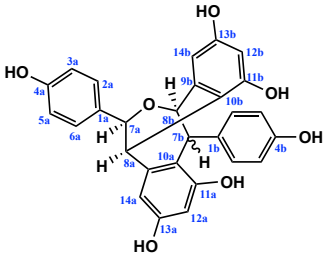

1 : H-7b = α
5 : H-7b = β

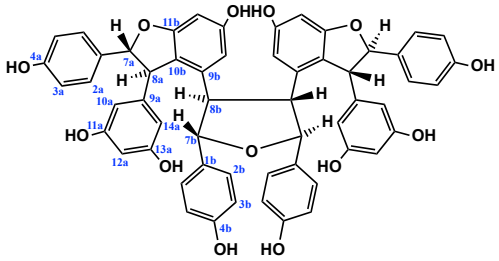

2

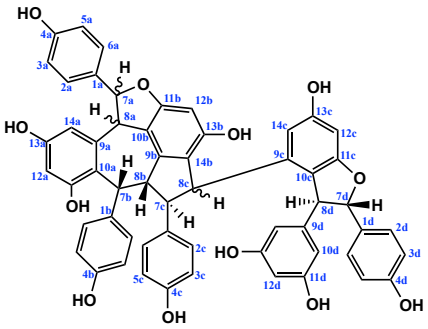

3 : H-7a=α H-8a=β H-8c=α
6 : H-7a=β H-8a=α H-8c=β

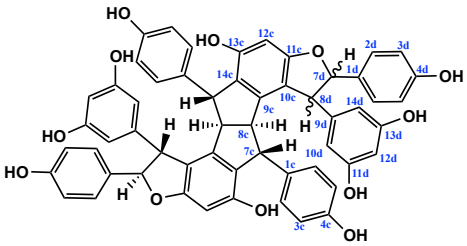

4 : H-7d=β H-8d=α
7 : H-7d=α H-8d=β

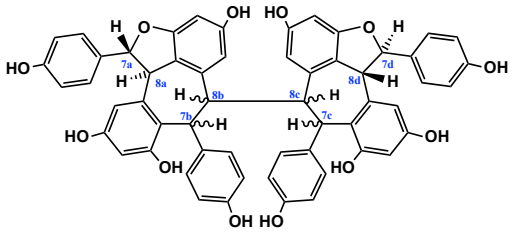

8 : H-7b=β H-8b=α H-7c=α H-8c=β
9 : H-7b=α H-8b=β H-7c=β H-8c=α
10 :H-7b=β H-8b=α H-7c=β H-8c=α
11 :H-7b=α H-8b=α H-7c=β H-8c=α

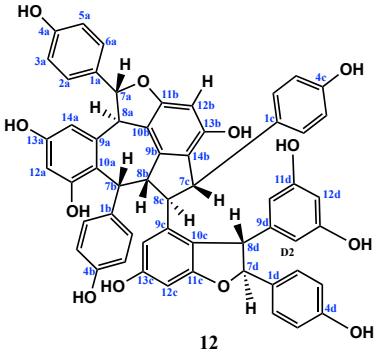

12

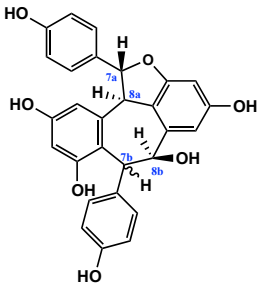

13 : H-7b=α
14 : H-7b=β

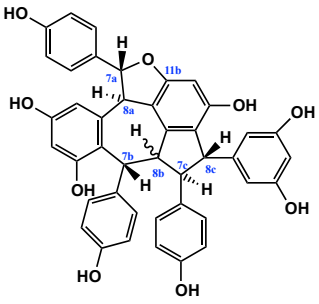

15 : H-8b=α
16 : H-8b=β

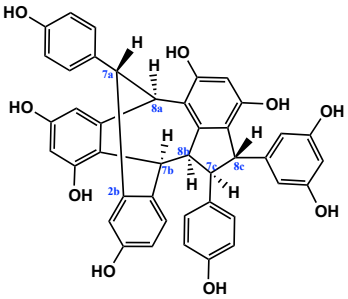

17

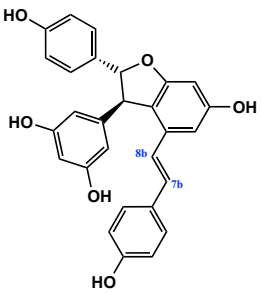

18

Figure 1. Oligostilbenes isolated from *Neobalanocarpus heimii* heartwood.

The HMBC spectrum also displayed H-7a/C-10b, H-8a/C-9b, H-8a/C-10b, H-8a/C-11b, H-7b/C-9a, H-7b/C-10a, H-7b/C-11a and H-8b/C-10a correlations indicating linkages between both resveratrol units of the dimer. Such correlations were similar to those obtained with ampelopsin A (**14**). However, the J_{H-H} of 2.0 Hz for the benzylic hydrogen at the 7a position was incongruent with the presence of a dihydrofuran ring. The ^{13}C signals at d 81.4 (C-7a) and 81.5 (C-8b) correspond to benzylic carbons bearing an oxygen atom. The excess of only one oxygen atom in the molecule suggested that both carbons were connected to the same oxygen atom, forming an ether linkage between C-7a and C-8b. The long-range correlation H-7b/C-9a indicated a linkage between C-7b and C-10a. Such correlations establish an oxygenated seven-membered ring. The cross peaks H-7a/C-10b, H-8a/C-9b, H-8a/C-10b and H-8a/C-11b showed the presence of a bridged framework in the molecule similar to that of heimiol A. Based on NOESY experiment, correlations between H-7a/H-8a and H-7b/H-8b were observed, which indicate *cis* configurations. Further assessment of NOE correlations revealed cross peaks between H-7a and H-8b, indicating *syn* orientation. The HMBC and NOE correlations and relative stereochemistry of **1** are shown in Figure 2. Based on this structure a conformational analysis was obtained at the DFT level (see Figure 2 and Method section for computational details). No intra H-bonding was observed in the most stable conformer.

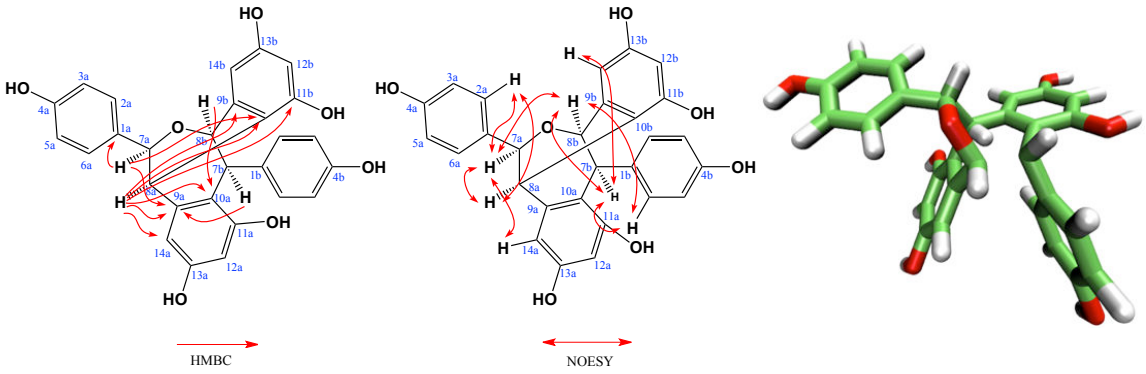

Figure 2. Selected HMBC and NOESY correlations and 3D computed most stable conformation of **1**.

❖ ***Heimiol C***

Heimiol C (2) was obtained as a dark brown amorphous solid. It exhibited a pseudomolecular [M+Na]+ ion peak at m/z 947.2679 in ESI-MS. On the basis of HR-MS data, the molecular formula of 2 was determined to be $C_{56}H_{44}O_{13}$, compatible with a tetramer of resveratrol composed of four resveratrol units with an additional oxygen atom. However, both the 1H and 13C-NMR spectra of compound 2 (Table 1) showed half the signals corresponding to the above molecular formula. This observation indicated that compound 2 is a symmetrical molecule with an additional oxygen atom being located along the axis of

symmetry. This suggested the presence of an ether linkage between both symmetrical moieties. The 1H-NMR and COSY spectra exhibited the signals of two sets of ortho-coupled aromatic protons in the form of AA'BB' systems at d 6.91, 6.68 (4 H each, d, J = 8.4 Hz) and d 6.67, 6.54 (4 H each, d, J = 8.4 Hz). They were assignable to four 4-hydroxyphenyl groups. Signals from a set of meta-coupled aromatic protons from a 1,2,3,5-tetra-substituted benzene ring were observed at d 6.06 and 6.83 (2 H each, d, J = 1.9 Hz). The 1H-NMR spectrum also included a signal at d 6.20 (2 H, t, J = 2.0 Hz). From the splitting pattern and chemical shift, the signal was assignable to the proton of a resorcinolic B ring. However, in the COSY spectrum, that signal did not show any correlation.

Table 1. ^{1}H- and ^{13}C-NMR spectral data for compounds **1-4**.

No	**1**		**2**		**3**		**4**	
	^{1}H	^{13}C	^{1}H	^{13}C	^{1}H	^{13}C	^{1}H	^{13}C
1a		133.4		131.5		134.2		134.7
2a, 6a	7.34 (d, 8.7)	128.7	6.91 (d, 8.4)	128.3	6.92 (d, 8.5)	127.2	7.10 (d, 8.5)	127.2
3a, 5a	6.75 (d, 8.7)	115.0	6.68 (d, 8.4)	114.8	6.68 (d, 8.5)	116.1	6.73 (d, 8.5)	116.4
4a		158.1		157.1		158.1		157.9
7a	4.90 (d, 2.0)	81.5	5.10 (d, 7.3)	94.3	5.44 (d, 4.3)	94.0	5.29 (d, 1.3)	93.9
8a	4.61 (d, 2.0)	46.2	3.42 (d, 7.3)	54.7	4.10 (d, 4.3)	57.3	4.29 (d, 1.3)	57.1
9a		142.8		146.5		147.9		148.5
10a		116.2	5.90 [a] (br s)	106.0 [b]		119.8	6.27 (d, 1.8)	106.5 [c]
11a		156.2		158.4		159.0		162.8
12a	6.08 (d, 2.1)	102.4	6.20 (t, 2.0)	101.2	5.94 (d, 1.9)	93.5	6.06 (t, 1.8)	102.1
13a		156.8		158.4				162.8
14a	6.24 (d, 2.1)	110.4	5.90 [a] (br s)	106.0 [b]	6.13 (d, 1.9)	109.2	6.28 (d, 2.0)	106.6
1b		136.8		130.9		136.6		138.7 [d]
2b, 6b	7.03 (d, 8.7)	130.8	6.67 (d, 8.4)	127.9	7.16 (d, 8.5)	130.8	6.77 (d, 8.5)	129.3 [e]
3b, 5b	6.71 (d, 8.7)	115.1	6.54 (d, 8.4)	114.8	6.73 (d, 8.5)	115.5	6.59 (d, 8.5)	115.4 [f]
4b		157.8		156.5		156.0		155.9
7b	4.22 (d, 2.0)	53.6	5.19 (dd, 6.9, 2.6)	84.1	3.72 (d, 1.9)	52.7	4.28 (br s)	50.6
8b	5.13 (d, 2.0)	82.9	3.59 (dd, 6.9, 2.6)	56.4	3.64 (d, 1.9)	62.1	4.02 (br d, 6.8)	60.5
9b		140.7		136.7		144.8		144.6
10b		121.3		121.8		123.4		116.0
11b		153.0		160.7		161.6		163.2
12b	6.36 (d, 2.1)	102.4	6.06 (d, 1.9)	95.7	6.10 (s)	96.3	6.16 (s)	96.8
13b		156.8		158.4		154.1		155.4
14b	6.36 (d, 2.1)	104.9	6.83 (d, 1.9)	105.6		118.7		126.5
1c				130.9		133.0		138.6 [d]
2c, 6c			6.67 (d, 8.4)	127.9	6.81 (d, 8.5)	131.2	6.75 (d, 8.5)	129.2 [e]
3c, 5c			6.54 (d, 8.4)	114.8	6.54 (d, 8.5)	115.2	6.56 (d, 8.5)	114.8 [f]
4c				156.5		156.4		155.9
7c			5.19 (dd, 6.9, 2.6)	84.1	4.00 (d, 7.0)	48.7	4.22 (br s)	50.3
8c			3.59 (dd, 6.9, 2.6)	56.4	4.62 (d, 7.0)	39.6	4.07 (br d, 6.8)	60.7
9c				136.7		143.5		143.9
10c				121.8		113.8		119.2
11c				160.7		157.9		162.5
12c			6.06 (d, 1.9)	95.7	6.31 (d, 1.6)	101.5	6.19 (s)	97.0
13c				158.4		157.8		155.4
14c			6.83 (d, 1.9)	105.6	4.45 (d, 1.6)	103.0		126.5
1d				131.5		133.4		129.1
2d, 6d			6.91 (d, 8.4)	128.3	7.10 (d, 8.5)	128.4	7.01 (d, 8.5)	128.9
3d, 5d			6.68 (d, 8.4)	114.8	6.79 (d, 8.5)	116.0	6.60 (d, 8.5)	115.4 [f]
4d				157.1		157.7		157.3
7d			5.10 (d, 7.3)	94.3	5.94 (d, 6.0)	85.2	5.69 (d, 7.0)	91.5
8d			3.42 (d, 7.3)	54.7	4.49 (d, 6.0)	49.7	4.43 (d, 7.0)	53.5
9d				146.5		147.0		143.1
10d			5.90 [a] (br s)	106.0 [b]	6.37 (br s)	129.6	5.87 (d, 2.0)	107.5
11d				158.4		159.6		160.0
12d			6.20 (t, 2.0)	101.2	6.23 (t, 2.0)	102.1	6.31 (t, 2.0)	102.2
13d				158.4		159.6		160.0
14d			5.90 [a] (br s)	106.0 [b]	6.37 (br s)	129.6	6.24 (d, 2.0)	106.5 [c]

^{1}H and ^{13}C NMR spectra were recorded in acetone-d6 at 400 and 100 MHz, respectively, unless otherwise stated. [a] NMR experiment at 60°C (500 MHz). [b] Signal not detected when spectrum recorded at RT; assignment made through ^{1}H-^{13}C cross peaks in HMQC experiment at 60°C (500 MHz). [c], [d], [e], [f] assignments respectively interchangeable.

Furthermore, the integration of signals observed in the ^{1}H-NMR spectrum did account for only eleven aromatic protons, instead of the expected thirteen (Figure 3a). It had been previously observed that aromatic protons H-10(14) of a free resorcinol moiety resonate either as a broad signal [245] or just as a hump [246], [247] and this was explained by steric hindrance restricting the rotation of this ring. These

authors recorded ^{1}H spectra at -20°C and/or -40°C in order to block the molecules in their different stable conformers and could observe these protons as two independent broad singlets. An opposite strategy consists of heating up the sample and facilitating the free rotation of that problematic ring, which would lead to a well-resolved averaged signal. A ^{1}H-NMR spectrum of **2** was recorded at 60°C and a broad signal was observed at d 5.90 (Figure 3b); a 1D-TOCSY experiment, also performed at 60°C, allowed to obtain correlation between that broad signal and the signal at d 6.20 (Figure 3c). The ^{1}H-NMR and COSY spectra also displayed two sets of coupled benzyl methine protons resonating at d 5.10 and 3.42 (2 H each, d, J = 7.3 Hz) on one hand, and d 5.19, 3.59 (2 H each, dd, J = 7.0, 2.6 Hz) on the other hand. The corresponding methine carbons were assigned from HMQC experiments.

In the HMBC spectrum, cross peaks observed between the methine protons and aromatic carbons allow the establishment of connections between the aromatic rings and their corresponding benzylic methine groups (Figure 4). The only correlation that connected the two resveratrol units (of one of the symmetric half) was H-8a/C-11b. This correlation, together with the deshielding of C-7a and the coupling constant of 7.3 Hz, suggested linkages through a dihydrobenzofuran ring. The HMBC cross peak H-8b/C-8b indicated the linkage (C-8b/C-8b') between both halves of the tetramer. The deshielding effect on methine carbon C-7b was compatible with the presence of an oxygen atom. This observation suggested the presence of an ether linkage between C-7b and C-7b'. The linkages between the two equivalent units of compound **2** resembled to those already observed for tricuspidatol A, a resveratrol dimer.[248] Indeed, the chemical shifts and coupling constants of the methine protons of the tetrahydrofuran ring of both compounds were found quite similar. Consequently, compound **2** was suggested to be a tricuspidatol A derivative having two additional symmetrically attached resveratrol units.

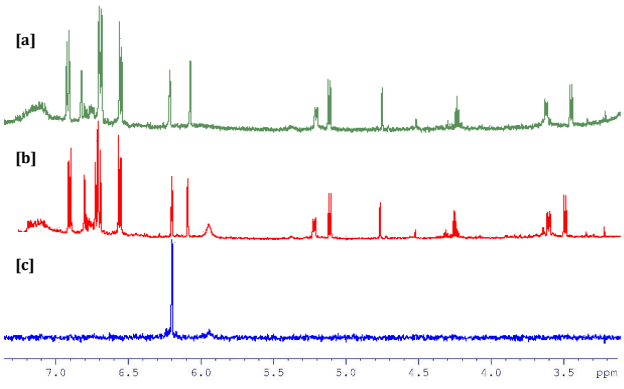

Figure 3. NMR spectra for **2**. [a] ^{1}H–NMR experiment at RT; [b] ^{1}H–NMR experiment at 60°C; [c] 1D TOCSY experiment at 60°C, irradiation at d 5.90.

From the NOESY spectrum, H-7a correlated with H-8a and H-2(6)a, while H-8a with H-7a and H-2(6)a. These observations first suggested a possible *cis* orientation. However, the ^{1}H-NMR spectrum, which displayed a $J_{7a,8a}$ of 7.3 Hz, supported *trans* configuration. The corresponding calculated molecular structure exhibited a H-7a/C-7a/C-8a/H-8a torsion angle of 104.0° and a H-7a/H-8a distance of 2.8 Å. The *trans* conformer slightly avoids steric repulsion and is significantly more stable than the *cis* by 6.9 kcal.mol^{-1}. Meanwhile, the strong nOe correlations H-7b/H-14b and H-8b/H-2(6)b are typical indications of *trans* configuration between H-7b and H-8b. The NOESY spectrum also revealed H-7a/H7b and H-8a/H-8b correlations, suggesting *syn* configurations. The fact that H-7a correlated with H-7b but not with H-8b and H-8a correlated with H-8b but not with H-7b further verified the *trans* configuration of H-7a/H-8a. The cross peak H-7b/H-8b was also explained by the calculated distance of 3.0 Å. The nOe correlations and relative stereochemistry of **2** are shown in Figure 4. The most stable conformer exhibits two H-bonds between 11a-OH/4b'-OH and 13a-OH/13a'-OH, with respective distances of 2.1 and 2.0 Å. The use of a dispersive-corrected DFT functional highlighted π–stacking-like interactions, which contribute to stabilization (Figure 4).

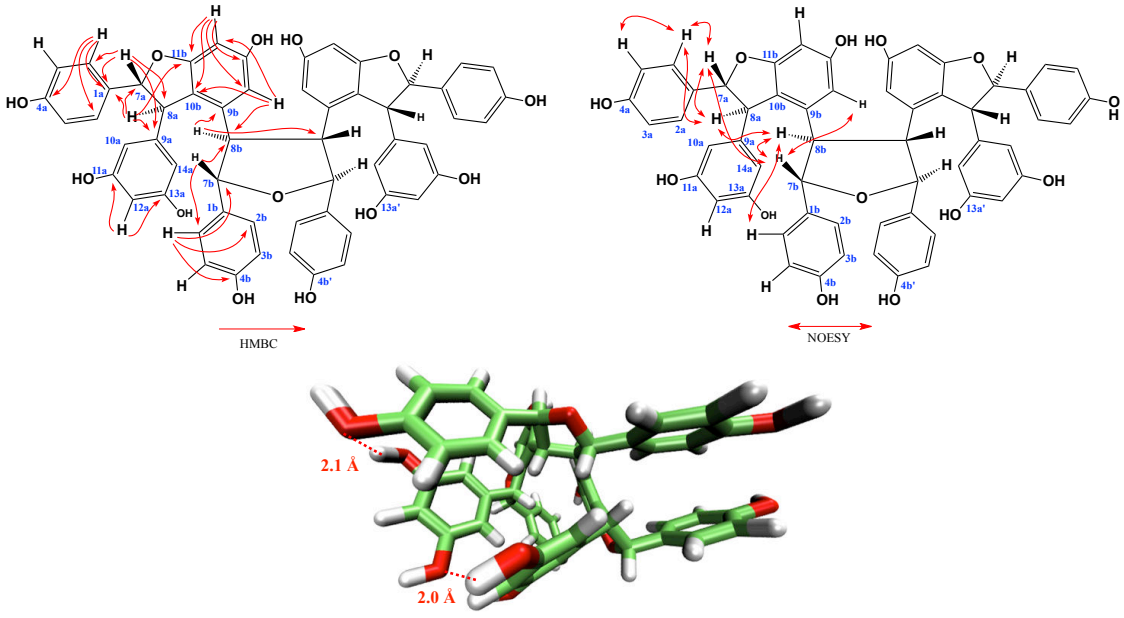

Figure 4. Selected correlations observed in HMBC and NOESY spectra and 3D computated most stable conformation of **2**.

❖ ***Heimiol D***

Heimiol D (**3**) was obtained as a pale yellow amorphous powder. The compound gave an $[M-H]^-$ ion peak at m/z 905.2581 in negative ion HR–ESI–TOF–MS, compatible with the molecular formula $C_{56}H_{42}O_{12}$ and suggesting **3** to be an oxidative tetramer of resveratrol. The analysis of ^{1}H–NMR (Table 1) and COSY spectra showed the presence of four sets of *ortho*–coupled aromatic hydrogen signals as

pseudo doublets typical of AA'BB' systems at d 6.92, 6.68 (2 H each, d, *J* = 8.5 Hz), 7.16, 6.73 (2 H each, d, *J* = 8.5 Hz), 6.81, 6.54 (2 H each, d, *J* = 8.5 Hz) and 7.10, 6.79 (2 H each, d, *J* = 8.5 Hz), assignable to four independent 4–hydroxy–phenyl groups. Two sets of meta–coupled aromatic hydrogen signals were observed at d 6.13, 5.94 (l H each, d, *J* = 1.9 Hz) and 6.31, 4.45 (l H each, d, *J* = 1.6 Hz), assignable to two di–substituted resorcinol moieties. A signal from an aromatic proton of a penta–substituted benzene ring was observed at d 6.10 (1 H, *s*). Further analysis of the ^{1}H–NMR spectrum revealed one set of signals due to a 3,5–dihydroxyphenyl group at d 6.37 (2 H, br s) and 6.23 (1 H, t, *J* = 2.0 Hz). Four olefinic hydrogen signals at d 5.44, 4.10 (l H each, d, *J* = 4.3 Hz), and 5.94, 4.49 (1 H, each d, *J* = 6.0 Hz) were attributed to two diaryl–dihydrobenzofuran moieties. A spin system formed of four aliphatic methine protons linearly attached is identified from the COSY spectrum at d 3.72 (1 H, d, *J* = 1.9 Hz), 3.64 (1 H, d, *J* = 1.9 Hz), 4.00 (1 H, d, *J* = 7.0 Hz) and 4.62 (1 H, d, *J* = 7.0 Hz). In the HMBC spectrum, significant cross peaks H–2(6)a/C–7a, H–8a/C–9a, H–8a/C–10a, H–2(6)b/C–7b, H–8b/C–9b, H–8b/C–10b, H–7c/C–9c, H–8c/C–9c, H–8c/C–10c, H–2d(6d)/C–7d, H–7d/C–1d, H–7c/C–19d, H–8d/C–1d, H–8d/C–9d and H–8d/C–10d established connections between the aromatic rings and their corresponding benzylic methine groups (Figure 5). Long–range correlations H–7a/C–10b, H–7a/C–11b, H–8a/C–9b, H–8a/C–10b, H–8a/C–11b, H–7d/C–11c and H–8d/C–9c suggested that the resveratrol units A and D form a dihydrofuran ring with rings B and C, respectively. The HMBC spectrum also showed correlations, namely H–7b/C–1c, H–7b/C–7c, H–8b/C–1c, H–7c/C–14b, and H–8c/C–14b, suggesting connection between the resveratrol units B and C, through the C–8b/C–7c linkage. This connection was previously not detected from the COSY spectrum as no cross peak between H–7c and H–8b could be observed. The relative stereochemistry was determined from the NOESY spectrum. The lack of correlation between H–7a/H–8a and H–7d/H–8d was a preliminary indication of *trans* orientations. Further evidence was obtained from the correlations between H–2(6)a and H–7a (but not H–8a), and H–2(6)d and H–8b (but not H–7a), see Figure 5. Such cross peaks suggested configurations of both chiral carbons 7d and 8d to be *S*. Some nOes were also observed between H–2(6)b/H–7c, H–7b/H–2(6)c, H-8c/H-8d and H–7d/H–12c indicated their respective *syn* orientations. The *J* values for the H–7b/H–8b and H–7c/H–8c correlations were 1.9 and 7.0 Hz, respectively, suggesting *cis* conformation. From the assignment on the dihedral angle of the respective protons, it may be concluded that the configurations for C–7b, C–8b, C–8c and C–7c were *R*, *R*, *S* and *R* respectively. The corresponding 3D structure was optimized at the DFT level (Figure 5). Neither H–bonding nor π–stacking interaction exist in the most stable conformer of **3**.

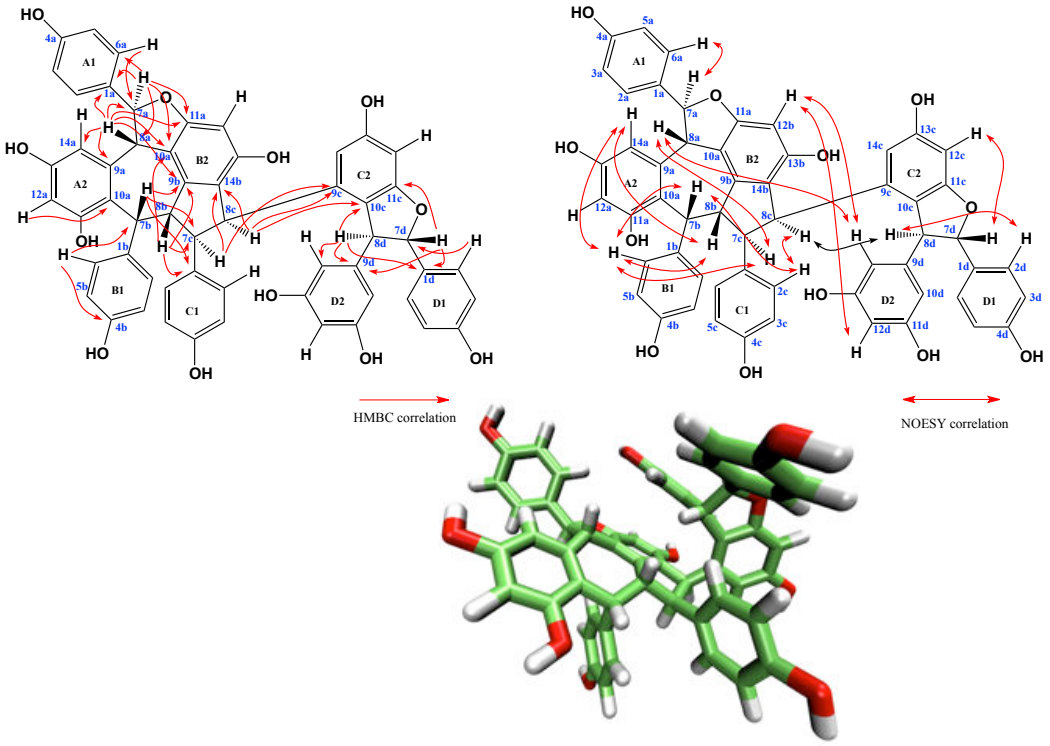

Figure 5. Selected correlations observed in HMBC and NOESY spectra and 3D computed most stable conformation of **3**.

❖ *Heimiol E*

Heimiol E (**4**) was obtained as a pale yellow amorphous powder. The compound gave a $[M-H]^-$ ion peak at m/z 907.2587 in negative ion HR–ESI–TOF–MS, compatible with the molecular formula $C_{56}H_{42}O_{12}$. Additional data from the ^{13}C-NMR spectrum (100 MHz, CD_3COCD_3), which showed signal related to fifty–six carbons (eight being sp^3– and forty eight sp^2–hybridized), suggested that the compound was a tetramer of resveratrol. A preliminary examination of the ^{1}H–NMR spectrum of compound **4** showed signals of aromatic rings appearing either in close pairs or even overlapping. The ^{13}C–NMR spectrum showed similar features for most of the sp^2–hybridized carbon signals. The signals for the aliphatic protons and sp^3–hybridized carbons were well distinguishable. This suggested a plane structure of **4** made of two symmetrical moieties, with differences in stereochemistry resulting in an asymmetrical molecule. The ^{1}H–NMR (Table 1) and COSY spectra exhibited four sets of *ortho*–coupled aromatic protons in AA'BB' spin systems assignable to four independent 4–hydroxyphenyl groups at d 7.10, 6.73 (2 H each, d, J = 8.5 Hz), 6.77, 6.59 (2 H each, d, J = 8.5 Hz), d 7.01, 6.60 (2 H each, d, J = 8.5 Hz), 6.75, 6.56 (2 H each, d, J = 8.5 Hz) resulting from the presence of four mono–substituted *p*–hydroxyphenyl groups. Two sets of *meta*–coupled aromatic protons in AA'B spin systems resonated at d 6.27 (1 H, d, J = 1.8 Hz), 6.28 (1 H, d, J = 1.8 Hz) and 6.06 (1 H, *t*, J = 1.8 Hz) on one hand and d 5.87 (1 H, d, J = 2.0 Hz) d 6.24

(1 H, d, *J* = 2.0 Hz) and 6.31 (1 H, *t*, *J* = 2.0 Hz), suggesting the presence of two independent 2,5−dihydroxyphenyl groups. The protons at positions 10 and 14 of the resorcinol rings resonated at different chemical shifts thus indicating a strong steric hindrance preventing the rings free rotation. Finally, the aromatic proton signals of two penta−substituted benzene rings were observed at d 6.16 and 6.19 (1 H, each br s). Two pairs of aliphatic hydrogen signals at d 5.29 and 4.29 (1 H each, d, *J* = 1.3 Hz) and 5.69 and 4.43 (1 H each, d, *J* = 7.0 Hz) respectively suggested the presence of a dihydrobenzofuran group bearing 4−hydroxyphenyl and 3,5−dihydroxyphenyl groups characteristic of oligostilbenes biosynthesized from resveratrol derivatives. The other two pairs of aliphatic ^{1}H−NMR signals, at d 4.07, 4.02 (1 H each, d, *J* = 6.8Hz) and 4.28, 4.22 (1 H each, br s) showed correlations in COSY as one spin system. In the HMBC spectrum, correlations between the methine protons and the aromatic carbons, as shown in Figure 6, allowed the establishment of connections between these aromatic rings and their corresponding benzylic methine group. Cross peaks H−7a/C−10b, H−7a/C−11b, 8a/C−10b, 8a/C−11b and 8d/C−10c, 8d/C−11c indicated the formation of dihydrofuran rings between the resveratrol units A and B as well as between units D and C. The H−7b/C−8c, H−7b/C−9c, H−7b/C−10c, H−7b/C−11c, H−8b/C−8c, H−8b/C−10c, H−7c/C−8b, H−7c/C−9b, H−7c/C−10b, H−7c/C−11b, H−8c/C−8b and H−8c/C−10b correlations suggested C−7b/C−10c, C−8b/C−8c and C−7c/C−10b linkages, thus establishing the connections between resveratrol units B and C. In addition, COSY assignments showed that H−7b, H−8b, H−8c and H−7c are linearly connected. The splitting patterns of the ^{1}H−NMR signals confirmed the linkage between C−8b and C−8c. The connections between the resveratrol units B and C are symmetrical. This was supported by the fact that the protons and carbons of both resveratrol units B and C resonated at similar chemical shifts, some of them being almost overlapped and became indistinguishable. The NOESY spectrum showed cross peaks H−2(6)a/H−7a, H−2(6)a/H−8a and H−7a/H−8a (Figure 6). Theoretically, these observations, together with the coupling constant value (*J* = 1.3 Hz) between H−7a and H−8a, match a *cis* conformation. However, the only configuration compatible with the *J* value of 10.5 Hz and NOE correlations more corresponds to *trans* (7a=a and 8a=b). Another significant NOE correlation H−7d/H−8d, together with a coupling constant of 7.0 Hz corresponded to a *trans* conformer of the second dihyrofuran ring. Cross peaks H−7b/H−10a and H−7d/H−12c were compatible with *syn* conformations. The H−8a/H−7b and H−8d/H−8c correlations suggested the conformation of H−8a/H−7b and H−8d/H−8c to be *syn*. The H−7a/H−8a, H−7a/H−2(6)a, H−7b/H−8b, H−7b/H−2(6)b, H−7c/H−8c, H−7c/H−2(6)c and H−7d/H−8d, H−7d/H−2(6)d correlations are explained by the close proximity of the protons. This is supported by the distances between the corresponding protons in the 3−dimensional molecular conformation, which were less than 3 Å. The HMBC and NOE correlations, as well as relative

stereochemistry of **4** is as shown in Figure 6. Both *trans* and *cis* conformers were optimized, and the *cis*–conformer appeared much more stable (-36.5 and -31.1 kcal.mol^{-1}.for H–a and H–b, respectively).

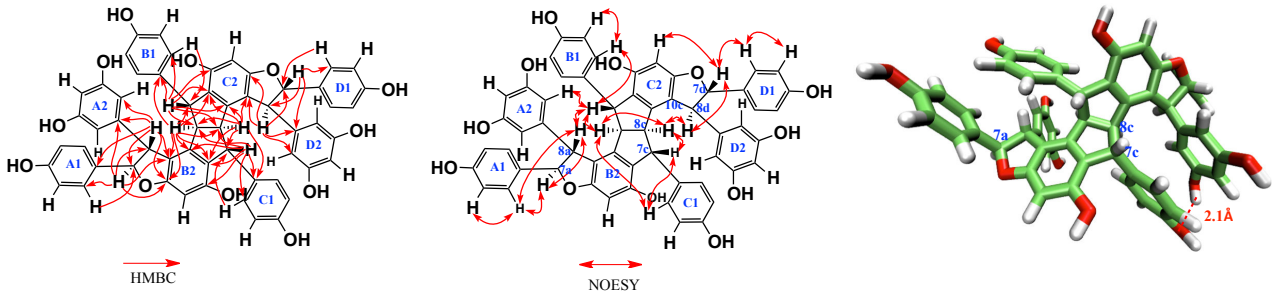

Figure 6. Selected correlations observed in HMBC and NOESY spectra and 3D computed most stable conformation of **4**.

❖ ***Other known oligostilbenes and stereoselectivity of the oxidative biosynthesis***

In addition to the above four new compounds, thirteen known compounds were isolated and their structures identified according to their spectral data and in agreement with those previously published. These known compounds include heimiol A (**5**),[244] vaticaphenol A (**6**),[245] ampelopsin H (**7**),[249] hopeaphenol (**8**),[250] isohopeaphenol (**9**),[251] hopeaphenol A (**10**), isohopeaphenol A (**11**),[252] hemsleyanol D (**12**),[253] balanocarpol (**13**),[256] ampelopsins A (**14**) and C (**15**),[259] vaticanol A (**16**)[246] and copalliferol A (**17**).[255] An HPLC analysis of the extract shows that virtually all–significant peaks can be assigned to the above listed compounds (Figure 7).

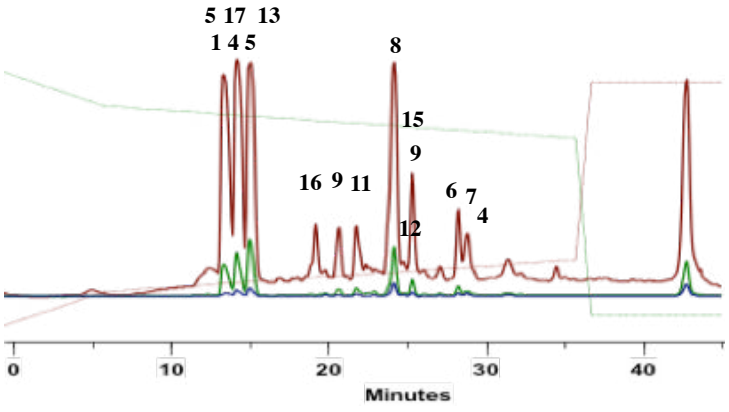

Figure 7. HPLC analysis of the extract.

A thorough examination of the overall oligostilbenoid composition of *N. heimii* wood raised many questions regarding the fascinating variety of chemical structures and biosynthesis of the above oligostilbenes, which is driven by stereo– and regio–selective processes. It clearly appears that all isolated compounds originate from resveratrol. As noted by previous workers,[243] the composition of this dipterocarp, like all members of this family, is dominated by derivatives that include a benzodihydrofuran

moiety. Even though we did not isolate ε−viniferin (**18**), it is their most likely precursor. Sotheeswaran, in his seminal review,[37] proposed a biosynthetic scheme for the generation of hopeaphenol. This scheme however is not without several flaws; one of them being that it does not address the issue of the stereoselectivity of the dimerization. The stereo−control of resveratrol oligomer synthesis was proposed following a unique three−stage design. This was discussed mainly in terms of functionalization, namely positional control through the introduction of a novel reagent of bromination.[55] In previous papers,[48], [203] we have proposed that the outcome of the stilbene dimerization depends on how species would approach toward each other within a pre−reaction complex, *i.e*. head−to−head (H/H) or head−to−tail (H/T) as well as approaching through their *Re*/*Si* or *Re*/*Re* (*Si*/*Si*) faces. Applying this concept to ε−viniferin as a substrate would explain the formation of most components of this plant extract. The starting point of such an oxidatively induced process is electron transfer from the polyphenol to an oxidative system, usually an oxidase in plants. The electron transfer occurs from either the neutral polyphenol or its deprotonated form. In the former case a radical cation is formed, which is highly unstable and undergoes heterolytic bond dissociation to form a phenoxy radical. The whole process is called SET−PT (sequential electron transfer – proton transfer). The latter case depends on the pKa of the molecule and the pH of the environment. In this instance the deprotonated polyphenol is somehow activated to favour electron transfer. This mechanism is called SPLET (sequential proton loss electron transfer). A phenoxy radical is formed here also. Disregarding the mechanism, a hydrogen atom transfer (HAT) occurs from one of the OH group to the oxidative system. Calculation of the bond dissociation enthalpy (BDE) of the different OH groups of stilbene derivatives shows that HAT occurs from the 4−OH group to form the corresponding phenoxy radical, for which the spin density is delocalized over the molecule with high values at C−1, C−3, C−5, C−8 and O−4 (Figure 8). While we are aware of debates on whether the stilbene dimerization occurs through radical−radical (as proposed by Stekhan [48], [203] following Barton's general mechanism for phenolic oxidative coupling [256]) or radical−to−neutral molecule reaction (as we proposed recently [57], [257]), we have chosen here to use the former hypothesis for simplicity purpose. This radical−radical reaction has been rationalized for the dimerization of flavonolignan derivatives on the basis of quantum chemical calculations .[258] It is shown that the radical−radical formation is relatively fast but, in order to be thermodynamically favourable, the whole dimerization mechanism requires subsequent molecular re-arrangements to form stable products. If one would consider the group of tetrameric species formed by hopeaphenol, isohopeaphenol, hopeaphenol A, isohopeaphenol A, one would recognized that they differ by the stereochemistry at C−8b and 8c in one hand and C−7b and 7c in the other hand. The determinism for C−8b and 8c will be discussed first.

❖ ***Determinism at carbon C-8***

Many oligostilbenoids reported in Figure 1 require, as a primary event, bond formation at C–8. The regioselectivity of this atom is not explained by the spin density distribution of the phenoxy radical (Figure 8), which exhibits five sites (C–8, C–6, C–4, C–2 and O–3) for further reactions following oxidation, like covalent bond formation. As already shown for stilbene dimerization, the regioselective dimerization of ε–viniferin units can be driven by the formation of non–covalent pre–reaction complexes that may occur in solution. The long–range interaction driving such association was assessed with quantum calculations describing dispersive forces, namely DFT–D calculations (see the Method section). Considering all possible supramolecular arrangements, H/H and H/T with four possible approaches *Re/Re*, *Si/Si*, *Re/Si* and *Si/Re*, eight geometries were obtained (Scheme 1). The differences in association energies between the various complexes are not of any significance (Table 2), indicating that all possibilities may occur in solution with an equal Boltzmann distribution. In these non–covalent complexes, intermolecular distances were around 3.5 Å, which is typical of π–stacking interactions. Yet, π–stacking is not the only driving force for such association, as H–bonding also plays a crucial role in stabilizing these non–covalent pre-reaction complexes (Scheme 1). The formation of these non–covalent complexes appears the only logical rationale for the stereoselectivity determinism at the C–8 of oligostilbenoid structures.[259]

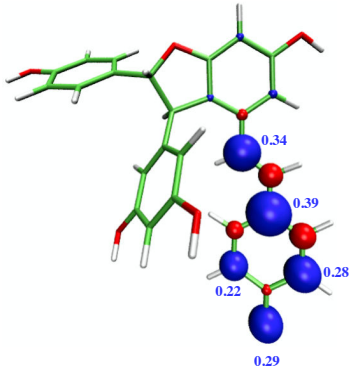

Figure 8. Spin density distribution of the phenoxy radical.

Table 2. Association energies (kcal.mol^{-1}) of the non-covalent pre–reaction complexes between two ε–viniferin units for the different alignments as obtained by *COSMO*–B3P86–D2(s_6=0.780)/def2–QZVP.

Non-covalent pre-reaction complexes	**[H/H]$_{Re/Re}$**	**[H/H]$_{Si/Si}$**	**[H/H]$_{Si/Re}$**	**[H/H]$_{Re/Si}$**	**[H/T]$_{Si/Re}$**	**[H/T]$_{Re/Si}$**	**[H/T]$_{Re/Re}$**	**[H/T]$_{Si/Si}$**
$E_{Association}$	-15.7	-19.8	-15.4	-15.0	-16.8	-10.0	-16.9	-10.9

[H/H]: head–to–head alignment; [H/T]: head–to–tail alignment.

From the $[H/H]_{Si/Si}$ and $[H/T]_{Si/Si}$ complexes, radical alignments **19** and **20** are obtained, respectively (Scheme 1). Atoms C−8b and 8c would readily establish a bond leading to the dimeric intermediate **21**. This intermediate has both C−8b and 8c in *S*−configuration as in hopeaphenol (**8**). Conversely, a *Re*/*Re* approach (alignments **22** and **23**, see Scheme 1) leads to an inverted configuration for these carbon atoms (intermediate **24**) as in isohopeaphenol (**9**). From *Re/Si* approach, alignments **25**–**28** (Scheme 1) are formed, all leading to a single intermediate (**29**), which would account for the formation of both hopeaphenol A (**10**) and isohopeaphenol A (**11)**.

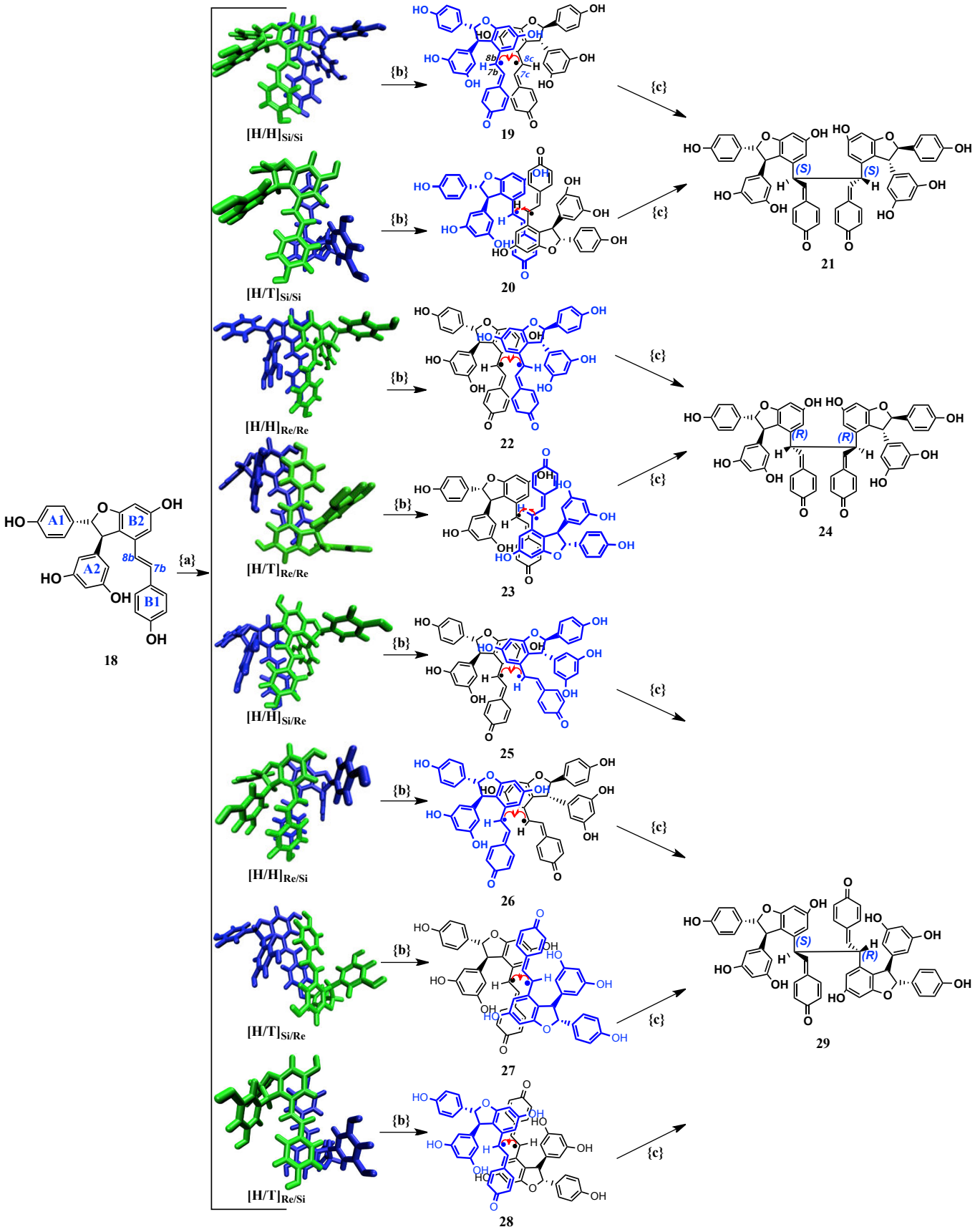

Scheme 1. Oxidation and initial step of ε–viniferin (**18**) dimerization: {a} non–covalent complexation; {b} oxidation; {c} C–C bond formation.

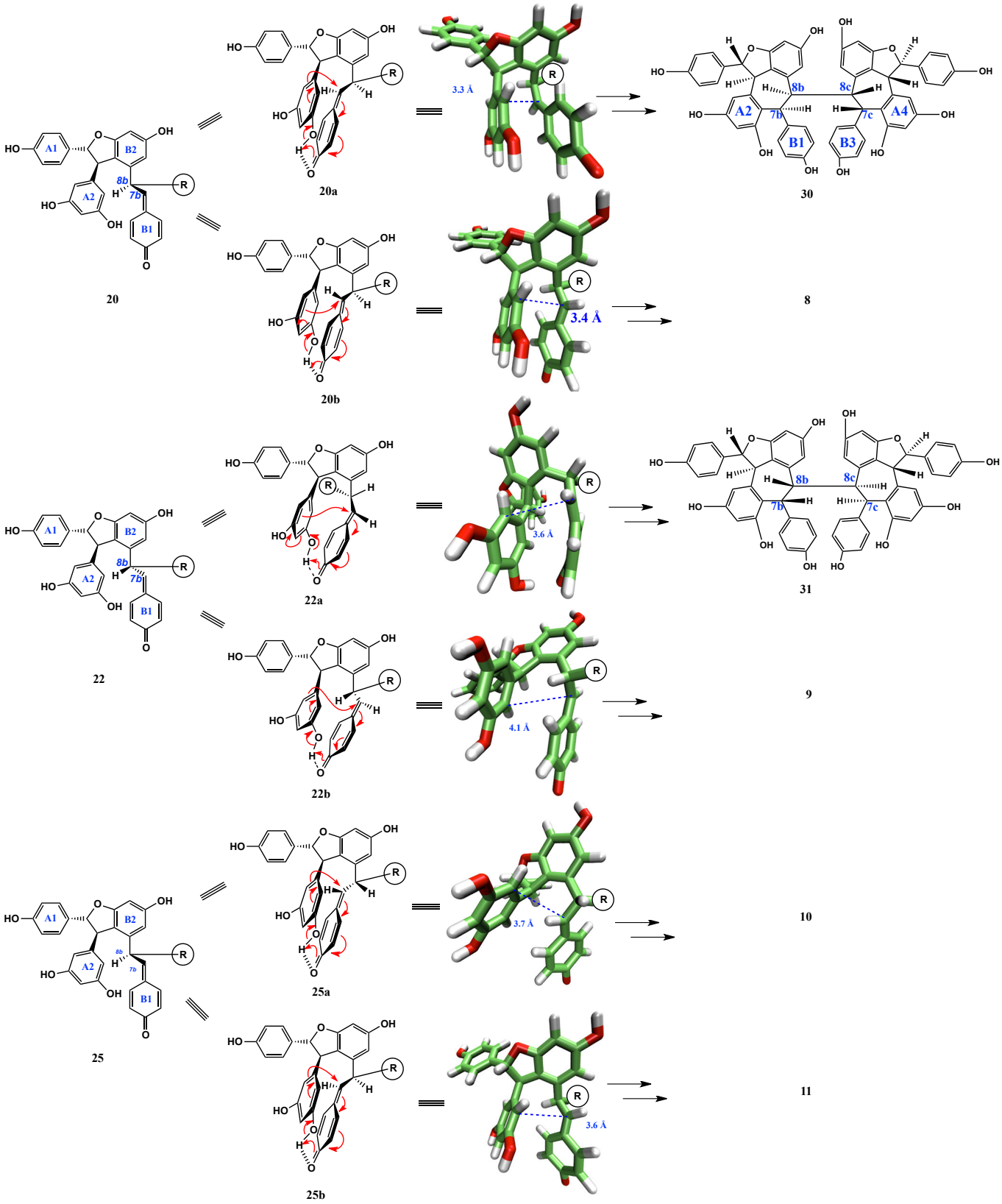

Scheme 2. Role of non–covalent interactions in determining the stereochemistry at C–7b of oligostilbenes with a dibenzocycloheptane moiety. ® represents either an OH group or an ε–viniferyl moiety.

The stability (given by the difference in Gibbs energy between the intermediate and the corresponding pair of phenoxy radicals) of the three intermediates (**21**, **24** and **29**) was evaluated by quantum calculations in the DFT formalism. The ΔG of formation of these intermediates were -16.4, -18.5 and -21.8 kcal.mol^{-1} for **21**, **24** and **29**, respectively, as obtained by B3P86-D2/def2-SVP, which confirm that all compounds are thermodynamically favoured, *i.e.* the feasibility of each process mainly depends on the stability of the respective non-covalent complexes. Therefore the ratio of the different products depends on both the relative thermodynamic stability of these intermediates, and the stability of the corresponding molecular approaches, the latter being driven by long-range interactions (π-stacking and H-bonding) and steric hindrance towards a given approach.

❖ ***Further reactions following the primary C-8/C-8 bonding event***

Once the C-8 configuration is set, the subsequent intermediates continue reacting according to intramolecular re-arrangements. Concerning C-7b and C-7c configurations, the key parameter is the re-arrangement of rings A2 and B1 on one hand and B3 and A4 (the corresponding rings in the other monomer) on the other hand (Scheme 2). Carbon C-8 of intermediates **21**, **24** and **29** is sp^3-hybridized and the changes of the torsion angle C-7/C-8/C-9/C-10 lead to conformational re-arrangements determining the C-7 stereochemistry. All intermediates are stabilized with π-stacking interactions between resorcinol ring A2 and semiquinone ring B1 holding them nearly parallel (Scheme 2). In addition, some intermediates are further stabilized by H-bonds with interatomic distances of ca. 2.0 Å. In these conformations, the C-7 atom of one unit is facing the resorcinol ring of the other unit, thus favouring the formation of the seven-membered rings of **8**, **9**, **10**, and **11** (Scheme 2). Ring closure follows an intra S_{N1} nucleophilic substitution from the carbon in *para* position to the OH group of the resorcinol ring onto C-7 of the other unit (Scheme 2). The nucleophilic attack is favoured since *i)* these two atoms are relatively close to each other in the intermediates (distance around 3.5 Å); and *ii)* the former atom is electron-rich with an atomic charge of -0.5, while the C-7 carries an atomic charge of -0.06.[***] According to the intermediate and molecular re-arrangement, one of the four isomers is formed.

[***] A similar chemical pathway is proposed to explain the formation of **13** and **14**. In this case, the semiquinone intermediate comes from the phenoxy radical formed after oxidation of ε-viniferin, which then catch one hydrogen atom from its neighboring environment.

In principle two other hypothetic compounds (**30** and **31**) could be formed (Scheme 2). However, detailed quantum mechanics–based calculations showed these two compounds to be energetically much less favoured (Table 3) and therefore in much lower occurrence if any in plants. The four identified compounds (**8-11**) exhibited Gibbs energies of formation (ΔG_f^0) of -25.3, -29.4, -22.1 and -17.3, respectively, indicating high stability (Table 3).

Table 3. ΔE of formation (kcal.mol^{-1}) of **8–11** and **26–27** as obtained by COSMO–B3P86–D2 (s_6=0.780)/QZVP

	8	**9**	**10**	**11**	**30**	**31**
ΔE	-64.7	-60.7	-60.1	-61.6	-41.2	-31.0
ΔG	-25.3	-29.4	-22.1	-17.3	-	-

It is remarkable that only isohopeaphenol A (**11**) includes a moiety where H–7b and H–8b are in *cis* configuration, while hopeaphenol (**8**), isohopeaphenol (**9**) and hopeaphenol A (**10**) only include *trans* configurations. At the same time, balanocarpol (**13**) with a 7b–8b *cis* configuration is far more abundant that its diastereoisomer ampelopsin A (**14**), which displays a *trans* configuration. This is probably related to the bulkiness of the substituent at C–8b, which would favour or disfavour the relative positioning of the rings A2 and B1 in intermediates **21, 24** and **29** (Scheme 1). Indeed, DFT calculations indicated **13** to be more stable than **14** by 3.7 kcal.mol^{-1}.

From intermediate **21**, another chemical pathway is allowed and rationalizes the biosynthesis of heimiol C (**2**). The molecular arrangement of **21** indeed exhibits short distances of around 3 Å between rings A2 and B1 as well as C1 and D2 (Scheme 3). In this case, the nucleophilic attack on the quinone methide group does not originate from the neighbouring resorcinol ring, but from a water molecule interacting with C–8b and C–8c. DFT calculations confirmed the stability of intermediate **32** since the hydrolysis reaction exhibits ΔG_f^0 of -3.4 kcal.mol^{-1}. Similar processes are expected from the other intermediates **24** and **29**, which would probably yield other stereoisomers of **2**. Even if this is still hypothetical (the compounds have not been observed yet), there are no particular molecular restraints forbidding the formation of these compounds.

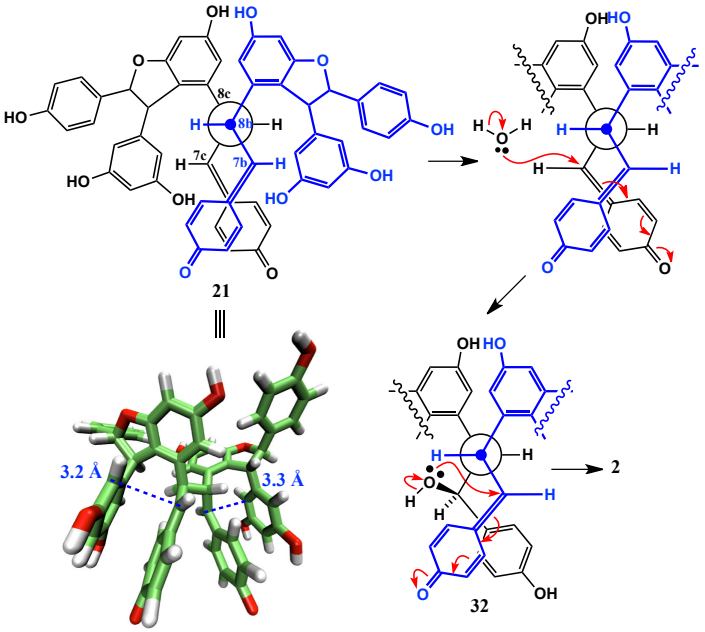

Scheme 3. Biosynthetic route to **2**.

Biosynthetic intermediates **21** and **29** (from $[H/T]_{Si/Si}$ and $[H/T]_{Si/Re}$ complexes, respectively) are the precursors of **4** and **7**. Through a mechanism similar to that described above, the quinone methide groups are subjected to nucleophilic attack from the resorcinol rings, though located on the opposite moieties (Scheme 4).

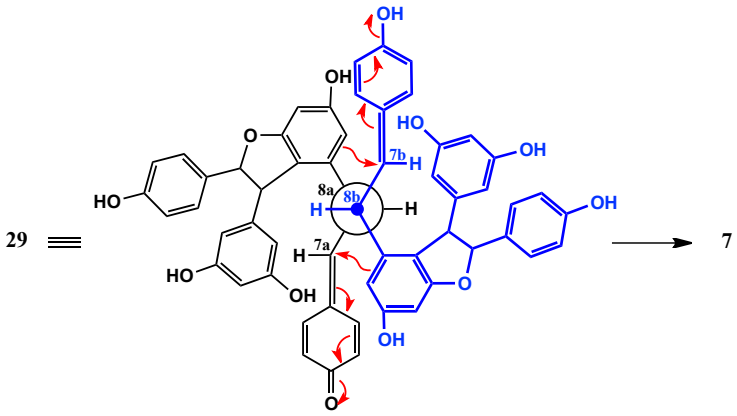

Scheme 4. Biosynthetic route to **7**.

The feasibility of this mechanism was here as well confirmed by DFT, which showed that **4** and **7** were more stable than their corresponding intermediates (**21** and **29**) according to their energies of formation of -42.7 and -44.3 kcal.mol^{-1}, respectively.

❖ ***Other pathways***

Hemsleyanol D (**12**) is likely to derive also from intermediate **29** deriving itself from the $[H/T]_{Re/Si}$ alignment (Scheme 1). In this case, both carbon atoms C–7b and C–7c are subjected to nucleophilic attack from the neighbouring resorcinol rings. Indeed, the 3D conformation allows C–7b and C–7c to be attacked by C–10a and C–14b, respectively (Scheme 5). This reaction is thermodynamically favoured, exhibiting a -44.3 kcal.mol^{-1} Gibbs energy of formation.

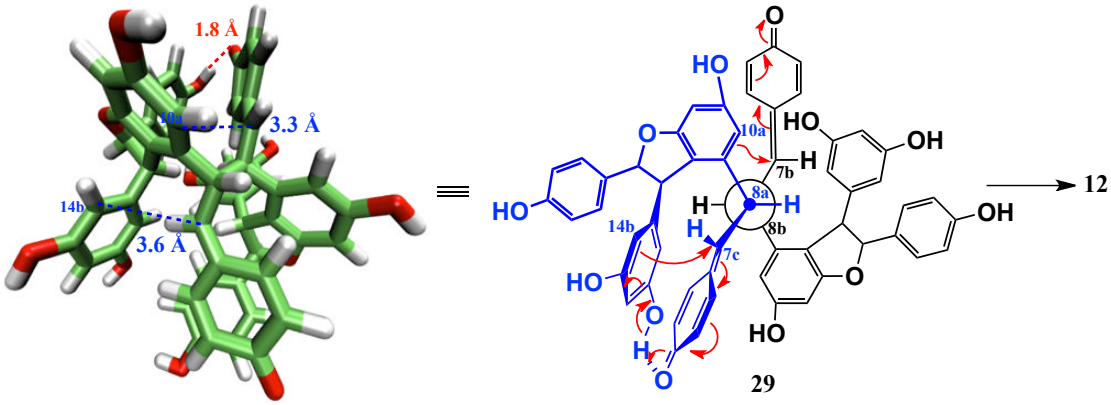

Scheme 5. Biosynthetic route to **12**.

Compounds **3**, **6**, **15** and **16** are obviously biosynthesized through a different mechanism. Even if less thermodynamically favoured than from the 4–OH group of the stilbenoid moiety, HAT from one resorcinolic OH group of resveratrol is thermodynamically feasible, leading to a quinoid radical that would combine with another radical originating from 4–OH oxidation (**32**, Scheme 6). The spin density distributions on both radicals allow various further linkages, including C–8a/C–10b bond formation. As a result, the first established inter–stilbene bond would be C-8a/C–10b (**33**). DFT calculation confirmed that **33** was the most stable intermediate by 2.1 kcal.mol^{-1} compared to the other possible dimers obtained by radical–radical dimerization. The bond formation breaks the planarity of the ring. The dimerization process is thus thermodynamically feasible only if followed by tautomerism with the adjacent OH group.[257] Next, the methide (C–7a) would be attacked by the 11–OH group leading eventually to ε–viniferin (**18**), or by C–8b, thus yielding intermediates **34** and **35.** The rigidity of the cyclopentane ring does not allow the quinone methide to be subjected to any intramolecular nucleophilic attack necessary for re-aromatization of ring A2. Therefore, intermediate **35** is ready

to react with the B–ring of another resveratrol unit followed by a new cycle of intramolecular phenolic oxidative coupling leading to **3**, **6**, **15** and **16**. The structure of copalliferol A (**17**) seems to vindicate these biosynthetic hypotheses. The only structural difference between **17** and **15** is the C–7a/C–2b instead of C–7a/O–11b bond (Figure 1). This C–7a/C–2b bond is very unusual and reflects the high reactivity of the quinone methide intermediate that would result from the addition of a resveratrol unit onto **35**. DFT calculation confirmed that **17** is much more stable than **16**, itself more stable than **15** based on the relative energies of -5.6 and -10.5 kcal.mol^{-1}, respectively.

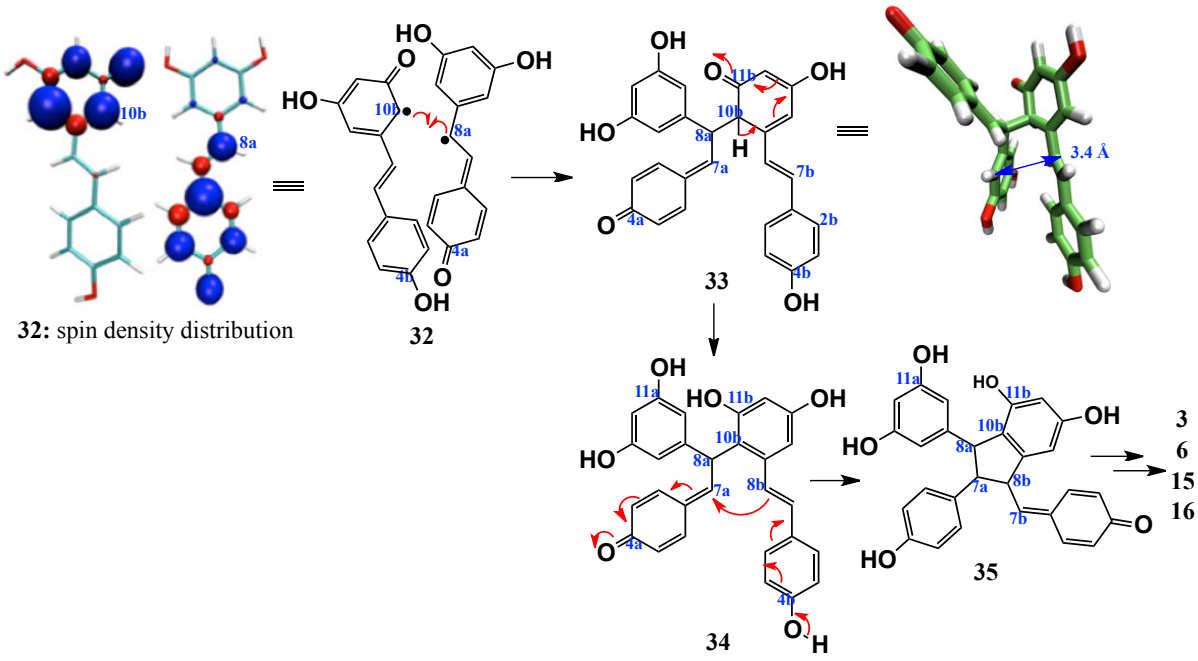

Scheme 6. Biosynthetic route to intermediates **3**, **6**, **15** and **16**.

Finally, the biosynthesis of 1 and 5 can also be understood by the nucleophilic attack of the methide (C−8b) of 33 with a water molecule, leading to intermediate 36 (Scheme 7). A second nucleophilic attack onto C−7a leads to isochroman 37. Depending on the orientation of the quinone methide moiety and its nucleophilic attack from C−10a, two diastereoisomers can be obtained, which correspond to heimiol A or B. The formation of both 1 and 5 was confirmed by

their low Gibbs energies of formation, i.e., -31.1 and -32.5 kcal.mol-1, respectively.

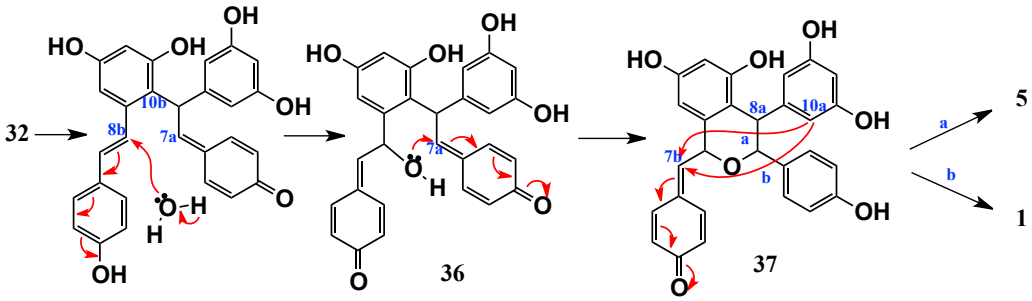

Scheme 7. Biosynthetic route to **1** and **5**.

3. Conclusion

Besides providing a series of new and structurally provocative compounds, namely heimiols B–E, the study of the oligostilbenes from the heartwood of *N. heimii* provided a series of derivatives characterized by a high consistency in their plausible biogenesis. In this respect, the dominant features consist of *i)* electron abstraction from the frontier orbitals of the polyphenol and the subsequent (or concomitant) proton loss from an OH group of a suitable precursor; *ii)* the combination of species aligned in specific supramolecular arrangements due to π–stacking and H–bonding interactions; and *iii)* the intra– or inter–molecular bond formation as a result of radical–radical reactions or nucleophilic substitutions, followed by the quenching of quinone methide intermediates. Electron transfer from the monomer or certain intermediates must be enzymatically controlled whereas the other steps of the whole process most probably result in chemical re-arrangements, thermodynamically favoured. Supramolecular self–assembly of units through non–covalent bonding is confirmed to be a significant driving force in some key–steps of the stereoselective oligostilbene biosynthesis. These molecular assemblies formed prior to oxidation provide powerful indications for the targeted stilbenoid oligomer synthesis.

Non–covalent trimers were also envisaged (Figure 9) explaining the origin of stilbenoids of higher degrees of polymerization. This work sheds new light on the biogenesis of a number of natural product classes. A proper understanding of oligostilbenoid biosynthesis may provide more refined approaches towards biomimetic syntheses, which are likely to become a most

practical approach to the generation of series of derivatives and analogues of some representatives endowed with interesting bioactivities.

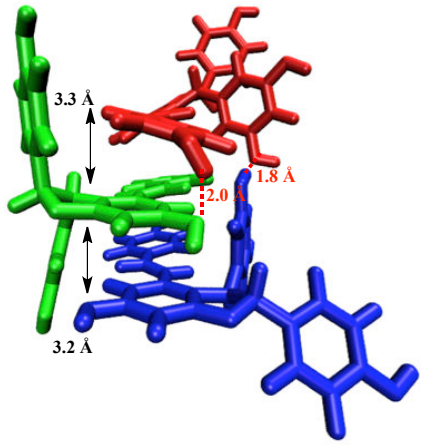

Figure 9. Predicted 3D geometry of a non-covalent trimer.

Here we have provided a comprehensive (bio)synthetic mechanism of different oligostilbenoids isolated from Neobalanocarpus heimii., whereas the enzyme was not taken into account. We believe that the enzyme mainly initiate oxidation but has a minor role in the further steps oligomerisation. Therefore, the active site of the corresponding (yet unknown) enzyme is most probably at the surface, relatively flexible and weakly specific. We are confident that our work is a first crucial step to get in-depth into the knowledge of the biosynthetic oligomerisation of stilbenes.[†††]

4. Method Section

General Procedures. The following instruments were used: optical rotation, JASCO J-715 CD Spectropolarimeter, 1D– and 2D–NMR spectra, BRUKER 300, 400 and 500 (chemical shifts given in d values); TOF–MS spectra, Agilent 6200 Series; C–18 Column, Genesis (Jones chromatography), Synergi Hydro–RP (Phenomenex), Hypersil (Thermo) and Chromolith (Merck).

[†††] This section in italic was not included in the published paper.

Plant material. Heartwood of *Neobalanocarpus heimii* was collected in Malaysia, see[244].

Methods of calculation. Geometries and energies of all compounds were obtained using the B3P86 functional. This hybrid functional provided most of the geometrical conformation of stand−alone oligostilbenoids at the DFT level while B3P86−D2 was used as this method includes dispersive corrections and allows high accuracy in the description of non−covalent interactions. This method was used systematically with s_6 = 0.780 as recently re-parameterized for phenolic derivatives.[184] The def2−SVP and QZVP basis sets were used for geometry optimization and energy calculations, respectively. All calculations were performed either with Gaussian 09 [260] or ORCA.[222]
The association energy ($E_{Association}$, Table 2) between fragments A and B was calculated as follow:

$$E_{Association} = E_{AB} - (E_A + E_B)$$

where (E_{AB}) is the energy of the non−covalent complex, (E_A) and (E_B) are the energies of isolated fragments A and B, respectively.

The solvent effect was accounted implicitly, in which the solute is embedded into a shape adapted cavity surrounded by a structure less continuum. Conformational analysis and interaction energies were carried out using PCM (Polarizable Continuum Model) [261] or COSMO (COnductor−like Screening Model).[262] Methanol was selected as being the solvent used to extract compounds and to measure their physical−chemical properties.

Extraction and isolation. Crude methanol extract (15 g) from the heartwood of *N. Heimii* was fractionated by semi−preparative chromatography on C18 and eluted by gradient elution of water and MeCN (84:16 to 77:23 in 7 minutes, followed by 77:23 to 66:34 in 18 minutes) to yield 57 fractions. Fraction 18 (R_T =11.2 min) was further analysed by HPLC on a Chromolith column, eluted by isocratic elution of H_2O/MeOH (84:16) to yield compounds **1** (31.0 mg) and **5** (116.8 mg). Compound **2** (5.3 mg) was obtained together with compound **11** (131.9 mg) from purification of fraction 29 (R_T =15.5 min) over a Genesis C18 column, eluted by isocratic elution of H_2O/MeOH (77:23). Fraction 40 (R_T =20.2 min) was further processed over a Synergi Hydro−RP (Phenomenex) column (eluted by H_2O/MeOH, 75:25) and yielded compounds **3** (14.3

mg), **8** (9.1 mg) and **15** (29.9 mg). Fraction 51 (R_T =25.5 min) yielded compounds **4** (5.2 mg) and **17** (7.6 mg) from purification over a Genesis C18 column eluted by H_2O/MeOH (75:25).

Heimiol B (**1**). Light brown amorphous powder; negative ion HR−TOF−MS $[M-H]^-$ m/z 469.1288 (calc. for $C_{28}H_{22}O_7$: 471.1444). ^{1}H− and ^{13}C−NMR data are listed in Table 1. HMBC correlations are as in Figure 2 (selected) and H-2(6)a/C-4a, H-3(5)a/C-4a, H-12a/C-10a, H-12a/C-13a, H-14a/C-10a, 14a/C-13a, H-2(6)b/C-4b, H-3(5)b/C-4b, H-7b/C-1b, H-7b/C-2(6)b, H-7b/C-9b, H-8b/C-1b, H-8b/C-9b, H-8b/C-10b, H-8b/C-14b H-12b/C-10b, H-12b/C-11b, H-12b/C-13b, H-14b/C-10b, H-14b/C-13b, H-7b/C-10a and H-7b/C-11a. NOESY correlations, see Figure 2.

Heimiol C (**2**). Dark brown amorphous powder; negative ion HR-TOF-MS $[M+Na]^+$ m/z 947.2679 (calc. for $C_{56}H_{44}O_{13}$: 925.2860). ^{1}H and ^{13}C NMR data are listed in Table 1. HMBC correlations are as in Figure 4 (selected) and H-2(6)a/C-6(2)a, H-2(6)a/C-1a, H-2(6)a/C-4a, H-2(6)a/C-7a, H-3(5)a/C-5(3)a, H-2(6)b/C-6(2)b, H-2(6)b/C-4b, H-3(5)a/C-1a, H-3(5)a/C-4a, H-3(5)b/C-1b, H-3(5)b/C-4b, H-3(5)b/C-5(3)b, H-12b/C-10b, H-12b/C-11b, H-12b/C-13b, H-12b/C-14b, H-14b/C-10b, H-14b/C-12b and H-14b/C-13b. NOESY correlations, see Figure 4.

Heimiol D (**3**). Pale yellow amorphous powder; negative ion HR-TOF-MS $[M-H]^-$ m/z 905.2581 (calc. for $C_{56}H_{42}O_{12}$: 907.2755). ^{1}H and ^{13}C NMR data are listed in Table 1. HMBC correlations are as in Figure 5 (selected) and H-2(6)a/C-6(2)a, H-2(6)a/C-4a, H-3(5)a/C-1a, H-3(5)a/C-2(6)a, H-3(5)a/C-4a, H-7a/C-1a, H-7a/C-2(6)a, H-7a/C-8a, H-7a/C-9a, H-8a/C-1a, H-8a/C-7a, H-8a/C-10a, H-12a/C-10a, H-14a/C-10a, H-14a/C-11a, H-2(6)b/C-6(2)b, H-2(6)b/C-3(5)b, H-2(6)b/C-4b, H-3(5)b/C-1b, H-3(5)b/C-5(3)b, H-3(5)b/C-4b, H-7b/C-1b, H-7b/C-2(6)b, H-7b/C-9b, H-8b/C-10b, H-8b/C-7c, H-2(6)c/C-6(2)c, H-2(6)c/C-1c, H-3(5)c/C-1c, H-3(5)c/C-5(3)c, H-3(5)c/C-4c, H-7c/C-10b, H-7c/C-8b, H-8c/C-7b, H-8c/C-7c, H-8c/C-10b, H-12c/C-10c, H-12c/C-11c, H-2(6)d/C-6(2)d, H-2(6)d/C-3(5)d, H-2(6)d/C-4d, H-3(5)d/C-1d, H-3(5)d/C-5(3)d, H-3(5)d/C-4d, H-7d/C-2(6)d, H-7d/C-1d, H-8d/C-11(13)d, H-8d/C-10c and H-12d/C-11(13)d. NOESY correlations, see Figure 5.

Heimiol E (**4**). Pale yellow amorphous powder; positive ion HR-TOF-MS $[M+H]^+$ m/z 907.2587 (calc. for $C_{56}H_{42}O_{12}$: 907.2755). ^{1}H and ^{13}C NMR data are listed in Table 1 and 2.

HMBC correlations are as in Figure 6 (selected) and H-2(6)a/C-6(2)a, H-2(6)a/C-4a, H-2(6)a/C-7a, H-3(5)a/C-1a, H-3(5)a/C-5(3)a, H-3(5)a/C-4a, H-7a/C-2(6)a, H-7a/C-8a, 7a/C-9a, 8a/C-1a, 8a/C-7a, 8a/C-9a, H-8a/C-10a, H-10a/C-11a, H-14a/C-13a, H-2(6)b/C-6(2)b, H-2(6)b/C-4b, H-2(6)b/C-7b, H-3(5)b/C-1b, H-3(5)b/C-5(3)b, H-3(5)b/C-4b, H-7b/C-1b, H-7b/C-2(6)b, H-7b/C-8b, H-7b/C-9b, H-7b/C-13c, H-7b/C-14c, H-8b/C-1b, H-8b/C-7b, H-8b/C-9b, H-8b/C-10b, H-8b/C-14b, H-8b/C-9c, H-12b/C-10b, H-12b/C-11b, H-12b/C-13b, H-12b/C-14b, H-12b/C-7c, H-2(6)c/C-6(2)c, H-2(6)c/C-4c, H-2(6)c/C-7c, H-3(5)c/C-1c, H-3(5)c/C-5(3)c, H-3(5)c/C-4c, H-7c/C-1c, H-7c/C-2(6)c, H-7c/C-8c, H-7c/C-13b, H-7c/C-14b, H-8c/C-1c, H-8c/C-7c, H-8c/C-9c, H-8c/C-10c, H-8c/C-11c, H-8c/C-14c, H-8c/C-9b, H-12c/C-10c, H-12c/C-11c, H-12c/C-13c, H-12c/C-14c, H-12c/C-7b, H-2(6)d/C-6(2)d, H-2(6)d/C-4d, H-2(6)d/C-7d, H-3(5)d/C-1d, H-3(5)d/C-5(3)d, H-3(5)d/C-4d, H-7d/C-8d, H-7d/C-2(6)d, H-7d/C-9d, H-8d/C-7d, H-8d/C-9d, H-8d/C-10d, H-10d/C-11d, H-10d/C-12d, H-12d/C-11d, H-12d/C-13d, H-12d/C-14d, H-14d/C-12d and H-14d/C-13d. NOESY correlations, see Figure 6.

Chapter 6 – Antioxidants

Chapter 6 – Antioxidants

The plant kingdom provides the largest number of antioxidants. There are mainly terpenoids (e.g. vitamin E, vitamin C) and polyphenols (e.g., flavonoids, stilbenoids, lignans, Schiff bases), and in a less extent alkaloids (e.g., caffeine, theobromine). The large variety of the chemical structures of polyphenols allows many important biological activities, including antioxidant activity. Over the past two decades, many works have been dedicated to theoretical elucidation of the free radical scavenging capacity of polyphenols.[263]–[268], [268]

QM allows calculating different physico−chemical parameters related to the antioxidant activity including OH−BDE (the major descriptor of the antioxidant activity), IP (Ionization Potential), ETE (Electron Transfer Energy) from deprotonated forms, and electronic and spin density distributions. The use of hybrid DFT functionals provides an accurate description of the structure-activity relationships of free radical scavenging, in agreement with experiments.[269]–[274] The aim of the theoretical calculations is to accurately predict activity of new compounds, as a crucial stage for pharmaceutical, cosmetic and food industries. The free radical scavenging by a polyphenol antioxidant proceeds by H atom transfer through four possible mechanisms (see section I).

This chapter includes two sections. Section I describes antioxidant properties of phenolic Schiff bases and section II describes non−covalent association of antioxidants in lipid−bilayer membranes.

Note for readers: *This article has been published in the Journal of Computer-Aided Molecular Design (Anouar et al., J Comput Aided Mol Des, 10.1007/s10822-013-9692-0). My contribution concerns the study of the SPLET mechanism. The entire manuscript is incorporated in this PhD to keep consistency.*

The figure and reference formats and positions are sometimes modified compared to the original article to keep homogeneity in the thesis.

Section I. Antioxidant properties of phenolic Schiff bases: Structure activity relationship and mechanism of action

El Hassane Anouar[a,*], Salwa Raweh[a,b], Imene Bayach[a,c], Muhammad Taha[a], Mohd Syukri Baharudin[a], Florent Di Meo[d], Mizaton Hazizul Hasan[b], Aishah Adam[b], Nor Hadiani Ismail[a,e], Jean-Frédéric F. Weber[a,b], Patrick Trouillas[d,f-g*]

Abstract: Phenolic Schiff bases are known for their diverse biological activities and ability to scavenge free radicals. To elucidate (i) the structure–antioxidant activity relationship of a series of thirty synthetic derivatives of 2–methoxybezohydrazide phenolic Schiff bases and (ii) to determine the major mechanism involved in free radical scavenging, we used density functional theory (DFT) calculations (B3P86/6–31+(d,p)) within polarizable continuum model. The results showed the importance of the bond dissociation enthalpies related to the first (BDE) and second (BDE_d) hydrogen atom transfer (intrinsic parameters) for rationalizing the antioxidant activity. In addition to the number of OH groups, the presence of a bromine substituent plays an interesting role in modulating the antioxidant activity. Theoretical thermodynamic and kinetic studies demonstrated that the free radical scavenging by these Schiff bases mainly proceeds through proton–coupled electron transfer (PCET) rather than sequential proton loss electron transfer (SPLET), the latter mechanism being only feasible at relatively high pH.

Keywords: Schiff bases, Antioxidant, DFT, kinetics, free–radical–scavenging, BDE, structure–activity–relationship.

[a]*Atta-ur-Rahman Institute For Natural Product Discovery (RiND), Universiti Teknologi MARA, 42300 Bandar Puncak Alam, Selangor D. E, Malaysia.*

[b]*Faculty of Pharmacy, Universiti Teknologi MARA, Puncak Alam Campus, Malaysia.*

[c]*LCSN - Faculté de Pharmacie, Université de Limoges, 2 rue du Dr Marcland, 87000 Limoges, France*

[d]*INSERM, UMR-S850 / Faculté de Pharmacie, Université de Limoges, 2 rue du Dr Marcland, 87000 Limoges, France*

[e]*Faculty of Applied Sciences, Universiti Teknologi MARA, 40450 Shah Alam. Malaysia.*

[f]*Laboratoire de Chimie des Matériaux Nouveaux, Université de Mons, Place du Parc, 20, B-7000, Mons, Belgium*

[g]*Regional Center of Advanced Technologies and Materials, Department of Physical Chemistry, Faculty of Science, Palacký University, 17. Listopadu 1192/12, 77146 Olomouc, Czech Republic*

Corresponding author:
Atta-ur-Rahman Institute for Natural Product Discovery (RiND), Universiti Teknologi MARA Kampus Puncak Alam, 42300 Bandar Puncak Alam, Selangor D. E, Malaysia.
Tel: +603 3258 4771; fax:+603 3258 4770
E-mail addresses: (E. Anouar), patrick.trouillas@unilim.fr (P. Trouillas).

1. Introduction

Natural and synthetic phenols including flavonoids, phenolic acids, stilbenoids and curcuminoids have been described as powerful antioxidants, being able to efficiently scavenge free radicals.[218], [275], [276] Schiff bases form an important class of synthetic phenolic compounds, substituted by a hydrazone moiety. They are known for their various fields of application including inorganic chemistry, biological and analytical chemistry.[277], [278] Several studies focused on their biological activities as antibacterial,[279]–[282] anticancer,[278] and antifungal activities.[283], [284] Recently, we reported the antileishmanial activity of the series of synthetic Schiff bases studied in the present work (Fig. 1).[285] Schiff bases also showed potent antioxidant activity to scavenge free radicals. In two recent studies, we reported the antioxidant activity of acylhydrazide and 2,4,6–trichlorophenylhydrazine Schiff bases as DPPH radical and super oxide anion scavengers.[286], [287] Free radical scavenging capacity of (poly)phenols is generally attributed to the hydrogen atom lability of the OH groups attached to aromatic rings (Ar);[269], [271], [288], [289] however in some other antioxidants, NH and SH groups may provide labile hydrogen.[290]–[296] Antioxidants (ArX-H) may scavenge free radicals ($R^{\bullet}$) by H atom transfer through one of the four mechanisms:

(i) HAT (hydrogen atom transfer) and PCET (proton-coupled electron transfer)

$$ArX–H + R^{\bullet} \rightarrow ArX^{\bullet} + R–H \quad \text{(eq. 1)}$$

This is the direct HAT, which is purely governed by the homolytic bond dissociation enthalpy (BDE) of X–H; note that the lower the BDE, the more important the role of the corresponding XH group in the antioxidant activity. PCET is distinguished from the pure HAT as it involves several molecular orbitals in an H–bonding pre–reaction complex.[297]–[300] The proton transfer is coupled to the electron transfer that occurs from a lone pair of the antioxidant to the SOMO (singly occupied molecular orbital) of the free radical.

ii) ET–PT (Electron Transfer – Proton Transfer) or SET–PT (Sequential ET–PT)

$$ArX–H + R^{\bullet} \rightarrow ArXH^{+\bullet} + R^{-} \rightarrow ArX^{\bullet} + R–H \quad \text{(eq. 2)}$$

The first step of this reaction leads to the formation of the radical cation $ArXH^{+\bullet}$, which easily undergoes heterolytic dissociation of X–H bond leading to the same final products than those yielded by PCET. The first step is mainly governed by the ionization potential (IP) of the antioxidant.

iii) SPLET (Sequential Proton–Loss–Electron–Transfer)

$$ArX–H \rightarrow ArO^- + H^+ \qquad \text{(eq. 3)}$$

$$ArX^- + R^\bullet \rightarrow ArX^\bullet + R^- \qquad \text{(eq. 4)}$$

$$R^- + H^+ \rightarrow RH \qquad \text{(eq. 5)}$$

In this mechanism, a proton is lost prior to electron transfer from the subsequent anion to the free radical. SPLET is strongly favoured under alkaline conditions, which may help in the proton loss of the first step.[301], [302]

iv) AF (Adduct Formation)

$$ArX–\mathbf{H} + R^\bullet \rightarrow [ArXH–R]^\bullet \rightarrow \text{metabolites or } ArX^\bullet + RH \qquad \text{(eq. 6)}$$

This mechanism is relatively specific to $^\bullet OH$ free radicals. It has been observed in radiolytic solutions. The radical may add on double bonds and aromatic rings. This mechanism is not considered in this work. As often shown in the literature, intrinsic parameters including BDE, IP and ETE (electron transfer enthalpy) rationalize free radical scavenging capacities [269], [271], [288], [303] as the thermodynamic balance of the first three mechanisms is the same ($\Delta G^{PCET} = \Delta G^{ET\text{-}PT} = \Delta G^{SPLET}$). However to tackle the mechanisms of action, kinetic parameters should be considered.[268], [271], [296], [301], [304], [305]

In the present study, we elucidate the structure–antioxidant activity relationship for a series of 30 synthetic derivatives of 2–methoxybezohydrazide phenolic Schiff bases (Fig. 1). The Schiff bases differ from the nature of the R– (aromatic) moiety attached to the nitrogen atom engaged in the –N=C double bond (Fig. 1). The compounds can be subdivided into three classes, namely (i) compounds **1**-**25**, where the aromatic ring is a benzene substituted with different OH,

OCH_3, halogen, $COOCH_3$ and NO_2 groups, (ii) compounds **26–28**, in which R is an unsubstituted pyridine attached at the three different possible positions and (iii) compounds **29–30**, in which R is an unsaturated five–membered ring containing one heteroatom. The positive or negative contributions of different descriptors (e.g, number and position of OH groups, BDE, double (BDEd), IP, spin density distribution, intramolecular hydrogen bonds, presence of electron donating or withdrawing groups, and structural parameters) have been examined. The elucidation of the mechanism of action is based on a combined experimental and theoretical approach. For the theoretical approach, transition state and Marcus–Levich–Jörtner theories were used to evaluate atom (PCET mechanism) and electron transfer (SPLET mechanism), respectively.

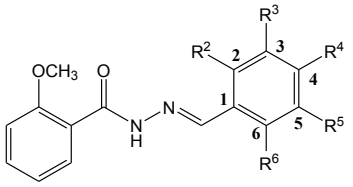

Monohydroxylated
1: $R^2 = OH$
2: $R^3 = OH$
3: $R^4 = OH$

Dihydroxylated
4: $R^2 = R^3 = OH$
5: $R^2 = R^4 = OH$
6: $R^2 = R^5 = OH$
7: $R^3 = R^4 = OH$
8: $R^3 = R^5 = OH$

Trihydroxylated
9: $R^2 = R^4 = R^6 = OH$
10: $R^3 = R^4 = R^5 = OH$

Monomethoxylated
11: $R^3 = OCH_3$
12: $R^4 = OCH_3$

Dimethoxylated
13: $R^3 = R^4 = OCH_3$
14: $R^3 = R^5 = OCH_3$

1-OH and 1-OCH_3
15: $R^2 = OH$, $R^4 = OCH_3$
16: $R^2 = OH$, $R^5 = OCH_3$
17: $R^3 = OH$, $R^4 = OCH_3$

Halogenated
18: $R^3 = Br$, $R^4 = OH$
19: $R^3 = Br$, $R^4 = Cl$
20: $R^4 = F$
21: $R^4 = Cl$
22: $R^2 = I$, $R^3 = OH$, $R^4 = OCH_3$

Other substitution
23: $R^4 = COOCH_3$
24: $R^4 = NO_2$

No substitution
25: $R^i = H$ (i = 2 to 6)

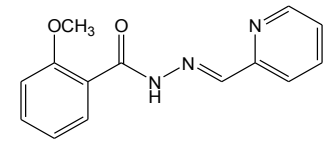

26

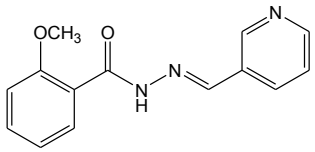

27

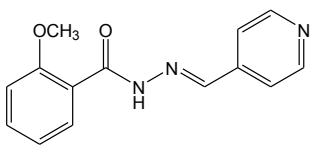

28

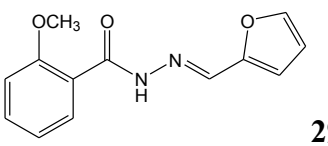

29

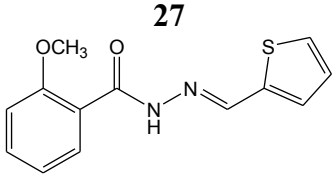

30

Figure 1. Structures of the synthesized Schiff bases.

2. Methodology

- ***Experimental synthesis***

The N–benzylidene–2–methoxybenzohydrazide phenolic derivatives were synthesized by refluxing mixtures of 2 mmol 2–methoxy–benzohydrazide and different aldehydes in methanol and in the presence of catalytical amount of acetic acid for 3 hours, according to the previously described method.[285] The reaction progress was monitored by thin layer chromatography (TLC); after completion, the solvent was evaporated under vacuum to afford the crude products, which were further re-crystallized in methanol. Needle–like pure products in good to excellent (0.40g (78%) - 0.58 (92%)) yields were obtained.[285]

- ***DPPH free radical scavenging capacity***

The antioxidant capacity was evaluated as the capacity of the 30 different compounds to scavenge the 1,1–diphenyl–2–picrylhydrazil (DPPH) free radical, following the Blois' method.[306] The reaction mixture contains 5 µL of test sample (1 mM in DMSO) and 95 µL of DPPH (Sigma, 300 µM) in ethanol; it was placed into a 96-well microtiter plate and incubated at 37º C for 30 min. The UV/Vis light absorbance was measured at 515 nm on microtiter plate reader (Molecular Devices, CA, and USA). The percentage of free radical scavenging was determined with respect to DMSO control. Following free radical scavenging vs. compound concentration, IC_{50} was measured, which represent the concentration of compounds that scavenge 50% of DPPH radicals (i.e., 50% of absorbance at 515 nm). Propyl gallate was used as a positive control. All chemicals used were of analytical grade (Sigma, USA).

- ***General computational details***

Geometry optimization and frequency calculations have been carried out using density functional theory (DFT) as implemented in Gaussian09.[260] To elucidate the structure–antioxidant activity relationship of polyphenols, the hybrid functional B3P86 appears reliable.[221], [270], [273]a Increasing the number of polarization and diffuse functions have no significant effects on theoretical results, especially on BDEs and IPs,[270], [271] therefore the calculations were

performed with the 6−31+G(d,p) basis set. The ground states (GSs) geometries were confirmed by the absence of any imaginary frequency, while for the transition states (TSs) of PCET one imaginary frequency was obtained, which corresponds to H atom transfer. It has been shown that the B3P86 hybrid functional underestimates activation energy ($\Delta G^{\#}$) especially for hydrogen atom transfer reactions [274], [307]; in this course, MPWB1K appears more recommended even if overestimation are sometimes observed.[308], [309] The kinetic calculations of the PCET mechanism were performed with both (U)B3P86/6−31+G (d,p) and MPWB1K/6−31+G(d,p) methods.

Solvent effects were taken into account implicitly using the polarizable continuum model (PCM). In PCM models, the substrate is embedded into a shape−adapted cavity surrounded by a dielectric continuum characterized by its dielectric constant (ε_{MeOH} = 32.613).[261] Using an explicit solvent were investigated by other authors,[310] confirming that PCM succeeded in providing a reasonably accurate description of BDE, the main descriptor of antioxidant capacity. Hybrid models (*i.e.*, one or two molecules in the surrounding of the OH groups + PCM) were also tested for quercetin, an antioxidant, showing only slight differences in terms of BDE when compared to pure PCM calculations, while computational time was dramatically increased.[288]

- ***Pre-reaction complexes, descriptions of non-covalent interactions and electron transfer kinetics***

The rate constants of electron transfer (i.e., for ET−PT and SPLET mechanism) were evaluated within the Marcus−Levich−Jortner ($k^{\text{LJ-Marcus}}$) formalism according the following expression:

$$k^{\mathrm{LJ-Marcus}} = \frac{4\pi^2}{h} \cdot V_{RP}^2 \sqrt{\frac{1}{4\pi\lambda_S k_b T}} \cdot \sum_{\upsilon'} \left\{ \frac{S^{\nu'}}{\nu'!} \cdot \exp(-S) \cdot \exp\left[-\frac{(\Delta G^\circ + \lambda_S + \nu' \hbar \langle\omega\rangle)^2}{4\lambda_S k_b T} \right] \right\}$$

where ΔG° is the Gibbs energy difference of ET reactions (i.e., eq. (2) or (4) for SET−PT and SPLET, respectively), λ_S is the outer−shell reorganisation energy attributed to the solvent, V_{RP} is the electronic coupling, S is the Huang−Rhys factor and ν' is the vibrational quantum number. The sum runs over all effective vibrational modes, namely in our case aromatic C−C, phenolic C−O and C−N bond stretching. These bonds are the most probable reaction coordinates involved

in electron transfer. $\Delta G°$, λ_S, S were calculated following the previous study on free radical scavenging of quercetin.[301] V_{RP} was calculated from the pre−reaction complex geometries. They were calculated following the Farazdel et al. approach with a def2−TZVP basis set:[311]

$$V_{RP} = \frac{H_{RP} - S_{RP}\frac{(E_R + E_P)}{2}}{1 - S_{RP}^2}$$

where H_{RP} is the total reactant−product interaction energy, S_{RP} is the reactant−product overlap, E_R and E_P are the electronic energies of reactants and products, respectively.

Pre−reaction complexes are of major importance in ET mechanisms since they drive the bimolecular mechanisms. These complexes involved either H−bond or [ν–π] dispersive interactions, which are poorly described by classical hybrid functionals. Dispersion−corrected DFT−D is a successful approach to circumvent the use of expensive post−HF methods.[211], [312], [313] The B3P86−D2 functional was recently re-parameterized, reaching accuracy to evaluate dispersion effects in the non−covalent complexes involving natural polyphenols.[184] The geometries of the pre−reaction complexes were obtained at the B3P86−D2/def2−TZVPP level of theory for all possible H-bond and [ν–π] complexes, i.e., either towards the OH groups or towards aromatic and N−N *p*−bonds. All calculations were carried out using Gaussian09,[260] Orca 2.8.1 [222] and NWCHEM 6.1.1 [314] packages for PCET, SPLET and electronic coupling calculations, respectively. When available, the RIJCOSX (resolution of identity and chain−of−sphere) approximations were used, allowing large speed−up of calculations for a minimal error.[224]

3. Results and discussion

- ***Experimentally-based (DPPH scavenging) structure activity relationship***

As usually observed for polyphenols, at least one phenolic OH group is required to provide an active compound (namely, **1–10**, **15–18**, **22** as seen in Table 1); the other compounds without OH group are inactive (namely, **11–14**, **19–21**, **23–30**). The position of OH groups is of crucial

importance to modulate antioxidant capacity. Based on the measured IC_{50} values (Table 1), the active phenolic Schiff bases can be divided into three classes, depending on the number and position of the OH groups.

*(i) One OH–group compounds (compounds **1-3**, IC_{50} ranging from 0.6 to 1.1 µg/mL)* - In this case, compound **3** with a *para*–OH group is a stronger antioxidant than **1** having an *ortho*–OH group, being as well more active than **2** with a *meta*–OH group.

*(ii) Two OH–group compounds (compounds **4-8**, IC_{50} ranging from 0.2 to 0.9 µg/mL)* - The following order in terms of antioxidant activity is observed **7** ≈ **4** < **5** < **8** ≈ **6**. In the active phenolic Schiff bases **7** and **4**, the two OH groups are *ortho* to each other, which makes the compounds particularly active (IC_{50} about 0.2 µg/mL). This positive contribution of the catechol moiety is in agreement with the general literature on the structure–antioxidant activity relationship of polyphenols.[270], [271], [275], [288] Compound **5**, having two OH groups *meta* to each other, one being in *para* with respect to the N=C double bond is less active. Compounds **6** and **8**, having two OH groups *meta* to each other (no OH group at C4), are even much less active (Table 1). This highlights the importance of the *para* substitution in the benzene moiety.
*(iii) Three OH–group compounds (compounds **9-10**)* - Compound **10** is a stronger antioxidant than **9**, is particularly due to the adjacent three OH groups.

The main trend observed here is that compounds of the first class are less active than those of the other two classes. Moreover the presence of two OH groups *ortho* to each other and one OH group *para* is of crucial importance to increase the activity. An additional third OH group is not mandatory to increase the antioxidant capacity, as already observed for myricetin with respect to quercetin.[275]

Another interesting feature derived from this series of compounds concern the effect of bromination and methoxylation of phenolic ring. To emphasize this effect on the antioxidant activity, compound **7** (3–OH, 4–OH) is compared to both **17** (3–OH, 4–OCH_3), and **18** (3–Br, 4–OH). The methoxylation significantly reduces the antioxidant activity (Table 1), while interestingly the bromine at C3 makes compound **18** as active as **7** (having the active catechol moiety).

Table 1 BDEs, IPs, spin density on the oxygen atom from which the hydrogen atom is removed, as obtained with PCM–B3P86/6–31+G (d,p), and experimental IC_{50} of the 30 Schiff bases.

Schiff base	BDEd (Kcal/mol)						IP (eV)	Spin density*	IC_{50} (μg/mL)
	NH	2-OH	3-OH	4-OH	5-OH	6-OH			
1	96.5	83.8	-	-	-	-	6.4	0.27	0.90± 0.045
2	97.7	-	87.1	-	-	-	6.6	0.37	1.1 ± 0.05
3	95.7	-		83.2	-	-	6.3	0.32	0.65± 0.045
4	96.7	77.5	79.7		-	-	6.5	0.31	0.22± 0.045
5	94.7	82.4	-	82.2	-	-	6.2	0.25	0.34 ± 0.045
6	96.4	78.8	-		82.2	-	6.3	0.31	0.92 ± 0.045
7	95.8	-	78.8	76.1	-	-	6.2	0.25	0.20± 0.045
8	97.9	-	86.6		87.4	-	6.6	0.34	0.91± 0.0045
9	94.8	83.9	-	83.0	-	84.9	6.1	0.23	0.35± 0.045
10	95.7		80.2	72.3	81.68	-	6.2	0.27	0.30 ± 0.045
11	97.7	-	-	-	-	-	6.6	0.50	No activity
12	95.6	-	-	-	-	-	6.3	0.46	>> 2
13	95.6	-	-	-	-	-	6.2	-	>> 2
14	97.7	-	-	-	-	-	6.6	0.50	>> 2
15	94.7	84.1	-	-	-	-	6.2	0.28	0.50 ± 0.071
16	97.2	79.2	-	-	-	-	6.2	0.31	1.01± 0.045
17	95.5		86.0	-	-	-	6.2	0.33	0.8 ± 0.002
18	96.6	-	-	82.2	-	-	6.4	0.26	0.22 ± 0.0045
19	99.0	-	-	-	-	-	6.7	0.53	>> 2
20	97.4	-	-	-	-	-	6.6	0.49	>> 2
21	97.7	-	-	-	-	-	6.6	0.49	>> 2
22	-	-	-	-	-	-	-	-	1.63 ± 0.21
23	98.6	-	-	-	-	-	6.8	0.45	>> 2
24	99.6	-	-	-	-	-	7.0	0.50	>> 2
25	97.5	-	-	-	-	-	6.6	0.51	>> 2
26	98.4	-	-	-	-	-	6.9	0.57	>> 2
27	98.5	-	-	-	-	-	6.8	0.51	>> 2
28	99.4	-	-	-	-	-	7.0	0.54	>> 2
29	94.9	-	-	-	-	-	6.4	0.45	>> 2
30	95.1	-	-	-	-	-	6.4	0.44	>> 2

*Spin density of the active OH site

❖ *Theoretical rationalization*

The free radical scavenging capacity has been extensively correlated to O–H BDEs, rationalized by spin density distribution and stability of the phenoxyl radical ($ArX^{\bullet}$ with X=O) formed after HAT. In principle, N–H BDE may also correlate with the free radical scavenging capacity, since the hydrogen of these groups may be labile according to the chemical neighboring. The inactive compounds (**11–14**, **19–21**, **23–30**) having no OH group, and thus no O–H BDE, could have only been active due to the NH group. However all N–H BDEs of this series of compounds are higher than 90 kcal/mol (Table 1), making these compounds inefficient to scavenge DPPH. Indeed, the BDE of DPPH–H is ca. 80 kcal/mol,[273], [315] thus for these compounds the thermodynamic balance of eq. 1 is positive with DPPH.

In the first class of active compounds (**1-3**), the low antioxidant activity of **2** is in agreement with the relatively high BDE of the *ortho*−2−OH group (87.1 kcal/mol) compared to those of the *meta*−3−OH and *para*−4−OH groups (83.8 and 83.1 kcal/mol, respectively). The BDE is related to the capacity of the phenoxy radical (ArO$^{\bullet}$) formed after HAT (eq. 1) to stabilize by π−conjugation. The higher BDE obtained for the 2−OH group is attributed to a lower spin density delocalization in the corresponding ArO$^{\bullet}$ (Fig. 2a-middle) compare to the better π−conjugation observed when HAT occurs at 3−OH (Fig. 2a-left and right). Regarding both compounds **1** and **3**, the BDEs are similar (difference in BDE ca. 0.5 kcal/mol as seen in Table 1), while the latter compound is more active as free radical scavenger (Table 1). This shows that BDE cannot be the only descriptor to fully rationalize slight antioxidant activities. In this case, the spin density distribution better explain this difference i.e., ArO$^{\bullet}$ obtained after HAT from **3** exhibits a better electron delocalization (Fig. 2a). In next section this is even better rationalized with another secondary descriptor.

In the second class of active compounds (**4**−**8**), the role of the catechol moiety (compounds **4** and **7**) is rationalized by the low BDE values, namely 76.1 and 77.5 kcal/mol for 2−OH (**4**) and 4−OH (**7**), respectively. The low BDEs obtained in the catechol moiety is attributed to the stabilization of the corresponding ArO$^{\bullet}$ by spin delocalization (Fig. 2b) and intramolecular H−bonding. In compound **7**, the 4−OH group has a lower BDE (76.1 kcal/mol) than the 3−OH group (78.8 kcal/mol), in agreement with the better spin density delocalization when HAT occurs from the former group (Fig. 2b). Compare to **4** and **7**, the Schiff bases **5**, **6** and **8** exhibit higher BDEs, as correlated by the higher IC_{50} values (Table 1). This again exemplified the importance of the catechol moiety in the antioxidant activity.

In the third class, the Schiff base **10** is more active than **9**. This is attributed to the low BDE of 4−OH in **10** (72.3 kcal/mol) (Table 1). The decrease in free radical scavenging capacity observed from **7** to **17** (after methylation of 4−OH) is simply attributed to the loss of the most active group (having the lowest BDE and no delocalization of spin density (Fig. 2c-left)). When methylation occurs on the other OH groups, the effects on BDE is lower and the free radical scavenging capacity is not significantly reduced (Table 1).

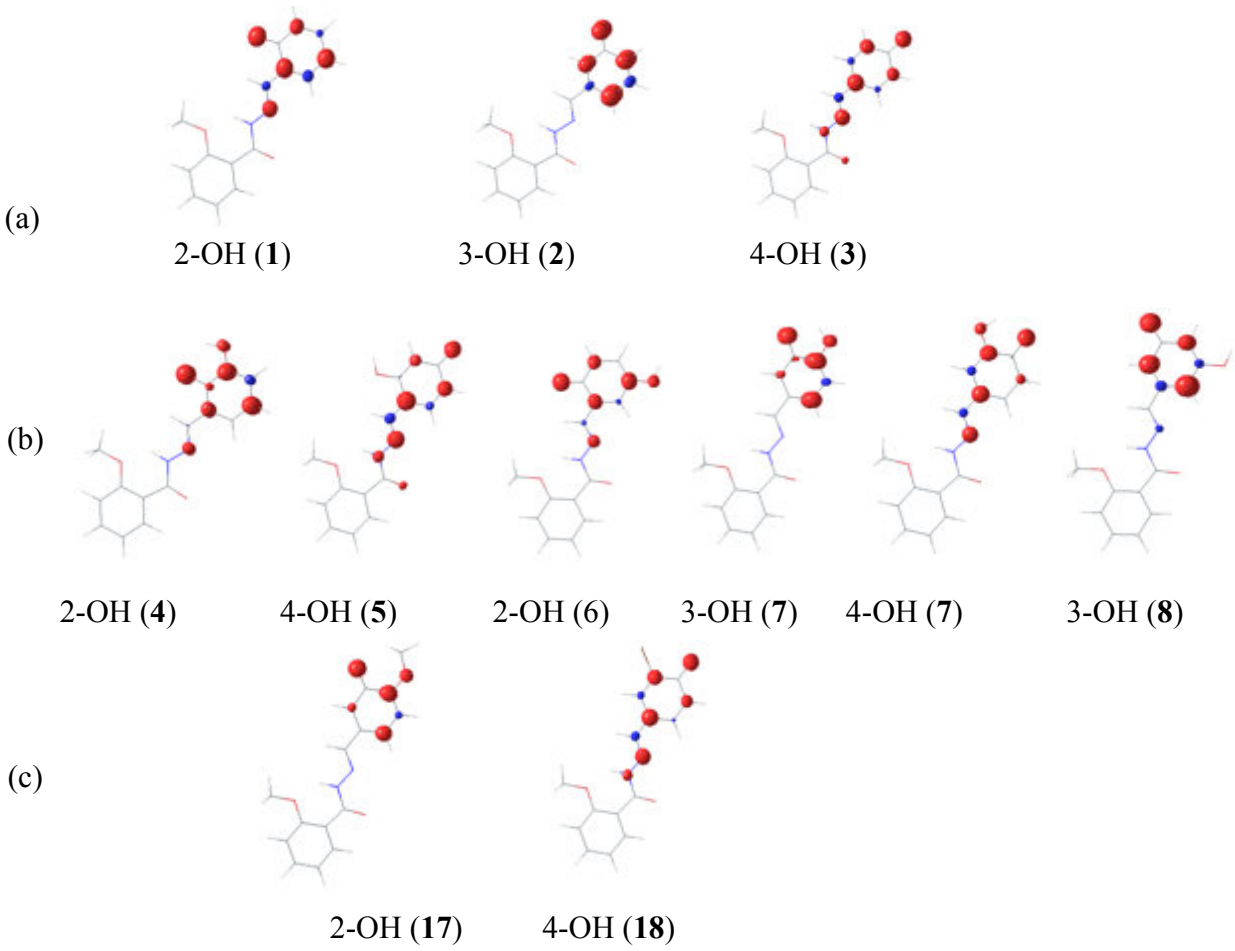

Figure 2. Spin density distribution of the AO$^{\bullet}$ obtained after first HAT transfer from (a) 2–OH, 3–OH, 4–OH groups for compounds **1**, **2** and **3**, respectively; (b) 2–OH, 4–OH, 2-OH, 3(4)-OH and 3–OH groups for compounds **4**, **5**, **6**, **7** and **8**, respectively; (c) 2-OH and 4-OH for compounds **17** and **18**, respectively.

The substitution of position 3 by a bromine (compound **18**) slightly decreases the 4–OH BDE compare to compound **3**, having only one OH group at C4 (Table 1) and increases spin delocalization in the related phenoxy radical compare to compound **7** (Fig. 2c-right). This agrees perfectly with a relatively good free radical scavenging capacity (Table 1), showing the role of bromine substitution in enhancing the antioxidant activity.

❖ ***Double BDE Analysis***

The free radical scavenging capacity can be rationalized by HAT from one of the active OH group, but it has also been explained that a second HAT may occurs from active compounds (to

scavenge a second free radical). This has been rationalized by the double BDE (BDE_d) descriptor. In case, the calculated BDEs have similar values, BDE_d may appear as an efficient descriptor to rationalize slight variations of the antioxidant activity. BDE_d appeared particularly adequate to differentiate the antioxidant activity of a series of synthetic oligomers of guaiacol.[271] BDE_d values of the second and third classes (two and three OH groups, respectively) of Schiff bases are reported in table 2. To highlight the potent role of this descriptor, compounds **8** and **17** were considered. After HAT from 3−OH (having very similar BDEs in both compounds), the BDE_ds from the NH group are 113.3 and 100.6 kcal/mol (Table 2), respectively, which agrees with the better activity for the latter compound. Another example concerns compounds **1** and **3**, for which the O−H BDEs are very similar (difference lower than 0.8 kcal/mol, as seen in Table 1) while the N−H BDE_d difference is 2.6 kcal/mol in favor of compound **3** (Table 2), in agreement with the better antioxidant activity of **3**.

Table 2 BDE_d and IP_d of Schiff bases, as calculated with PCM−B3P86/6−31+G(d,p).

Schiff base	BDEd (Kcal/mol)							IC_{50} (μg/mL)
	NH	2-OH	3-OH	4-OH	5-OH	6-OH	IPd (eV)	
1-(2-OH)	88.7	-	-	-	-	-	6.5	0.90± 0.045
2-(3-OH)	112.1	-	-	-	-	-	7.1	1.1 ± 0.05
3-(4-OH)	86.1	-	-	-	-	-	6.4	0.65± 0.045
4-(2-OH)	91.8	-	76.7	-	-	-	6.5	0.22± 0.045
5-(4-OH)	84.9	94.1	-	-	-	-	6.4	0.34 ± 0.045
6-(2-OH)	90.7	-	-	-	68.8	-	6.2	0.92 ± 0.045
7-(4-OH)	87.3	-	75.9	-	-	-	6.2	0.20± 0.045
8-(3-OH)	113.3	-	-	-	107.9	-	7.1	0.91± 0.0045
9-(4-OH)	84.6	95.0	-	-	-	83.6	6.4	0.35± 0.045
10-(4-OH)	88.1	-	76.6	-	79.1	-	6.2	0.30 ± 0.045
15-(2-OH)	86.3	-	-	-	-	-	6.4	0.50 ± 0.071
16-(2-OH)	91.8	-	-	-	-	-	6.1	1.01 ± 0.045
17-(3-OH)	100.6	-	-	-	-	-	6.3	0.8 ± 0.002
18-(4-OH)	86.8	-	-	-	-	-	6.4	0.22 ± 0.0045
22-(3-OH)	-	-	-	-	-	-	-	1.63 ± 0.21

❖ ***Mechanism of free radical scavenging***

The capacity of antioxidant to scavenge free radicals depends on intrinsic parameters as BDE but also on the nature of the free radical itself. In terms of thermodynamics, the radical scavenging depends on the Gibbs energy of eq. 1. Here we focus on DPPH and a prototype of peroxy radical ($CH_3OO^{\bullet}$). The free radical scavenging of DPPH usually correlate relatively well with that of peroxy radicals even if both radicals are chemically different.[303] The thermodynamic balance is calculated for both reactions:

$$ArO–\mathbf{H} + DPPH^{\bullet} \rightarrow ArO^{\bullet} + DPPH–\mathbf{H} \quad \text{(eq. 1')}$$

$$ArO–\mathbf{H} + CH_3OO^{\bullet} \rightarrow ArO^{\bullet} + CH_3OO–\mathbf{H} \quad \text{(eq. 1'')}$$

Table 3. Gibbs energies of the HAT and ET processes (ΔG^{HAT} and ΔG^{ET}) of Schiff bases with the DPPH and $CH_3OO^{\bullet}$ free radical, as obtained with B3P86/6–31+G (d,p).

Schiff base	HAT mechanism				ET mechanism			
	ΔG^{HAT} with DPPH		ΔG^{HAT} with $CH_3OO^{\bullet}$		ΔG^{ET} with DPPH		ΔG^{ET} with $CH_3OO^{\bullet}$	
	Gas	Solvent	Gas	Solvent	Gas	Solvent	Gas	Solvent
(a) First HAT								
1	2.9	7.5	-1.6	-0.5	88.0	26.3	143.1	45.7
2	7.1	10.8	2.6	2.8	91.3	29.4	146.5	48.7
3	4.1	6.8	-0.4	-1.2	85.8	23.8	141.0	-1.2
4	-4.1	1.5	-8.6	-6.5	87.4	26.2	142.6	45.6
5	0.9	5.7	-3.5	-2.3	81.9	21.9	137.1	41.3
6	-1.3	2.3	-7.8	-5.6	85.4	24.1	140.5	43.5
7	-4.6	0.2	-9.1	-7.9	84.4	21.7	139.5	41.1
8	6.2	10.3	1.7	2.3	91.2	29.2	146.4	48.6
9	2.7	6.6	-1.8	-1.4	79.1	21.4	134.2	40.8
10	-8.1	-2.7	-12.6	-10.7	83.6	23.5	138.7	42.9
11	15.8	20.5	11.3	12.5	89.4	28.8	144.5	48.1
12	14.5	18.5	10.0	10.4	82.8	-	137.9	-
13	14.8	18.2	10.3	10.2	79.2	20.7	143.4	40.4
14	15.9	20.4	11.4	12.4	87.6	28.1	142.7	47.5
15	7.4	7.7	-0.7	-0.4	79.7	20.0	134.8	39.3
16	-1.2	0.0	-5.7	-8.0	83.5	21.0	138.6	40.4
17	5.4	9.3	0.8	1.3	81.3	20.1	136.4	39.4
18	14.9	6.0	10.5	-2.1	88.4	25.9	143.5	39.8
19	16.0	21.0	11.5	13.0	95.7	32.3	150.8	51.6
20	15.8	20.4	11.3	12.4	93.7	30.0	148.8	49.4
21	16.0	20.7	11.5	12.7	93.5	30.5	148.6	49.8
22	-	-	-	-	-	-	-	-
23	16.3	21.3	11.8	13.3	95.6	33.2	150.7	52.5
24	17.1	21.2	12.6	14.2	104.2	37.4	159.3	56.8
25	15.8	20.3	11.4	12.4	92.9	30.2	148.0	49.5
26	14.6	20.8	10.1	12.8	97.3	35.2	152.4	54.6
27	16.3	21.2	11.8	13.2	98.1	33.7	153.2	53.0
28	16.2	21.7	11.8	13.7	103.3	38.2	158.4	57.6
29	13.7	18.0	9.2	10.0	88.5	24.5	143.6	43.8
30	13.6	18.2	9.1	10.2	88.5	25.0	143.7	44.3
(b) Second HAT								
1	7.0	11.9	1.0	-1.6	91.8	28.0	146.9	42.0
2	33.5	35.2	27.5	21.7	106.9	42.5	161.9	56.5
3	10.2	9.4	4.2	-3.9	90.3	25.7	145.4	39.7
4	-0.4	-0.5	-6.4	-14.0	92.0	29.5	147.0	43.4
5	18.8	18.1	12.8	4.6	88.7	25.0	143.7	38.9
6	-12.5	-7.6	-18.5	-21.0	84.5	21.4	139.5	35.4
7	-0.8	-0.6	-6.8	-14.1	85.8	23.4	140.8	37.3
8	32.3	30.3	26.3	16.9	107.1	43.9	162.1	57.8
9	5.3	9.3	-0.8	-4.2	87.6	26.7	142.6	40.6
10	-0.5	0.1	-6.5	-13.4	85.3	21.2	140.3	35.2
15	5.5	9.7	-0.5	-3.7	88.7	27.5	143.7	41.5
16	10.1	15.7	4.1	2.3	81.7	22.1	136.7	36.1
17	21.6	24.2	15.6	10.8	87.1	25.1	142.1	39.1
18	3.9	9.8	-2.1	-3.6	90.4	26.5	145.4	40.5

In order to tackle the mechanism of action of free radical scavenging, the kinetics of the limiting step should be evaluated. Here only the kinetics of $CH_3OO^{\bullet}$ scavenging was evaluated. Regarding the large Gibbs energy of the ET step in the SET−PT process (higher than 40 kcal/mol as seen in Table 4), this mechanism appears unlikely, as usually described in the literature.[271] The competition may occur between PCET and SPLET.

Table 4. Free energies of activation ($\Delta G^{\#}$) and rate constants (k^{TST}, $k^{TST/W}$ and $k^{TST/ST}$) of HAT mechanism of the active Schiff bases with the CH_3OO ($R^{\bullet}$) free radical, as obtained with hybrid functionals B3P86 and MPWB1K.

		B3P86			
N° of OH in aromatic ring	Compound	$\Delta G^{\#}$	K^{TST}	$K^{TST/W}$	$K^{TST/ST}$
	1	12.26	6.5×10^{3}	2.9×10^{4}	6.5×10^{3}
1-OH	**2**	15.09	5.5 x10	2.2×10^{2}	5.5 x10
	3	11.99	1.0×10^{4}	5.2×10^{4}	1.0×10^{4}
	4	10.73	8.6×10^{4}	2.3×10^{5}	8.6×10^{4}
	5	11.47	2.5×10^{4}	1.2×10^{5}	2.5×10^{4}
2-OH	**6**	9.39	8.3×10^{5}	3.3×10^{6}	8.3×10^{5}
	7	8.82	2.2×10^{6}	9.3×10^{6}	2.2×10^{6}
	8	14.36	1.9×10^{2}	1.1×10^{3}	1.9×10^{2}
	9	11.55	2.2×10^{4}	1.0×10^{5}	2.2×10^{4}
3-OH	**10**	11.53	2.2×10^{4}	3.9×10^{4}	2.2×10^{4}
		MPWB1K			
	1	22.44	2.3×10^{-4}	1.0×10^{-3}	2.3×10^{-4}
1-OH	**2**	23.76	2.5×10^{-5}	1.0×10^{-4}	2.5×10^{-5}
	3	23.20	6.4×10^{-5}	3.2×10^{-4}	6.4×10^{-5}
	4	22.00	4.8×10^{-4}	1.3×10^{-3}	4.8×10^{-4}
	5	22.26	3.1×10^{-4}	1.5×10^{-3}	3.1×10^{-4}
2-OH	**6**	17.97	4.3×10^{-1}	1.7 x10	4.3×10^{-1}
	7	18.10	3.5×10^{-1}	1.5 x10	3.5×10^{-1}
	8	24.16	1.3×10^{-5}	7.1×10^{-5}	1.3×10^{-5}
	9	21.09	2.2×10^{-3}	1.1×10^{-2}	2.2×10^{-3}
3-OH	**10**	20.02	1.4×10^{-2}	2.3×10^{-2}	1.4×10^{-2}

The former mechanism is described by the transition state theory. In the transition state, the hydrogen atom is approximately located between the phenoxyl and peroxyl radicals (Fig. 3).

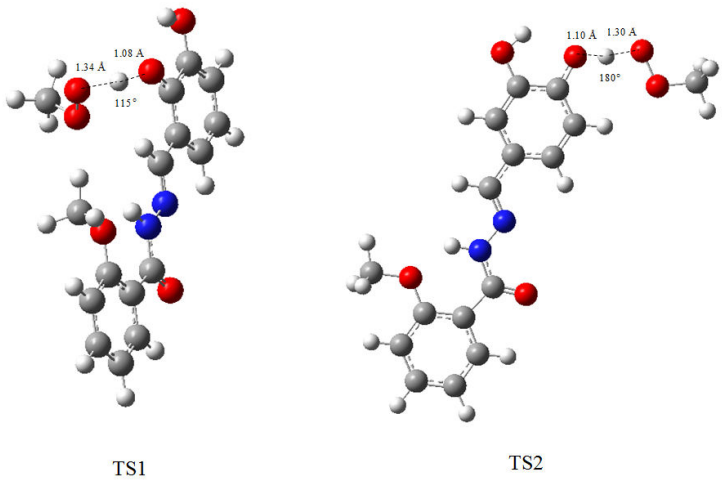

Fig. 3. Geometries of the PCET transition states between the Schiff bases **4** (left) and **7** (right), and the peroxyl radical $CH_3OO^{\bullet}$.

As explained above the B3P86 hybrid functional underestimates Gibbs energy of activation, while MPWB1K give a better description of PCET.[274], [307] Therefore the values reported in Table 5 only provide a range. In this process, tunneling appears crucial thus rate constants are more relevant than $\Delta G^{\#}$ in order to discuss on PCET. The rate constant of the most active compounds (e.g. compound **7**) is ranging from 10^{-1} to 10^{6} $M^{-1}.s^{-1}$ (Table 4), probably within an intermediate value. Compounds having only one OH group (**1**-**3**) are 10^{3} less active than **7**. Interestingly, BDE correlates with $\Delta G^{\#}$ (R^2=0.99) when the two most active compounds are excluded (Fig. 4). Regarding these two compounds, the intramolecular H–bonding may strongly influence kinetics.

Table 5. Structural parameters of the transition state of active Schiff bases and the peroxyl $CH_3OO^{\bullet}$ obtained with B3P86 functional.

	Distance (Å)				Angle (Degree)				Torsional angle (Degree)		
Schiff base	C_a-O_a	O_a-H_a	H_a-O_r	O_r-O_r	C_a-O_a-H_a	O_a-H_a-O_r	H_a-O_r-O_r	O_r-O_r-C_r	C_a-O_a-H_a-O_r	O_a-H_a-O_r-O_r	C_a-O_a-O_r-O_r
1	1.302	1.181	1.204	1.378	120	169	105	110	180	-180	0
2	1.311	1.161	1.214	1.378	115	167	104	109	94	-102	-10
3	1.304	1.139	1.257	1.380	119	170	105	109	-179	179	0
4	-	-	-	-	-	-	-	-	-	-	-
5	1.305	1.127	1.275	1.381	119	170	106	109	-180	180	0
6	1.313	1.103	1.307	1.376	118	169	106	109	180	-180	0
7	1.314	1.110	1.295	1.370	118	171	106	109	-180	180	0
8	1.304	1.173	1.212	1.380	120	170	105	109	167	-170	-3
9	1.305	1.126	1.278	1.382	118	170	106	109	-178	178	0
10	-	-	-	-	-	-	-	-	-	-	-

a: refers to the atom of antioxidant, r: refers to atom of peroxyl radical

The mechanism of antioxidant activity of polyphenols is known to be dependent on pH,[274], [302] due to the capacity of these compounds to deprotonate, leading to an anion having a better capacity to release an electron to the free radical (SPLET mechanism as described in eq. 3-5). SPLET is investigated on the most active compound studied here (**7**). In this case, only the two OH groups of the catechol moiety (3–OH and 4–OH) can be deprotonated. From our calculations, the 4–OH group appears slightly more acidic than 3–OH by 2.6 kcal/mol (Table 6); here we quote **7**– [4H+] and **7**– [3H+] the deprotonated form of **7** at C4 and C3, respectively.

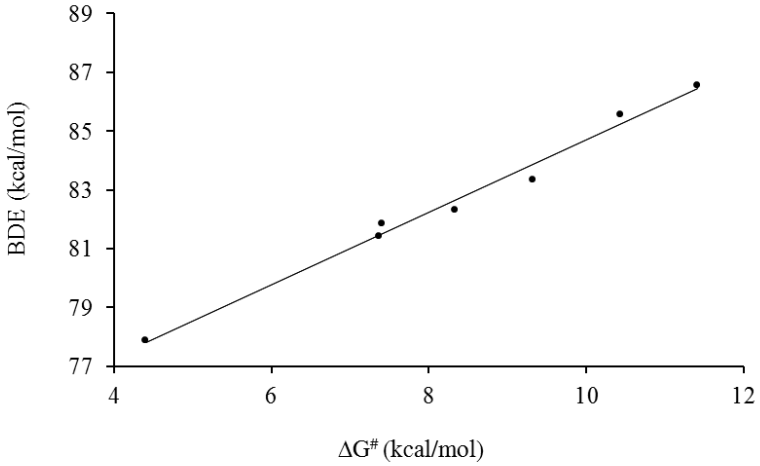

Figure 4. Correlation between BDE and free activation energy ($\Delta G^{\#}$) for peroxyl radical scavenging by active Schiff bases (**1**-**10**).

As expected, IP of the deprotonated form is lower than that of parent molecule by 1.32 and 1.27 eV for **7**–[3H+] and **7**–[4H+], respectively. No significant difference is observed between the electron donor capacities of **7**–[3H+] and **7**–[4H+] (IP = 4.14 and 4.19 eV, respectively). This highlights that the electron donor capacity of **7** is related to the catechol moiety and not only one specific OH group.

The electron transfer towards the free radical is expected only if a non–covalent pre–reaction complex is formed between the antioxidant and the free radical. Two types of pre–reaction complexes may exist, both involving the O–atom lone pair of the free radical. The first type involves a H–bond with the OH group of the antioxidant ([**HB**]–type complex), as observed in the PCET mechanism; the second involves a [ν–π] dispersive interaction with

aromatic π–electrons (i.e., [$\boldsymbol{\nu-\pi}$]–type). It must be stressed that quantum calculations did not allow obtaining [$\boldsymbol{\nu-\pi}$]-type interactions with N–N p–electrons.

From these pre–reaction complexes, the calculated SPLET rate constants are in the range from 10^{-30} to 10^{-3} $M^{-1}.s^{-1}$ (Table 6). These rate constants strongly depend on (i) the electron donor anion (i.e., **7**–[3H+] and **7**–[4H+]) and (ii) the geometry of pre–reaction complexes (Fig. 5). The **7**–[4H+] anion exhibits the highest rate constants (10^{-3} and 10^{-5} $M^{-1}.s^{-1}$ for **7**–[3H+] and **7**–[4H+], respectively). Moreover the **7**–[4H+] anion and the subsequent (post–ET) phenoxyl radical (i.e., **7**–[4H$^{\bullet}$]) show a better π–conjugation than **7**–[3H+] (Fig. 6). Furthermore, the electronic coupling is significantly different between the reactions of both anions (Table 6). According to V_{RP} formula, the lower the molecular orbital (MO) modification along the reaction, the higher the reactant–product overlap S_{RP}, the higher the electron coupling V_{RP} and therefore the higher the rate constant k^{SPLET}. The highest occupied MO (HOMO) modification from **7**–[4H+] to **7**–[4H$^{\bullet}$] is low while HOMOs of **7**–[3H+] and **7**–[3H$^{\bullet}$] have the same location but with opposite sign (Fig. 6), highlighting a broken orbital symmetry and thus decreasing the corresponding rate constants.

Table 6. Relative energy stabilization (**Δ**E) of both studied anion **7**–[3H+] and **7**–[4H+], internal λ_i and external λ_s reorganization energies (kcal.mol^{-1}), electronic coupling V_{RP} (kcal.mol^{-1}), Gibbs energy of the reaction ΔG° (kcal.mol^{-1}), SPLET rate constants k ($M^{-1}.s^{-1}$) for all H–bond and [$\boldsymbol{\nu-\pi}$] complexes.

Anion	ΔE	Conformation	λ_i	λ_s	V_{RP}	ΔG°	k^{SPLET}
	0.00	$[\boldsymbol{\nu-\pi}]_{Abot}$	14.78	20.22	0.12	21.96	$1.4x10^{-6}$
		$[\boldsymbol{\nu-\pi}]_{Atop}$	14.78	14.30	1.53	21.89	$5.6x10^{-5}$
7– [3H+]		$[\boldsymbol{\nu-\pi}]_{Bbot}$	14.78	4.31	1.45	21.53	$3.0x10^{-17}$
		$[\mathbf{n-p}]_{Btop}$	14.78	2.70	0.27	21.70	$1.5x10^{-30}$
		[HB-4]	14.78	14.32	1.54	22.01	$5.7x10^{-5}$
	-2.60	$[\boldsymbol{\nu-\pi}]_{Abot}$	14.08	18.33	3.71	21.90	$1.7x10^{-3}$
		$[\boldsymbol{\nu-\pi}]_{Atop}$	14.08	25.00	4.61	21.83	$2.6x10^{-3}$
7– [4H+]		$[\boldsymbol{\nu-\pi}]_{Bbot}$	14.08	7.29	3.90	22.18	$1.9x10^{-8}$
		$[\boldsymbol{\nu-\pi}]_{Btop}$	14.08	14.61	1.50	21.68	$9.3x10^{-5}$
		[HB-3]	14.08	13.85	0.43	21.98	$5.2x10^{-6}$

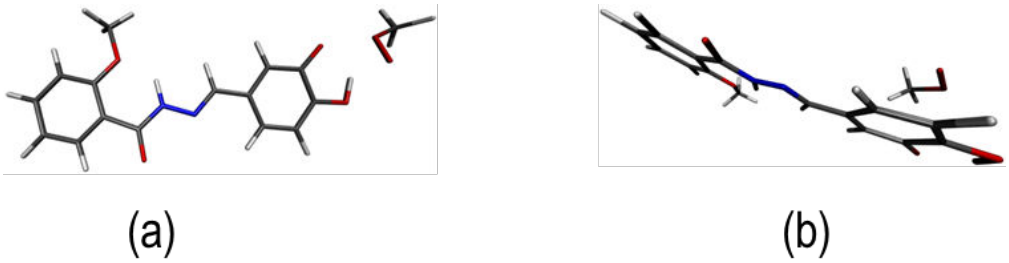

Fig. 1. Optimized geometries of pre-reaction complexes of **7**-[4H+]: (a) [**HB**-3] and (b) $[\boldsymbol{\nu-\pi}]^{Atop}$.

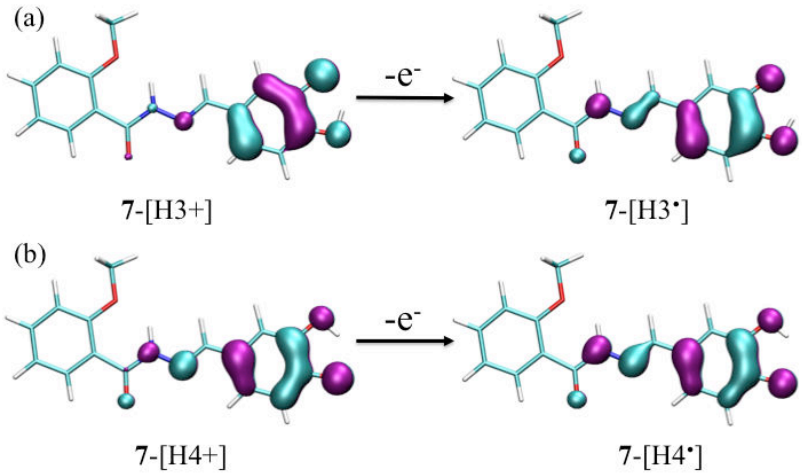

Figure 6. HOMOs modification along electron abstraction (a) from **7**–[3H+] to **7**– [3H$^{\bullet}$] and (b) from **7**– [4H+] to **7**-[4H$^{\bullet}$].

Compare to quercetin, an antioxidant of reference, the SPLET rate constants are significantly lower.[274] Therefore, the present series of compounds are not expected to be powerful free radical scavenging by ET process, even from the deprotonated (activated) forms. The π–delocalization in the Schiff bases studied here is less extended than in quercetin, thus significantly decreasing the positive energetic contributions (e.g., internal reorganization λ_i, $\Delta G°$) along the electron transfer process.

5. Conclusion

Based on a series of synthetized Schiff bases, the present study has confirmed the role of the catechol moiety and the importance of the O–H BDE descriptor. Other minor descriptors succeeded in explaining slight differences in antioxidant activity, namely spin density distribution and BDE_d. The latter descriptor elegantly rationalizes the role of the NH group that, according to the chemical structure, may provide a hydrogen atom for a second HAT. Bromine substitution may slightly enhance antioxidant activity. The free radical scavenging capacity of these compounds mainly proceeds by PCET rather than SPLET, the latter mechanism being only feasible at relatively high pH.

Note for readers: *This article has been submitted and is still under revision. My contribution concerns the evaluation of the stability of the non-covalent complexes between antioxidants within lipid-bilayer membranes. Since the article is not yet published, we have only incorporated the part in which I contributed together with the abstract and a part of the conclusion.*

The figures and reference formats and positions are sometimes modified compared to the original article to keep the homogeneity of the thesis.

Section II. Atomistic description of collaborative antioxidant effects between vitamins E, C and natural polyphenols in lipid−bilayer membranes

Gabin Fabre[1,2], Imene Bayach[1,3], Karel Berka[2], Marketa Paloncýová[2], Jean-Luc Duroux[1], Michal Otyepka*[,2], Patrick Trouillas*[,4,2,5]

[1]LCSN EA1069, Faculté de Pharmacie, Université de Limoges, 2 rue de Dr. Marcland, 87025 Limoges, France

[2]Regional Centre of Advanced Technologies and Materials, Department of Physical Chemistry, Faculty of Science, Palacký University, tř. 17 listopadu 12, 771 46 Olomouc, Czech Republic

[3]Atta-ur-Rahman Research Institute for Natural Product Discovery, Faculty of Pharmacy, Universiti Teknologi MARA, 42300 Puncak Alam, Malaysia

[4]INSERM UMR-S850, Faculté de Pharmacie, Université de Limoges, 2 rue du Docteur Marcland, 87025 Limoges Cedex, France

[5]Laboratoire de Chimie des Matériaux Nouveaux, Université de Mons, Place du Parc 20, B-7000 Mons, Belgium

Abstract: Vitamin E, vitamin C and natural polyphenols (flavonoids and non-flavonoids) are considered major natural antioxidants capable of preventing damage generated by oxidative stress. Here, we show the capacity of vitamin E and vitamin C to interact and form non−covalent complexes within lipid bilayers, close to the membrane/cytosol interface. The formation of such non-covalent complexes contributes to the synergism existing between these two antioxidants (vitamin E being regenerated by vitamin C). Quercetin, considered here as a representative polyphenol, also forms non−covalent complexes with both vitamins C and E. Therefore, in

addition to their inherent capacity to scavenge free radicals in membranes, flavonoids forming such complexes within lipid bilayer membranes can function as enhancers of the regeneration process

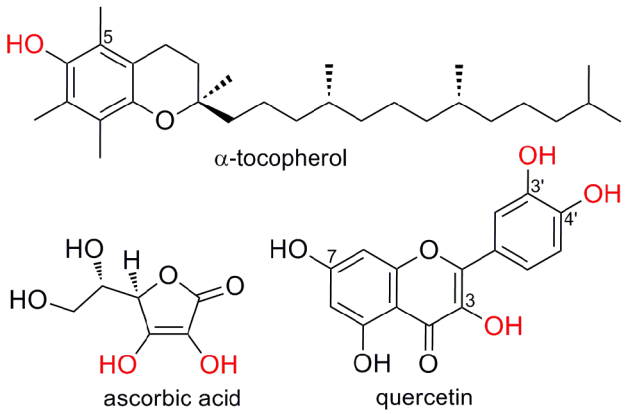

Figure 1. Antioxidant compounds evaluated in this study. The active antioxidant OH groups are shown in red.

1. Results/Discussion

1.1. Association energies

The strength of the non–covalent intermolecular interaction between antioxidants was evaluated by using quantum calculations. Computations were made with density functional theory (DFT) augmented by an empirical dispersion term, allowing high accuracy.[313] After exploring the conformational space, we analyzed the thirteen, ten, eight and four stable geometries of quercetin:vitE, quercetin:vitC, vitC:vitE and vitE:vitE complexes, respectively (see Figure 4 for the most stable geometries per type of complex). The Gibbs energies of association were obtained with B3P86–D2, recently re-parameterized for polyphenol non–covalent complexes [316]. To simulate an environment with polarity similar to the inner bilayer, a diethylether–like polarizable continuum model was used. Different arrangements were observed, namely head–to–head and head–to–tail. The calculated Gibbs energies of association of the most stable conformer for each complex were in the range –4.0 to –4.9 kcal.mol^{-1} (Table 1). The QM

calculations confirmed that the association–complexes are stabilized by a combination of π–stacking (the ring–to–ring distance is around 3.6 Å, which is a typical distance for π–stacking of aromatic rings [317]) and intermolecular hydrogen bonds (Figure 4). According to this quantum evaluation, strong attractive forces exist between the three antioxidants, favoring the formation of non–covalent dimers.

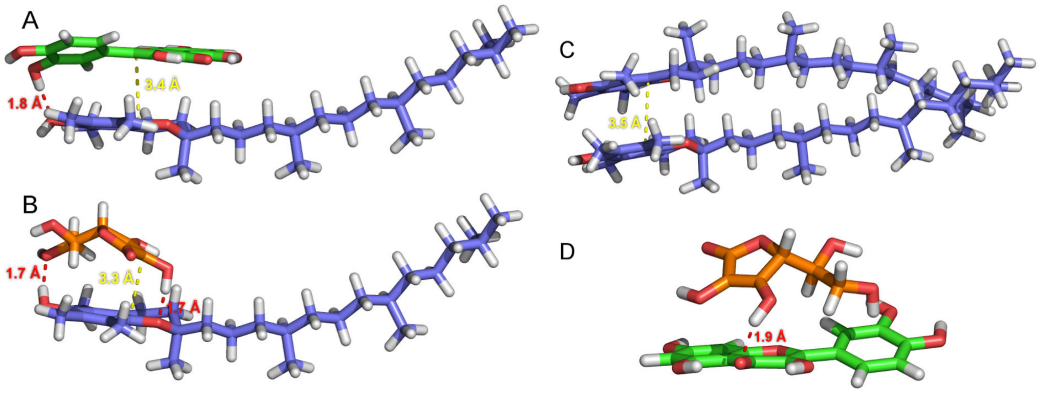

Figure 4. Geometries of the most stable association–complexes as obtained by quantum DFT–D calculations. (A) quercetin:vitE, (B) vitC:vitE, (C) vitE:vitE and (D) quercetin:vitC.

1.2. Critical analysis of the association Gibbs energy evaluation

The first attempt to evaluate the Gibbs energies of association at the QM level provided surprisingly positive values. Such positive values are inconsistent with previous findings, as association enthalpies of -13.7 kcal.mol^{-1} between two flavonoid derivatives [184] have been attributed to formation of non–covalent complexes, which have been repeatedly evidenced experimentally [318], [319]. As in this study the association enthalpies are (favorable) in the range (Table 1), it seems plausible that the entropy correction to the Gibbs energy was overestimated as assessed by the statistical thermodynamic apparatus used. The entropy term consisted of three major components arising from translational, rotational and vibrational modes. As these contributions were estimated under ideal gas, rigid rotor and harmonic approximations, one might expect that the loss of translational entropy accompanying formation of the non–covalent complexes in the lipid bilayer was dramatically overestimated. Therefore, a rough

estimation of the Gibbs energies of association in the membrane can be obtained by taking account of rotational and vibrational entropies but neglecting translational entropy (Table 2).

These data provide collective evidence that non-covalent aggregation is likely to occur in a membrane–type environment. All types of simulations (DFT–D calculations, and free and constrained MD simulations) clearly show that with regard to the non–covalent association (e.g., quercetin:vitE), the inter–molecular interaction is sufficiently strong to give stable complexes inside lipid bilayers under physiological conditions.

Table 2. Association energies (kcal.mol^{-1}) calculated as the difference in energy between the most stable complex and the isolated fragments.

	ΔE	ΔH	ΔS_{vib}	ΔS_{rot}	ΔS_{trans}	$\Delta G_{corrected}$
quercetin:vitE	-13.2	-12.6	1.2	-9.1	-12.4	-4.6
quercetin:vitC	-9.3	-8.2	4.1	-8.0	-11.9	-4.3
vitC:vitE	-11.0	-10.3	1.8	-8.1	-12.0	-4.0
vitE:vitE	-9.8	-12.8	2.0	-9.9	-12.5	-4.9
quercetin:quercetin	-13.7[a]	-	-	-	-	-

Negative values indicate that the association is thermodynamically favored compared to the pair of isolated fragments quercetin and vitE. The calculation was performed with B3P86–D2/def2–QZVP//B3P86–D2/def2–SVP [184]. The vibrational, rotational, translational, and entropic corrections at 298 K are also given in kcal.mol^{-1}.

[a]As obtained in ref. [184] with B3P86–D2/cc–pVDZ (BSSE corrected).

2. Methods

❖ Quantum mechanics calculations

The potential energy surface of the various dimers was explored using our previously reported method [259]. Association energies (ΔE) of the complexes were calculated as the difference in energy between the complex and the isolated fragments (Table 1). The association enthalpies (ΔH) were calculated for all conformers of all complexes using a frequency analysis, a

temperature of 298 K and a pressure of 1 atm. Negative values indicated that the association was thermodynamically favored compared to the pair of isolated compounds. The calculations were performed with B3P86−D2(s6=0.78)/def2−QZVP//B3P86−D2(s6=0.78)/def2−SVP. This re−parameterized DFT functional, which includes Grimme's dispersive term with the s_6 parameter adjusted to a value of 0.780, has been validated by high−level SCS−MP2 calculations and experimental values on polyphenol non−covalent complexes [184], [320]. The COSMO implicit solvent was used to model diethylether solvation. This solvent was chosen as it exhibits a dielectric constant of 4.24, which is close to the polarity of phospholipid headgroups. Bond dissociation enthalpy calculations were performed with B3P86/6−311+G(d,p) as previously reported [220].

4. Conclusion

Quercetin can readily form strong non−covalent association complexes with vitE and vitC. In summary, we have presented a molecular picture of the possible intermolecular interaction between vitE, vitC and polyphenols. This may favour regeneration of vitE and mediation of vitE regeneration by vitC, thus rationalizing antioxidant synergism between these compounds. This behaviour may also be observed in membranes.

Chapter 7 – Tuning optical properties of chalcone derivatives

Chapter 7 – Tuning optical properties of chalcone derivatives

Abstract: The conformational feature of non-covalent complexes of two borondifluoride chalcone derivatives was assessed using DFT-D2. The corresponding optical properties were analysed based on TD-DFT calculations. As already described in such complexes, the π–stacking interaction existing between both fragments allowed formation of a new absorption band corresponding to the $S_0 \rightarrow S_1$ transition. However, this band appears very close to the most intense band corresponding the $S_0 \rightarrow S_2$ transition.

Keywords: Borondifluoride chalcones • non-covalent complexes • UV/Vis absorption • Molecular orbitals • DFT-D2/TD-DFT • π–stacking interactions

1. Introduction

Chalcones represent a specific group of polyphenols. They are present in common fruit and cereals e.g., apples, pears, strawberries, tomatoes and wheat. The most common natural chalcones are phloretin, phloridzin, chalconaringenin and arbutin. They are key intermediates in the biosynthesis of flavonoids (shikimate pathway, see chapter 1).

Chalcones are known to exhibit many biological activities.[321] For example, significant chemoprotective effects have been evidenced.[322]–[327] These activities can be partly correlated to their antioxidant properties. Among other important properties, chalcones have antibacterial, antifungal, antiviral, anti-inflammatory and capillary strengthening properties.[328] Chalcones may be used in novel therapeutic approach in the treatment of inflammatory disorders. In addition, some chalcones exhibit insulin like activities, which impart to them anti-diabetic properties.

As π–conjugated systems, chalcones are optically active in the UV/Vis range; most of natural chalcones being yellowish. They have thus inspired spectroscopic studies aiming at

adapting their optical features (by chemical functionalization) to be used as dyes for new optically active materials. As π−conjugated systems, these compounds have also the capacity to interact by π−stacking interactions. The chapter aims at describing and rationalizing π−stacking interactions[329] and optical properties of two chemically−modified chalcones, namely borondifluoride complexes of 2'−hydroxychalcones (Fig. 1).[330] To achieve these purposes, we first provide a full conformational analysis that has been followed by the systematic evaluation of their optical properties with TD−DFT[331] calculations. We have taken advantages of the expertise on theoretical electronic spectroscopy studies of polyphenols that has been developed in our lab, mainly using adequate functionals for an accurate description of dispersive effects.[258], [332], [333] Those two functionalized chalcones, which have similar structures (i.e., they only differ by the position of the chlorine and bromine atoms, see Fig. 1), are expected to exhibit interesting optical properties for medical and material applications. They can form non-covalent complexes in solution mainly driven by π−stacking. The interaction energies and UV/Vis properties have been investigated for all possible non−covalent complexes.

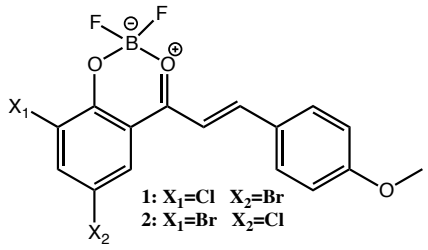

Figure 1. Chemical structures of both borondifluoride complexes of 2'-hydroxychalcones **1** and **2**.

2. Methodology

Over the last years, QM has become an adapted and powerful tool to describe non−covalent complexes and related optical properties.[334] Within the DFT formalism, classical hybrid functionals well describe medium size chemical systems. For example, B3P86 is well adapted to describe thermodynamic and optical properties of chalcones.[335] Nevertheless, as previously described in this manuscript, hybrid functionals failed at describing charge transfer and

non−covalent interactions e.g., π−stacking. So including dispersive terms in the energy calculation is crucial to describe non−covalent complexes. One of the most used approach is the so-called DFT−D as developed by Grimme (See Chapter 3), which provide good accuracy/computational time ratio.[312] Following the native DFT−D formalism, the refined dispersive DFT−D2 method has been widely used.[336] As described in Chapter 3, various parameterizations and benchmarking were performed for polyphenol derivatives, B3P86−D2 with the parameterized scaling factor s_6 = 0.78 has been selected as adequate to perform geometry optimizations and to evaluate interaction energies. This method was combined with COSMO (COnductor-like Solvation MOdel) to describe implicitly solvent effect.[262] The def2−SVP//QZVP basis set was used for the DFT−D2 calculations as it provides good compromise between accuracy and computational time; in this case the BSSE can be neglected.

Once the ground state (GS) structure of the complexes is studied, the excited−states (ESs) are described by the use of a range separated hybrid (RSH)−corrected functionals (i.e., ωB97X) developed in particular to improve charge transfer (CT) description in ESs. This functional was also corrected to describe non−covalent interactions by including a dispersion term in the ωB97XD version. Therefore, ωB97XD was used to calculate ES and optical properties within the TD−DFT framework. In this case, the PCM implicit solvent model is used. The chalcone derivatives studied in this work are not phenolic compounds, they differ from our previous methodological studies not from the skeleton but from the chemical functionalization. Therefore, other functionals were tested on one prototype complex (C1‡‡‡, see section 3.1), including CAMB3LYP, M062X, MPW1K, with the 6−31+G(d,p) basis set (Fig.2). Solvents with different polarities (i.e., CCl_4 (ε=2.23), CH_2Cl_2 (ε=8.93) and H_20 (ε=78.36)) were used to evaluate solvent effects and the results were consistently compared to experimental data. All absorption wavelengths calculated were shifted compared to those obtained experimentally (Fig. 2), and none of the tested functionals performed better than our previous methodology validated for phenolic compounds. For all this study, the B3P86 functional and def2−SVP//QZVP basis set were chosen within the DFT−D2 formalism whereas ωB97XD/6−31+G(d,p) was selected for the TD−DFT study. It is important to highlight that the choice of the functional does not influence

‡‡‡ C1 is a non−covalent complex between two molecules **1** as identified from crystallography.

the MO description and electronic transition assignment.

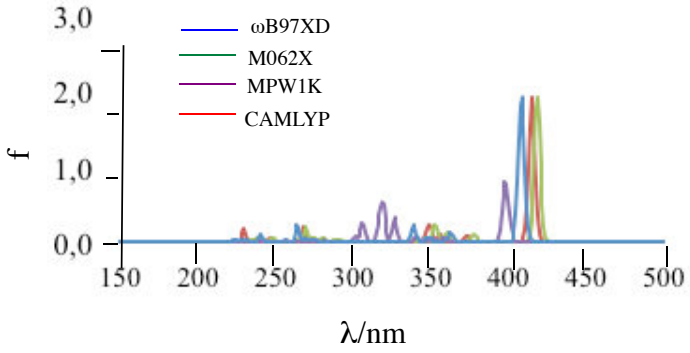

Figure 2. Theoretical UV/Vis absorption spectra of C1 complex.

3. π−π non−covalent chalcone dimers

This section describes the non−covalent conformations in the solid state and solvent (sections 3.1 and 3.2, respectively).

3.1. 3D arrangements issued from X-ray crystal structures

We first studied the two non−covalent dimers, named C1 and C2, issued from the X−ray crystal structures of molecules **1** and **2**, respectively (Fig. 3). C1 and C2 are the corresponding arrangements of two stacked units of **1** and **2**, respectively. B3P86−D2(s_6=0.780)/def2−SVZ single point calculation confirmed the energetic stability of these two arrangements with association energies of -18.8 and -19.2 kcal.mol^{-1} for C1 and C2, respectively, as obtained in the gas phase (Fig. 5). The stability is mainly attributed to π−stacking interactions between both partners being distant from each other by 3.5 Å (Fig.3).

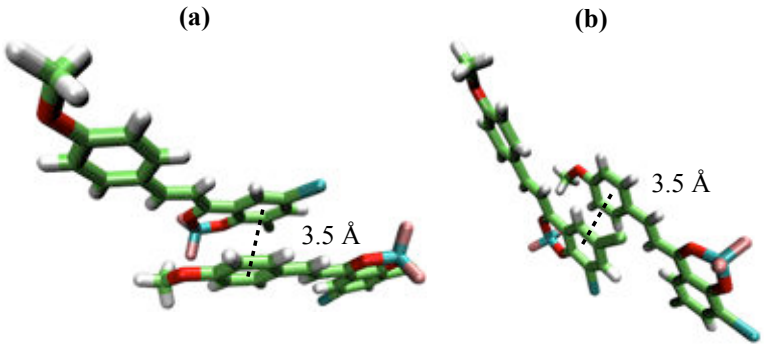

Figure 3. (a) C1 and (b) C2 geometries issued from the crystal structures of molecules **1** and **2**, respectively.

As C1 and C2 corresponded to solid-state geometries, they may exist in a specific restrained environment. In order to understand how these non–covalent dimers may arrange without these restrains, both geometries were optimized. After optimization, these geometries were significantly modified, both partners slid along each other (Fig. 4). Due to the relaxation within the implicit PCM environment, the optimized structures appeared slightly more stable by providing slightly lower association energies, e.g., in CCl_4, the associations energies are *i)* -14.7 and-15.0 for the C1 and its corresponding optimized complex, respectively and *ii)* -14.5 and -14.9 for C2 and its corresponding optimized complex, respectively (see Table 1).

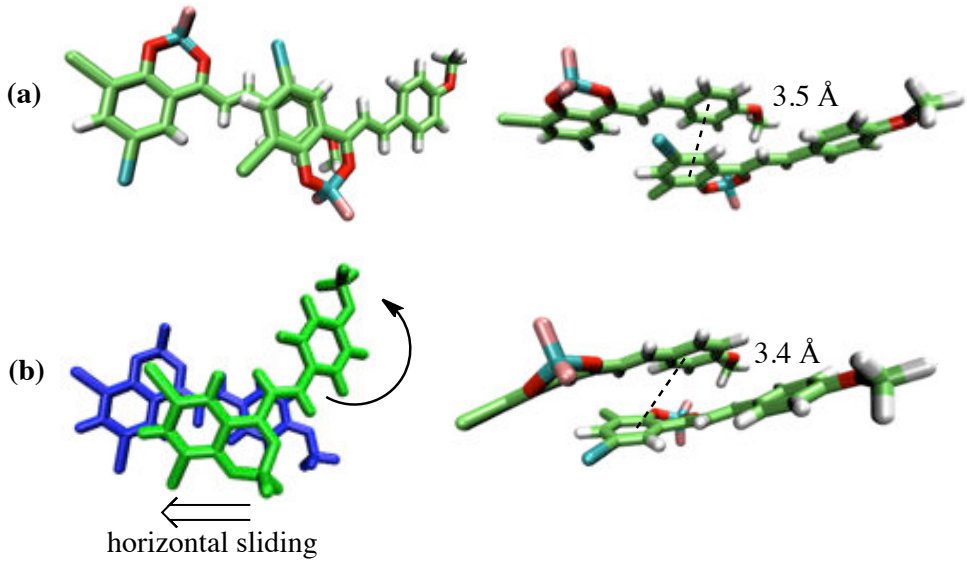

Figure 4. (a) Complex C1 issued from the crystal structure of **1** and (b) the corresponding (B3P86–D2/def2–SVP) –Optimized geometry.

Table 1. (B3P86−D2/def2−TZVP) −Association energies of the C1 and C2 complexes in nonpolar (CCl_4) and polar (H_2O) solvents, (**a)** Single Point and (**b)** Optimization.

Complex	**C1**		**C2**	
	(a)	(b)	(a)	(b)
CCl_4	-14.7	-15.0	-14.5	-14.9
H_2O	-8.2	-10.5	-8.0	-10.1

When increasing the polarity of the solvent, the interaction energies are lowered in absolute value (Table 1 and Fig. 5). Here we are aware that the solvent is taken into account implicitly therefore loosing the description of specific interactions (H−bonds) and the global hydrophobic effects. This can be particularly true for polar and protic solvent such as water.

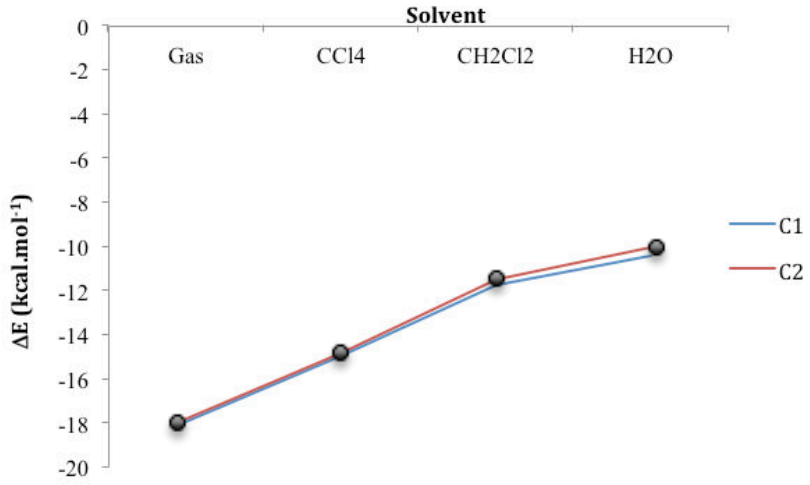

Figure 5. B3P86−D2/def2−TZVP Association energies for C1 and C2 in the gas phase and in PCM-type different solvents.

3.2. Non−restrained conformational analysis

The orientations of non−covalent association may considerably influence optical properties. Therefore it appears crucial to explore the entire potential energy hypersurface for the

non−covalent dimers, other than the two described above (i.e., the optimized geometries from C1 and C2). One must consider either *i)* offset−dimers, in which both fragments are slid along each other within a 1:1 cofacial aromatic rings (Fig. 7 & 8), or *ii)* aligned−dimers, exhibiting 2:2 cofacial rings thus enhancing π−stacking alignment (Fig. 9). For asymmetric compounds (asymmetric substitutions), head−to−head and head−to−tail arrangements must be considered as well as *Re/Re* and *Re/Si* approaches. For each chalcone (**1** and **2**), six offset−dimer geometries (Fig. 8) and eight aligned−dimer geometries (Fig. 9) were elucidated.

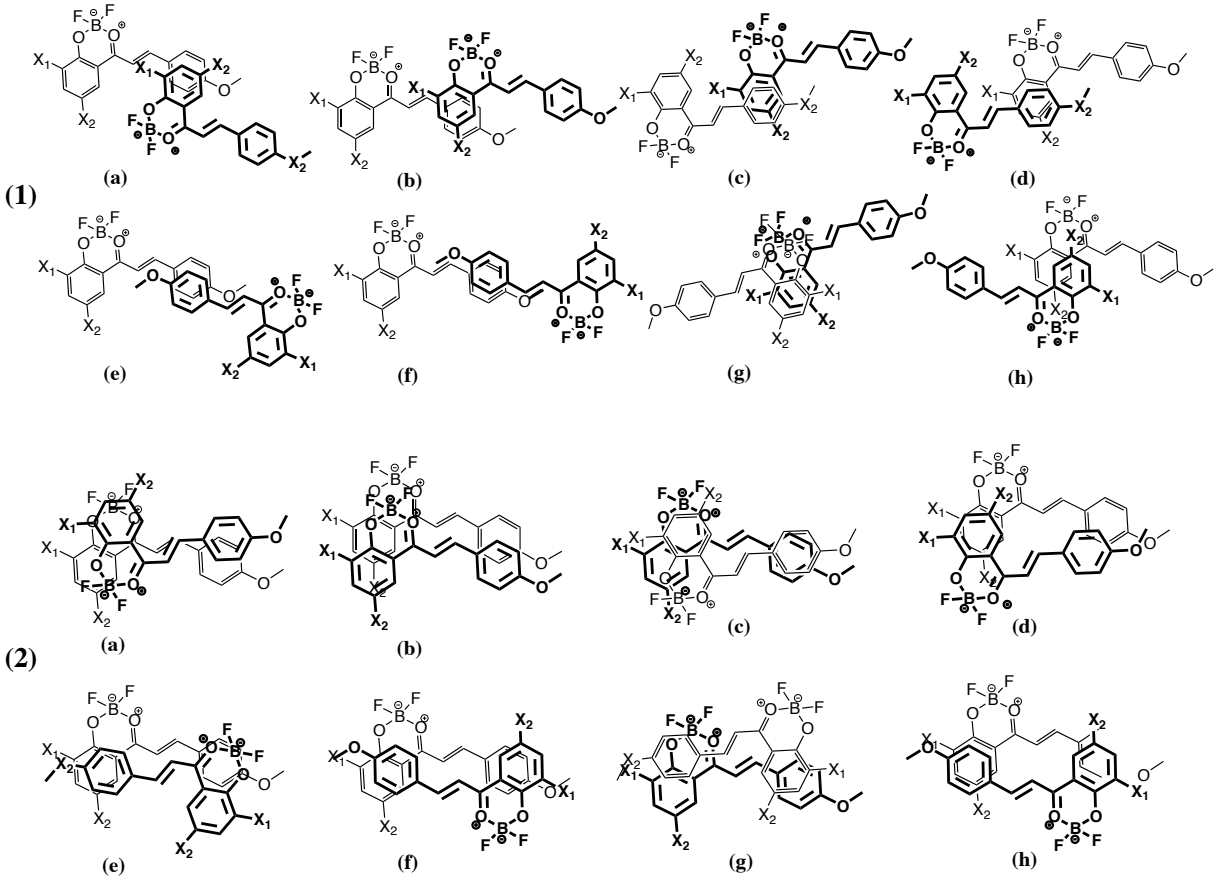

Figure 7. Chemical structures of the different (1) offset− and (2) aligned−dimers.

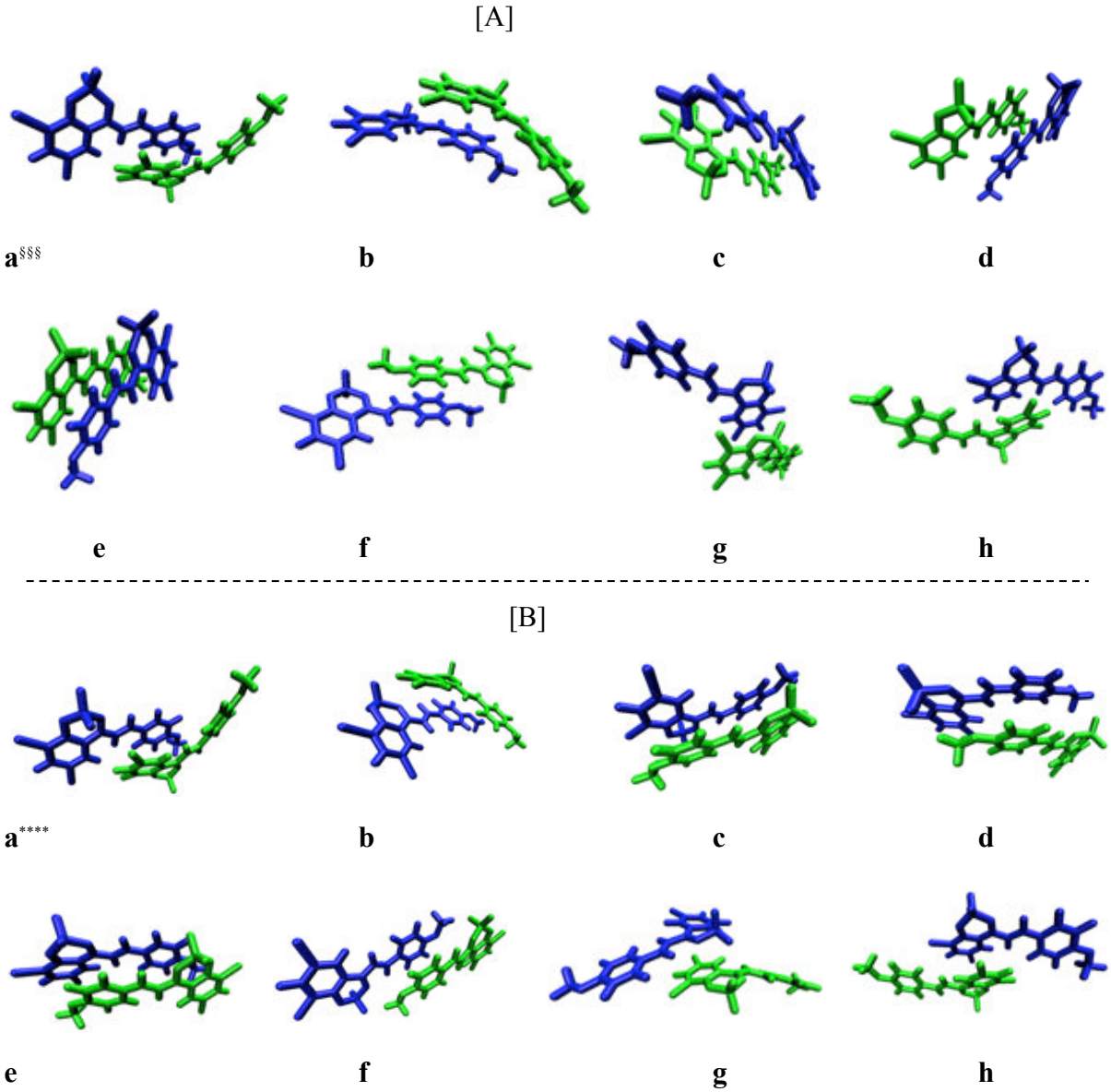

Figure 8. (B3P86–D2(s_6 = 0.780)/def2–SVP)–Optimized geometries from the eight possible offset-dimers of **1** [A] and **2** [B].

Starting with eight offset–dimer conformations, the optimization procedure led to two aligned–dimers conformations (**c** and **e**) and to six offset–dimers including the optimized complex issued from the crystal structure (conformation **a**) (Fig. 8). Due to better π–stacking

§§§ This orientation corresponds to the optimized conformation of C1 as described in Fig.4.

**** This orientation corresponds to the optimized conformation of C2.

overlap, conformations **c** and **e** are more stable than the six offset−dimers (Table 2).

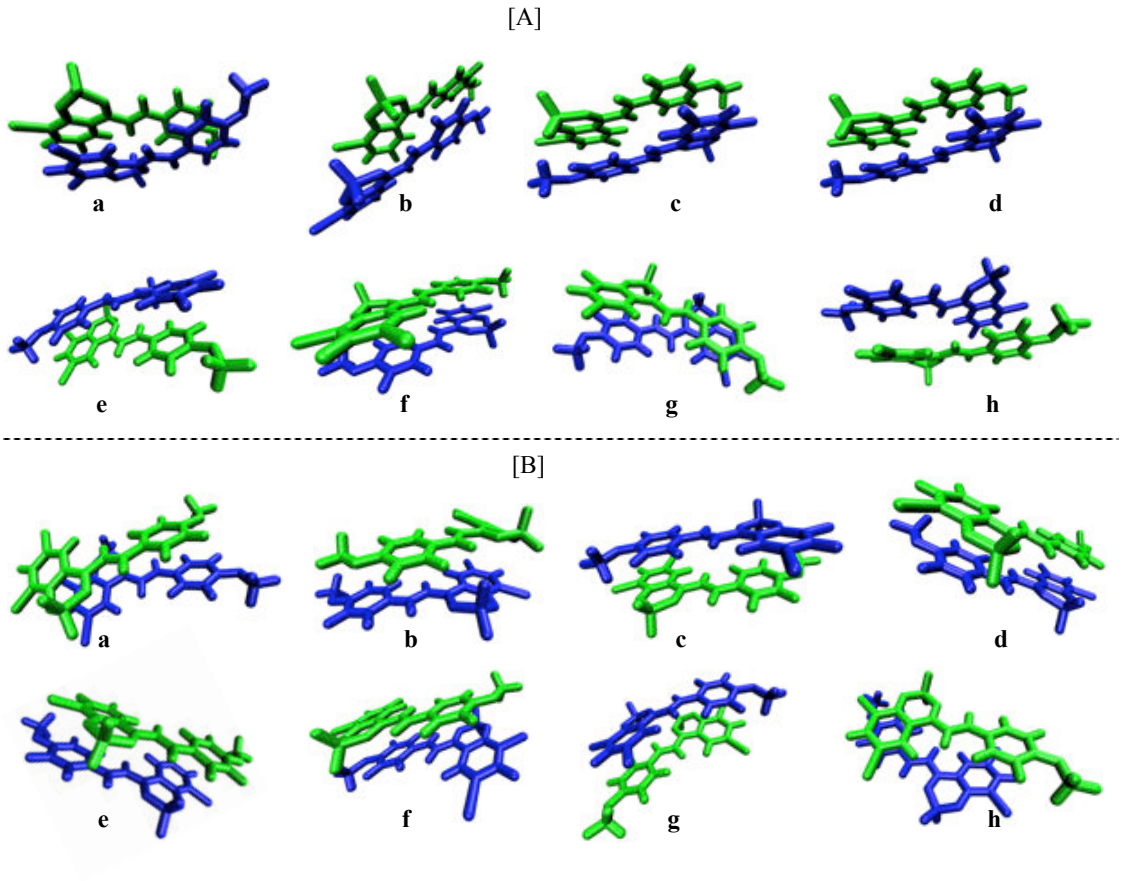

Figure 9. (B3P86−D2/def2−SVP)−Optimized geometries of the eight aligned−dimer from [A] **1** and [B] **2**.

While all orientations exhibit considerable negative association energies, there are significant differences between the various complexes (Table 2). The intermolecular distances within all non−covalent complexes were around 3.5 Å, typical of π−stacking.

Table 2. (B3P86−D2/def2−QZVP)−Association energies (ΔE_{int} in kcal.mol^{-1}) of the non−covalent complexes and Boltzmann weights (D_{bolt} in %) calculated for the different alignments.

	1					**2**				
	offset			aligned			offset			aligned	
	ΔE_{int}	D_{bolt}		ΔE_{int}	D_{bolt}		ΔE_{int}	D_{bolt}		ΔE_{int}	D_{bolt}
a	-13.2	0.0	a	-19.7	0.0	a	-15.0	0.0	a	-17.3	0.0
b	-9.7	0.0	b	-11.6	0.0	b	-13.1	0.0	b	-13.8	0.0
c	-22.6	99.8	c	-24.1	37.1	c	-22.6	100.0	c	-24.5	57.7
d	-8.1	0.0	d	-19.0	0.0	d	-11.2	0.0	d	-19.3	0.0
e	-18.9	0.2	e	-17.6	0.0	e	-17.1	0.0	e	-18.3	0.0
f	-9.8	0.0	f	-24.4	62.8	f	-10.7	0.0	f	-24.3	42.1
g	-4.2	0.0	g	-17.3	0.0	g	-6.4	0.0	g	-14.5	0.0
h	-17.0	0.0	h	-17.0	0.0	h	-12,7	0.0	h	-20.8	0.1

As expected, the aligned-dimers are much more stable than the offset−dimers. In the former type of dimers indeed, π−stacking is favored along an extended region. The most stable energies were obtained for the head−to−tail alignments (Fig. 9). The position for bromine and chlorine substitution also influences significantly the stabilizing energies. The non−covalent dimers are particularly stable because they exhibit adequate charge distribution. Nevertheless, as we pointed out in our recent paper,[337] considering only association energies is not enough to conclude, ΔG calculations would be required. Therefore all complexes are considered for the following comprehensive optical analysis.

4. Optical properties

4.1. Monomers 1 and 2

For both monomers **1** and **2**, the global shape of the theoretical UV/Vis absorption spectra (i.e., peaks and intensity) agrees with the corresponding experimental spectra with all functionals tested (Fig. 11). Only B3P86 (i.e., the functional well adapted for polyphenols [335]) correctly predicts maximum absorption wavelengths i.e., the error being 5 and 4 nm for both compounds, respectively (Fig.10 and Fig.11). The ωB97XD functional provided 60 nm errors both for **1** and **2**, respectively (Fig. 11). We also confirm that the BP86 functional is totally inaccurate (Fig. 11). For both **1** and **2**, λ_{max} is assigned to the first excited state S1, mainly described by the HOMO (H) → LUMO (L) electronic transition, both MO overlapping efficiently (Fig. 15). The overlapping between the π and π^* orbitals involved in the electronic transitions is a major requirement to increase oscillator strengths (*i.e.*, to increase band intensities).

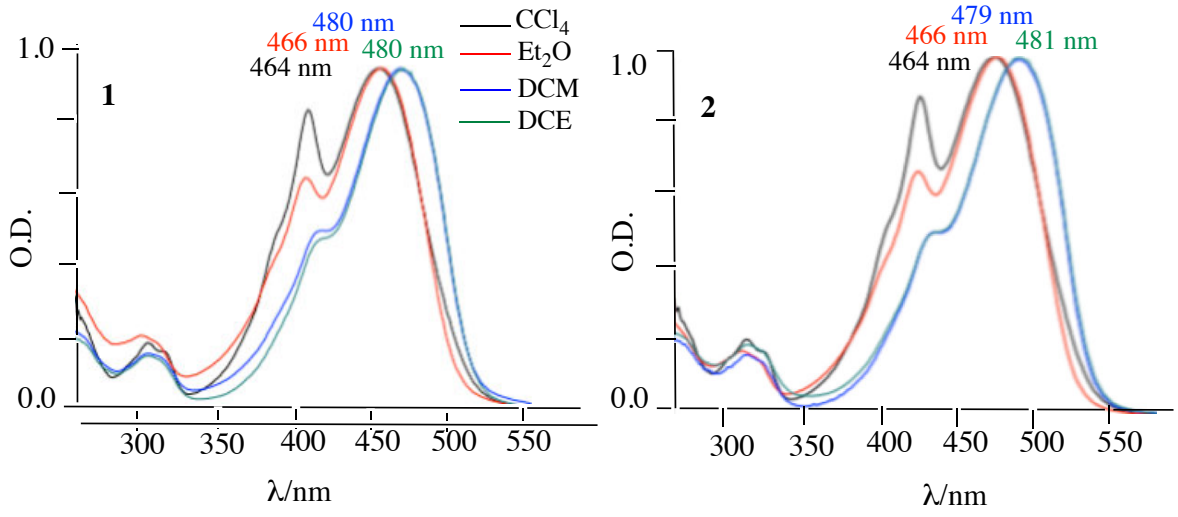

Figure 10. Experimental UV/Vis absorption spectra for **1** and **2** in four selected solvents.

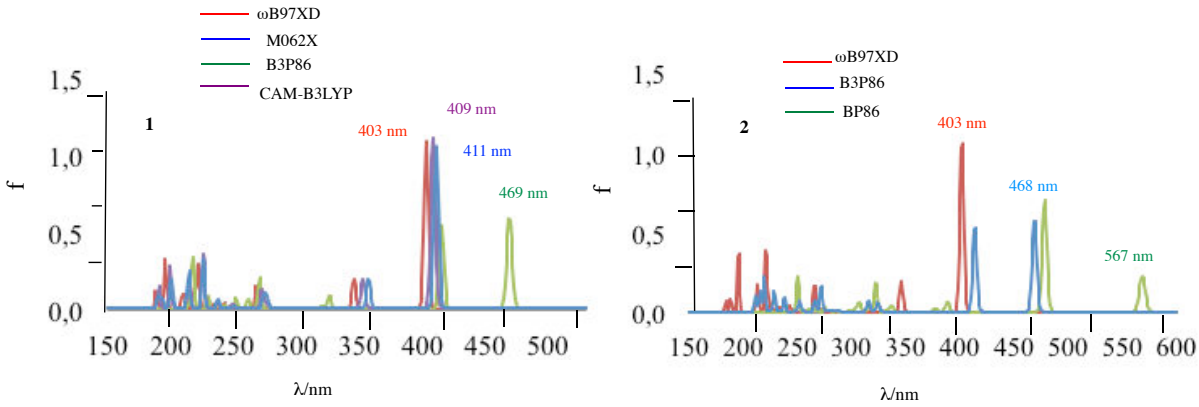

Figure 11. Theoretical UV/Vis absorption spectra in CCl_4 with different functionals.

Contrary to what is observed for polyphenols,[335] increasing the polarity of the solvent induces a slight hypsochromic shift of λ_{max} by 8 nm and 9 nm for **1** and **2**, respectively (Fig. 12).

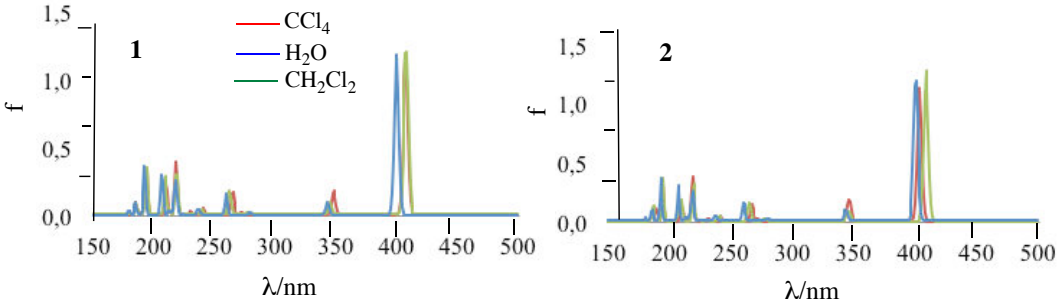

Figure 12. Theoretical UV/Vis absorption spectra in different solvents for **1** and **2**.

4.2. Non−covalent complexes

Even if the optimized geometries appeared more stable in a solvent-type environment, the understanding of optical properties of the X-ray crystal structures (C1 and C2) is a crucial step, mainly because aiming at a comparison between solvent and solid state behaviors.

The UV/Vis spectra of C1 and C2 looks very similar to that of the corresponding monomers, with a clear maximum absorption band at 409.26 and 405.90 nm for both frozen non−covalent dimers C1 and C2, respectively (Fig. 14). Interestingly, in the relaxed non−covalent dimers, the band is split into two main (and clearly separated) bands (Fig. 14). The maximum absorption band is actually a new peak resulting from the non−covalent complexation

located at 416.13 and 415.58 nm for conformers **a** and **b** (the optimized C1 and C2), respectively. It is assigned to the first excited state S1 that is mainly described by the H−1→L electronic transition and exhibits a strong CT (charge transfer) character. The corresponding oscillator strength is rather high (f = 1.21 and 0.93 for conformers **a** and **b**, respectively (Table 3)), due to efficient overlap of the MO involved in the electronic transition constituting S1. The S2 is described by different electronic transitions, mainly the H−1→L, H→L and H→L+1 electronic transitions. The oscillator strengths are rather important (f = 0.87 and 1.17 for C1 and C2, respectively) (Table 3) also due to an efficient MO overlapping. In the solid−state arrangement, both S1 and S2 exist as well, however they correspond to two very similar absorption wavelengths, thus being hardly separated, therefore not expected to be observable experimentally.

The oscillator strengths of the two optimized complexes are lower than for the C1 and C2 (f = 0.43 and 0.47 for optimized C1 and C2, respectively). In another hand, the absorption band at 399.82 and 400.68 nm for conformers **a** and **b**, respectively, is much more intense (i.e., f = 1.30 and 1.31, respectively, Table 3). This band is described mainly by a combination of H−1→L and H−1→L+1 transitions (Fig. 15).

The solvent polarity greatly influences electronic transitions and MO distributions. For instance, S1 of the C1 complex is described by H−1→L and H→L in CCl_4 and H_2O, respectively (Table 4). The difference in intensity of these peaks is well explained by the MO description (Fig.15).

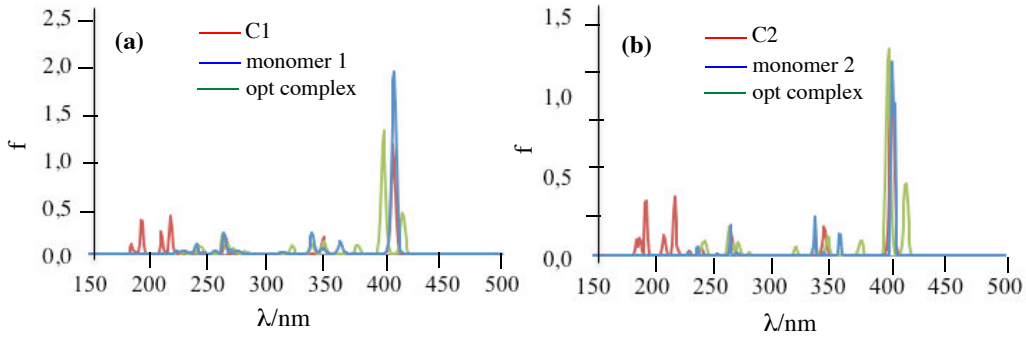

Figure 14. Theoretical UV/Vis spectra of obtained by TD−DFT for (a) **C1** and (b) **C2**.

Table 3. Maximum vertical excitation energies (E_{max}, eV), absorption wavelengths (λ_{max}, nm), oscillator strengths (f) and MO descriptions of C1 and C2 and their corresponding optimization at the PCM (CCl_4)−TD−ωB97XD/6−31+G(d,p) level.

	Optimization				**SP**			
	E_{max}	**λ_{max}**	**f**	**MO**	**E_{max}**	**λ_{max}**	**f**	**MO**
C1	2.98	416.13	0.43	H→L (49%) H→L+1(-36%)	3.03	409.26	1.21	H-1→L (57%) H-1→L+1 (29%)
	3.10	399.82	1.30	H-1→L (53%) H-1→L+1 (31%)	3.04	407.83	0.87	H→L (-43%) H→L+1(47%)
C2	2.98	415.58	0.47	H→L (47%) H→L+1(-37%) H-1→L (-30%)	3.05	405.90	0.93	H-1→L (60%)
	3.09	400.68	1.31	H→L (51%) H-1→L+1 (31%) H→L (29%)	3.07	403.89	1.17	H→L (-45%) H→L+1(47%)

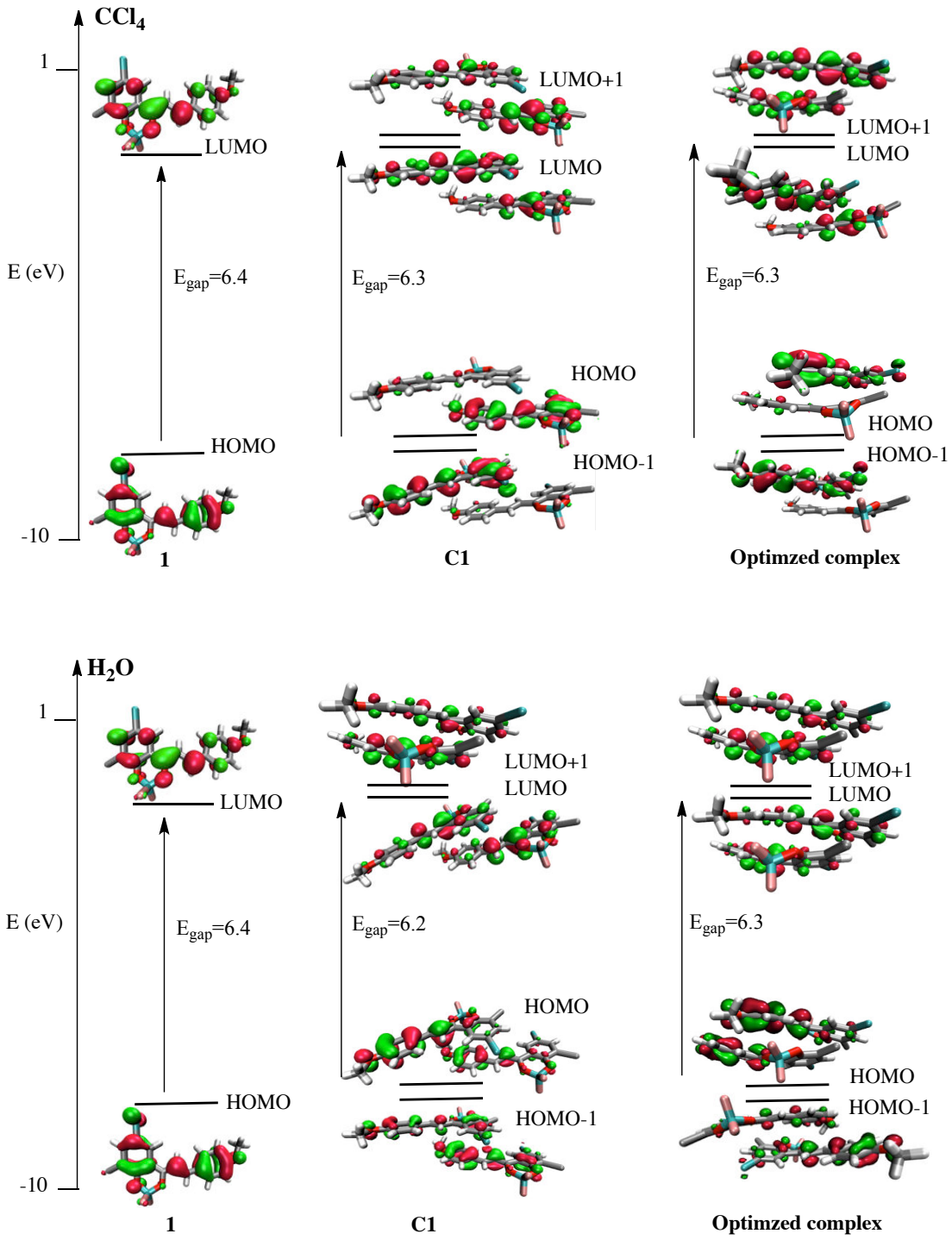

Figure 15. MO diagram of monomer **1**, **C1** and its corresponding optimized complex in CCl_4 and H_2O solvents.

Table 4. E_{max} (eV), λmax (nm), f and MO descriptions of C1 at the PCM–TD–ωB97XD/6-31+G(d,p) level.

CCl_4				H_20			
OPT		**SP**		**OPT**		**SP**	
2.98eV 416.13nm f=0.43		2.99eV 414.86nm f=0.48		3.03eV 409.26nm f=1.21		3.05eV 406.57nm f=2.12	
H-2→L+1	(11%)	H-2→L+1	(-11%)	H-3→L+2	(11%)	H-1→L	(14%)
H-1→L	(27%)	H-1→L	(45%)	H-1→L	(57%)	H-1→L+1	(-35%)
H→L	(49%)	H→L	(-43%)	H-1→L+1	(29%)	H→L	(54%)
H→L+1	(-36%)	H→L+1	(23%)	H→L	(-20%)		
3.10eV 399.82 nm f=1.30		3.10eV 399.48nm f=1.25		3.04eV 407.83nm f=0.87		3.07eV 404.25nm f=0.12	
H-1 →L	(53%)	H-1→L	(29%)	H-2 → L+1	(-12%)	H-2→L+1	(-12%)
H-1 →L+1	(31%)	H-1→L+1	(36%)	H-2→L+3	(-12%)	H-1→L	(53%)
H →L	(-25%)	H→L	(41%)	H-1→L	(-17%)	H→L+1	(-39%)
		H→L+1	(25%)	H→L	(-43%)		
				H→L+1	(47%)		

The ES description of all conformers was studied as well (Tables 5 and 6). However, MO diagrams were given for the significant complexes (high D_{bolt}), i.e., orientations **c** and **f** only for aligned-dimer (Table 2 and Fig. 16–19). As for C1, C2 and their corresponding optimized complexes, the UV/vis spectra of all other complexes consist of two main absorption bands. From Tables 5 and 6 and the MO diagrams, these two bands are well understood following the same explanation as previously. Again, both absorption wavelengths and oscillator strengths are highly influenced by the conformation, some electronic transitions being interchanged.

Table 5. Maximum vertical excitation energies (E_{max}, eV), absorption wavelengths (λ_{max}, nm), oscillator strengths (f) and MO descriptions of different complexes from two units of **1** at the PCM (CCl_4)–TD–ωB97XD/6–31+G(d,p) level.

	offset–dimers				aligned–dimers			
	E_{max}	**λ_{max}**	**f**	**MO**	**E_{max}**	**λ_{max}**	**f**	**MO**
a	2.93	421.75	1.45	H→L	2.85	435.36	0.08	H→L
	3.03	409.55	0.34	H–1→L (42%) H→L+1 (45%)	3.07	403.25	1.58	H–1→L
b	3.01	411.88	1.70	H→L	3.00	413.34	0.03	H–1→L
	3.08	402.86	0.30	H–1→L (49%) H→L+1 (38%)	3.12	397.57	1.75	H–1→L (41%) H→L+1 (51%)
c	2.69	460.12	0.00	H→L	2.76	448.75	0.00	H→L
	3.09	401.68	1.85	H–1→L (43%) H→L+1 (47%)	3.08	402.60	1.80	H–1→L (-44%) H→L+1 (47%)
d	2.94	421.10	0.11	H→L	2.90	428.42	0.04	H→L+1
	3.04	407.49	1.84	H–1→L (40%) H→L+1 (53%)	3.11	398.34	1.67	H–1→L (35%) H–1→L+1 (38%)
e	2.90	427.87	0.08	H–1→L	2.80	443.07	0.08	H→L
	3.12	397.93	1.61	H→L+1	3.12	397.26	1.71	H–1→L (46%) H→L+1 (47%)
f	2.95	420.14	2.30	H→L	2.78	446.69	0.00	H→L
	3.02	410.32	0.01	H→L+1	3.09	401.11	2.03	H→L+1 (58%)
g	3.02	409.94	0.67	H-1→L (54%) H→L (35%)	2.91	426.60	0.11	H→L
	3.07	403.52	1.78	H→L+1	3.14	394.81	1.67	H–1→L (43%) H–1→L+1 (48%)
h	3.00	414.60	0.00	H→L	2.85	435.32	0.10	H→L+1
	3.04	407.29	2.22	H–1→L (51%) H→L+1 (43%)	3.03	408.59	1.77	H-1→L+1 (-31%) H→L+1 (55%)

Table 6. Maximum vertical excitation energies (E_{max}, eV), absorption wavelengths (λ_{max}, nm), oscillator strengths (f) and MO descriptions of different complexes from two units of **2** at the PCM(CCl_4)–TD–ωB97XD/6–31+G(d,p) level.

	offset–dimers				aligned–dimers			
	E_{max}	**λ_{max}**	**f**	**MO**	**E_{max}**	**λ_{max}**	**f**	**MO**
a	2.91	425.75	0.96	H→L	2.83	438.05	0.07	H→L
	3.01	410.18	0.79	H–1→L (32%) H→L+1 (54%)	3.10	400.59	1.51	H–1→L (49%) H→L+1 (-45%)
b	2.97	416.25	0.48	H→L	2.96	419.47	0.09	H-1→L
	3.07	403.42	1.22	H–1→L (45%) H→L+1 (48%)	3.13	396.53	1.59	H–1→L (42%) H→L+1 (49%)
c	2.72	454.80	0.00	H→L	2.76	449.47	0.00	H→L
	3.10	399.15	1.91	H–1→L (36%) H→L+1 (55%)	3.09	401.46	1.88	H–1→L (-35%) H→L+1 (58%)
d	2.99	415.30	0.35	H→L	2.88	430.69	0.02	H→L
	3.02	410.98	1.76	H–1→L (49%) H→L+1 (-43%)	3.13	396.27	1.75	H–1→L (41%) H→L+1 (49%)
e	2.84	435.15	0.01	H→L	2.77	447.38	0.00	H→L
	3.07	403.44	1.74	H→L+1	3.11	398.13	2.08	H→L+1
f	2.95	420.89	2.01	H→L	2.79	445.17	0.00	H→L
	3.00	413.27	0.14	H→L+1	3.10	399.60	1.99	H→L+1
g	3.00	412.44	0.47	H–1→L	2.79	443.93	0.04	H→L
	3.07	403.34	1.66	H→L+1	3.15	393.09	1.72	H–1→L (47%) H→L+1 (48%)
h	2.94	421.06	0.00	H→L	2.87	432.68	0.04	H–1→L (49%) H→L+1 (45%)
	3.04	407.93	2.18	H–1→L (52%) H→L+1 (42%)	2.99	414.83	1.68	H→L

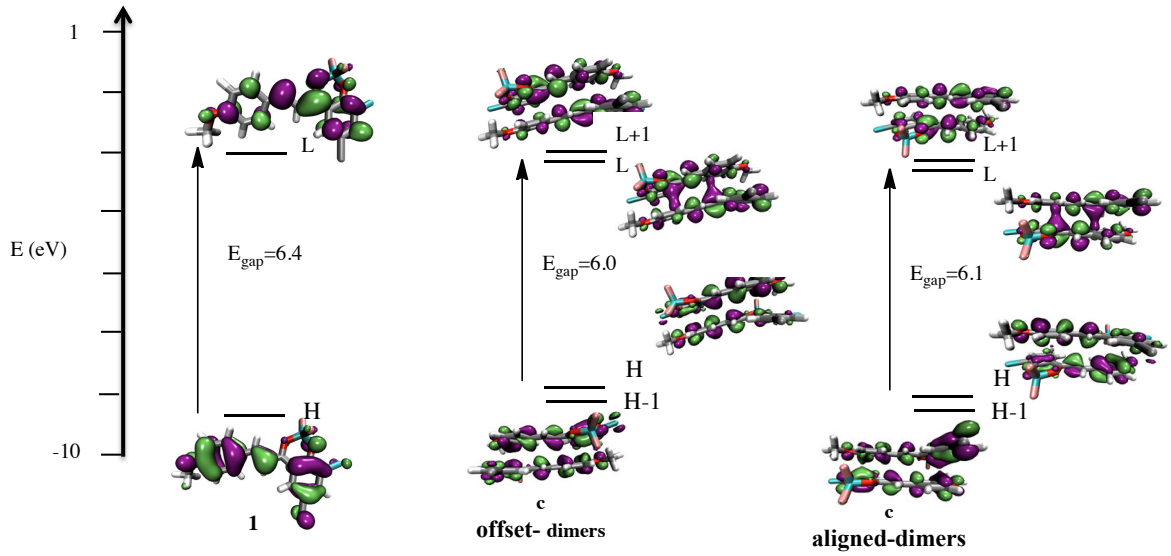

Figure 16. MO diagram of monomer **1** and complex **c**.

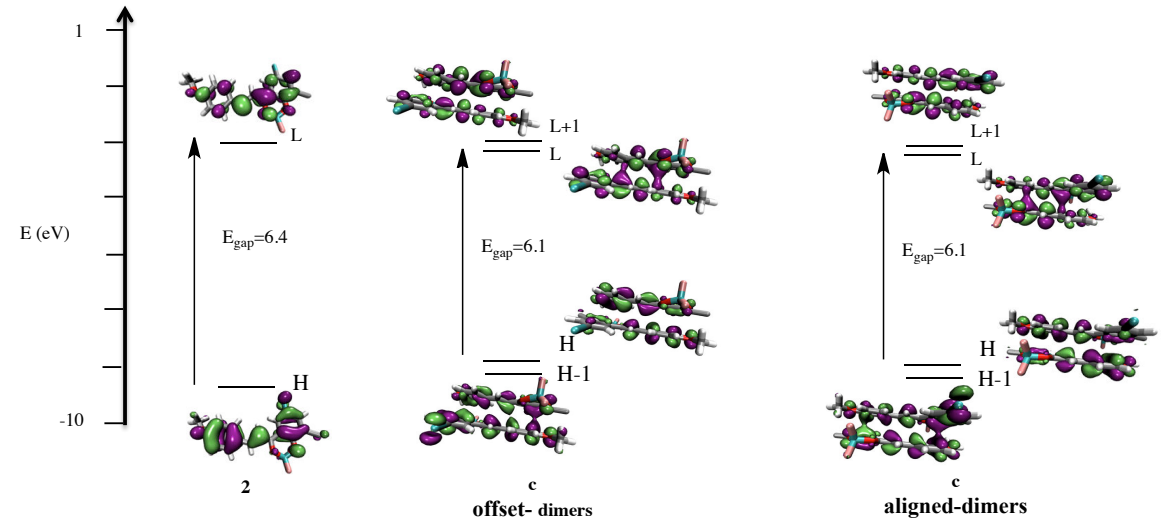

Figure 17. MO diagram of monomer **2** and complex **c**.

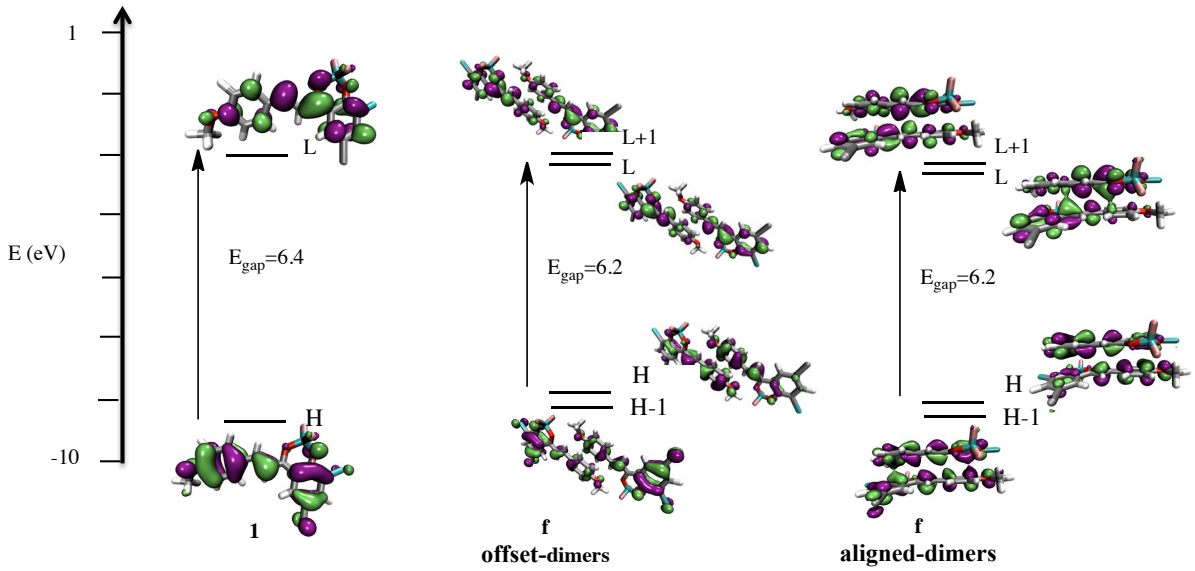

Figure 18. MO diagram of monomer **1** and complex **f**.

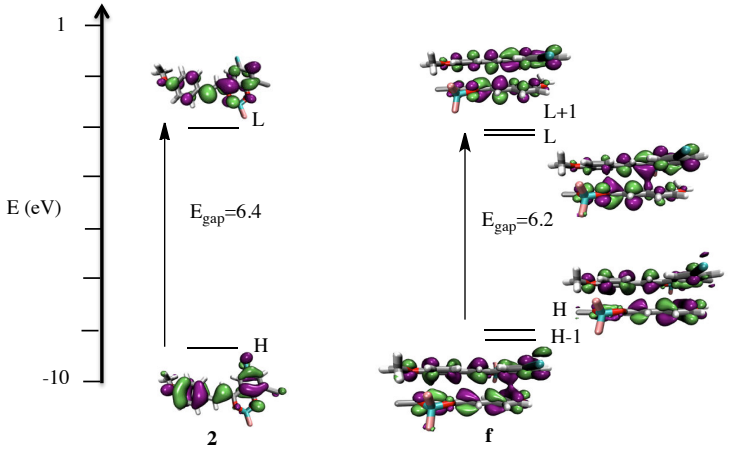

Figure 19. MO diagram of monomer **2** and complex **f**.

5. Conclusion

Quantum chemical calculations have allowed providing a detailed MO picture and thus a complete spectroscopic understanding of non−covalent association between the complexes of borondifluoride 2'−hydroxychalcones. We provided a quantum rationalization of UV/Vis spectra of single molecules and different possible non-covalent arrangements driven by π−stacking. As expected, the B3P86 functional within the TD-DFT formalism provided accurate results for the

monomers. However, even if less accurate for the monomer, the ωB97XD functional was required to describe CT within the π−stacking complexes.

Within the non-covalent complexes, a new band due to the π−stacking interaction attributed to the $S_0 \rightarrow S_1$ transition (mainly described by a H→L electronic transition) with a CT character. However, the supramolecular arrangements only slightly influence the MO scheme since the global shape of the UV/Vis spectrum is conserved. The solvent description influences the optical properties i.e., solvent polarity induces slight hypsochromic shifts of λ_{max}. The halogen substituent position poorly influenced the MO description and the subsequent optical properties.

This computational study of monomer and non-covalent dimers in solution is a first step towards full rationalization of optical properties of these compounds in the solid phase. In this case, stacking description and spectral influence is mandatory.

Conclusion

Conclusion

The purpose of this PhD was to rationalize the role of non−covalent interactions through three examples covering three fields of applications. First, in chemistry, our results constitute efficient weapons to help proceeding of supramolecular synthesis. Non−covalent complexes formed prior to oxidation have been shown to be specific precursors of the regio− and stereo−selective stilbenoid oligomer synthesis. Supramolecular self−assembly of oligostilbenoids units through non−covalent bonding is the driving force in some key−steps of the oligostilbene biosynthesis.

QM calculations, carefully including dispersive effects, have brought new understanding for biogenesis of different classes of natural products. This understanding may provide more refined approaches to biomimetic syntheses, which are likely to become more practical in the production of series of new derivatives from lead drugs with enhanced biological activities.

Second, in biochemistry, our work provides a new molecular picture of antioxidants (i.e., vitamins and polyphenols) and their antioxidant action in membranes. We demonstrated that antioxidants form non−covalent complexes that eventually affect their activities. In lipid bilayer membranes, vitamin E could form stable non−covalent association-complexes with vitamin C and quercetin, considered as a representative polyphenol, can also form strong non−covalent association−complexes with either vitamin E or C. We believe that non−covalent complexation of these antioxidants promotes vitamin E regeneration and mediation of vitamin E regeneration by vitamin C and polyphenols. These effects due to the non−covalent complexation would be even more enhanced in larger aggregates possibly forming part nanodomains.

Third, in materials science, DFT−D and TD−DFT have provided a preliminary spectroscopic understanding of non−covalent complexation of chalcone derivatives through a detailed molecular orbitals picture. The non−covalent association (3D arrangement) affects optical properties of these selected chalcones. Solvent and position of halogen substituent (Br or Cl) also influence the optical properties.

This thesis highlights the importance of non−covalent interactions that have increasingly attracted interest from food and pharmaceutical applications. Theoretical chemistry represents an accurate tool to describe these non−covalent interactions with practical perspectives.

Thanks to all refinements that have allowed reaching high accuracy, DFT has become indispensable for Science to improve understanding, especially for natural products. In this work, the robustness of dispersion−corrected calculations (DFT−D2, DFT−D3 and DFT−NL) was assessed, with large basis sets (def2−QZVP) to avoid incompleteness effects for one real−world polyphenol dimer chosen as an appropriate model. Our benchmark study predicts the existence of natural polyphenols complexes mainly driven by both π–stacking and H−bonding interactions. The adequate comparison of lower−cost DFT−based methods allowed bracketing their expected accuracy. These results thus pave the way towards reliable studies of challenging aggregation processes of natural products. However, theoretical chemistry still has its limits to be enhanced since the choice of the functional and the basis set is not always obvious and is system−dependent. The challenging task in QM is still to find the best compromise between accuracy and computational time.

Theoretical chemistry is a crucial tool to rationalize many other chemical and biological properties of natural or synthetic compounds, as is the case of the synthetized phenolic Schiff bases for which the structure–antioxidant activity relationship have been elucidated and have confirmed the importance of the O–H groups together with the catechol moiety as well as other minor descriptors in modulating the antioxidant activity. We also demonstrated the role of the NH group to provide a hydrogen atom for a second HAT according to the chemical structure and the bromine substitution to slightly enhance antioxidant activity. Moreover, this part of the work allowed determining the major mechanism involved in free radical scavenging using DFT calculations by confirming that the free radical scavenging by these Schiff bases mainly proceeds through atom transfer (PCET) rather than electron transfer (SPLET).

BIBLIOGRAPHY

[1] M. B. Austin, M. E. Bowman, J.-L. Ferrer, J. Schröder, and J. P. Noel, "An Aldol Switch Discovered in Stilbene Synthases Mediates Cyclization Specificity of Type III Polyketide Synthases," *Chem. Biol.*, vol. 11, no. 9, pp. 1179–1194, Sep. 2004.

[2] T. Iwashina, "The Structure and Distribution of the Flavonoids in Plants," *J. Plant Res.*, vol. 113, no. 3, pp. 287–299, Sep. 2000.

[3] J. Koukol and E. E. Conn, "The metabolism of aromatic compounds in higher plants. IV. Purification and properties of the phenylalanine deaminase of Hordeum vulgare," *J. Biol. Chem.*, vol. 236, pp. 2692–2698, Oct. 1961.

[4] H. Grisebach and S. Kellner, "studies on the mechanism of transformation of 4,2',4',6'-tetrahydroxychalcone into taxifoline in *Chamaecyparis obtusa*," *Z. Für Naturforschung Teil B Chem. Biochem. Biophys. Biol.*, vol. 20, pp. 446–450, May 1965.

[5] M. L. Falcone Ferreyra, S. P. Rius, and P. Casati, "Flavonoids: biosynthesis, biological functions, and biotechnological applications," *Front. Plant Sci.*, vol. 3, Sep. 2012.

[6] S. Martens, A. Preuss, and U. Matern, "Multifunctional flavonoid dioxygenases: flavonol and anthocyanin biosynthesis in Arabidopsis thaliana L," *Phytochemistry*, vol. 71, no. 10, pp. 1040–1049, Jul. 2010.

[7] D. Bowles, J. Isayenkova, E.-K. Lim, and B. Poppenberger, "Glycosyltransferases: managers of small molecules," *Curr. Opin. Plant Biol.*, vol. 8, no. 3, pp. 254–263, Jun. 2005.

[8] J.-L. Ferrer, M. B. Austin, C. Stewart Jr, and J. P. Noel, "Structure and function of enzymes involved in the biosynthesis of phenylpropanoids," *Plant Physiol. Biochem. PPB Société Fr. Physiol. Végétale*, vol. 46, no. 3, pp. 356–370, Mar. 2008.

[9] M. G. Simic, "Mechanisms of inhibition of free-radical processes in mutagenesis and carcinogenesis," *Mutat. Res.*, vol. 202, no. 2, pp. 377–386, Dec. 1988.

[10] J.-H. Yang, H.-C. Lin, and J.-L. Mau, "Antioxidant properties of several commercial mushrooms," *Food Chem.*, vol. 77, no. 2, pp. 229–235, May 2002.

[11] S. Hercberg, P. Galan, P. Preziosi, S. Bertrais, L. Mennen, D. Malvy, A.-M. Roussel, A. Favier, and S. Briançon, "The SU.VI.MAX Study: a randomized, placebo-controlled trial of the health effects of antioxidant vitamins and minerals," *Arch. Intern. Med.*, vol. 164, no. 21, pp. 2335–2342, Nov. 2004.

[12] O. Dangles, "Antioxidant Activity of Plant Phenols: Chemical Mechanisms and Biological Significance," *Curr. Org. Chem.*, vol. 16, no. 6, pp. 692–714, Apr. 2012.

[13] B. W. Shirley, "Flavonoid biosynthesis: 'new' functions for an 'old' pathway," *Trends Plant Sci.*, vol. 1, no. 11, pp. 377–382, Jan. 1996.

[14] G. R. Beecher, "Overview of dietary flavonoids: nomenclature, occurrence and intake," *J. Nutr.*, vol. 133, no. 10, p. 3248S–3254S, Oct. 2003.

[15] R. J. Williams, J. P. E. Spencer, and C. Rice-Evans, "Flavonoids: antioxidants or signalling molecules?," *Free Radic. Biol. Med.*, vol. 36, no. 7, pp. 838–849, Apr. 2004.

[16] A. García-Lafuente, E. Guillamón, A. Villares, M. A. Rostagno, and J. A. Martínez, "Flavonoids as anti-inflammatory agents: implications in cancer and cardiovascular disease," *Inflamm. Res. Off. J. Eur. Histamine Res. Soc. Al*, vol. 58, no. 9, pp. 537–552, Sep. 2009.

[17] A. E. Rotelli, T. Guardia, A. O. Juárez, N. E. de la Rocha, and L. E. Pelzer, "Comparative study of flavonoids in experimental models of inflammation," *Pharmacol. Res. Off. J. Ital. Pharmacol. Soc.*, vol. 48, no. 6, pp. 601–606, Dec. 2003.
[18] P. N. Paradkar, P. S. Blum, M. A. Berhow, H. Baumann, and S.-M. Kuo, "Dietary isoflavones suppress endotoxin-induced inflammatory reaction in liver and intestine," *Cancer Lett.*, vol. 215, no. 1, pp. 21–28, Nov. 2004.
[19] W. Duan, I. C. Kuo, S. Selvarajan, K. Y. Chua, B. H. Bay, and W. S. F. Wong, "Antiinflammatory effects of genistein, a tyrosine kinase inhibitor, on a guinea pig model of asthma," *Am. J. Respir. Crit. Care Med.*, vol. 167, no. 2, pp. 185–192, Jan. 2003.
[20] T. Guardia, A. E. Rotelli, A. O. Juarez, and L. E. Pelzer, "Anti-inflammatory properties of plant flavonoids. Effects of rutin, quercetin and hesperidin on adjuvant arthritis in rat," *Farm. Soc. Chim. Ital. 1989*, vol. 56, no. 9, pp. 683–687, Sep. 2001.
[21] A. J. Afolayan and J. J. Meyer, "The antimicrobial activity of 3,5,7-trihydroxyflavone isolated from the shoots of Helichrysum aureonitens," *J. Ethnopharmacol.*, vol. 57, no. 3, pp. 177–181, Aug. 1997.
[22] Y. M. Lin, H. Anderson, M. T. Flavin, Y. H. Pai, E. Mata-Greenwood, T. Pengsuparp, J. M. Pezzuto, R. F. Schinazi, S. H. Hughes, and F. C. Chen, "In vitro anti-HIV activity of biflavonoids isolated from Rhus succedanea and Garcinia multiflora," *J. Nat. Prod.*, vol. 60, no. 9, pp. 884–888, Sep. 1997.
[23] R. I. Brinkworth, M. J. Stoermer, and D. P. Fairlie, "Flavones are inhibitors of HIV-1 proteinase," *Biochem. Biophys. Res. Commun.*, vol. 188, no. 2, pp. 631–637, Oct. 1992.
[24] M. R. Fesen, Y. Pommier, F. Leteurtre, S. Hiroguchi, J. Yung, and K. W. Kohn, "Inhibition of HIV-1 integrase by flavones, caffeic acid phenethyl ester (CAPE) and related compounds," *Biochem. Pharmacol.*, vol. 48, no. 3, pp. 595–608, Aug. 1994.
[25] J. W. Critchfield, S. T. Butera, and T. M. Folks, "Inhibition of HIV activation in latently infected cells by flavonoid compounds," *AIDS Res. Hum. Retroviruses*, vol. 12, no. 1, pp. 39–46, Jan. 1996.
[26] E. M. Jr and C. Kandaswami, "The impact of plant flavonoids on mammalian biology: implications for immunity, inflammation and cancer," in *The Flavonoids*, J. B. Harborne, Ed. Springer US, 1994, pp. 619–652.
[27] S. M. Colegate and R. J. Molyneux, *Bioactive Natural Products Detection, Isolation, and Structural Determination*. CRC Press, 1993.
[28] R. Dall'Agnol, A. Ferraz, A. P. Bernardi, D. Albring, C. Nör, L. Sarmento, L. Lamb, M. Hass, G. von Poser, and E. E. S. Schapoval, "Antimicrobial activity of some Hypericum species," *Phytomedicine Int. J. Phytother. Phytopharm.*, vol. 10, no. 6–7, pp. 511–516, 2003.
[29] M. S. El-Abyad, N. M. Morsi, D. A. Zaki, and M. T. Shaaban, "Preliminary screening of some Egyptian weeds for antimicrobial activity," *Microbios*, vol. 62, no. 250, pp. 47–57, 1990.
[30] J. B. Harborne and C. A. Williams, "Advances in flavonoid research since 1992," *Phytochemistry*, vol. 55, no. 6, pp. 481–504, Nov. 2000.
[31] Atta-ur-Rahman, *Studies in Natural Products Chemistry*. Elsevier, 2008.
[32] J. Gorham and S. J. Coughlan, "Inhibition of photosynthesis by stilbenoids," *Phytochemistry*, vol. 19, no. 10, pp. 2059–2064, 1980.
[33] H.-J. Z. Kai Xiao, "Stilbenoids: Chemistry and bioactivities," *Stud. Nat. Prod. Chem.*, vol. 34, pp. 453–646, 2008.

[34] G. J. Soleas, E. P. Diamandis, and D. M. Goldberg, “The world of resveratrol,” *Adv. Exp. Med. Biol.*, vol. 492, pp. 159–182, 2001.
[35] S. He and X. Yan, “From resveratrol to its derivatives: new sources of natural antioxidant,” *Curr. Med. Chem.*, vol. 20, no. 8, pp. 1005–1017, 2013.
[36] P. Coggon, N. F. Janes, F. E. King, T. J. King, R. J. Molyneux, J. W. W. Morgan, and K. Sellars, “61. Hopeaphenol, an extractive of the heartwood of Hopea odorata and Balanocarpus heimii,” *J. Chem. Soc. Resumed*, no. 0, pp. 406–409, Jan. 1965.
[37] S. Sotheeswaran and V. Pasupathy, “Distribution of resveratrol oligomers in plants,” *Phytochemistry*, vol. 32, no. 5, pp. 1083–1092, Mar. 1993.
[38] I. Iliya, Z. Ali, T. Tanaka, M. Iinuma, M. Furusawa, K. ichi Nakaya, J. Murata, and D. Darnaedi, “Stilbenoids from the stem of Gnetum latifolium (Gnetaceae),” *Phytochemistry*, vol. 61, no. 8, pp. 959–961, Dec. 2002.
[39] T. Ito, Z. Ali, M. Furusawa, I. Iliya, T. Tanaka, K. Nakaya, J. Murata, D. Darnaedi, M. Oyama, and M. Iinuma, “Two novel trimeric resveratrol derivatives from Cotylelobium lanceolatum,” *Chem. Biodivers.*, vol. 2, no. 9, pp. 1200–1216, Sep. 2005.
[40] N. M. Packter, “Biochemistry of stilbenoids: By J Gorham (with contributions by M Tori and Y Asakawa). pp 262. Chapman & Hall, London. 1995. £59 ISBN 0-412-55070-9,” *Biochem. Educ.*, vol. 23, no. 3, pp. 179–179, Jul. 1995.
[41] M. B. Austin, M. E. Bowman, J.-L. Ferrer, J. Schröder, and J. P. Noel, “An aldol switch discovered in stilbene synthases mediates cyclization specificity of type III polyketide synthases,” *Chem. Biol.*, vol. 11, no. 9, pp. 1179–1194, Sep. 2004.
[42] H. Morita, H. Noguchi, J. Schröder, and I. Abe, “Novel polyketides synthesized with a higher plant stilbene synthase,” *Eur. J. Biochem. FEBS*, vol. 268, no. 13, pp. 3759–3766, Jul. 2001.
[43] H. Shuilin, Z. Jingui, W. Xiaofeng, W. Yanhua, X. Ming, L. Binlian, and L. Ming, “Plant secondary metabolism: Function, regulation and gene engineering,” *Chin. J. Appl. Environ. Biol. Zhongguo Ke Xue Yuan Chengdu Sheng Wu Yan Jiu Suo Zhu Ban*, vol. 8, no. 5, pp. 558–563, Dec. 2001.
[44] F. Melchior and H. Kindl, “Coordinate- and elicitor-dependent expression of stilbene synthase and phenylalanine ammonia-lyase genes in Vitis cv. Optima,” *Arch. Biochem. Biophys.*, vol. 288, no. 2, pp. 552–557, Aug. 1991.
[45] K. T. Watts, P. C. Lee, and C. Schmidt-Dannert, “Biosynthesis of plant-specific stilbene polyketides in metabolically engineered Escherichia coli,” *BMC Biotechnol.*, vol. 6, no. 1, p. 22, Mar. 2006.
[46] S. S. Velu, I. Buniyamin, L. K. Ching, F. Feroz, I. Noorbatcha, L. C. Gee, K. Awang, I. A. Wahab, and J.-F. F. Weber, “Regio- and stereoselective biomimetic synthesis of oligostilbenoid dimers from resveratrol analogues: influence of the solvent, oxidant, and substitution,” *Chem. Weinh. Bergstr. Ger.*, vol. 14, no. 36, pp. 11376–11384, 2008.
[47] A.- Rahman, *Studies in Natural Products Chemistry: Bioactive Natural Products (Part L)*. Gulf Professional Publishing, 2011.
[48] S. S. Velu, F. Di Meo, P. Trouillas, J.-C. Sancho-Garcia, and J.-F. F. Weber, “Regio- and stereocontrolled synthesis of oligostilbenoids: theoretical highlights at the supramolecular level,” *J. Nat. Prod.*, vol. 76, no. 4, pp. 538–546, Apr. 2013.
[49] K. C. L. Noel F. Thomas, “Tandem Stereospecific Radical Cation-Mediated Syntheses of Oligostilbenoid Dimers,” *Front. Nat. Prod. Chem.*, vol. 1, no. 1, pp. 19–30, 2004.

[50] Y. Takaya, K. Terashima, J. Ito, Y.-H. He, M. Tateoka, N. Yamaguchi, and M. Niwa, "Biomimic transformation of resveratrol," *Tetrahedron*, vol. 61, no. 43, pp. 10285–10290, Oct. 2005.
[51] Y. Takaya, K.-X. Yan, K. Terashima, Y.-H. He, and M. Niwa, "Biogenetic reactions on stilbenetetramers from Vitaceaeous plants," *Tetrahedron*, vol. 58, no. 45, pp. 9265–9271, Nov. 2002.
[52] M. Sako, H. Hosokawa, T. Ito, and M. Iinuma, "Regioselective Oxidative Coupling of 4-Hydroxystilbenes: Synthesis of Resveratrol and ε-Viniferin (E)-Dehydrodimers," *J. Org. Chem.*, vol. 69, no. 7, pp. 2598–2600, Apr. 2004.
[53] C.-S. Yao, L.-X. Zhou, and M. Lin, "Preparation on Oligostilbenes of Isorhapontigenin by Oxidative Coupling Reaction," *Chem. Pharm. Bull. (Tokyo)*, vol. 52, no. 2, pp. 238–243, 2004.
[54] W. Li, H. Li, Y. Li, and Z. Hou, "Total Synthesis of (±)-Quadrangularin A," *Angew. Chem. Int. Ed.*, vol. 45, no. 45, pp. 7609–7611, Nov. 2006.
[55] S. A. Snyder, A. Gollner, and M. I. Chiriac, "Regioselective Reactions for Programmable Resveratrol Oligomer Synthesis," *Nature*, vol. 474, no. 7352, pp. 461–466, Jun. 2011.
[56] S. S. Velu, I. Buniyamin, L. K. Ching, F. Feroz, I. Noorbatcha, L. C. Gee, K. Awang, I. A. Wahab, and J.-F. F. Weber, "Regio- and Stereoselective Biomimetic Synthesis of Oligostilbenoid Dimers from Resveratrol Analogues: Influence of the Solvent, Oxidant, and Substitution," *Chem. – Eur. J.*, vol. 14, no. 36, pp. 11376–11384, Dec. 2008.
[57] S. S. Velu, F. Di Meo, P. Trouillas, J.-C. Sancho-Garcia, and J.-F. F. Weber, "Regio- and Stereocontrolled Synthesis of Oligostilbenoids: Theoretical Highlights at the Supramolecular Level," *J. Nat. Prod.*, vol. 76, no. 4, pp. 538–546, Apr. 2013.
[58] J. C. S.-G. I. Bayach, "π-Stacked polyphenolic dimers: A case study using dispersion-corrected methods," *Chem. Phys. Lett.*, vol. 578, pp. 120–125, 2013.
[59] S. Friederich, U. H. Maier, B. Deus-Neumann, Yoshinori Asakawa, and M. H. Zenk, "Biosynthesis of cyclic bis(bibenzyls) in Marchantia polymorpha," *Phytochemistry*, vol. 50, no. 4, pp. 589–598, Feb. 1999.
[60] Y. Ohta, S. Abe, H. Komura, and M. Kobayashi, "Prelunularic acid, a probable immediate precursor of lunularic acid. First example of a 'prearomatic' intermediate in the phenylpropanoid-polymalonate pathway," *J. Am. Chem. Soc.*, vol. 105, no. 13, pp. 4480–4481, Jun. 1983.
[61] S. Friederich, M. Rueffer, Y. Asakawa, and M. H. Zenk, "Cytochromes P-450 catalyze the formation of marchantins A and C in Marchantia polymorpha," *Phytochemistry*, vol. 52, no. 7, pp. 1195–1202, Dec. 1999.
[62] H. Yang, M. K. Lee, and Y. C. Kim, "Protective activities of stilbene glycosides from Acer mono leaves against H2O2-induced oxidative damage in primary cultured rat hepatocytes," *J. Agric. Food Chem.*, vol. 53, no. 10, pp. 4182–4186, May 2005.
[63] K. Ohguchi, T. Tanaka, I. Iliya, T. Ito, M. Iinuma, K. Matsumoto, Y. Akao, and Y. Nozawa, "Gnetol as a potent tyrosinase inhibitor from genus Gnetum," *Biosci. Biotechnol. Biochem.*, vol. 67, no. 3, pp. 663–665, Mar. 2003.
[64] C. Cal, H. Garban, A. Jazirehi, C. Yeh, Y. Mizutani, and B. Bonavida, "Resveratrol and cancer: chemoprevention, apoptosis, and chemo-immunosensitizing activities," *Curr. Med. Chem. Anti-Cancer Agents*, vol. 3, no. 2, pp. 77–93, Mar. 2003.

[65] B. B. Aggarwal, A. Bhardwaj, R. S. Aggarwal, N. P. Seeram, S. Shishodia, and Y. Takada, "Role of resveratrol in prevention and therapy of cancer: preclinical and clinical studies," *Anticancer Res.*, vol. 24, no. 5A, pp. 2783–2840, Oct. 2004.
[66] B. B. Aggarwal and S. Shishodia, *Resveratrol in Health and Disease*. CRC Press, 2005.
[67] A. R. Martín, I. Villegas, M. Sánchez-Hidalgo, and C. A. de la Lastra, "The effects of resveratrol, a phytoalexin derived from red wines, on chronic inflammation induced in an experimentally induced colitis model," *Br. J. Pharmacol.*, vol. 147, no. 8, pp. 873–885, Apr. 2006.
[68] N. Elmali, I. Esenkaya, A. Harma, K. Ertem, Y. Turkoz, and B. Mizrak, "Effect of resveratrol in experimental osteoarthritis in rabbits," *Inflamm. Res. Off. J. Eur. Histamine Res. Soc. Al*, vol. 54, no. 4, pp. 158–162, Apr. 2005.
[69] B.-N. Su, M. Cuendet, M. E. Hawthorne, L. B. S. Kardono, S. Riswan, H. H. S. Fong, R. G. Mehta, J. M. Pezzuto, and A. D. Kinghorn, "Constituents of the bark and twigs of Artocarpus dadah with cyclooxygenase inhibitory activity," *J. Nat. Prod.*, vol. 65, no. 2, pp. 163–169, Feb. 2002.
[70] S. H. Lee, N. H. Shin, S. H. Kang, J. S. Park, S. R. Chung, K. R. Min, and Y. Kim, "Alpha-viniferin: a prostaglandin H2 synthase inhibitor from root of Carex humilis," *Planta Med.*, vol. 64, no. 3, pp. 204–207, Apr. 1998.
[71] E. Y. Chung, B. H. Kim, M. K. Lee, Y.-P. Yun, S. H. Lee, K. R. Min, and Y. Kim, "Anti-inflammatory effect of the oligomeric stilbene alpha-Viniferin and its mode of the action through inhibition of cyclooxygenase-2 and inducible nitric oxide synthase," *Planta Med.*, vol. 69, no. 8, pp. 710–714, Aug. 2003.
[72] H. Matsuda, T. Morikawa, H. Xie, and M. Yoshikawa, "Antiallergic phenanthrenes and stilbenes from the tubers of Gymnadenia conopsea," *Planta Med.*, vol. 70, no. 9, pp. 847–855, Sep. 2004.
[73] L. Harinantenaina, D. N. Quang, N. Takeshi, T. Hashimoto, C. Kohchi, G.-I. Soma, and Y. Asakawa, "Bis(bibenzyls) from liverworts inhibit lipopolysaccharide-induced inducible NOS in RAW 264.7 cells: a study of structure-activity relationships and molecular mechanism," *J. Nat. Prod.*, vol. 68, no. 12, pp. 1779–1781, Dec. 2005.
[74] A. M. Pridgeon, P. J. Cribb, M. W. Chase, and F. N. Rasmussen, *Genera Orchidacearum Volume 6: Epidendroideae*. Oxford University Press, 2014.
[75] Y.-H. Lu, C.-N. Lin, H.-H. Ko, S.-Z. Yang, L.-T. Tsao, and J.-P. Wang, "Novel Anti-Inflammatory Constituents of Artocarpus rigida," *Helv. Chim. Acta*, vol. 86, no. 7, pp. 2566–2572, Jul. 2003.
[76] W. Li, *Exploration of the Underlying Mechanisms for the Superinduction Effects of Phytoestrogens*. ProQuest, 2006.
[77] B. B. Aggarwal and S. Shishodia, *Resveratrol in Health and Disease*. CRC Press, 2005.
[78] R. Hain, H. J. Reif, E. Krause, R. Langebartels, H. Kindl, B. Vornam, W. Wiese, E. Schmelzer, P. H. Schreier, and R. H. Stöcker, "Disease resistance results from foreign phytoalexin expression in a novel plant," *Nature*, vol. 361, no. 6408, pp. 153–156, Jan. 1993.
[79] J. M. Mérillon and K. G. Ramawat, *Plant Defence: Biological Control: Biological Control*. Springer, 2011.
[80] P. Jeandet, A.-C. Douillet-Breuil, R. Bessis, S. Debord, M. Sbaghi, and M. Adrian, "Phytoalexins from the Vitaceae: biosynthesis, phytoalexin gene expression in transgenic plants, antifungal activity, and metabolism," *J. Agric. Food Chem.*, vol. 50, no. 10, pp. 2731–2741, May 2002.

[81] T. Pacher, C. Seger, D. Engelmeier, S. Vajrodaya, O. Hofer, and H. Greger, "Antifungal Stilbenoids from Stemona collinsae," *J. Nat. Prod.*, vol. 65, no. 6, pp. 820–827, Jun. 2002.
[82] C. Niu, J.-B. Qu, and H.-X. Lou, "Antifungal Bis[bibenzyls] from the Chinese Liverwort Marchantia polymorpha L.," *Chem. Biodivers.*, vol. 3, no. 1, pp. 34–40, Jan. 2006.
[83] J. M. Scher, J.-B. Speakman, J. Zapp, and H. Becker, "Bioactivity guided isolation of antifungal compounds from the liverwort Bazzania trilobata (L.) S.F. Gray," *Phytochemistry*, vol. 65, no. 18, pp. 2583–2588, Sep. 2004.
[84] P.-H. Ducrot, A. Kollmann, A. E. Bala, A. Majira, L. Kerhoas, R. Delorme, and J. Einhorn, "Cyphostemmins A-B, two new antifungal oligostilbenes from Cyphostemma crotalarioides (Vitaceae)," *Tetrahedron Lett.*, vol. 39, no. 52, pp. 9655–9658, Dec. 1998.
[85] S. Wang, D. Ma, and C. Hu, "Three New Compounds from the Aerial Parts of Caragana sinica," *Helv. Chim. Acta*, vol. 88, no. 8, pp. 2315–2321, Aug. 2005.
[86] I. Rivero-Cruz, L. Acevedo, J. A. Guerrero, S. Martínez, R. Bye, R. Pereda-Miranda, S. Franzblau, B. N. Timmermann, and R. Mata, "Antimycobacterial agents from selected Mexican medicinal plants," *J. Pharm. Pharmacol.*, vol. 57, no. 9, pp. 1117–1126, Sep. 2005.
[87] T. A. Tomoko Nitta, "Antibacterial Activity of Extracts Prepared from Tropical and Subtropical Plants on Methicillin-Resistant Staphylococcus aureus," *J. Health Sci. - J Health SCI*, vol. 48, no. 3, pp. 273–276, 2002.
[88] J. R. Zgoda, A. J. Freyer, L. B. Killmer, and J. R. Porter, "Polyacetylene carboxylic acids from Mitrephora celebica," *J. Nat. Prod.*, vol. 64, no. 10, pp. 1348–1349, Oct. 2001.
[89] F. Hanawa, M. Okamoto, and G. H. N. Towers, "Antimicrobial DNA-binding photosensitizers from the common rush, Juncus effusus," *Photochem. Photobiol.*, vol. 76, no. 1, pp. 51–56, Jul. 2002.
[90] K. P. Manfredi, V. Vallurupalli, M. Demidova, K. Kindscher, and L. K. Pannell, "Isolation of an anti-HIV diprenylated bibenzyl from Glycyrrhiza lepidota," *Phytochemistry*, vol. 58, no. 1, pp. 153–157, Sep. 2001.
[91] G. Yang, J. Zhou, Y. Li, and C. Hu, "Anti-HIV bioactive stilbene dimers of Caragana rosea," *Planta Med.*, vol. 71, no. 6, pp. 569–571, Jun. 2005.
[92] J. T. Romeo, *Phytochemicals in Human Health Protection, Nutrition, and Plant Defense*. Springer, 1999.
[93] V. Cardile, L. Lombardo, C. Spatafora, and C. Tringali, "Chemo-enzymatic synthesis and cell-growth inhibition activity of resveratrol analogues," *Bioorganic Chem.*, vol. 33, no. 1, pp. 22–33, Feb. 2005.
[94] A. Gosslau, M. Chen, C.-T. Ho, and K. Y. Chen, "A methoxy derivative of resveratrol analogue selectively induced activation of the mitochondrial apoptotic pathway in transformed fibroblasts," *Br. J. Cancer*, vol. 92, no. 3, pp. 513–521, Feb. 2005.
[95] M. Murias, W. Jäger, N. Handler, T. Erker, Z. Horvath, T. Szekeres, H. Nohl, and L. Gille, "Antioxidant, prooxidant and cytotoxic activity of hydroxylated resveratrol analogues: structure-activity relationship," *Biochem. Pharmacol.*, vol. 69, no. 6, pp. 903–912, Mar. 2005.
[96] G. R. Pettit, S. B. Singh, M. R. Boyd, E. Hamel, R. K. Pettit, J. M. Schmidt, and F. Hogan, "Antineoplastic agents. 291. Isolation and synthesis of combretastatins A-4, A-5, and A-6(1a)," *J. Med. Chem.*, vol. 38, no. 10, pp. 1666–1672, May 1995.
[97] S. L. Young and D. J. Chaplin, "Combretastatin A4 phosphate: background and current clinical status," *Expert Opin. Investig. Drugs*, vol. 13, no. 9, pp. 1171–1182, Sep. 2004.

[98] M. Jang, L. Cai, G. O. Udeani, K. V. Slowing, C. F. Thomas, C. W. Beecher, H. H. Fong, N. R. Farnsworth, A. D. Kinghorn, R. G. Mehta, R. C. Moon, and J. M. Pezzuto, "Cancer chemopreventive activity of resveratrol, a natural product derived from grapes," *Science*, vol. 275, no. 5297, pp. 218–220, Jan. 1997.

[99] G. J. Soleas, E. P. Diamandis, and D. M. Goldberg, "Resveratrol: a molecule whose time has come? And gone?," *Clin. Biochem.*, vol. 30, no. 2, pp. 91–113, Mar. 1997.

[100] T. Ito, Y. Akao, H. Yi, K. Ohguchi, K. Matsumoto, T. Tanaka, M. Iinuma, and Y. Nozawa, "Antitumor effect of resveratrol oligomers against human cancer cell lines and the molecular mechanism of apoptosis induced by vaticanol C," *Carcinogenesis*, vol. 24, no. 9, pp. 1489–1497, Sep. 2003.

[101] K. Ohguchi, Y. Akao, K. Matsumoto, T. Tanaka, T. Ito, M. Iinuma, and Y. Nozawa, "Vaticanol C-induced cell death is associated with inhibition of pro-survival signaling in HL60 human leukemia cell line," *Biosci. Biotechnol. Biochem.*, vol. 69, no. 2, pp. 353–356, Feb. 2005.

[102] M. Yamada, K.-I. Hayashi, H. Hayashi, S. Ikeda, T. Hoshino, K. Tsutsui, K. Tsutsui, M. Iinuma, and H. Nozaki, "Stilbenoids of Kobresia nepalensis (Cyperaceae) exhibiting DNA topoisomerase II inhibition," *Phytochemistry*, vol. 67, no. 3, pp. 307–313, Feb. 2006.

[103] S. Mishima, K. Matsumoto, Y. Futamura, Y. Araki, T. Ito, T. Tanaka, M. Iinuma, Y. Nozawa, and Y. Akao, "Antitumor effect of stilbenoids from Vateria indica against allografted sarcoma S-180 in animal model," *J. Exp. Ther. Oncol.*, vol. 3, no. 5, pp. 283–288, Sep. 2003.

[104] A. M. Pridgeon, P. J. Cribb, M. W. Chase, and F. N. Rasmussen, *Genera Orchidacearum Volume 6: Epidendroideae*. Oxford University Press, 2014.

[105] G.-N. Zhang, L.-Y. Zhong, S. W. A. Bligh, Y.-L. Guo, C.-F. Zhang, M. Zhang, Z.-T. Wang, and L.-S. Xu, "Bi-bicyclic and bi-tricyclic compounds from Dendrobium thyrsiflorum," *Phytochemistry*, vol. 66, no. 10, pp. 1113–1120, May 2005.

[106] P. Kittakoop, K. Kirtikara, M. Tanticharoen, and Y. Thebtaranonth, "Antimalarial preracemosols A and B, possible biogenetic precursors of racemosol from Bauhinia malabarica Roxb," *Phytochemistry*, vol. 55, no. 4, pp. 349–352, Oct. 2000.

[107] Y. Hernández-Romero, L. Acevedo, M. de los A. Sánchez, W. T. Shier, H. K. Abbas, and R. Mata, "Phytotoxic activity of bibenzyl derivatives from the orchid Epidendrum rigidum," *J. Agric. Food Chem.*, vol. 53, no. 16, pp. 6276–6280, Aug. 2005.

[108] N. A. Valencia-Islas, R. N. Paul, W. T. Shier, R. Mata, and H. K. Abbas, "Phytotoxicity and ultrastructural effects of gymnopusin from the orchid Maxillaria densa on duckweed (Lemna pausicostata) frond and root tissues," *Phytochemistry*, vol. 61, no. 2, pp. 141–148, Sep. 2002.

[109] J. Harmatha and L. Dinan, "Biological activities of lignans and stilbenoids associated with plant-insect chemical interactions," *Phytochem. Rev.*, vol. 2, no. 3, pp. 321–330, Jan. 2003.

[110] G. Smagghe, *Ecdysone: Structures and Functions: Structures and Functions*. Springer, 2009.

[111] Y. Meng1, P. C. Bourne, P. Whiting, V. Sik, and L. Dinan, "Identification and ecdysteroid antagonist activity of three oligostilbenes from the seeds of Carex pendula (Cyperaceae)," *Phytochemistry*, vol. 57, no. 3, pp. 393–400, Jun. 2001.

[112] Y. Hirano, R. Kondo, and K. Sakai, “Compounds inhibitory to rat liver 5α-reductase from tropical commercial wood species: resveratrol trimers from melapi (Shorea sp.) heartwood,” *J. Wood Sci.*, vol. 47, no. 4, pp. 308–312, Aug. 2001.
[113] Y. Hirano, R. Kondo, and K. Sakai, “5α-Reductase inhibitory compounds produced by polymerization of resveratrol with horseradish peroxidase,” *J. Wood Sci.*, vol. 48, no. 1, pp. 64–68, Feb. 2002.
[114] S. Sanoh, S. Kitamura, K. Sugihara, and S. Ohta, “Cytochrome P450 1A1/2 mediated metabolism of trans-stilbene in rats and humans,” *Biol. Pharm. Bull.*, vol. 25, no. 3, pp. 397–400, Mar. 2002.
[115] V. Farines, M.-C. Monje, J. P. Telo, E. Hnawia, M. Sauvain, and F. Nepveu, “Polyphenols as superoxide dismutase modulators and ligands for estrogen receptors,” *Anal. Chim. Acta*, vol. 513, no. 1, pp. 103–111, Jun. 2004.
[116] J. Y. Liu, Y. H. Ye, L. Wang, D. H. Shi, and R. X. Tan, “New Resveratrol Oligomers from the Stem Bark of Hopea hainanensis,” *Helv. Chim. Acta*, vol. 88, no. 11, pp. 2910–2917, Nov. 2005.
[117] S. H. Sung, S. Y. Kang, K. Y. Lee, M. J. Park, J. H. Kim, J. H. Park, Y. C. Kim, J. Kim, and Y. C. Kim, “(+)-Alpha-viniferin, a stilbene trimer from Caragana chamlague, inhibits acetylcholinesterase,” *Biol. Pharm. Bull.*, vol. 25, no. 1, pp. 125–127, Jan. 2002.
[118] C. Fan, W. Wang, Y. Wang, G. Qin, and W. Zhao, “Chemical constituents from Dendrobium densiflorum,” *Phytochemistry*, vol. 57, no. 8, pp. 1255–1258, Aug. 2001.
[119] Y.-L. Huang, W.-J. Tsai, C.-C. Shen, and C.-C. Chen, “Resveratrol derivatives from the roots of Vitis thunbergii,” *J. Nat. Prod.*, vol. 68, no. 2, pp. 217–220, Feb. 2005.
[120] A. Soumyanath, *Traditional Medicines for Modern Times: Antidiabetic Plants*. CRC Press, 2005.
[121] S. Z. Choi, S. O. Lee, K. U. Jang, S. H. Chung, S. H. Park, H. C. Kang, E. Y. Yang, H. J. Cho, and K. R. Lee, “Antidiabetic stilbene and anthraquinone derivatives from Rheum undulatum,” *Arch. Pharm. Res.*, vol. 28, no. 9, pp. 1027–1030, Sep. 2005.
[122] M. Manickam, M. Ramanathan, M. A. Jahromi, J. P. Chansouria, and A. B. Ray, “Antihyperglycemic activity of phenolics from Pterocarpus marsupium,” *J. Nat. Prod.*, vol. 60, no. 6, pp. 609–610, Jun. 1997.
[123] Y. Oshima, K. Namao, A. Kamijou, S. Matsuoka, M. Nakano, K. Terao, and Y. Ohizumi, “Powerful hepatoprotective and hepatotoxic plant oligostilbenes, isolated from the Oriental medicinal plant Vitis coignetiae (Vitaceae),” *Experientia*, vol. 51, no. 1, pp. 63–66, Jan. 1995.
[124] S. Estrada-Soto, J. J. López-Guerrero, R. Villalobos-Molina, and R. Mata, “Endothelium-independent relaxation of aorta rings by two stilbenoids from the orchids Scaphyglottis livida,” *Fitoterapia*, vol. 77, no. 3, pp. 236–239, Apr. 2006.
[125] Y. Hernández-Romero, J.-I. Rojas, R. Castillo, A. Rojas, and R. Mata, “Spasmolytic effects, mode of action, and structure-activity relationships of stilbenoids from Nidema boothii,” *J. Nat. Prod.*, vol. 67, no. 2, pp. 160–167, Feb. 2004.
[126] S. Estrada, J. J. López-Guerrero, R. Villalobos-Molina, and R. Mata, “Spasmolytic stilbenoids from Maxillaria densa,” *Fitoterapia*, vol. 75, no. 7–8, pp. 690–695, Dec. 2004.
[127] S. Yannai, *Dictionary of Food Compounds with CD-ROM, Second Edition*. CRC Press, 2012.

[128] A. Puntumchai, P. Kittakoop, S. Rajviroongit, S. Vimuttipong, K. Likhitwitayawuid, and Y. Thebtaranonth, “Lakoochins A and B, new antimycobacterial stilbene derivatives from Artocarpus lakoocha,” *J. Nat. Prod.*, vol. 67, no. 3, pp. 485–486, Mar. 2004.
[129] B. Piver, F. Berthou, Y. Dreano, and D. Lucas, “Differential inhibition of human cytochrome P450 enzymes by epsilon-viniferin, the dimer of resveratrol: comparison with resveratrol and polyphenols from alcoholized beverages,” *Life Sci.*, vol. 73, no. 9, pp. 1199–1213, Jul. 2003.
[130] O. Dangles, C. Dufour, and G. Fargeix, “Inhibition of lipid peroxidation by quercetin and quercetin derivatives: antioxidant and prooxidant effects,” *J. Chem. Soc. Perkin Trans. 2*, no. 6, pp. 1215–1222, Jan. 2000.
[131] L. Pauling, “THE NATURE OF THE CHEMICAL BOND. IV. THE ENERGY OF SINGLE BONDS AND THE RELATIVE ELECTRONEGATIVITY OF ATOMS,” *J. Am. Chem. Soc.*, vol. 54, no. 9, pp. 3570–3582, Sep. 1932.
[132] L. Pauling, “THE NATURE OF THE CHEMICAL BOND. APPLICATION OF RESULTS OBTAINED FROM THE QUANTUM MECHANICS AND FROM A THEORY OF PARAMAGNETIC SUSCEPTIBILITY TO THE STRUCTURE OF MOLECULES,” *J. Am. Chem. Soc.*, vol. 53, no. 4, pp. 1367–1400, Apr. 1931.
[133] F. London, “The general theory of molecular forces,” *Trans. Faraday Soc.*, vol. 33, no. 0, p. 8b–26, Jan. 1937.
[134] W. M. Latimer and W. H. Rodebush, “POLARITY AND IONIZATION FROM THE STANDPOINT OF THE LEWIS THEORY OF VALENCE.,” *J. Am. Chem. Soc.*, vol. 42, no. 7, pp. 1419–1433, Jul. 1920.
[135] L. Pauling, *The Nature of the Chemical Bond and the Structure of Molecules and Crystals: An Introduction to Modern Structural Chemistry*. Cornell University Press, 1960.
[136] G. Gilli and P. Gilli, *The Nature of the Hydrogen Bond: Outline of a Comprehensive Hydrogen Bond Theory*. Oxford ; New York: Oxford University Press, 2009.
[137] P. Hobza, “2 Theoretical studies of hydrogen bonding,” *Annu. Rep. Sect. C Phys. Chem.*, vol. 100, p. 3, 2004.
[138] T. Steiner and G. R. Desiraju, “Distinction between the weak hydrogen bond and the van der Waals interaction,” *Chem. Commun.*, no. 8, pp. 891–892, Jan. 1998.
[139] A. P. West, S. Mecozzi, and D. A. Dougherty, “Theoretical Studies of the Supramolecular Synthon Benzene · · · Hexafluorobenzene,” *J. Phys. Org. Chem.*, vol. 10, no. 5, pp. 347–350, May 1997.
[140] I. Geronimo, E. C. Lee, N. J. Singh, and K. S. Kim, “How Different are Electron-Rich and Electron-Deficient π Interactions?,” *J. Chem. Theory Comput.*, vol. 6, no. 7, pp. 1931–1934, Jul. 2010.
[141] D. A. Dougherty and D. A. Stauffer, “Acetylcholine binding by a synthetic receptor: implications for biological recognition,” *Science*, vol. 250, no. 4987, pp. 1558–1560, Dec. 1990.
[142] E. C. Lee, D. Kim, P. Jurecka, P. Tarakeshwar, P. Hobza, and K. S. Kim, “Understanding of assembly phenomena by aromatic-aromatic interactions: benzene dimer and the substituted systems,” *J. Phys. Chem. A*, vol. 111, no. 18, pp. 3446–3457, May 2007.
[143] E. C. Lee, B. H. Hong, J. Y. Lee, J. C. Kim, D. Kim, Y. Kim, P. Tarakeshwar, and K. S. Kim, “Substituent effects on the edge-to-face aromatic interactions,” *J. Am. Chem. Soc.*, vol. 127, no. 12, pp. 4530–4537, Mar. 2005.

[144] H. G. Kim, C.-W. Lee, S. Yun, B. H. Hong, Y.-O. Kim, D. Kim, H. Ihm, J. W. Lee, E. C. Lee, P. Tarakeshwar, S.-M. Park, and K. S. Kim, "An electrochemically controllable nanomechanical molecular system utilizing edge-to-face and face-to-face aromatic interactions," *Org. Lett.*, vol. 4, no. 22, pp. 3971–3974, Oct. 2002.
[145] W. Wang and P. Hobza, "Theoretical Study on the Complexes of Benzene with Isoelectronic Nitrogen-Containing Heterocycles," *ChemPhysChem*, vol. 9, no. 7, pp. 1003–1009, May 2008.
[146] T. van der Wijst, C. F. Guerra, M. Swart, and F. M. Bickelhaupt, "Performance of various density functionals for the hydrogen bonds in DNA base pairs," *Chem. Phys. Lett.*, vol. 426, no. 4–6, pp. 415–421, Aug. 2006.
[147] G. M. Robinson and R. Robinson, "A survey of anthocyanins. I," *Biochem. J.*, vol. 25, no. 5, pp. 1687–1705, 1931.
[148] N. Malaj, B. C. De Simone, A. D. Quartarolo, and N. Russo, "Spectrophotometric study of the copigmentation of malvidin 3-O-glucoside with p-coumaric, vanillic and syringic acids," *Food Chem.*, vol. 141, no. 4, pp. 3614–3620, Dec. 2013.
[149] F. Di Meo, J. C. Sancho Garcia, O. Dangles, and P. Trouillas, "Highlights on Anthocyanin Pigmentation and Copigmentation: A Matter of Flavonoid π-Stacking Complexation To Be Described by DFT-D," *J. Chem. Theory Comput.*, vol. 8, no. 6, pp. 2034–2043, Jun. 2012.
[150] L. Rustioni, R. Basilico, S. Fiori, A. Leoni, D. Maghradze, and O. Failla, "Grape Colour Phenotyping: Development of a Method Based on the Reflectance Spectrum," *Phytochem. Anal.*, vol. 24, no. 5, pp. 453–459, Sep. 2013.
[151] H. Mizuno and Vitis, "Effect of anthocyanin composition in grape skin on anthocyanic vacuolar inclusion development and skin coloration," *Vitis*, 2006.
[152] Kenji Fukuda, Kazuhiko Kikuya, Kennichi Isono, and Masaki Yoshio, "Foliated natural graphite as the anode material for rechargeable lithium-ion cells," *J. Power Sources*, vol. 69, no. 1–2, pp. 165–168, Nov. 1997.
[153] W. Primak and L. H. Fuchs, "Electrical Conductivities of Natural Graphite Crystals," *Phys. Rev.*, vol. 95, no. 1, pp. 22–30, Jul. 1954.
[154] A. K. Geim and K. S. Novoselov, "The rise of graphene," *Nat. Mater.*, vol. 6, no. 3, pp. 183–191, Mar. 2007.
[155] K. S. Kim, S. B. Suh, J. C. Kim, B. H. Hong, E. C. Lee, S. Yun, P. Tarakeshwar, J. Y. Lee, Y. Kim, H. Ihm, H. G. Kim, J. W. Lee, J. K. Kim, H. M. Lee, D. Kim, C. Cui, S. J. Youn, H. Y. Chung, H. S. Choi, C.-W. Lee, S. J. Cho, S. Jeong, and J.-H. Cho, "Assembling phenomena of calix[4]hydroquinone nanotube bundles by one-dimensional short hydrogen bonding and displaced pi-pi stacking," *J. Am. Chem. Soc.*, vol. 124, no. 47, pp. 14268–14279, Nov. 2002.
[156] A. Facchetti, "π-Conjugated Polymers for Organic Electronics and Photovoltaic Cell Applications †," *Chem. Mater.*, vol. 23, no. 3, pp. 733–758, Feb. 2011.
[157] D. Musmade, "Research Journal of Pharmaceutical, Biological and Chemical Sciences." [Online]. Available: http://www.academia.edu/797890/Research_Journal_of_Pharmaceutical_Biological_and_Chemical_Sciences. [Accessed: 04-Jul-2014].
[158] J. Mattsson, O. Zava, A. K. Renfrew, Y. Sei, K. Yamaguchi, P. J. Dyson, and B. Therrien, "Drug delivery of lipophilic pyrenyl derivatives by encapsulation in a water soluble metalla-cage," *Dalton Trans.*, vol. 39, no. 35, pp. 8248–8255, Aug. 2010.

[159] N. Bertrand, M. A. Gauthier, C. Bouvet, P. Moreau, A. Petitjean, J.-C. Leroux, and J. Leblond, "New pharmaceutical applications for macromolecular binders," *J. Controlled Release*, vol. 155, no. 2, pp. 200–210, Oct. 2011.
[160] E. Schrödinger, "An Undulatory Theory of the Mechanics of Atoms and Molecules," *Phys. Rev.*, vol. 28, no. 6, pp. 1049–1070, Dec. 1926.
[161] M. Born and R. Oppenheimer, "Zur Quantentheorie der Molekeln," *Ann. Phys.*, vol. 389, no. 20, pp. 457–484, Jan. 1927.
[162] M. Klein, A. Martinez, and X. P. Wang, "On the Born-Oppenheimer approximation of wave operators in molecular scattering theory," *Commun. Math. Phys.*, vol. 152, no. 1, pp. 73–95, Feb. 1993.
[163] R. G. Parr and Yang, *Density-functional theory of atoms and molecules*. New York; Oxford [England]: Oxford University Press ; Clarendon Press, 1989.
[164] W. Koch and M. C. Holthausen, *A chemist's guide to density functional theory*. Weinheim; New York: Wiley-VCH, 2001.
[165] C. C. J. Roothaan, "New Developments in Molecular Orbital Theory," *Rev. Mod. Phys.*, vol. 23, no. 2, pp. 69–89, Apr. 1951.
[166] G. G. Hall, "The Molecular Orbital Theory of Chemical Valency. VIII. A Method of Calculating Ionization Potentials," *Proc. R. Soc. Lond. Ser. Math. Phys. Sci.*, vol. 205, no. 1083, pp. 541–552, Mar. 1951.
[167] W. J. Hehre, R. F. Stewart, and J. A. Pople, "Self-Consistent Molecular-Orbital Methods. I. Use of Gaussian Expansions of Slater-Type Atomic Orbitals," *J. Chem. Phys.*, vol. 51, no. 6, pp. 2657–2664, Sep. 2003.
[168] W. Kohn and L. J. Sham, "Self-Consistent Equations Including Exchange and Correlation Effects," *Phys. Rev.*, vol. 140, no. 4A, pp. A1133–A1138, Nov. 1965.
[169] C. Møller and M. S. Plesset, "Note on an Approximation Treatment for Many-Electron Systems," *Phys. Rev.*, vol. 46, no. 7, pp. 618–622, Oct. 1934.
[170] C. Møller and M. S. Plesset, "Note on an Approximation Treatment for Many-Electron Systems," *Phys. Rev.*, vol. 46, no. 7, pp. 618–622, Oct. 1934.
[171] M. Head-Gordon, J. A. Pople, and M. J. Frisch, "MP2 energy evaluation by direct methods," *Chem. Phys. Lett.*, vol. 153, no. 6, pp. 503–506, Dec. 1988.
[172] J. A. Pople, R. Seeger, and R. Krishnan, "Variational configuration interaction methods and comparison with perturbation theory," *Int. J. Quantum Chem.*, vol. 12, no. S11, pp. 149–163, Jan. 1977.
[173] R. Krishnan and J. A. Pople, "Approximate fourth-order perturbation theory of the electron correlation energy," *Int. J. Quantum Chem.*, vol. 14, no. 1, pp. 91–100, Jul. 1978.
[174] K. Raghavachari, J. A. Pople, E. S. Replogle, and M. Head-Gordon, "Fifth order Moeller-Plesset perturbation theory: comparison of existing correlation methods and implementation of new methods correct to fifth order," *J. Phys. Chem.*, vol. 94, no. 14, pp. 5579–5586, Jul. 1990.
[175] Y. Jung, R. C. Lochan, A. D. Dutoi, and M. Head-Gordon, "Scaled opposite-spin second order Møller–Plesset correlation energy: An economical electronic structure method," *J. Chem. Phys.*, vol. 121, no. 20, pp. 9793–9802, Nov. 2004.
[176] J. Grant Hill, J. A. Platts, and H.-J. Werner, "Calculation of intermolecular interactions in the benzene dimer using coupled-cluster and local electron correlation methods," *Phys. Chem. Chem. Phys.*, vol. 8, no. 35, p. 4072, 2006.

[177] J. Antony and S. Grimme, “Is spin-component scaled second-order Møller-Plesset perturbation theory an appropriate method for the study of noncovalent interactions in molecules?,” *J. Phys. Chem. A*, vol. 111, no. 22, pp. 4862–4868, Jun. 2007.
[178] T. Takatani and C. David Sherrill, “Performance of spin-component-scaled Møller-Plesset theory (SCS-MP2) for potential energy curves of noncovalent interactions,” *Phys. Chem. Chem. Phys. PCCP*, vol. 9, no. 46, pp. 6106–6114, Dec. 2007.
[179] P. Hohenberg and W. Kohn, “Inhomogeneous Electron Gas,” *Phys. Rev.*, vol. 136, no. 3B, pp. B864–B871, Nov. 1964.
[180] S. Grimme, “Improved second-order Møller–Plesset perturbation theory by separate scaling of parallel- and antiparallel-spin pair correlation energies,” *J. Chem. Phys.*, vol. 118, no. 20, pp. 9095–9102, May 2003.
[181] J. P. Perdew and A. Zunger, “Self-interaction correction to density-functional approximations for many-electron systems,” *Phys. Rev. B*, vol. 23, no. 10, pp. 5048–5079, May 1981.
[182] S. Grimme, “Accurate description of van der Waals complexes by density functional theory including empirical corrections,” *J. Comput. Chem.*, vol. 25, no. 12, pp. 1463–1473, Sep. 2004.
[183] A. D. Becke, “A new mixing of Hartree–Fock and local density-functional theories,” *J. Chem. Phys.*, vol. 98, no. 2, pp. 1372–1377, Jan. 1993.
[184] F. Di Meo, J. C. Sancho Garcia, O. Dangles, and P. Trouillas, “Highlights on Anthocyanin Pigmentation and Copigmentation: A Matter of Flavonoid π-Stacking Complexation To Be Described by DFT-D,” *J. Chem. Theory Comput.*, vol. 8, no. 6, pp. 2034–2043, juin 2012.
[185] Q. Wu and W. Yang, “Empirical correction to density functional theory for van der Waals interactions,” *J. Chem. Phys.*, vol. 116, no. 2, pp. 515–524, Jan. 2002.
[186] S. Grimme, S. Ehrlich, and L. Goerigk, “Effect of the damping function in dispersion corrected density functional theory,” *J. Comput. Chem.*, vol. 32, no. 7, pp. 1456–1465, May 2011.
[187] R. A. Heaton, J. G. Harrison, and C. C. Lin, “Self-interaction correction for density-functional theory of electronic energy bands of solids,” *Phys. Rev. B*, vol. 28, no. 10, pp. 5992–6007, Nov. 1983.
[188] M. Dion, H. Rydberg, E. Schröder, D. C. Langreth, and B. I. Lundqvist, “Van der Waals Density Functional for General Geometries,” *Phys. Rev. Lett.*, vol. 92, no. 24, p. 246401, Jun. 2004.
[189] C. Lee, W. Yang, and R. G. Parr, “Development of the Colle-Salvetti correlation-energy formula into a functional of the electron density,” *Phys. Rev. B*, vol. 37, no. 2, pp. 785–789, Jan. 1988.
[190] S. KÜMMEL and J. P. PERDEW, “Two avenues to self-interaction correction within Kohn—Sham theory: unitary invariance is the shortcut,” *Mol. Phys.*, vol. 101, no. 9, pp. 1363–1368, 2003.
[191] G. Román-Pérez and J. M. Soler, “Efficient Implementation of a van der Waals Density Functional: Application to Double-Wall Carbon Nanotubes,” *Phys. Rev. Lett.*, vol. 103, no. 9, p. 096102, Aug. 2009.
[192] L. Goerigk, “How Do DFT-DCP, DFT-NL, and DFT-D3 Compare for the Description of London-Dispersion Effects in Conformers and General Thermochemistry?,” *J. Chem. Theory Comput.*, vol. 10, no. 3, pp. 968–980, Mar. 2014.

[193] E. Runge and E. K. U. Gross, “Density-Functional Theory for Time-Dependent Systems,” *Phys. Rev. Lett.*, vol. 52, no. 12, pp. 997–1000, Mar. 1984.
[194] “Why bother with Polyphenols ? : Groupe Polyphenols.” .
[195] N. Authors, “Dictionary of Natural Products on DVD,” 2011.
[196] C. C. Tangney and H. E. Rasmussen, “Polyphenols, inflammation, and cardiovascular disease,” *Curr. Atheroscler. Rep.*, vol. 15, no. 5, p. 324, May 2013.
[197] V. Habauzit and C. Morand, “Evidence for a protective effect of polyphenols-containing foods on cardiovascular health: an update for clinicians,” *Ther. Adv. Chronic Dis.*, vol. 3, no. 2, pp. 87–106, Mar. 2012.
[198] J. S. G. Florent Di Meo, “Highlights on Anthocyanin Pigmentation and Copigmentation: A Matter of Flavonoid π-Stacking Complexation To Be Described by DFT-D,” *J. Chem. Theory Comput.*, vol. 8, no. 6, pp. 2034–2043, 2012.
[199] F. Nave, N. F. Brás, L. Cruz, N. Teixeira, N. Mateus, M. J. Ramos, F. Di Meo, P. Trouillas, O. Dangles, and V. De Freitas, “Influence of a Flavan-3-ol Substituent on the Affinity of Anthocyanins (Pigments) toward Vinylcatechin Dimers and Proanthocyanidins (Copigments),” *J. Phys. Chem. B*, vol. 116, no. 48, pp. 14089–14099, Dec. 2012.
[200] T. Tanaka, I. Kouno, and G.-I. Nonaka, “Biomimetic Synthesis and Related Reactions of Ellagitannins,” in *Biomimetic Organic Synthesis*, E. Poupon and B. Nay, Eds. Wiley-VCH Verlag GmbH & Co. KGaA, 2011, pp. 637–675.
[201] J. Gorham, *Biochemistry of the Stilbenoids*. Springer, 1995.
[202] S. S. Velu, N. F. Thomas, and J.-F. F. Weber, “Strategies and Methods for the Syntheses of Natural Oligomeric Stilbenoids and Analogues,” *Curr. Org. Chem.*, vol. 16, no. 5, pp. 605–662, Mar. 2012.
[203] S. S. Velu, I. Buniyamin, L. K. Ching, F. Feroz, I. Noorbatcha, L. C. Gee, K. Awang, I. A. Wahab, and J.-F. F. Weber, “Regio- and stereoselective biomimetic synthesis of oligostilbenoid dimers from resveratrol analogues: influence of the solvent, oxidant, and substitution,” *Chem. Weinh. Bergstr. Ger.*, vol. 14, no. 36, pp. 11376–11384, 2008.
[204] C. Bonechi, S. Martini, A. Magnani, and C. Rossi, “Stacking interaction study of trans-resveratrol (trans-3,5,4’-trihydroxystilbene) in solution by Nuclear Magnetic Resonance and Fourier Transform Infrared Spectroscopy,” *Magn. Reson. Chem. MRC*, vol. 46, no. 7, pp. 625–629, Jul. 2008.
[205] J. F. Dobson and T. Gould, “Calculation of dispersion energies,” *J. Phys. Condens. Matter*, vol. 24, no. 7, p. 073201, Feb. 2012.
[206] J. Klimeš and A. Michaelides, “Perspective: Advances and challenges in treating van der Waals dispersion forces in density functional theory,” *J. Chem. Phys.*, vol. 137, no. 12, p. 120901, Sep. 2012.
[207] S. Grimme, “Semiempirical GGA-type density functional constructed with a long-range dispersion correction,” *J. Comput. Chem.*, vol. 27, no. 15, pp. 1787–1799, Nov. 2006.
[208] G. Yi Liu, “A Universal Damping Function for Empirical Dispersion Correction on Density Functional Theory,” 2009.
[209] S. Grimme, “Density functional theory with London dispersion corrections,” *Wiley Interdiscip. Rev. Comput. Mol. Sci.*, vol. 1, no. 2, pp. 211–228, Mar. 2011.
[210] M. E. Foster and K. Sohlberg, “Empirically corrected DFT and semi-empirical methods for non-bonding interactions,” *Phys. Chem. Chem. Phys. PCCP*, vol. 12, no. 2, pp. 307–322, Jan. 2010.

[211] S. Grimme, J. Antony, S. Ehrlich, and H. Krieg, “A consistent and accurate ab initio parametrization of density functional dispersion correction (DFT-D) for the 94 elements H-Pu,” *J. Chem. Phys.*, vol. 132, no. 15, p. 154104, Apr. 2010.
[212] S. Grimme, S. Ehrlich, and L. Goerigk, “Effect of the damping function in dispersion corrected density functional theory,” *J. Comput. Chem.*, vol. 32, no. 7, pp. 1456–1465, May 2011.
[213] O. A. Vydrov and T. Van Voorhis, “Dispersion interactions from a local polarizability model,” *Phys. Rev. A*, vol. 81, no. 6, Jun. 2010.
[214] K. Lee, É. D. Murray, L. Kong, B. I. Lundqvist, and D. C. Langreth, “Higher-accuracy van der Waals density functional,” *Phys. Rev. B*, vol. 82, no. 8, p. 081101, Aug. 2010.
[215] M. Dion, H. Rydberg, E. Schröder, D. C. Langreth, and B. I. Lundqvist, “Van der Waals Density Functional for General Geometries,” *Phys. Rev. Lett.*, vol. 92, no. 24, p. 246401, Jun. 2004.
[216] O. A. Vydrov and T. Van Voorhis, “Nonlocal van der Waals density functional: the simpler the better,” *J. Chem. Phys.*, vol. 133, no. 24, p. 244103, Dec. 2010.
[217] G. Román-Pérez and J. M. Soler, “Efficient Implementation of a van der Waals Density Functional: Application to Double-Wall Carbon Nanotubes,” *Phys. Rev. Lett.*, vol. 103, no. 9, p. 096102, Aug. 2009.
[218] E. Anouar, P. Kosinová, D. Kozlowski, R. Mokrini, J. L. Duroux, and P. Trouillas, “New aspects of the antioxidant properties of phenolic acids: a combined theoretical and experimental approach,” *Phys. Chem. Chem. Phys. PCCP*, vol. 11, no. 35, pp. 7659–7668, Sep. 2009.
[219] P. Trouillas, C. Fagnère, R. Lazzaroni, C. Calliste, A. Marfak, and J.-L. Duroux, “A theoretical study of the conformational behavior and electronic structure of taxifolin correlated with the free radical-scavenging activity,” *Food Chem.*, vol. 88, no. 4, pp. 571–582, Dec. 2004.
[220] P. Trouillas, P. Marsal, D. Siri, R. Lazzaroni, and J.-L. Duroux, “A DFT study of the reactivity of OH groups in quercetin and taxifolin antioxidants: The specificity of the 3-OH site,” *Food Chem.*, vol. 97, no. 4, pp. 679–688, août 2006.
[221] E. H. Anouar, J. Gierschner, J.-L. Duroux, and P. Trouillas, “UV/Visible spectra of natural polyphenols: A time-dependent density functional theory study,” *Food Chem.*, vol. 131, no. 1, pp. 79–89, Mar. 2012.
[222] F. Neese, “The ORCA program system,” *Wiley Interdiscip. Rev. Comput. Mol. Sci.*, vol. 2, no. 1, pp. 73–78, Jan. 2012.
[223] K. Eichkorn, O. Treutler, H. Öhm, M. Häser, and R. Ahlrichs, “Auxiliary basis sets to approximate Coulomb potentials,” *Chem. Phys. Lett.*, vol. 240, no. 4, pp. 283–290, Jun. 1995.
[224] F. Neese, F. Wennmohs, and A. Hansen, “Efficient and accurate local approximations to coupled-electron pair approaches: An attempt to revive the pair natural orbital method,” *J. Chem. Phys.*, vol. 130, no. 11, p. 114108, Mar. 2009.
[225] J. Řezáč, K. E. Riley, and P. Hobza, “Benchmark Calculations of Noncovalent Interactions of Halogenated Molecules,” *J. Chem. Theory Comput.*, vol. 8, no. 11, pp. 4285–4292, Nov. 2012.
[226] K. E. Riley, M. Pitoňák, P. Jurečka, and P. Hobza, “Stabilization and Structure Calculations for Noncovalent Interactions in Extended Molecular Systems Based on Wave

Function and Density Functional Theories," *Chem. Rev.*, vol. 110, no. 9, pp. 5023–5063, Sep. 2010.
[227] T. Schwabe, "Accurate and fast treatment of large molecular systems: Assessment of CEPA and pCCSD within the local pair natural orbital approximation," *J. Comput. Chem.*, vol. 33, no. 26, pp. 2067–2072, Oct. 2012.
[228] S. Grimme, "Improved second-order Møller–Plesset perturbation theory by separate scaling of parallel- and antiparallel-spin pair correlation energies," *J. Chem. Phys.*, vol. 118, no. 20, pp. 9095–9102, May 2003.
[229] T. Schwabe and S. Grimme, "Theoretical thermodynamics for large molecules: walking the thin line between accuracy and computational cost," *Acc. Chem. Res.*, vol. 41, no. 4, pp. 569–579, Apr. 2008.
[230] C. R. Taylor, P. J. Bygrave, J. N. Hart, N. L. Allan, and F. R. Manby, "Improving density functional theory for crystal polymorph energetics," *Phys. Chem. Chem. Phys. PCCP*, vol. 14, no. 21, pp. 7739–7743, Jun. 2012.
[231] J. C. Sancho-García and Y. Olivier, "Reliable DFT-based estimates of cohesive energies of organic solids: The anthracene crystal," *J. Chem. Phys.*, vol. 137, no. 19, p. 194311, Nov. 2012.
[232] P. Hemberger, A. Bodi, C. Schon, M. Steinbauer, K. H. Fischer, C. Kaiser, and I. Fischer, "A pass too far: dissociation of internal energy selected paracyclophane cations, theory and experiment," *Phys. Chem. Chem. Phys.*, vol. 14, no. 34, pp. 11920–11929, Aug. 2012.
[233] A. Karton, A. Tarnopolsky, J.-F. Lamère, G. C. Schatz, and J. M. L. Martin, "Highly accurate first-principles benchmark data sets for the parametrization and validation of density functional and other approximate methods. Derivation of a robust, generally applicable, double-hybrid functional for thermochemistry and thermochemical kinetics," *J. Phys. Chem. A*, vol. 112, no. 50, pp. 12868–12886, Dec. 2008.
[234] K. E. Riley, J. A. Platts, J. Řezáč, P. Hobza, and J. G. Hill, "Assessment of the Performance of MP2 and MP2 Variants for the Treatment of Noncovalent Interactions," *J. Phys. Chem. A*, vol. 116, no. 16, pp. 4159–4169, Apr. 2012.
[235] S. Grimme, C. Mück-Lichtenfeld, and J. Antony, "Noncovalent Interactions between Graphene Sheets and in Multishell (Hyper)Fullerenes," *J. Phys. Chem. C*, vol. 111, no. 30, pp. 11199–11207, Aug. 2007.
[236] T. Risthaus and S. Grimme, "Benchmarking of London Dispersion-Accounting Density Functional Theory Methods on Very Large Molecular Complexes," *J. Chem. Theory Comput.*, vol. 9, no. 3, pp. 1580–1591, Mar. 2013.
[237] O. A. von Lilienfeld and A. Tkatchenko, "Two- and three-body interatomic dispersion energy contributions to binding in molecules and solids," *J. Chem. Phys.*, vol. 132, no. 23, p. 234109, Jun. 2010.
[238] S. Grimme, "Supramolecular Binding Thermodynamics by Dispersion-Corrected Density Functional Theory," *Chem. – Eur. J.*, vol. 18, no. 32, pp. 9955–9964, Aug. 2012.
[239] W. Hujo and S. Grimme, "Comparison of the performance of dispersion-corrected density functional theory for weak hydrogen bonds," *Phys. Chem. Chem. Phys.*, vol. 13, no. 31, pp. 13942–13950, Jul. 2011.
[240] J. Řezáč, K. E. Riley, and P. Hobza, "S66: A Well-balanced Database of Benchmark Interaction Energies Relevant to Biomolecular Structures," *J. Chem. Theory Comput.*, vol. 7, no. 8, pp. 2427–2438, Aug. 2011.

[241] M. S. Marshall, L. A. Burns, and C. D. Sherrill, “Basis set convergence of the coupled-cluster correction, δ[sub MP2][sup CCSD(T)]: Best practices for benchmarking non-covalent interactions and the attendant revision of the S22, NBC10, HBC6, and HSG databases,” *J. Chem. Phys.*, vol. 135, no. 19, p. 194102, 2011.
[242] T. Shen, X.-N. Wang, and H.-X. Lou, “Natural stilbenes: an overview,” *Nat. Prod. Rep.*, vol. 26, no. 7, pp. 916–935, Jun. 2009.
[243] E. . Hakim, S. A. Nanik, S. Atun, Tukiran, S. A. Achmad, Y. M. Syah, and D. J. Lia, “Prosiding Seminar Kimia bersama UKM-ITB ke-5,” pp. 29–41, 2001.
[244] J.-F. F. Weber, I. A. Wahab, A. Marzuki, N. F. Thomas, A. A. Kadir, A. H. A. Hadi, K. Awang, A. A. Latiff, P. Richomme, and J. Delaunay, “Heimiol A, a new dimeric stilbenoid from Neobalanocarpus heimii,” *Tetrahedron Lett.*, vol. 42, no. 29, pp. 4895–4897, Jul. 2001.
[245] E. K. Seo, M. E. Wall, M. C. Wani, H. Navarro, R. Mukherjee, N. R. Farnsworth, and A. D. Kinghorn, “Cytotoxic constituents from the roots of Tovomita brevistaminea,” *Phytochemistry*, vol. 52, no. 4, pp. 669–674, Oct. 1999.
[246] T. Tanaka, T. Ito, K. Nakaya, M. Iinuma, and S. Riswan, “Oligostilbenoids in stem bark of Vatica rassak,” *Phytochemistry*, vol. 54, no. 1, pp. 63–69, May 2000.
[247] T. Ito, T. Tanaka, M. Iinuma, I. Iliya, K. Nakaya, Z. Ali, Y. Takahashi, R. Sawa, Y. Shirataki, J. Murata, and D. Darnaedi, “New resveratrol oligomers in the stem bark of Vatica pauciflora,” *Tetrahedron*, vol. 59, no. 28, pp. 5347–5363, Jul. 2003.
[248] A. P. Lins, J. D. Felicio, M. M. Braggio, and L. C. Roque, “A resveratrol dimer from Parthenocissus tricuspidata,” *Phytochemistry*, vol. 30, no. 9, pp. 3144–3146, 1991.
[249] Y. Oshima, A. Kamijou, H. Moritani, K.-I. Namao, and Y. Ohizumi, “Vitisin A and cis-vitisin A, strongly hepatotoxic plant oligostilbenes from Vitis coignetiae (vitaceae),” *J. Org. Chem.*, vol. 58, no. 4, pp. 850–853, 1993.
[250] R. Madhav, T. R. Seshadri, and G. B. V. Subramanian, “Chemical components of Shorea talura,” *Tetrahedron Lett.*, vol. 6, no. 31, pp. 2713–2716, 1965.
[251] T. Ito, N. Abe, M. Oyama, and M. Iinuma, “Oligostilbenoids from Dipterocarpaceaeous Plants: A New Resveratrol Tetramer from Vateria indica and the Revised Structure of Isohopeaphenol,” *Helv. Chim. Acta*, vol. 91, no. 10, pp. 1989–1998, Oct. 2008.
[252] J. R. Zgoda-Pols, A. J. Freyer, L. B. Killmer, and J. R. Porter, “Antimicrobial resveratrol tetramers from the stem bark of Vatica oblongifoliassp. oblongifolia,” *J. Nat. Prod.*, vol. 65, no. 11, pp. 1554–1559, Nov. 2002.
[253] T. I. Toshiyuki Tanaka, “Six New Heterocyclic Stilbene Oligomers from Stem Bark of Shorea hemsleyana,” *Heterocycles*, vol. 55, no. 4, 2001.
[254] M. N. C. Diyasena, S. Sotheeswaran, S. Surendrakumar, S. Balasubramanian, M. Bokel, and W. Kraus, “Balanocarpol, a new polyphenol from Balanocarpus zeylanicus(trimen) and Hopea jucunda(Thw.)(Dipterocarpaceae),” *J. Chem. Soc. [Perkin 1]*, no. 0, pp. 1807–1809, Jan. 1985.
[255] T. Ito, T. Tanaka, K. Nakaya, M. Iinuma, Y. Takahashi, H. Naganawa, M. Ohyama, Y. Nakanishi, K. F. Bastow, and K.-H. Lee, “A novel bridged stilbenoid trimer and four highly condensed stilbenoid oligomers in Vatica rassak,” *Tetrahedron*, vol. 57, no. 34, pp. 7309–7321, Aug. 2001.
[256] D. H. R. Barton and P. de Mayo, “27. Sesquiterpenoids. Part VII. The constitution of tenulin, a novel sesquiterpenoid lactone,” *J. Chem. Soc. Resumed*, no. 0, pp. 142–149, Jan. 1956.

[257] P. Košinová, R. Gažák, J.-L. Duroux, R. Lazzaroni, V. Křen, X. Assfeld, and P. Trouillas, “Dimerisation process of silybin-type flavonolignans: insights from theory,” *Chemphyschem Eur. J. Chem. Phys. Phys. Chem.*, vol. 12, no. 6, pp. 1135–1142, Apr. 2011.
[258] F. Di Meo, J. C. Sancho Garcia, O. Dangles, and P. Trouillas, “Highlights on Anthocyanin Pigmentation and Copigmentation: A Matter of Flavonoid π-Stacking Complexation To Be Described by DFT-D,” *J. Chem. Theory Comput.*, vol. 8, no. 6, pp. 2034–2043, Jun. 2012.
[259] I. Bayach, J. C. Sancho-García, F. Di Meo, J.-F. F. Weber, and P. Trouillas, “π-Stacked polyphenolic dimers: A case study using dispersion-corrected methods,” *Chem. Phys. Lett.*, vol. 578, pp. 120–125, juillet 2013.
[260] Frisch, Trucks, Schlegel, Scuseria, Robb, Cheeseman, Scalmani, Barone, Mennucci, Petersson, Nakatsuji, Caricato, Li, Hratchian, Izmaylov, Bloino, Zheng, Sonnenberg, Hada, Ehara, Toyota, Fukuda, Hasegawa, Ishida, Nakajima, Honda, Kitao, Nakai, Vreven, Montgomery, Peralta, Ogliaro, Bearpark, Heyd, Brothers, Kudin, Staroverov, Kobayashi, Normand, Raghavachari, Rendell, Burant, Iyengar, Tomasi, Cossi, Rega, and Millam, “Gaussian 09, Revision A. 1. Wallingford CT: Gaussian,” 2009.
[261] J. Tomasi, B. Mennucci, and R. Cammi, “Quantum mechanical continuum solvation models,” *Chem. Rev.*, vol. 105, no. 8, pp. 2999–3093, Aug. 2005.
[262] S. Sinnecker, A. Rajendran, A. Klamt, M. Diedenhofen, and F. Neese, “Calculation of solvent shifts on electronic g-tensors with the conductor-like screening model (COSMO) and its self-consistent generalization to real solvents (direct COSMO-RS),” *J. Phys. Chem. A*, vol. 110, no. 6, pp. 2235–2245, Feb. 2006.
[263] Z. M. Ana Amić, “Towards an improved prediction of the free radical scavenging potency of flavonoids: The significance of double PCET mechanisms.,” *Food Chem.*, vol. 152C, pp. 578–585, 2014.
[264] S. R. Jeremić, S. F. Šehović, N. T. Manojlović, and Z. S. Marković, “Antioxidant and free radical scavenging activity of purpurin,” *Monatshefte Für Chem. - Chem. Mon.*, vol. 143, no. 3, pp. 427–435, Mar. 2012.
[265] J. Đ. Zoran Markovi, “DFT study of free radical scavenging activity of erodiol,” 2013.
[266] J. M. D. M. Zoran S Marković, “Mechanistic study of the structure-activity relationship for the free radical scavenging activity of baicalein.,” *J. Mol. Model.*, vol. 17, no. 10, pp. 2575–84, 2011.
[267] S. V. M. Zoran S Marković, “Electrochemical and density functional theory study on the reactivity of fisetin and its radicals: implications on in vitro antioxidant activity.,” *J. Phys. Chem. A*, vol. 113, no. 51, pp. 14170–9, 2009.
[268] M. E. Alberto, N. Russo, A. Grand, and A. Galano, “A physicochemical examination of the free radical scavenging activity of Trolox: mechanism, kinetics and influence of the environment,” *Phys. Chem. Chem. Phys. PCCP*, vol. 15, no. 13, pp. 4642–4650, Apr. 2013.
[269] P. Trouillas, P. Marsal, D. Siri, R. Lazzaroni, and J.-L. Duroux, “A DFT study of the reactivity of OH groups in quercetin and taxifolin antioxidants: The specificity of the 3-OH site,” *Food Chem.*, vol. 97, no. 4, pp. 679–688, Aug. 2006.
[270] P. Trouillas, P. Marsal, D. Siri, R. Lazzaroni, and J.-L. Duroux, “A DFT study of the reactivity of OH groups in quercetin and taxifolin antioxidants: The specificity of the 3-OH site,” *Food Chem.*, vol. 97, no. 4, pp. 679–688, Aug. 2006.
[271] E. Anouar, C. A. Calliste, P. Kosinová, F. Di Meo, J. L. Duroux, Y. Champavier, K. Marakchi, and P. Trouillas, “Free radical scavenging properties of guaiacol oligomers: a

combined experimental and quantum study of the guaiacyl-moiety role," *J. Phys. Chem. A*, vol. 113, no. 50, pp. 13881–13891, Dec. 2009.
[272] E. Anouar, P. Kosinová, D. Kozlowski, R. Mokrini, J. L. Duroux, and P. Trouillas, "New aspects of the antioxidant properties of phenolic acids: a combined theoretical and experimental approach," *Phys. Chem. Chem. Phys. PCCP*, vol. 11, no. 35, pp. 7659–7668, Sep. 2009.
[273] P. Košinová, F. Di Meo, E. H. Anouar, J.-L. Duroux, and P. Trouillas, "H-atom acceptor capacity of free radicals used in antioxidant measurements," *Int. J. Quantum Chem.*, vol. 111, no. 6, pp. 1131–1142, May 2011.
[274] F. Di Meo, V. Lemaur, J. Cornil, R. Lazzaroni, J.-L. Duroux, Y. Olivier, and P. Trouillas, "Free radical scavenging by natural polyphenols: atom versus electron transfer," *J. Phys. Chem. A*, vol. 117, no. 10, pp. 2082–2092, Mar. 2013.
[275] C. A. Rice-Evans, N. J. Miller, and G. Paganga, "Structure-antioxidant activity relationships of flavonoids and phenolic acids," *Free Radic. Biol. Med.*, vol. 20, no. 7, pp. 933–956, 1996.
[276] B. Halliwell, R. Aeschbach, J. Löliger, and O. I. Aruoma, "The characterization of antioxidants," *Food Chem. Toxicol.*, vol. 33, no. 7, pp. 601–617, Jul. 1995.
[277] P. Vicini, A. Geronikaki, M. Incerti, B. Busonera, G. Poni, C. A. Cabras, and P. La Colla, "Synthesis and biological evaluation of benzo[d]isothiazole, benzothiazole and thiazole Schiff bases," *Bioorg. Med. Chem.*, vol. 11, no. 22, pp. 4785–4789, Nov. 2003.
[278] M. T. H. Tarafder, A. Kasbollah, N. Saravanan, K. A. Crouse, A. M. Ali, and K. Tin Oo, "S-methyldithiocarbazate and its Schiff bases: evaluation of bondings and biological properties," *J. Biochem. Mol. Biol. Biophys. JBMBB Off. J. Fed. Asian Ocean. Biochem. Mol. Biol. FAOBMB*, vol. 6, no. 2, pp. 85–91, Apr. 2002.
[279] A. A. Khalid M. Khan, "Schiff Bases of 3-Formylchromones as Antibacterial, Antifungal, and Phytotoxic Agents (Supplementry Table)," *Lett. Drug Des. Amp Discov.*, vol. 6, no. 5, pp. 363–373, 2009.
[280] Z. H. Chohan, H. Pervez, A. Rauf, K. M. Khan, and C. T. Supuran, "Antibacterial cobalt (II), copper (II), nickel (II) and zinc (II) complexes of mercaptothiadiazole--derived furanyl, thienyl, pyrrolyl, salicylyl and pyridinyl Schiff bases," *J. Enzyme Inhib. Med. Chem.*, vol. 21, no. 2, pp. 193–201, Apr. 2006.
[281] Z. H. Chohan, H. Pervez, A. Rauf, K. M. Khan, G. M. Maharvi, and C. T. Supuran, "Antibacterial and antifugal mono- and di-substituted symmetrical and unsymmetrical triazine-derived Schiff-bases and their transition metal complexes," *J. Enzyme Inhib. Med. Chem.*, vol. 19, no. 2, pp. 161–168, Apr. 2004.
[282] A. Kabeer, M. Baseer, and N. Mote, "Synthesis and antimicro- bial activity of some Schiff bases from benzothiazoles.," *Asian J Chem*, pp. 496–500, 2001.
[283] Z. H. Chohan, M. Arif, Z. Shafiq, M. Yaqub, and C. T. Supuran, "In vitro antibacterial, antifungal & cytotoxic activity of some isonicotinoylhydrazide Schiff's bases and their cobalt (II), copper (II), nickel (II) and zinc (II) complexes," *J. Enzyme Inhib. Med. Chem.*, vol. 21, no. 1, pp. 95–103, Feb. 2006.
[284] Z. Guo, R. Xing, S. Liu, Z. Zhong, X. Ji, L. Wang, and P. Li, "Antifungal properties of Schiff bases of chitosan, N-substituted chitosan and quaternized chitosan," *Carbohydr. Res.*, vol. 342, no. 10, pp. 1329–1332, Jul. 2007.
[285] M. Taha, M. S. Baharudin, N. H. Ismail, K. M. Khan, F. M. Jaafar, null Samreen, S. Siddiqui, and M. I. Choudhary, "Synthesis of 2-methoxybenzoylhydrazone and evaluation of

their antileishmanial activity," *Bioorg. Med. Chem. Lett.*, vol. 23, no. 11, pp. 3463–3466, Jun. 2013.
[286] K. M. Khan, M. Taha, F. Naz, S. Siddiqui, S. Ali, F. Rahim, S. Perveen, and M. I. Choudhary, "Acylhydrazide Schiff bases: DPPH radical and superoxide anion scavengers," *Med. Chem. Shāriqah United Arab Emir.*, vol. 8, no. 4, pp. 705–710, Jul. 2012.
[287] K. M. Khan, Z. Shah, V. U. Ahmad, M. Khan, M. Taha, F. Rahim, S. Ali, N. Ambreen, S. Perveen, M. I. Choudhary, and W. Voelter, "2,4,6-Trichlorophenylhydrazine Schiff bases as DPPH radical and super oxide anion scavengers," *Med. Chem. Shāriqah United Arab Emir.*, vol. 8, no. 3, pp. 452–461, May 2012.
[288] D. Kozlowski, P. Trouillas, C. Calliste, P. Marsal, R. Lazzaroni, and J.-L. Duroux, "Density functional theory study of the conformational, electronic, and antioxidant properties of natural chalcones," *J. Phys. Chem. A*, vol. 111, no. 6, pp. 1138–1145, Feb. 2007.
[289] M. Leopoldini, N. Russo, and M. Toscano, "The molecular basis of working mechanism of natural polyphenolic antioxidants," *Food Chem.*, vol. 125, no. 2, pp. 288–306, Mar. 2011.
[290] L.-F. Wang and H.-Y. Zhang, "A theoretical investigation on DPPH radical-scavenging mechanism of edaravone," *Bioorg. Med. Chem. Lett.*, vol. 13, no. 21, pp. 3789–3792, Nov. 2003.
[291] L. E. S. Netto, H. Z. Chae, S.-W. Kang, S. G. Rhee, and E. R. Stadtman, "Removal of Hydrogen Peroxide by Thiol-specific Antioxidant Enzyme (TSA) Is Involved with Its Antioxidant Properties TSA POSSESSES THIOL PEROXIDASE ACTIVITY," *J. Biol. Chem.*, vol. 271, no. 26, pp. 15315–15321, Jun. 1996.
[292] B. Halliwell, "Reactive oxygen species in living systems: Source, biochemistry, and role in human disease," *Am. J. Med.*, vol. 91, no. 3, Supplement 3, pp. S14–S22, Sep. 1991.
[293] P. Di Mascio, M. E. Murphy, and H. Sies, "Antioxidant defense systems: the role of carotenoids, tocopherols, and thiols," *Am. J. Clin. Nutr.*, vol. 53, no. 1 Suppl, p. 194S–200S, Jan. 1991.
[294] H. Saito and K. Ishihara, "Antioxidant activity and active sites of phospholipids as antioxidants," *J. Am. Oil Chem. Soc.*, vol. 74, no. 12, pp. 1531–1536, Dec. 1997.
[295] A. Padmaja, C. Rajasekhar, A. Muralikrishna, and V. Padmavathi, "Synthesis and antioxidant activity of oxazolyl/thiazolylsulfonylmethyl pyrazoles and isoxazoles," *Eur. J. Med. Chem.*, vol. 46, no. 10, pp. 5034–5038, Oct. 2011.
[296] O. Brede, M. R. Ganapathi, S. Naumov, W. Naumann, and R. Hermann, "Localized Electron Transfer in Nonpolar Solution: Reaction of Phenols and Thiophenols with Free Solvent Radical Cations," *J. Phys. Chem. A*, vol. 105, no. 15, pp. 3757–3764, Apr. 2001.
[297] G. A. DiLabio and E. R. Johnson, "Lone pair-pi and pi-pi interactions play an important role in proton-coupled electron transfer reactions," *J. Am. Chem. Soc.*, vol. 129, no. 19, pp. 6199–6203, May 2007.
[298] E. Hatcher, A. V. Soudackov, and S. Hammes-Schiffer, "Proton-Coupled Electron Transfer in Soybean Lipoxygenase: Dynamical Behavior and Temperature Dependence of Kinetic Isotope Effects," *J. Am. Chem. Soc.*, vol. 129, no. 1, pp. 187–196, Jan. 2007.
[299] S. Hammes-Schiffer, "Proton-coupled electron transfer: classification scheme and guide to theoretical methods," *Energy Environ. Sci.*, vol. 5, no. 7, pp. 7696–7703, Jun. 2012.
[300] M. Lingwood, J. R. Hammond, D. A. Hrovat, J. M. Mayer, and W. T. Borden, "MPW1K Performs Much Better than B3LYP in DFT Calculations on Reactions that Proceed by Proton-Coupled Electron Transfer (PCET)," *J. Chem. Theory Comput.*, vol. 2, no. 3, pp. 740–745, 2006.

[301] F. Di Meo, V. Lemaur, J. Cornil, R. Lazzaroni, J.-L. Duroux, Y. Olivier, and P. Trouillas, "Free Radical Scavenging by Natural Polyphenols: Atom versus Electron Transfer," *J. Phys. Chem. A*, vol. 117, no. 10, pp. 2082–2092, Mar. 2013.

[302] M. Musialik, R. Kuzmicz, T. S. Pawłowski, and G. Litwinienko, "Acidity of hydroxyl groups: an overlooked influence on antiradical properties of flavonoids," *J. Org. Chem.*, vol. 74, no. 7, pp. 2699–2709, Apr. 2009.

[303] P. Trouillas, P. Marsal, A. Svobodová, J. Vostálová, R. Gazák, J. Hrbác, P. Sedmera, V. Kren, R. Lazzaroni, J.-L. Duroux, and D. Walterová, "Mechanism of the antioxidant action of silybin and 2,3-dehydrosilybin flavonolignans: a joint experimental and theoretical study," *J. Phys. Chem. A*, vol. 112, no. 5, pp. 1054–1063, Feb. 2008.

[304] C. Iuga, J. R. Alvarez-Idaboy, and N. Russo, "Antioxidant Activity of trans-Resveratrol toward Hydroxyl and Hydroperoxyl Radicals: A Quantum Chemical and Computational Kinetics Study," *J. Org. Chem.*, vol. 77, no. 8, pp. 3868–3877, Apr. 2012.

[305] M. Leopoldini, S. G. Chiodo, N. Russo, and M. Toscano, "Detailed Investigation of the OH Radical Quenching by Natural Antioxidant Caffeic Acid Studied by Quantum Mechanical Models," *J. Chem. Theory Comput.*, vol. 7, no. 12, pp. 4218–4233, Dec. 2011.

[306] M. S. Blois, "Antioxidant Determinations by the Use of a Stable Free Radical," *Nature*, vol. 181, no. 4617, pp. 1199–1200, Apr. 1958.

[307] S. G. Chiodo, M. Leopoldini, N. Russo, and M. Toscano, "The inactivation of lipid peroxide radical by quercetin. A theoretical insight," *Phys. Chem. Chem. Phys. PCCP*, vol. 12, no. 27, pp. 7662–7670, Jul. 2010.

[308] Y. Zhao and D. G. Truhlar, "Hybrid Meta Density Functional Theory Methods for Thermochemistry, Thermochemical Kinetics, and Noncovalent Interactions: The MPW1B95 and MPWB1K Models and Comparative Assessments for Hydrogen Bonding and van der Waals Interactions," *J. Phys. Chem. A*, vol. 108, no. 33, pp. 6908–6918, Aug. 2004.

[309] I. Tejero, N. González-García, À. González-Lafont, and J. M. Lluch, "Tunneling in Green Tea: Understanding the Antioxidant Activity of Catechol-Containing Compounds. A Variational Transition-State Theory Study," *J. Am. Chem. Soc.*, vol. 129, no. 18, pp. 5846–5854, May 2007.

[310] M. Guerra, R. Amorati, and G. F. Pedulli, "Water effect on the o-h dissociation enthalpy of para-substituted phenols: a DFT study," *J. Org. Chem.*, vol. 69, no. 16, pp. 5460–5467, Aug. 2004.

[311] A. Farazdel, M. Dupuis, E. Clementi, and A. Aviram, "Electric-field induced intramolecular electron transfer in spiro .pi.-electron systems and their suitability as molecular electronic devices. A theoretical study," *J. Am. Chem. Soc.*, vol. 112, no. 11, pp. 4206–4214, May 1990.

[312] S. Grimme, "Accurate description of van der Waals complexes by density functional theory including empirical corrections," *J. Comput. Chem.*, vol. 25, no. 12, pp. 1463–1473, Sep. 2004.

[313] S. Grimme, "Semiempirical GGA-type density functional constructed with a long-range dispersion correction," *J. Comput. Chem.*, vol. 27, no. 15, pp. 1787–1799, Nov. 2006.

[314] M. Valiev, E. J. Bylaska, N. Govind, K. Kowalski, T. P. Straatsma, H. J. J. Van Dam, D. Wang, J. Nieplocha, E. Apra, T. L. Windus, and W. A. de Jong, "NWChem: A comprehensive and scalable open-source solution for large scale molecular simulations," *Comput. Phys. Commun.*, vol. 181, no. 9, pp. 1477–1489, Sep. 2010.

[315] L. R. Mahoney, G. D. Mendenhall, and K. U. Ingold, “Calorimetric and equilibrium studies on some stable nitroxide and iminoxy radicals. Approximate oxygen-hydrogen bond dissociation energies in hydroxylamines and oximes,” *J. Am. Chem. Soc.*, vol. 95, no. 26, pp. 8610–8614, Dec. 1973.
[316] Y. Kimura and A. Ikegami, “Local dielectric properties around polar region of lipid bilayer membranes,” *J. Membr. Biol.*, vol. 85, no. 3, pp. 225–231, Oct. 1985.
[317] K. E. Riley and P. Hobza, “Noncovalent interactions in biochemistry,” *Wiley Interdiscip. Rev. Comput. Mol. Sci.*, vol. 1, no. 1, pp. 3–17, 2011.
[318] J. M. Dimitrić Marković, J. M. Baranac, and T. P. Brdarić, “Electronic and infrared vibrational analysis of cyanidin-quercetin copigment complex,” *Spectrochim. Acta. A. Mol. Biomol. Spectrosc.*, vol. 62, no. 1–3, pp. 673–680, Nov. 2005.
[319] P. Figueiredo, M. Elhabiri, K. Toki, N. Saito, O. Dangles, and R. Brouillard, “New aspects of anthocyanin complexation. Intramolecular copigmentation as a means for colour loss?,” *Phytochemistry*, vol. 41, no. 1, pp. 301–308, Jan. 1996.
[320] D. Marquardt, J. A. Williams, J. J. Kinnun, N. Kučerka, J. Atkinson, S. R. Wassall, J. Katsaras, and T. A. Harroun, “Dimyristoyl Phosphatidylcholine: A Remarkable Exception to α-Tocopherol’s Membrane Presence,” *J. Am. Chem. Soc.*, vol. 136, no. 1, pp. 203–210, Jan. 2014.
[321] “Bioavailability of chalcones Arbutin,” *Docstoc.com*. [Online]. Available: http://www.docstoc.com/docs/47364588/Bioavailability-of-chalcones-Arbutin. [Accessed: 09-Apr-2014].
[322] S.-J. Won, C.-T. Liu, L.-T. Tsao, J.-R. Weng, H.-H. Ko, J.-P. Wang, and C.-N. Lin, “Synthetic chalcones as potential anti-inflammatory and cancer chemopreventive agents,” *Eur. J. Med. Chem.*, vol. 40, no. 1, pp. 103–112, Jan. 2005.
[323] H. Forejtníková, K. Lunerová, R. Kubínová, D. Jankovská, R. Marek, R. Kareš, V. Suchý, J. Vondráček, and M. Machala, “Chemoprotective and toxic potentials of synthetic and natural chalcones and dihydrochalcones in vitro,” *Toxicology*, vol. 208, no. 1, pp. 81–93, Mar. 2005.
[324] Y. L. Hsu, P. L. Kuo, W. S. Tzeng, and C. C. Lin, “Chalcone inhibits the proliferation of human breast cancer cell by blocking cell cycle progression and inducing apoptosis,” *Food Chem. Toxicol.*, vol. 44, no. 5, pp. 704–713, May 2006.
[325] T. Akihisa, H. Tokuda, D. Hasegawa, M. Ukiya, Y. Kimura, F. Enjo, T. Suzuki, and H. Nishino, “Chalcones and Other Compounds from the Exudates of Angelica keiskei and Their Cancer Chemopreventive Effects,” *J. Nat. Prod.*, vol. 69, no. 1, pp. 38–42, Jan. 2006.
[326] T. Akihisa, H. Tokuda, M. Ukiya, M. Iizuka, S. Schneider, K. Ogasawara, T. Mukainaka, K. Iwatsuki, T. Suzuki, and H. Nishino, “Chalcones, coumarins, and flavanones from the exudate of Angelica keiskei and their chemopreventive effects,” *Cancer Lett.*, vol. 201, no. 2, pp. 133–137, Nov. 2003.
[327] M. L. Go, X. Wu, and X. L. Liu, “Chalcones: An Update on Cytotoxic and Chemoprotective Properties,” *Curr. Med. Chem.*, vol. 12, no. 4, pp. 483–499, Feb. 2005.
[328] B. S. Publishers, *Current Medicinal Chemistry*. Bentham Science Publishers, 1999.
[329] S. Grimme, “Do Special Noncovalent π–π Stacking Interactions Really Exist?,” *Angew. Chem. Int. Ed.*, vol. 47, no. 18, pp. 3430–3434, Apr. 2008.
[330] A. D’Aléo, D. Gachet, V. Heresanu, M. Giorgi, and F. Fages, “Efficient NIR-Light Emission from Solid-State Complexes of Boron Difluoride with 2′-Hydroxychalcone Derivatives,” *Chem. – Eur. J.*, vol. 18, no. 40, pp. 12764–12772, Oct. 2012.

[331] E. Runge and E. K. U. Gross, “Density-Functional Theory for Time-Dependent Systems,” *Phys. Rev. Lett.*, vol. 52, no. 12, pp. 997–1000, Mar. 1984.
[332] E. H. Anouar, J. Gierschner, J.-L. Duroux, and P. Trouillas, “UV/Visible spectra of natural polyphenols: A time-dependent density functional theory study,” *Food Chem.*, vol. 131, no. 1, pp. 79–89, Mar. 2012.
[333] M. Millot, F. Di Meo, S. Tomasi, J. Boustie, and P. Trouillas, “Photoprotective capacities of lichen metabolites: A joint theoretical and experimental study,” *J. Photochem. Photobiol. B*, vol. 111, pp. 17–26, Jun. 2012.
[334] J. Fabian, “TDDFT-calculations of Vis/NIR absorbing compounds,” *Dyes Pigments*, vol. 84, no. 1, pp. 36–53, Jan. 2010.
[335] E. H. Anouar, J. Gierschner, J.-L. Duroux, and P. Trouillas, “UV/Visible spectra of natural polyphenols: A time-dependent density functional theory study,” *Food Chem.*, vol. 131, no. 1, pp. 79–89, Mar. 2012.
[336] S. Grimme, “Semiempirical GGA-type density functional constructed with a long-range dispersion correction,” *J. Comput. Chem.*, vol. 27, no. 15, pp. 1787–1799, Nov. 2006.
[337] G. Fabre, I. Bayach, K. Berka, M. Paloncyova, J.-L. Duroux, M. Otyepka, and P. Trouillas, “Atomistic description of collaborative antioxidant effects between vitamins and natural polyphenols in lipid-bilayer membranes,” 2014.

Annex

Annex

Flavonoids

1. 6–hydroxyflavone
2. apigenin
3. baicalein
4. catechin
5. chrysin
6. daidzin
7. dihydrofisetin (fustin)
8. dihydroquercetin
9. galangin
10. genistein
11. glycitein
12. hesperetin
13. hesperidin
14. leucocyanidin
15. luteolin
16. morin
17. naringenin
18. pelargonidin (taxifolin)
19. quercetin
20. rutin
21. scutellarein
22. tangeritin
23. vitamin E
24. wogonin
25. Xanthohumol

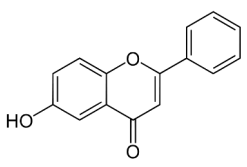

1

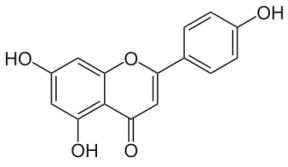

2

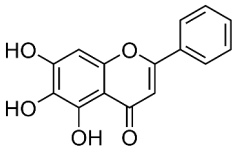

3

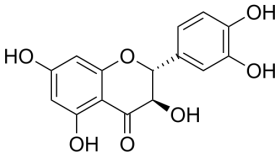

4

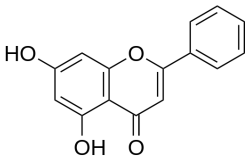

5

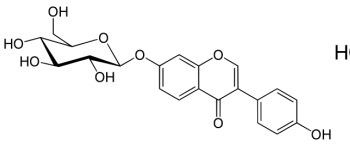

6

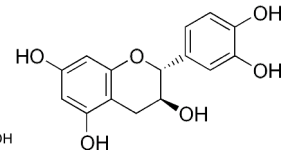

7

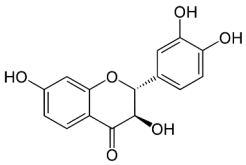

8

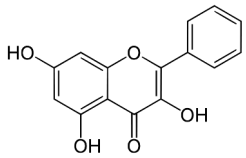

9

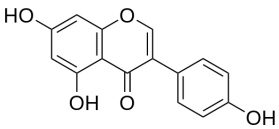

10

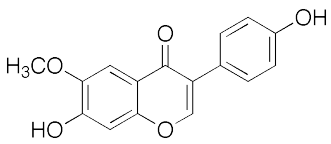

11

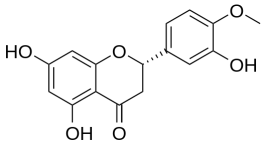

12

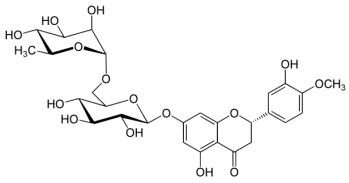

13

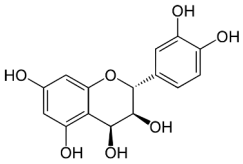

14

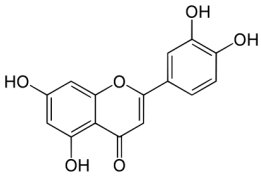

15

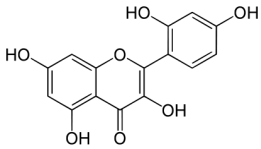

16

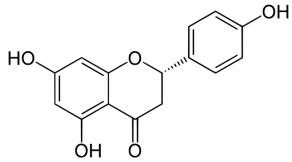

17

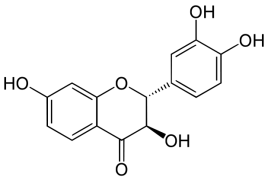

18

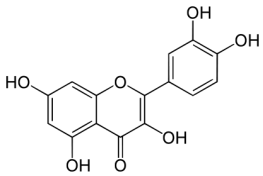

19

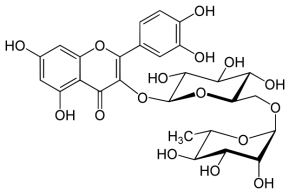

20

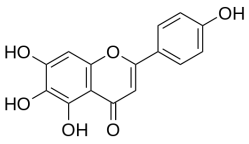

21

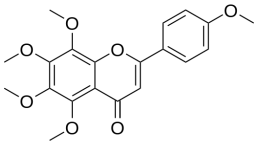

22

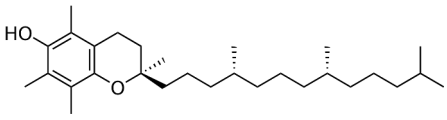

23

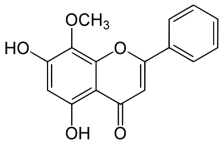

24

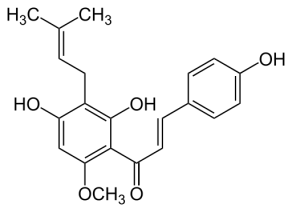

25

Stilbenoids

26. (-)−hopeaphenol
27. (+)−parviflorol
28. 13,13'−*O*−isoproylidenericcardin D
29. 3−hydroxy−4'-methoxybibenzyl

30. astringin
31. balanocarpol
32. Bazzanin B
33. bazzanin S
34. blestriarene A
35. carasiphenol D
36. corsifuran C
37. cyphostemmins A
38. cyphostemmins B
39. davidiol A
40. dibalanocarpol
41. glepidotin D
42. gnetofuran A
43. gymconopin D
44. hemsleyanol E
45. isoplagiochin D
46. isorhapontigenin
47. Lakoochins A
48. Lakoochins B
49. lespedezol H
50. marchantin A
51. miyabenol C
52. oxyresveratrol
53. parthenocissin A
54. piceatannol
55. pterostilbene
56. resveratrol
57. rhapontigenin
58. Riccardin C
59. scirpusin B
60. shanciguol
61. stemanthrene A
62. stemanthrene D
63. upunaphenols I
64. upunaphenols J
65. vaticanol C
66. α-viniferin
67. ε-viniferin

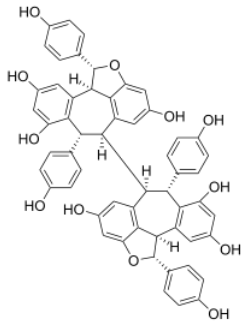

26

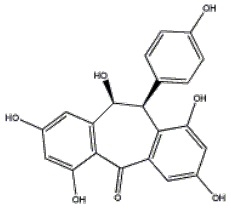

27

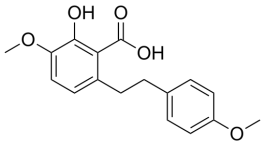

28

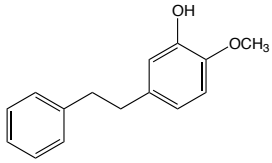

29

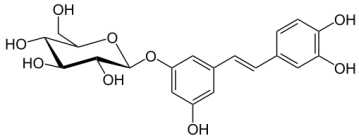

30

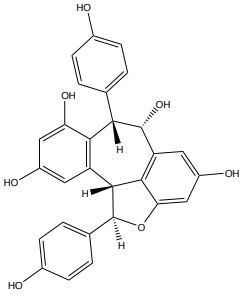

31

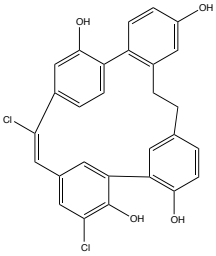

32

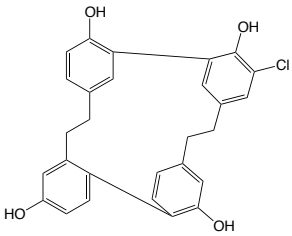

33

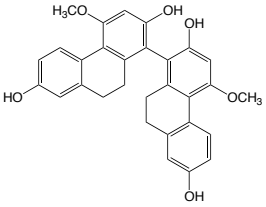

34

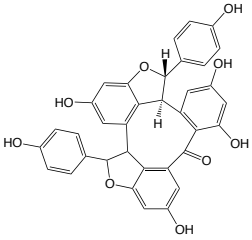

35

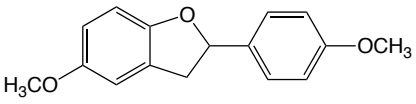

36

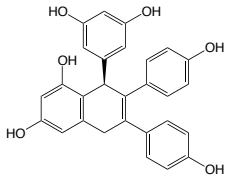

37

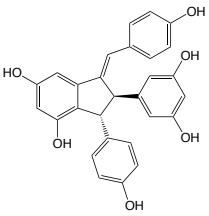

38

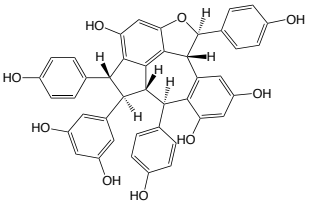

39

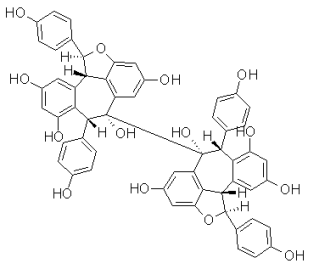

40

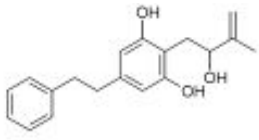

41

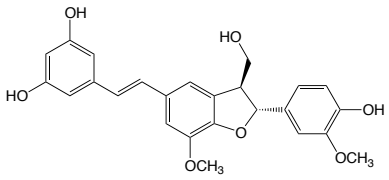

42

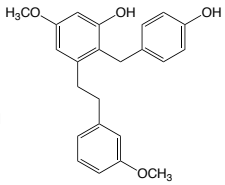

43

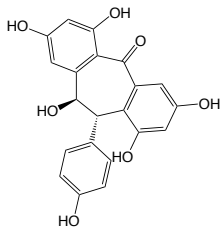

44

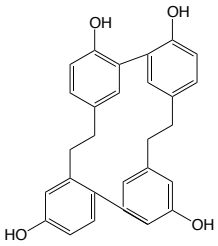

45

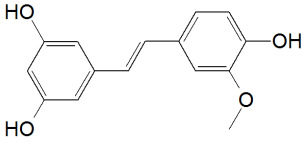

46

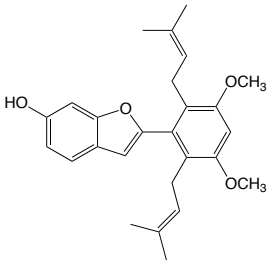

47

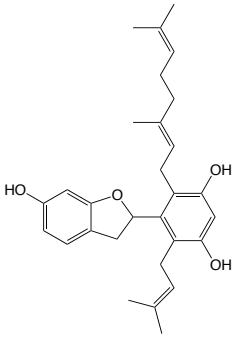

48

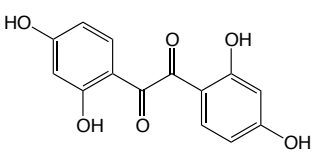

49

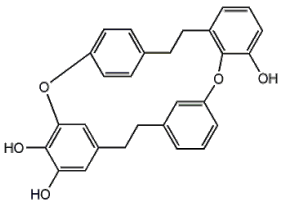

50

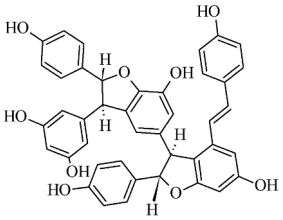

51

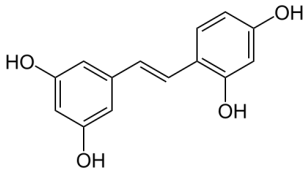

52

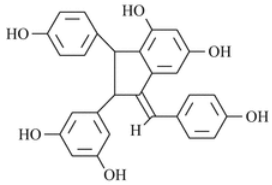

53

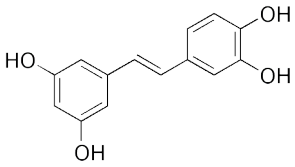

54

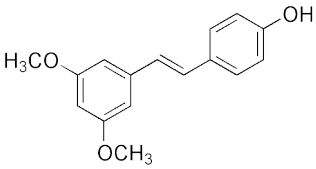

55

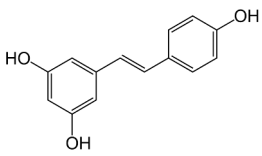

56

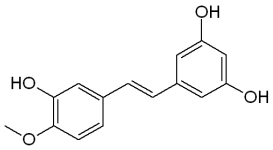

57

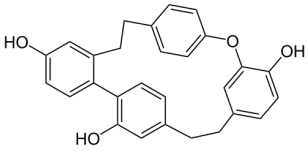

58

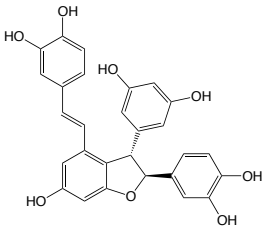

59

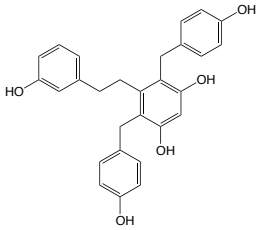

60

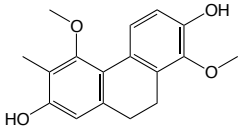

61

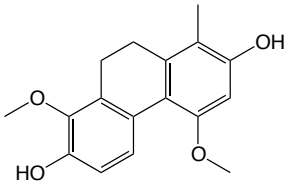

62

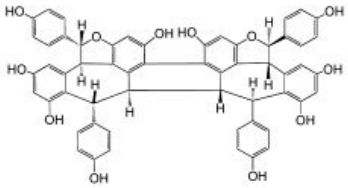

63

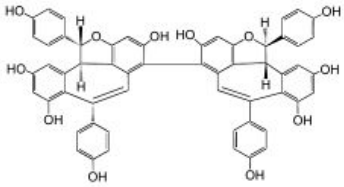

64

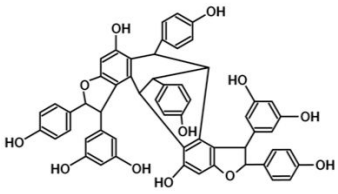

65

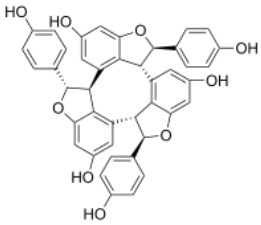

66

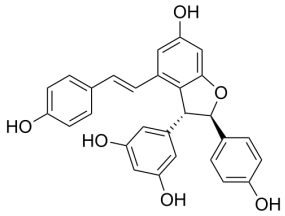

67

Abstract

Natural polyphenols form non-covalent complexes in which π–stacking and H–bonding play a key-stabilizing role. The dispersion–corrected DFT calculations have paved the way towards reliable description of aggregation processes of natural products. In this work, these methods are applied at i) understanding of stereo– and regio–selective oligostilbenoids biosynthesis; ii) predicting natural antioxidant aggregation within lipid bilayer membrane, which may allow rationalizing the synergism of vitamin E, vitamin C and polyphenols in their antioxidant action; and iii) modulating optical properties of chalcone derivatives.

Keywords: DFT–D(dispersion-corrected); non–covalent association; polyphenols; stilbenoids; antioxidants.

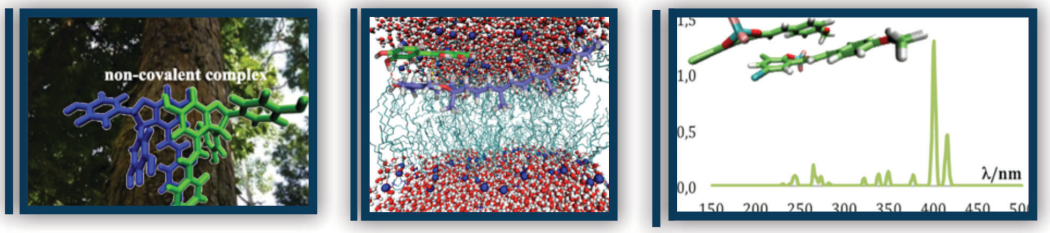

Les polyphénols naturels forment des complexes non–covalents dans lesquels le π–stacking et les liaisons hydrogène jouent un rôle clé dans la stabilisation. Les calculs DFT incluant la dispersion (DFT–D), la description des processus d'agrégation non–covalente de produits naturels devient fiable. Dans ce travail, les méthodes DFT–D sont appliquées à i) la compréhension de la biosynthèse stéréo– et régio–sélective des oligostilbenoïdes, ii) la prédiction de l'agrégation des antioxydants naturels au sein de la membrane bicouche lipidique, qui pourrait rationaliser la synergie de la vitamine E, la vitamine C et polyphénols dans leur action antioxydante, et iii) la modulation des propriétés optiques de dérivés de chalcones.

Mots-clés: DFT–D ; associations non–covalentes ; polyphénols ; stilbénoïdes ; antioxydants.